学位申請論文

芥川　智行

Studies on Multiplex Proton-Transfer and Electron-Transfer Natures Based on 2,2'-bi-1*H*-imidazole System

A Thesis Submitted to Kyoto University for the Degree of Doctor of Science

by Tomoyuki Akutagawa

December, 1996

Contents

Chapter 1. General Introduction

One of the purposes of the studies in the organic materials is to create the molecular aggregate, which shows the desired electronic properties, by the method of organic synthesis. The electronic structure of each molecules is possible to design and synthesis, but the construction of the desired molecular aggregate is very difficult to control. Both of the physical and chemical methods to control the molecular arrangements, intermolecular distances, intermolecular bond (covalent, ionic, van der Waals, and metal types), and dimensionality of intermolecular interaction in the molecular aggregate are not enough to develop.

There are many states of molecular aggregation; for examples, powder, polycrystalline, single crystals, evaporated film, and Langmuir-Blodgett (LB) film. Based on the studies of electrically conducting organic charge transfer (CT) complexes in the form of single crystals, the synthetic strategies of molecular metal and superconductor have been proposed and accumulated in these day.[1] In addition, the molecular magnet and metallic LB film were also reported,[2] and the researches of new organic materials, which shows an interesting chemical and physical properties, will be important to deduce the functions of organic materials. I focused on the interaction of the proton transfer (PT) and tried to combine the CT and PT interactions.

1-1 Organic Charge Transfer (CT) Complex

The first highly conducting organic compound (perylene)(bromine)$_X$, which showed the conductivity at room temperature of ca. 0.1 Scm^{-1}, was discovered by Japanese group in 1954.[3] This work indicated that the mobile carrier bearing high conductivity was generated on the organic molecule. The large numbers of organic metals were developed until now, and about 70 kinds of organic superconductors with 12 kinds of molecular systems; for examples, tetrathiafulvalene (TTF), metal[2-thioxo-1,3-

dithiol-4,5-dithiolate]$_2$ (M(dmit)$_2$), and carbon sixty (C_{60}), were found until 1995. The transition temperature to the superconducting state (T_c) raised above 30 K in the C_{60} system. These metallic or superconducting organic systems are the CT complex, which is composed of electron donor and acceptor molecules. Figure 1-1 summarizes the representative electron donor and acceptor molecules.

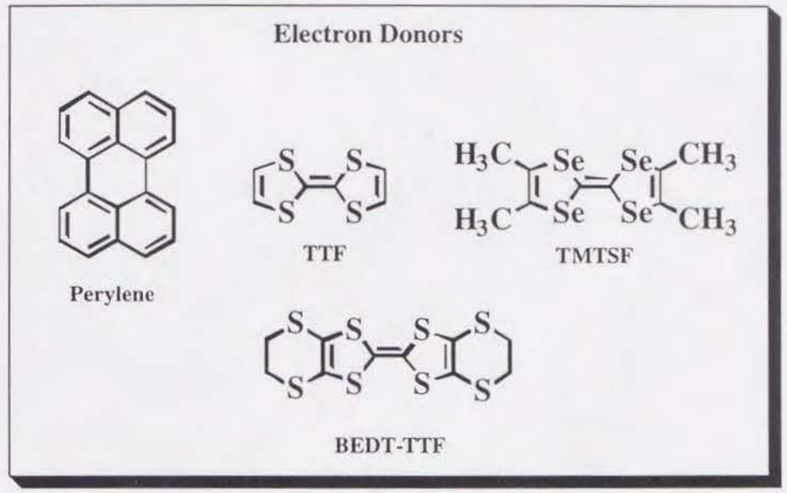

Fig. 1-1 Molecular structures of representative electron donor and acceptor molecules

In the 1960s, the crystal structures and physical properties of a number of anion radical salts of 7,7,8,8-tetracyanoquinodimethane (TCNQ) were examined.[4] A theory of the high T_c superconductor using the organic molecule was proposed by Little in 1964.[5] He proposed that the T_c value will rise up to room temperature if the formation of the Cooper pair is mediated by the electron-exciton interaction instead of the electron - lattice one. This idea was expanded to the two-dimensional electronic system as the surface superconductor by Ginzburg.[6] They pointed out that the enhancement of molecular polarizability was necessary to increase the electron-exciton interaction. Although many synthetic attempts have been done for above mentioned excitonic superconductors, no successful results have yet been reported. However, the studies of many kinds of TCNQ anion radicals have revealed the importance of molecular polarizability of counter cation on transport of electron in solid. The counter cation of large molecular polarizability in the TCNQ complexes increased the electrical conductivity compared with that of small molecular polarizability.[7, 8] The large size of molecular has many electron compared with small size one, so the molecular polarizability enhances according to the increase of volume of molecule. However, the size mismatch between the TCNQ and counter cation destroyed the stacking structure of TCNQ column, and the electrical conductivity is decreased in the combination of very large cation molecule. As a result, it was pointed out that the small size of molecule with large molecular polarizability increased the electrical conductivity.

In 1969, the TTF, which is the most representative electron donor molecule until now, was synthesized by several groups.[9] The fulvalene molecule was interested from a viewpoint of aromaticity. This molecule has the stable 7π - 7π electronic structure by the delocalization of the π-electron and gives the aromatic 7π - 6π and 6π - 6π electronic structures by the stepwise oxidations (Fig. 1-2). Since the chemical stabilities of cation radical (6π - 7π) and dication (6π - 6π) states in the heptafulvalene were insufficient, the isoelectronic substitution from the ethylene moiety to the sulphur atoms was tried to increase the stabilities of open shell electronic structure (Fig. 1-2). As a result, the

radical cation and dication states of TTF existed as stable species, and used as an electron donor molecule in the field of organic conductor.

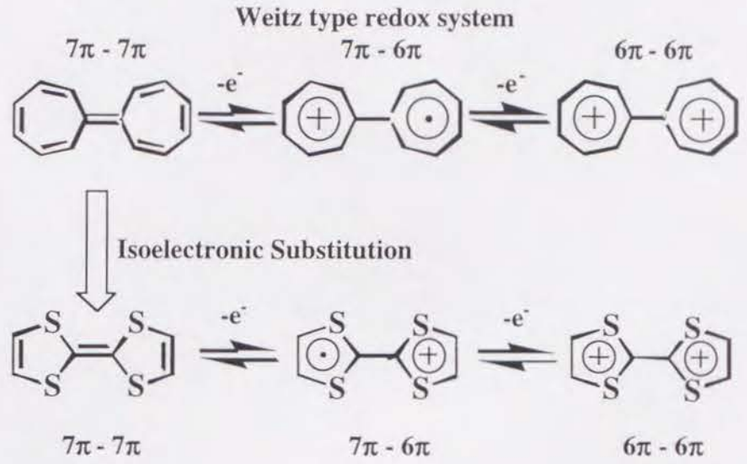

Fig. 1-2 Isoelectronic substitutions of heptafulvalene and redox characters of Weitz (TTF) and Würster (TCNQ) type molecules.

In the multi redox system, a conventional classification of redox character of the π - electron was proposed by Hünig et al.[10] Here, I explain the redox systems of TTF and TCNQ, which belong to the Weitz and Würster types, respectively (Fig. 1-2). This classification was based on the differences of redox system whether the redox reaction occurred at the end of the molecule (dicyanomethylene part of TCNQ) or the within the cyclic system of π-electron (five-membered ring of TTF). The aromatic 6π - 7π and 6π - 6π characters appear by two stage oxidations of TTF, while the quinoide structure of TCNQ changes to the aromatic 6π structure by one step reduction. However, no further contribution of aromaticity exists at the $TCNQ^{2-}$. This classification is conventional

nomenclature, and there are no detailed discussion concerning to the differences between the Weitz and Würster redox systems.

The first organic metal (TTF)(TCNQ) was discovered in 1973. This complex showed the metallic conducting behaviour from room temperature to 60 K, and changed to insulator below 60 K.[11]. It is known that three stable low temperature phases exist in the low dimensional conductor; that is, i) the charge density wave (CDW) phase by the strong electron - lattice interaction, ii) the spin density wave (SDW) phase by the antiferromagnetic interaction, and iii) the superconducting (SC) phase by the formation of Cooper pair. In the case of (TTF)(TCNQ), the insulating phase at low temperature (< 60 K) was ascribable to the CDW phase due to the one dimensional character of Fermi surface. The suppression of CDW and/or SDW phases at low temperature is indispensable to generate the SC phase in organic metal.

To suppress the low temperature insulating phases, two chemical methods were applied for one dimensional electronic system; i) the destruction of periodicity in the one dimensional Fermi surface, ii) the increase of the dimensionality from one to two or three dimensional electronic states of Fermi surface. The first method was succeeded in the case of the $(DEPE^{2+})(TCNQ)_4(H_2O)_x$, $x < 0.2$ (DEPE is 1,2-di(*N*-ethyl-4-pyridinium)ethylene^{2+}). This salt contains the incommensurate water molecule as solvent, which influences the periodicity of one dimensional Fermi surface. As a result, the complete nesting of Fermi surface at low temperatures was suppressed due to the blurred Fermi surface, and the metallic conducting behaviour was observed from room temperature (σ_{RT} = 150 ~ 2200 Scm^{-1}) to 20 mK.[12]. The second method was succeeded for the tetramethyltetraselenafulvalene (TMTSF) and bis(ethylenedithio) tetrathiafulvalene (BEDT-TTF) molecules. The replacements from the sulphur atoms (S) to selenium atoms (Se) increased the intermolecular interaction along the side-by-side direction to the conducting column, while multi chalcogen substitutions of TTF framework also enhanced the dimensional property of electronic structure. The application of pressure has also the same effect as the above mentioned chemical modifications. The first organic superconductor was discovered by the application of

pressure to the $(TMTSF)_2(PF_6^-)$; T_c = 0.6 K (0.6 kbar).[13] The cation radical salts of the BEDT-TTF system provided the organic superconductors with the T_c > 10 K.[14] From the studies of BEDT-TTF superconductors, it was pointed out that the small intermolecular transfer and high density of state at Fermi level were required to increase the T_c, the alkali metal - C_{60} system fulfilled this criteria fortunately. The first superconductor of C_{60} system was discovered in or on $(K)_3(C_{60})$.[15] Since the linear correlation between the T_c and lattice parameter was found, it was expected that the large size of alkali metal increased the T_c. In this sense, the Cs_3C_{60} was developed at the T_c of 40 K under the application of pressure.[16]

In these days, the appearance of superconducting state is common character even in the organic molecules. The controls of the crystal structure and band filling are the important subjects to increase the T_c of superconductor in the organic system. In the CuO_X high-T_c superconductors, the precise control of band filing largely increased the T_c.

1-2 Proton-Transfer (PT) and Charge-Transfer (CT) Complex

The phase transition, which interplays between electron (charge)-transfer (CT) and proton-transfer (PT) interactions, in the solid state was studied by Hertel in 1924.[17] The CT and PT properties of the picric acid complexes with some anilines were examined by Briegleb and Delle,[18] Kofler et al.,[19] Saito and Matsunaga,[20] Bernstein et al.,[21] and Tanaka et al.[22]. The 3,3',5,5'-tetranitrobiphenol and 2,4,6-trinitrobenzoic acid were also employed for the electron acceptor and proton donor instead of picric acid.[23] Until the 1970s, the researches of the CT and PT system in the solid state were mainly carried out for the polynitrophenol - aromatic amine systems. Only a few synthetic strategies have been proposed for these CT and PT system.[20a, d, g, h, 24] After the 1980s, the new systems; quinhydrones,[25] *N*-salicylideneanilines,[26] and metal(diaminoglyoxime)$_2$ complexes,[27] have been examined from a viewpoint of simultaneous operation of the CT and PT interactions. At first, I describe the

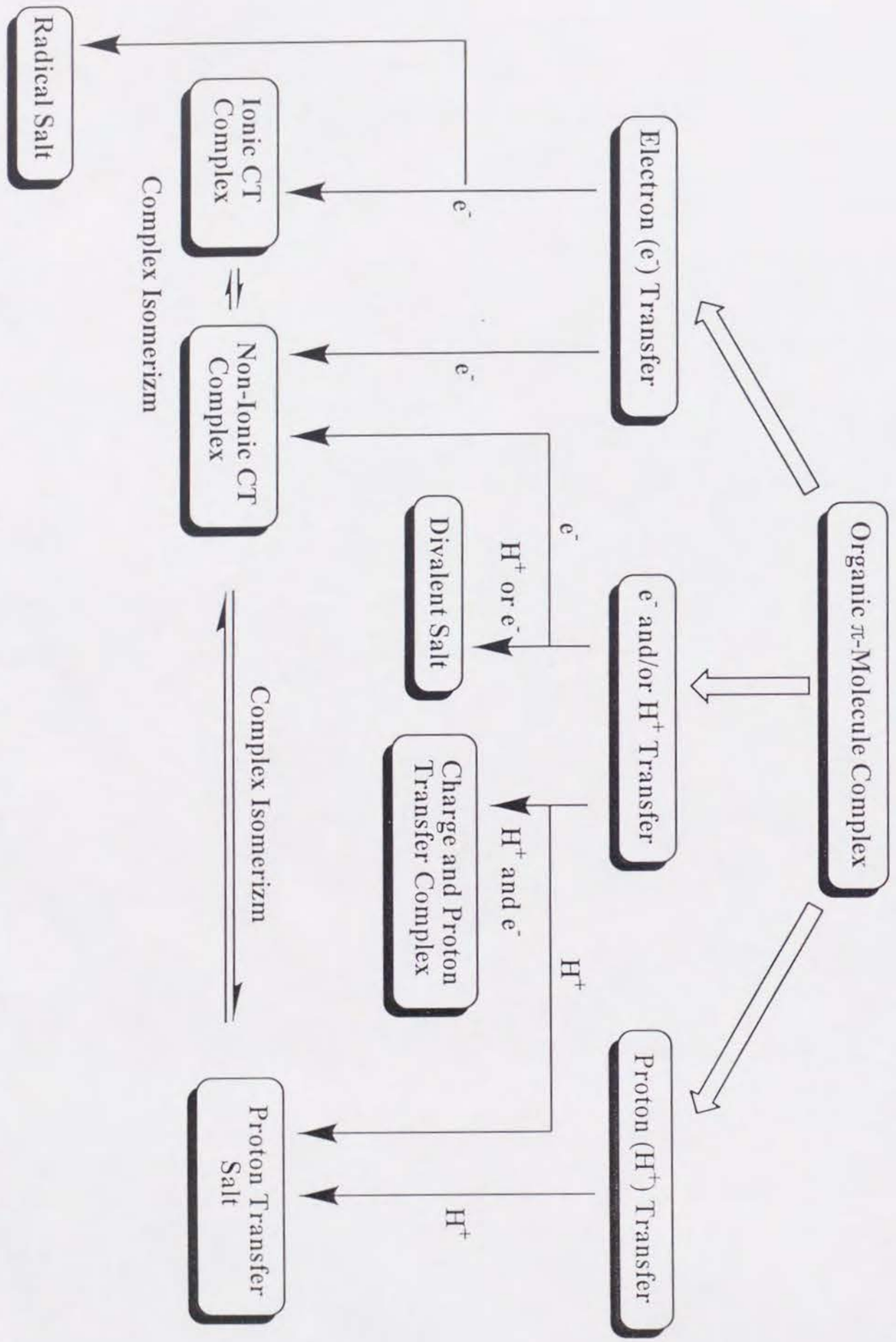

Fig. 1-3 Classification of Organic π-electron System based on CT and PT Interactions

relationship between CT and PT interactions based on the family tree of the molecular complex of π - electron system (Fig. 1-3).[24b, 28]

There are two main categories of the CT complex, one is one chain conductor (radical salt), and another is two chain conductor such as (TTF)(TCNQ). The latter class can be further divided into the ionic ($\delta > 0.5$) and non-ionic ($\delta < 0.5$) CT complexes based on the boundary of degree of CT (δ) in the ground state. The organic metals and superconductors are obtained from the ionic two chain CT complex or radical salt. In these categories, the reversible phase transition from non-ionic CT ($\delta \sim 0.3$) to ionic CT ($\delta \sim 0.7$) types (Scheme 1-1) was reported for the (TTF)(p-chloranile), which occurred at 81 K or applying the pressure above 10 kbar.[29]

< 81K or 10kbar <

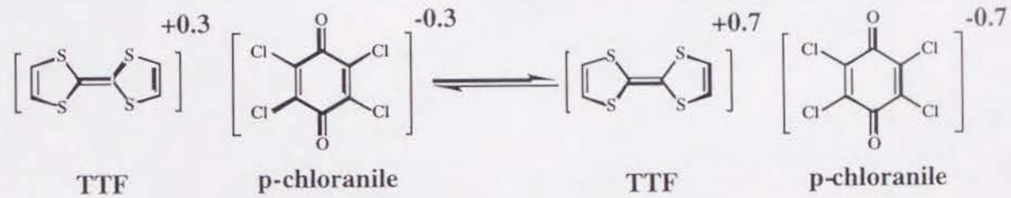

Scheme 1-1

In the case of CT and PT system, the balance of Brønsted's acid-base interaction, CT interaction, and Madelung energy decides the types of the obtained complex in the solid state. If the acidity of proton donor: $pK_a(DH)$, is higher than that of proton acceptor: $pK_a(AH^+)$, the proton of the HD molecule moves to the A molecule, which gives a PT salt: $[D^+][AH^-]$ (Scheme 1-2a). On the other hand, no PT reaction from the DH molecule to A molecule occurs in the condition of $pK_a(AH^+) < pK_a(DH)$. If the DH and A molecules have the electron donating and accepting abilities, respectively, at the same time, the formation of a CT complex can be observed as the $[DH^{+\delta}][A^{-\delta}]$ form (Scheme 1-2b).

$$a;\ DH + A \rightarrow D^- + AH^+ \rightarrow [D^-][AH^+]$$

$$b;\ DH + A \rightarrow [DH^{+\delta}]\ [A^{-\delta}]$$

Scheme 1-2

In 1924, Hertel reported the phase diagram of the molecular complexes between picric acid (electron acceptor and/or proton donor) and halogeno anilines (electron donor and/or proton acceptor).[17a] The molecular complex: (o-bromoaniline)(picric acid), indicated the colour change from yellow to red by the thermal treatment at 95 °C. Since colour of complex (o-bromoaniline)(s-trinitrobenzene) was red, the yellow and red phases of (o-bromoaniline)(picric acid) complex were classified as the PT salt with no CT: [o-bromoanilinium$^+$][picrate$^-$], and the molecular complex with no PT: [o-bromoaniline][picric acid], respectively, as shown in Scheme 1-3 (the PT and CT interactions are denoted as allows with the notations of H^+ and e^-, respectively). He found eight kinds of molecular complexes, which indicated the colour change by the thermal treatments (Table 1-1).[17]

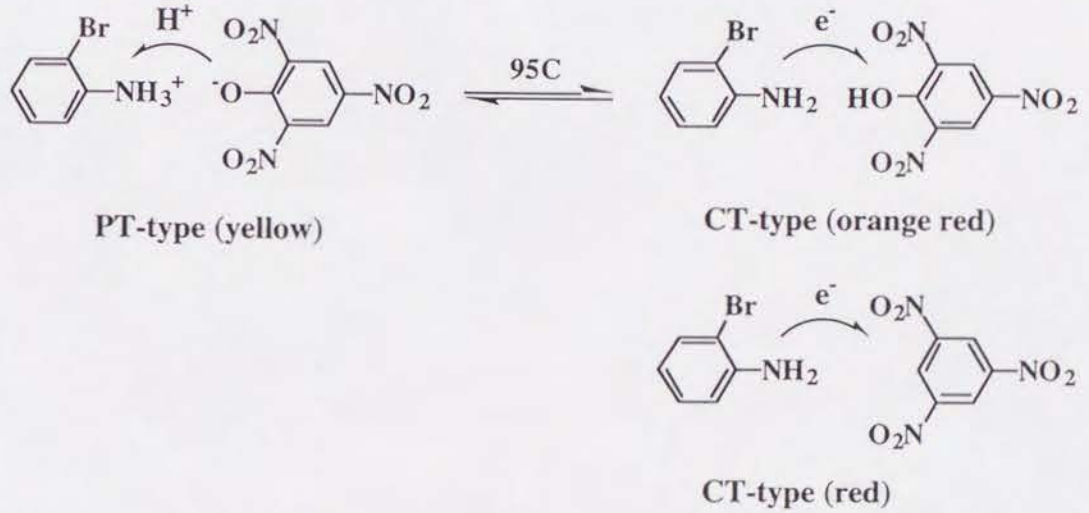

Scheme 1-3

In 1927, Pfeiffer summarized about one thousand of molecular complexes in his book, *Organisch Molekülverbindungen*, and introduced the work of Hertel as *complex*

Table 1-1. Molecular complexes between anilines and polynitrophenol.

Proton and electron donor	Proton and electron acceptor[a]	Colour change (T_c/°C)[b]	Electron acceptor[c]	Colour
		CT and PT complex		
o-bromoaniline	picric acid	yellow-orange red (95)	s-trinitrobenzene	orange
o-iodoaniline	picric acid	yellow-deep orange (90)	s-trinitrobenzene	orange
1-chloro-2-napthylamine	picric acid	yellow-dark red (130)	s-trinitrobenzene	bright red
1-bromo-2-napthylamine	picric acid	yellow-violet red (114)	s-trinitrobenzene	bright red
1,6-bromo-2-napthylamine	picric acid	yellow-dark red (96)	s-trinitrobenzene	bright red
4-bromo-1-napthylamine	2,6-dinitrophenol	yellow-dark red (91)	2,6-dinitrobenzene	red
4-chloro-1-napthylamine	2,6-dinitrophenol	yellow-red (76)	2,6-dinitrobenzene	orange
2,4-dichloro-1-napthylamine	2,6-dinitrophenol	yellow-red (72)	2,6-dinitrobenzene	-

a) The PT interaction occurs due to the existence of phenolic protons. b) The colour of high temperature phase is yellow with PT type and low temperature phase is CT type with no PT interaction. c) There are no PT interaction in the absence of the phenolic protons.

isomerizm .[30] The reason of the colour change was explained as follow. If the acid-base interaction was added to the force of molecular complex formation (CT interaction), the phenomena of the complex isomerizm occurred by the balance between the CT and the acid - base interactions. In the low temperature region, the acid - base interaction is superior to the CT one, while the CT interaction is important at the high temperature region.

In the PT and CT system, the types of the obtained complex depend on the acid - base dissociation constants (pK_a), ionization potential (I_p), electron affinity (E_a) of the component molecules, and Madelung energy (M) in the solid state. In the case of polynitrophenol - aromatic amine system, the difference of pK_a values (ΔpK_a = $pK_a(DH)$ - $pK_a(AH^+)$) between polynitrophenol ($pK_a(DH)$) and aromatic amine ($pK_a(AH^+)$) dominated to decide whether the obtained complex was the PT salt or CT complex. The clear boundary between CT ($\Delta pK_a > 0$) and PT ($\Delta pK_a < 0$) types was indicated at around the $\Delta pK_a \sim 0$ in the polynitrophenol - aromatic amine systems.[24b] The complex locating at $\Delta pK_a \sim 0$ region was sensitive to the condition of complex formation.

There are some examples that both of the CT and PT interactions operate simultaneously in the solid state. Kofler obtained yellow and red coloured (1-naphthylamine)(picric acid) complexes from pyridine solution.[19] The explanation of this colour changes was carried out by Matsunaga and Saito.[20b] The phenolic proton of picric acid was transferred to the amino group of 1-naphthylamine, which gave the yellow salt of [1-naphthylammonium$^+$][picrate$^-$]. In the red form, both of the CT and PT interactions coexisted simultaneously, and the real chemical formula was deduced as the [1-naphthylamine][picrate$^-$][pyridinium$^+$]. The picrate anion was acted as the electron acceptor, and the red colour was attributed to the CT interaction between 1-naphthylamine and picrate anion (Scheme 1-4).

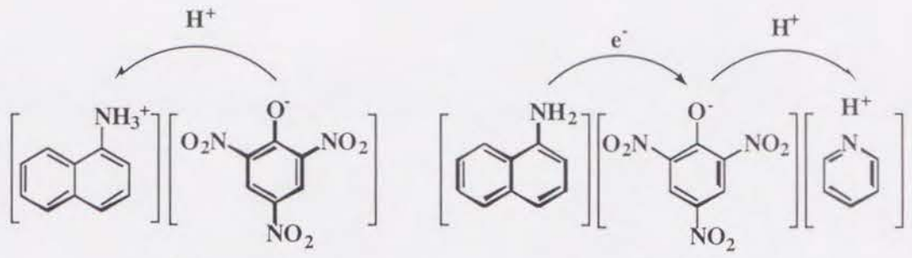

Scheme 1-4

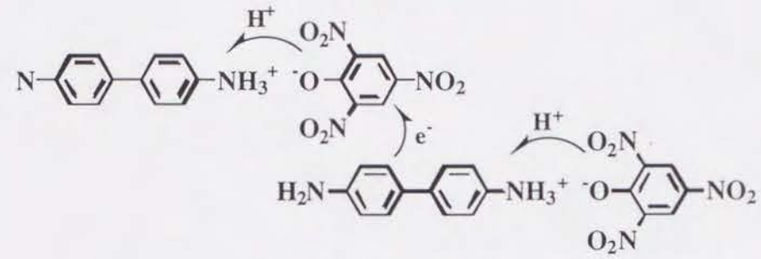

Benzidine - picric acid (1 : 2)

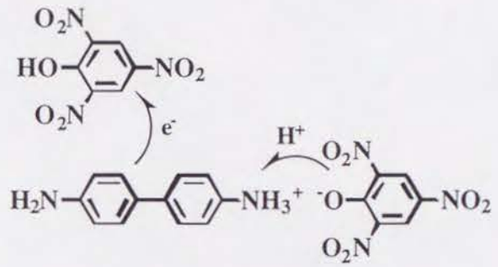

Benzidine - picric acid (1 : 2)

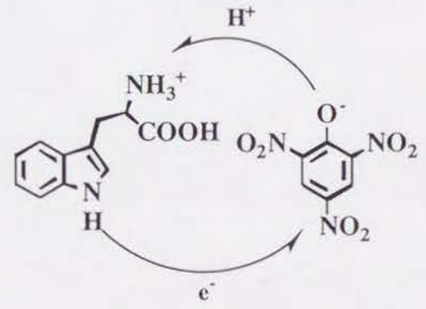

Tryptophan - picrate

Fig. 1-4. CPT complexes of (benzidine)(picric acid), (benzidine)(picric acid)$_2$, and (tryptophan)(picrate).

The molecular arrangement of 1-naphthylamine and picrate anion in the solid state was also preferred to occur the CT interaction between 1-naphthylamine and picrate, which was confirmed by the X-ray crystal structural analysis.[21] The complex, coexisting both of the PT and CT interactions simultaneously, was called as the charge and proton transfer (CPT) type. Fig. 1-4 shows another example of CPT complexes; (benzidine)(picric acid), (benzidine)(picric acid)$_2$ [20d, 20g, 23a] and (tryptophan)(picric acid).[20e] The [o-dibromotolidine$^{+\delta}$][picric acid$^{-\delta}$] was obtained as black coloured crystal with non-ionic CT complex from chloroform, while the cation radical [o-dibromotolidine$^{+\bullet}$][picrate^{-}] was also formed from ethanol (Scheme 1-5).[20d] This is also an example of complex isomerizm, which depends on the solvent system of crystal growth.

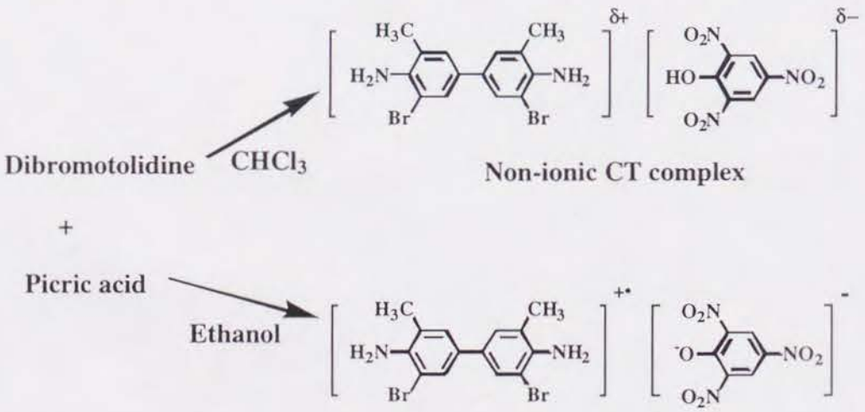

Scheme 1-5

The intermolecular transfer processes of hydrogen ($H^+ + e^- = H^\bullet$) and hydride ($H^+ + 2e^- = H^-$) were also examined. The hydrogen ($H^\bullet$) - transfer reaction of organic molecules was examined by Braude and Listead.[31] The hydride (H^-) - transfer (HT) and PT processes were also employed for the CT complex formation between TCNQ and some heterocyclic molecule (for examples, *N*-methylacridan and *N*-propyl-1,4-

dihydronicotinamide).[32] The TCNQ molecule changes to the 1,4-benzenedimalononitrile (H2TCNQ) by two step CT and PT processes (Fig. 1-5). Nine independent chemical species can be speculated for H2TCNQs - TCNQs system. Among nine species, there are no reports for the species; H2TCNQs^{2+}, H2TCNQs$^{+\bullet}$, and HTCNQs^{+}.

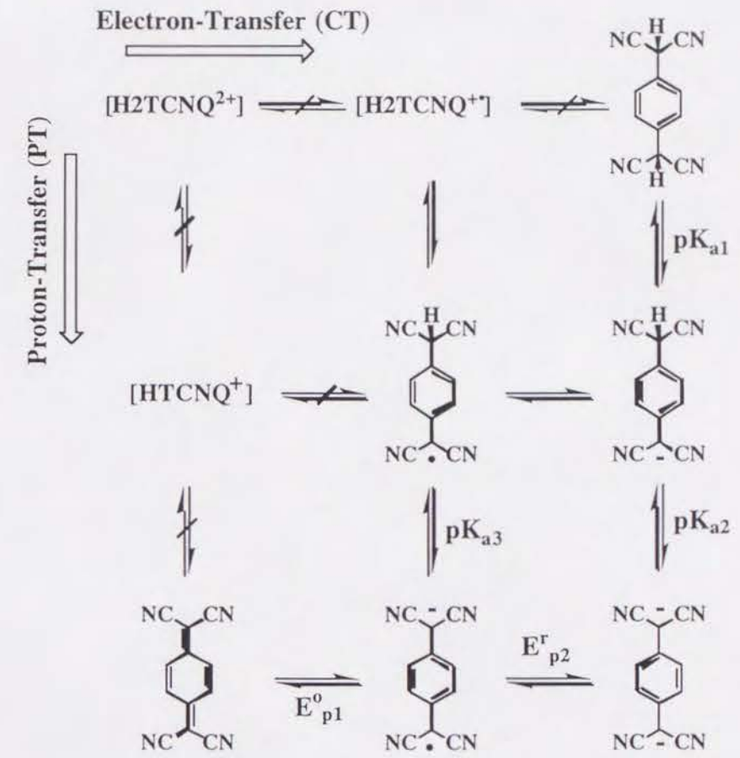

Fig. 1-5. 3 x 3 PT and CT diagram of H2TCNQ - TCNQ system. Each vertical and horizontal line corresponds to two-step PT and CT processes, respectively. The species in bracket are considered to be unstable. pK_{a1} ~ pK_{a3}, E^{o}_{p1}, and E^{r}_{p2} describe the processes in figure.

Scheme 1-6 shows an example of complex formation between TCNQ and *N*-alkylacridan. The hydride of *N*-alkylacridan is transferred to TCNQ, which forms *N*-alkylacridinium^{+} and HTCNQ^{-}. The HTCNQ^{-} molecule reacts with TCNQ, which forms the H2TCNQ and TCNQ$^{-\bullet}$ ($HTCNQ^- + 0.5TCNQ \rightarrow 0.5H2TCNQ + TCNQ^{-\bullet}$).

As a result, the complex (*N*-alkylacridinium^{+})(TCNQ)$_2$ was formed in addition to the H2TCNQ.

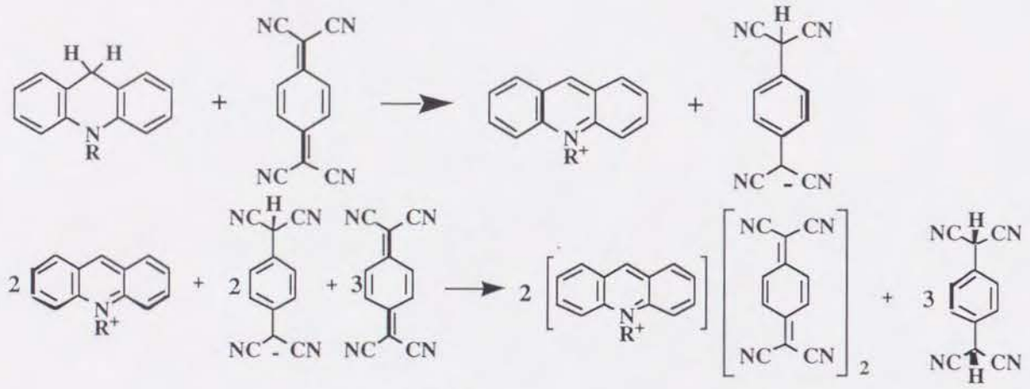

Scheme 1-6

Next, I explain three representative CT and PT systems: i) quinhydrone, which is composed of *p*-benzoquinone (BQ) as the electron acceptor and hydroquinone (H2Q) as the electron donor, ii) flavine nucleus as the biological redox processes, and iii) polyanilines as the conducting polymer system.

i) Quinhydrone. Since the transformation from H2Q to BQ occurs by two step PT and CT processes, nine independent species exist in this system (Fig. 1-6).[33] The oxidation of H2Q forms the cation radical: $H2Q^{+\bullet}$, and reduction of BQ produces the anion radical; $BQ^{-\bullet}$. The quinhydrone belongs to non-ionic CT complex due to the δ of 0.2 from the crystal structural analysis,[34] and the open shell species in the crystal are $H2Q^{+\bullet}$ and $BQ^{-\bullet}$. If a proton is removed from $H2Q^{+\bullet}$ or added to $BQ^{-\bullet}$, the neutral radical ($HQ^{\bullet}$) appears at the center of 3 x 3 diagram. The application of the pressure changed the optical spectra of quinhydrone crystal discontinuously, which is speculated to be the occurrence of transformation from the weak CT complex to the neutral radical ($HBQ^{\bullet}$) state.[25a] The direct evidence of the formation of semiquinone radical species ($HBQ^{\bullet}$) is not obtained. Nakasuji et al. proposed two chemical methods to stabilize the neutral radical state. The quinhydrone with small CT gap stabilizes the $HBQ^{\bullet}$ state through the excess charge effect of PT state, and the second method is the direct

stabilization by the push-pull substitution effect.[25b] They synthesized the extended π-electron systems; naphthoquinhydrone or pyrenoquinhydrone, to decrease the CT gap, but both of the direct detection of neutral radical species and the relationship between the CT gap and stabilization were not carried out.

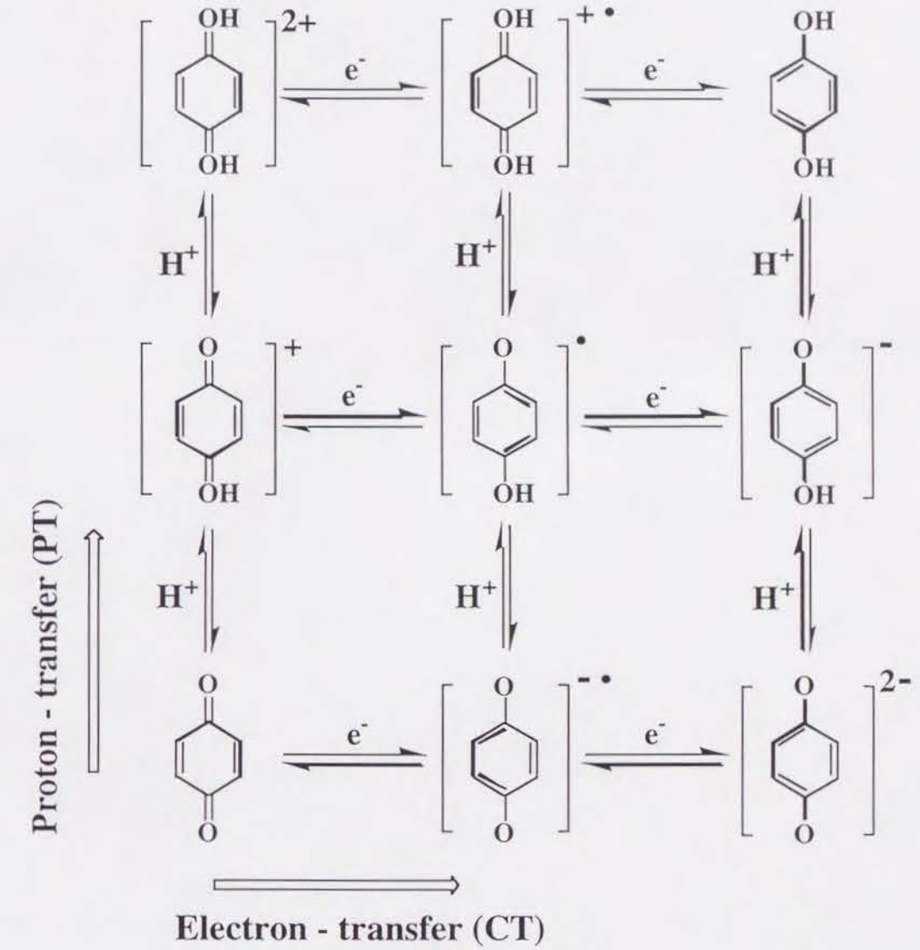

Fig. 1-6 3 x 3 (two-proton and two-electron matrix) diagram of quinone (BQ) - hydroquinone (H2Q) system. Each vertical and horizontal line corresponds to multiplex PT and CT processes, respectively.

*ii) **Flavine nucleus**.* The PT and CT interactions are also important in the biological system. The flavine nucleus is one of the typical components of CT and PT system in a biological redox moiety.[35)]

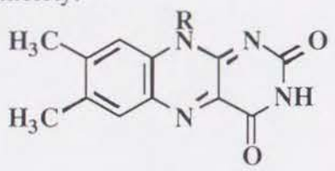

Flavine

The redox interconversions of flavine give cationic, neutral, or anionic species depending on the CT and PT processes. The HT reaction between the coenzyme of pyridinenucleotide and the substrate of the dehydrogenation enzyme is indispensable biological process in the biological energy transformation. In a viewpoint of the biological CT and PT system, the CT interaction between the tryptophan or serotonine and picrate was examined by the spectroscopic method.[20e)] The crystal structural analysis of these picrate complexes also showed the preferable arrangements between the donor and acceptor molecules to occur the CT interaction in the solid state.[36)]

*iii) **Polyaniline**.* The electrical conducting behaviour of polyaniline have been extensively studied by many researchers. The electrical conducting behaviour largely changes according to the protonated states of polyaniline.[37)] Scheme 1-7 indicates three representative forms of polyaniline.

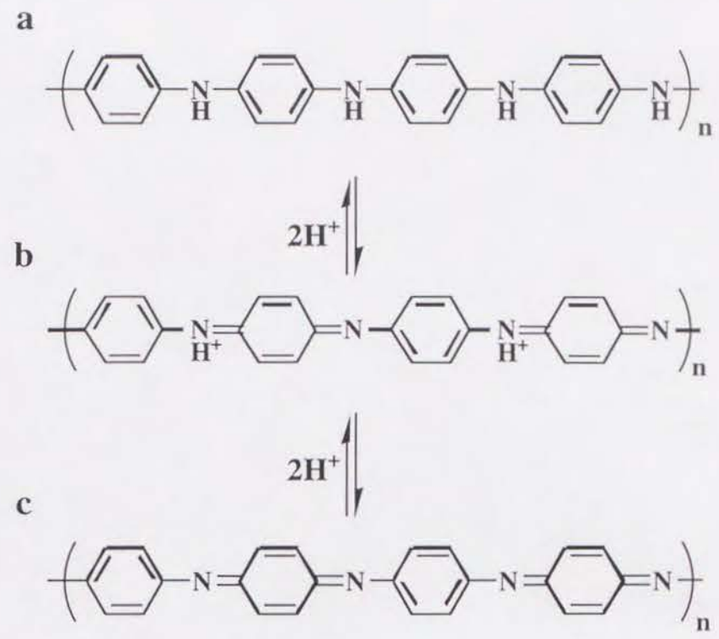

Scheme 1-7

The full protonated white polymer (a) is called as leucoemerardine, while fully deprotonated dark-purple form (c) is perigraniline. The form b, which has the equivalent amount of protonated and deprotonated units, is called as emerardine, and this state is important for a starting material of conducting polyaniline. The conductivity changed from 10^{-10} to 1 Scm^{-1} continuously by the proton doping in aqueous HCl solution.

1-3 CT and PT Nature of 2,2'-bi-1H-imidazole (H2BIM) System

Figure 1-7 showed the electron donor and acceptor molecules, which have been employed for the studies of CT and PT system in the solid state. All molecules in Fig. 1-7 (aromatic amines, hydroquinones, biphenols, polynitrophenols, and quinones) have a Würster type redox system. On the other hand, the representative electron donor molecule: TTF, belongs to the Weitz type redox system, which give a number of organic metals. Since the research of CT and PT system is not carried out for the Weitz type redox system, I focused on Weitz type molecule for a candidate of study. The 2,2'-bi-

1*H*-imidazole (H2BIM) system has Weitz type redox structure and same electronic structure to the TTF by the changes of the protonated and electronic states (Scheme 1-8). Thus, I selected H2BIM system as molecular framework of the CT and PT examination.

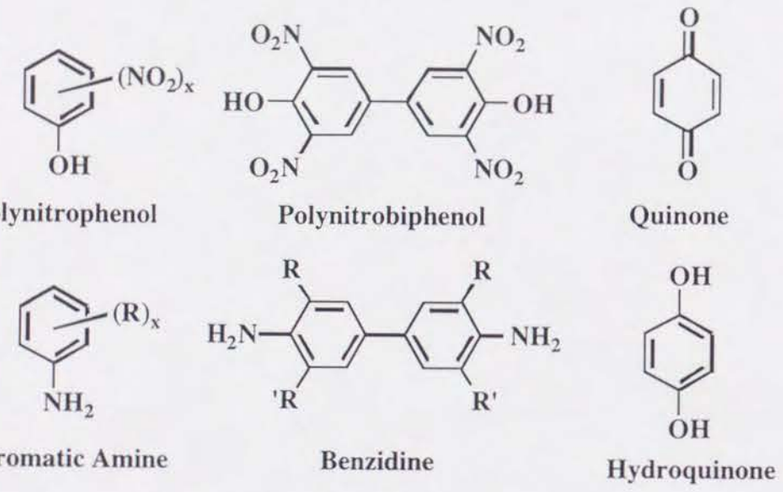

Fig. 1-7. Weitz type electron donor and acceptor molecules.

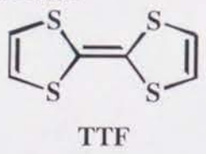

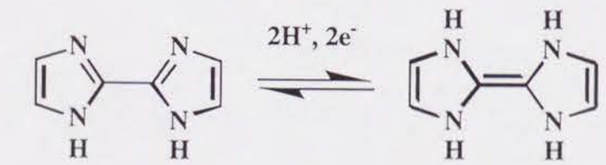

2,2'-bi-1*H*-imidazole

Scheme 1-8

The H2BIM system has complicated CT and PT character due to the existence of four nitrogens in the molecular framework. This four nitrogens can accept or donate the protons, which changes the chemical species step-by-step. Fig. 1-8 indicated the PT and CT scheme of H2BIM system, and each vertical and horizontal processes indicate the PT and CT processes, respectively. The existence of four-step CT and PT processes

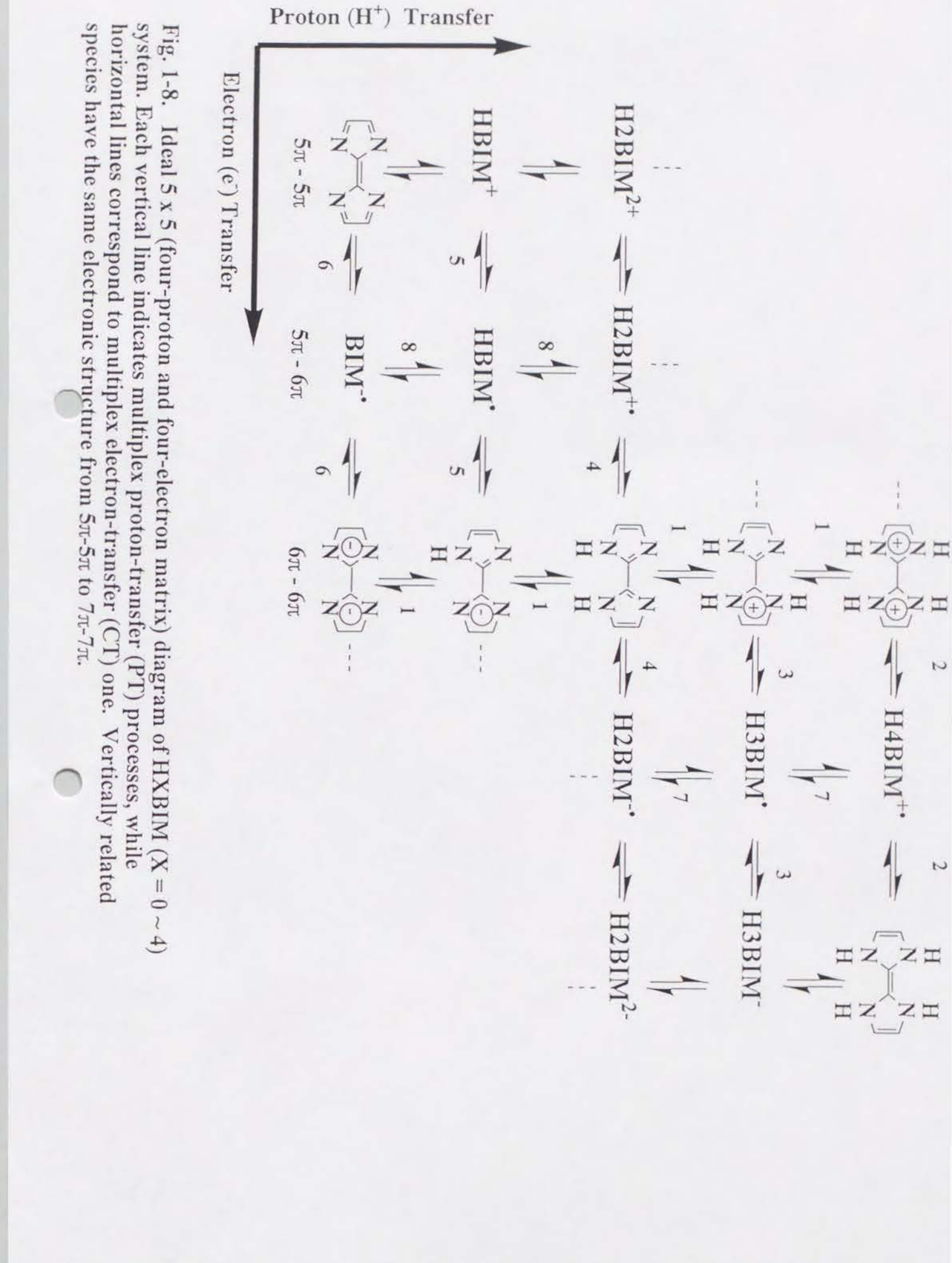

Fig. 1-8. Ideal 5 x 5 (four-proton and four-electron matrix) diagram of HXBIM (X = 0 ~ 4) system. Each vertical line indicates multiplex proton-transfer (PT) processes, while horizontal lines correspond to multiplex electron-transfer (CT) one. Vertically related species have the same electronic structure from 5π-5π to 7π-7π.

gives the twenty-five independent chemical species. I explain the CT and PT processes of H2BIM system using the routes **1** ~ **8**.

Route 1; The neutral H2BIM changes to 2-(2-1*H*-imidazolyl)-1*H*-imidazolium ($H3BIM^+$), then 2,2'-bi-imidazolium ($H4BIM^{2+}$) by the stepwise protonations. Also, 2-(2-1*H*-imidazolyl)-1*H*-imidazolide ($HBIM^-$) and 2,2'-biimidazolide (BIM^{2-}) were formed by the deprotonation processes of H2BIM. The electronic structure of these species is a close shell of 6π - 6π. Among four PT processes, only the acid dissociation constant of $H3BIM^+$ ($H3BIM^+ \rightleftarrows H2BIM^0 + H^+$) was reported ($pK_a$ =4.60).[89] **Route 2**; The one step reduction of $H4BIM^{2+}$ gives the open shell radical cation of $H4BIM^{+\bullet}$ with 6π - 7π electronic structure, and further reduction gives the neutral H4BIM with 7π - 7π electronic structure. This two step reduction processes are similar to that of TTF^{2+}. **Route 3**; The reduction of $H3BIM^+$ generates the neutral radical species: $H3BIM^{\bullet}$, and further reduction of $H3BIM^{\bullet}$ produces the anion species of $H3BIM^-$. **Route 4**; The reduction and oxidation processes of H2BIM change the chemical species to the anion radical ($H2BIM^{-\bullet}$) or cation radical ($H2BIM^{+\bullet}$), respectively. Since the H2BIM has a 6π - 6π electronic structure, the redox character of H2BIM is similar to the biphenyl. **Route 5**; The oxidation of $HBIM^-$ species provides the neutral radical of $HBIM^{\bullet}$. **Route 6**; The two-step oxidation of BIM^{2-} generates the anion radical species of $BIM^{-\bullet}$, and further oxidation of $BIM^{-\bullet}$ produces the neutral BIM with 5π - 5π electronic structure. Within 25 species, three neutral species (H2BIM, H4BIM, and BIM) and two neutral radical ($H3BIM^{\bullet}$ and $HBIM^{\bullet}$) exist in the CT and PT diagram. **Routes 7 and 8**; The PT process also changes the character of radical species. The neutral radical $H3BIM^{\bullet}$ is formed by the deprotonation of the $H4BIM^{+\bullet}$ or protonation of $H2BIM^{-\bullet}$, while $HBIM^{\bullet}$ is also obtained by the protonation of $BIM^{-\bullet}$ or deprotonation of the $H2BIM^{+\bullet}$.

The H2BIM system has been known to the ligand for the metal coordination compounds. The lone pair of nitrogen has highly coordination ability to the various kinds of metal ions such as Co, Ni, Cu, Zn, Pd, Ir, Ru, and Rh. The BIM^{2-} was used either as a ligand to the transition metals Rh, Ir, Ru, Pd, or Cu in chelate compounds,

such as $[Cu^{II}_2(BIM)(Me_5dien)_2][BPh_4]_2$,[39a] or as a counter anion in $[Ti(Cp)_2]_2[BIM]$.[39b] Some of their crystal structures have been reported.[39, 40] The preparation of the $HBIM^-$ compounds with $[Rh^{I}_4(CO)_8(HBIM)_2]$, $[Rh^{I}(CO)(PPh_3)(HBIM)]$, $[Pd^{II}_4(\eta^3\text{-}C_3H_5)_4(\mu\text{-}BIM)_2]$, and even with Fe, Co, Ni, and Cu, have been elucidated.[40, 41] Only the crystal structure of $[Cu(salenNMe_2)(HBIM^-)]_2$, $salenNMe_2$ is *N*-salycylidene-*N*,*N*'- dimethyl ethylenediamine, was reported recently.[42] The neutral $H2BIM^0$ has been known to give such compounds as $[Ni^{II}(H2BIM)_2][H_2O][NO_3^-]_2$, $[Zn^{II}_2(H2BIM)_5][ClO_4]_4[H_2O]_3$, and $[Zn^{II}(H2BIM)_2(HCO_2)][ClO_4]$, the crystal structures of which have been reported[43] besides that of pristine $H2BIM^0$.[44] However, there are no report concerning to the crystal structures of the $H3BIM^+$ and $H4BIM^{2+}$ states.

The CT complex formation between the ethylene bridged tetracyano-biimidazole ($(CH_2)_2$TCN-BIM) and TTF was reported (Scheme 1-9).[45] The crystal structure was composed of the mixed stack of $(CH_2)_2$TCN-BIM and TTF.

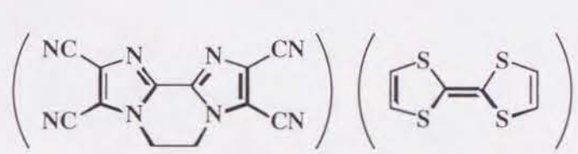

$(CH_2)_2$TCN-BIM **TTF**

Scheme 1-9

Since the $(CH_2)_2$TCN-BIM was a weak electron acceptor by the reason of the low reduction potential (-1.84 V in CH_3CN vs Ag/AgCl), the CT complex ($(CH_2)_2$TCN-BIM)(TTF) was classified as the neutral complex. On the other hands, the crystal structures of anion radical salts of Ir complexes with tetracyano-bi-1*H*-imidazole (TCN-BIM) molecule were reported for $[NEt_4^+]_5[Ir(CO)_2TCN\text{-}BIM]_6[ClO_4^-]$ and $[NEt_4^+]_5[Ir(CO)_2TCN\text{-}BIM]_6[BF_4^-]$, which showed the conductivities at room temperature (σ_{RT}) of 2 x 10^{-4} and 7 x 10^{-4} Scm^{-1}.[45]

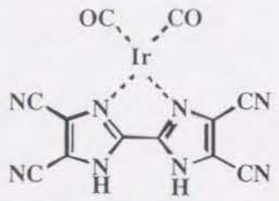

Ir(CO)$_2$TCN-BIM

The most conducting salt in this series was the [NPrEt$_2$Me]$_5$[Ir(CO)$_2$TCN-BIM]$_6$[HSO_4^-] with σ_{RT} of 2 x 10^{-2} Scm^{-1}. The crystal structures of [NEt_4^+][Ir(CO)$_2$TCN-BIM]$_2$ and mixed metal complex [NEt_3Me^+][Ir(CO)$_2$TCN-BIM]$_2$[Pt(CN)$_2$TCN-BIM] were also reported, and the σ_{RT} of these were 10^{-4} Scm^{-1} in both cases. The crystal structures were composed of the non-uniform segregated stacking of Ir(CO)$_2$TCN-BIM molecules, and the one - dimensional stacking structure was formed by the strong metal-metal interaction.

Since the neutral BIM molecule has a 5π - 5π electronic structure , this species is an electron acceptor molecule. The neutral 4,4',5,5'-tetrachloro-BIM (Cl$_4$-BIM), 4,4',5,5'-tetrabromo-BIM (Br$_4$-BIM), and dibenzo-BIM (BBIM) have been already prepared.[46] The reduction potentials of Cl$_4$-BIM, Br$_4$-BIM, and BBIM were 0.30, 0.38, and -0.65 V (vs. Ag/AgCl in dichloromethane), respectively. The electron accepting abilities of Cl$_4$-BIM and Br$_4$-BIM molecules are higher than that of TCNQ, but the CT complex formations have not been examined until now.

1-4 Scope of this Thesis

For the H2BIM system, there are no systematic researches concerning to the CT and PT nature. To construct a new CT and PT system based on the H2BIM system, it is need to evaluate the CT and PT abilities of individual species in solution. If the CT complex formation is carried out in solution, both of the redox potentials (E_{redox}) and acid dissociation constants (pK_a) of each component molecules decide the types of the obtained complex.

In Chapter 2, I examined the E_{redox} and pK_a of H2BIM derivatives in addition to the tetracyano-, tetrachlaoro-, tetrabromo-, tetramethyl-H2BIM, and related systems. Both of the E_{redox} and pK_a values of H2BIM system are compared with another redox or acid dissociation system, and I try to deduce the structural parameter, which relates to the on-site Coulomb repulsion energies (U) of CT and PT. Since the H2BIM system is the first example of Weitz type redox system, I focus on the difference of PT and CT characters from a viewpoint of U between the Weitz and Würster molecular framework.

In Chapter 3, I discuss the CT complex formations between the $H3BIM^+$ or $H4BIM^{2+}$ and some kinds of TCNQ derivatives. Since the TCNQ has both of electron and proton accepting abilities, the PT and CT characters of TCNQ system are examined to explain the results of CT complex formation. The types of obtained complex (complete ionic CT, mixed CT, and neutral CT) can explain from the differences of pK_a and E_{redox} of the initial $H3BIM^+$, $H4BIM^{2+}$, and $TCNQs^{-\bullet}$ molecules. The evaluation of PT state using the spectroscopic method is useful to distinguish the protonated species in the CT complex. The mechanism of CT complex formation can be discussed from the spectroscopic analysis of CT complex and both of the E_{redox} and pK_a of initial components ($H3BIM^+$, $H4BIM^{2+}$, and $TCNQ^{-\bullet}$ molecules). Since the structural characters of the H2BIM, $H3BIM^+$, and $H4BIM^{2+}$ molecules are also important for the CT complex formation, the crystal structures of close shell cations and TCNQ complex are shown from a viewpoint of hydrogen bond.

The complex formation of 2,2'-bi-1*H*-benzoimidazole (H2BBIM) systems with TCNQ is discussed in Chapter 4. The effect of expansion of π-electron system to the parent H2BIM molecule is examined from the viewpoints of pK_a, E_{redox}, and crystal structures (H2BBIM and 2,2'-bi-1*H*-benzoimidazolium ($H4BBIM^{2+}$)). To obtain the TCNQ complex, the new method of crystal preparation was carried out in the acetonitrile - buffer solution. The obtained TCNQ salt showed the high electrical conductivity at room temperature, thus the crystal structure, temperature and pressure dependences of conductivity, magnetic and optical properties were examined to clarify the CT and PT

states in the TCNQ complex. Finally, I summarize the CT and PT nature of the 2,2-bi-1*H*-imidazole system in Chapter 5.

1-5 References

1) There are many reviews of organic conductor; a) J. B. Torrance, *Acc. Chem. Res*, **12**, 79 (1979); b) D. Jérome and H. J. Schultz, *Adv. Phys.*, **31**, 299 (1982); c) F. Wudl, *Acc. Chem. Res.*, **17**, 227 (1984); d) J. M. Williams, M. A. Beno, H. H. Wang, P. C. Leung, T.J.Emge, U.Geiser, and K.D.Carlson, *Acc. Chem. Res.*, **18**, 261 (1985); e) D.O.Cowan, *New Aspects of Organic Chemistry*, edited by Z.Yoshida, T.Shiba, and Y.Oshiro, Proc. 4th Int. Kyoto Conf., Kodansha Ltd, Tokyo (1989); f) T.Ishiguro and K.Yamaji, *Organic Superconductors*, Spring Ser. Solid State Sci., 88, Springer, Berlin (1990); g) M.R.Bryce, *Chem. Soc. Rev.*, **20**, 355 (1991); h) D.Jérome, *Science*, **252**, 1509 (1991); i) J.M.Williams, J.R.Ferraro, R.J.Thorn, K.D.Carlson, U.Geiser, H.H.Wang, A.M.Kini, and M.-H.Whangbo, *Organic Superconductor (including Fullerenes)*, Prentice Hall, New Jersey (1992); j) G.Saito, *Metal-Insulator Transition Revisited*, edited by P.P.Edwards and C.N.R.Rao, Taylor & Francis, London. UK (1995). The synthetic strategy of organic metal and superconductor is referred in 1a), 1c), 1d), 1e), k) G.Saito and J.P.Ferraris, *Bull. Chem. Soc. Jpn.*, **53**, 2141 (1980), and l) H.Yamochi, T.Komatsu, N.Matsukawa, G.Saito, H.Mori, M.Kusunoki, and K.Sakaguchi, *J. Am. Chem. Soc.*, **115**, 11319 (1993).

2) a) J.S.Miller and A.J.Epstein, *Angew. Chem. Int. Ed. Engl.*, **33**, 385 (1994); b) T.Nakamura, *Handbook of Organic Conductive Molecules and Polymers*, edited by H.S.Nalwa, John Wiely & Sons, to be published; c) M.R.Bryce and M.C.Petty, *Nature*, **374**, 771 (1995); d) M.C.Petty, *Langmuir-Blodgett films*, Cambridge University Press (1996).

3) H.Akamatsu, H.Inokuchi, and Y.Matsunaga, *Nature*, **173**, 168 (1954).

4) '*Extended Linear Chain Compounds*', edited by J.S.Miller, Prenum Press, New York (1982), and the references are cited therein.

5) a) W.A.Little, *Phys. Revs. A*, **134**, 146 (1964).

6) V.Ginzburg, *Sov. Phys. JETP* **20**, 1549 (1965).

7) a) R.C.Wheland, *J. Am. Chem. Soc.*, **98**, 3926 (1976); b) R.C.Wheland and J.L.Gillson, *J. Am. Chem.Soc.*, **98**, 3916 (1976).

8) O.H.LeBlanc, *J.Chem. Phys.*, **72**, 4307 (1965).

9) a) The first TTF derivative was prepared in 1965: H.Pninzbach, H.Berger, and A.Lüttringhaus, *Angew. Chem. Int. Ed. Engl.*, **4**, 436 (1965); b) Thesis of G.Kiesslich, Würzburg (1968); c) D.L.Coffen and P.E.Garrett, *Tetrahedron Lett*, 2043 (1969); d) F.Wudl, G.M.Smith, and E.J.Hufnagel, *J. Chem. Soc. Chem. Commun.*, 1453 (1970); e) R.Zahradnik, P.Carsky, S.Hünig, G.Kiesslich, D.Scheutzow, *Int. J. Sulfur Chem.*, C, **6**, 109 (1971).

10) a) K.Deuchert and S.Hünig, *Angew. Chem. Int. Ed. Engl.*, **17**, 875 (1978); b) S.Hünig and H.Berneth, *Top. Curr. Chem.*, **92**, 1 (1980).

11) J. Ferraris, D.O.Cowan, V.V.Walatka, and J.H.Perlstein., *J. Am. Chem. Soc.*, **95**, 948 (1973).

12) a) G.J.Ashwell, *phys. stat. sol.*, **B86**, 705 (1978); b) G.J.Ashwell, D.D.Eley, M.R.Willis, and J.Woodward, *phys. stat. sol*, **B79**, 629(1977); c) G.J.Ashwell, *phys. stat. sol.*, **B109**, 89 (1982).

13) a) D.Jérome, A.Mazand, M.Ribault, and K.Bechgaard, *J. Phys. Lett.*, **41**, L95 (1980); b) K.Bechgaard, C.S.Jacobsen, K.Mortensen, H.J.Pedersen, and T.Thorup, *Solid. State Commun.*, **33**, 119 (1980).

14) a) H.Urayama, H.Yamochi, G.Saito, K.Nozawa, T.Sugano, M.Kinoshita, S.Sato, K.Oshima, A.Kawamoto, and J.Tanaka, *Chem. Lett.*, 55 (1988). b) A.M.Kini, U.Geiser, H.H.Wang, K.D.Carlson, J.M.Williams, W.K.Kwok, K.G.Vandervoot, J.E.Thompson, D.L.Stupka, D.Jung, and M.-H.Whangbo, *Inorg. Chem.*, **29**, 2555 (1990); c) J.M.Williams, A.M.Kini, H.H.Wang, K.D.Carlson, U.Geiser, L.K.Montgomery, G.J.Pyrka, D.M.Watkins, J.K.Kommers, S.J.Boryshuk, A.V.Crouch, W.K.Kwok, J.E.Schirber, D.L.Overmyer, D.Jung, and M.-H.Whangbo, *Inorg. Chem.*, **29**, 3274 (1990); d) T.Komatsu, T.Nakamura, N.Matuskawa, H.Yamochi, G.Saito, H.Ito, T.Ishiguro, M.Kusunoki, and K.Sakaguchi, *Solid State Commun.*, **80**, 843 (1991).

15) a) R.C.Haddon, A.F.Hebard, M.J.Rosseinsky, D.W.Murphy, S.D.Duclos, K.B.Lyons, B.Miller, J.M.Rosamilia, R.M.Fleming, A.R.KOrtan, S.H.Glarum, A.V.Makhja, A.J.Muller, R.H.Eick, S.Z.Zahurak, R.Tycko, G.Dabbagh, and F.A.Thiel, *Nature*, **350**, 320 (1991); b) A.F.Hebard, M.J.Rosseinsky, R.C.Haddon, D.W.Murphy, S.H.Glarum, T.T.M.Palstra, A.P.Ramirez, and A.R.Kortan, *Nature*, **350**, 600 (1991).

16) T.T.M.Palstra, O.Zhou, Y.Iwasa, P.E.Sulewski, R.M.Fleming, and B.R.Zegarski,

17) a) E.Hertel, *Ber. Dtsch. Chem. Ges.*, **57**, 1559(1924); b) E.Hertel, *Liebigs Ann. Chem.*, **415**, 179 (1926); c) E.Hertel and J. Cleef, *Ber. Dtsch. Chem. Ges*, **61**, 1545 (1928); d) E.Hertel and K.Schneider, *Z. Physik. Chem.* **A 151**, 413 (1930); e) E.Hertel and K.Schneider, *Z. Physik. Chem.* **B 12**, 109 (1931); f) E.Hertel and K.Schneider, *Z. Physik. Chem.* **B 13**, 387 (1931); g) E.Hertel and H.Frank, *Z. Physik. Chem.* **B 27**, 460 (1934).

18) a) G.Briegleb and H.Delle, *Z. Electrochem.*, **64**, 347(1960); b) G.Briegleb and H.Delle, *Z. Phys. Chem. Neue Folg.*, **24**, 359(1960).

19) A.Z.Kofler, *Electrochem.*, **50**, 200 (1944).

20) a) G.Saito and Y.Matsunaga, *Bull. Chem., Soc. Jpn.*, **44**, 3328 (1972); b) Y.Matsunaga and G.Saito, *Bull. Chem., Soc. Jpn.*, **45**, 963 (1972); c) N.Inoue and Y.Matsunaga, *Bull. Chem., Soc. Jpn.*, **45**, 3478 (1972); d) G.Saito and Y.Matsunaga, *Bull. Chem., Soc. Jpn.*, **46**, 714 (1973); e) Y.Matsunaga, *Bull. Chem., Soc. Jpn.*, **46**, 998 (1973); f) N.Inoue and Y.Matsunaga, *Bull. Chem., Soc. Jpn.*, **46**, 3345 (1973); g) G.Saito and Y.Matsunaga, *Bull. Chem., Soc. Jpn.*, **47**, 1020 (1974); h) Y.Matsunaga, G.Saito, and N.Sakai, *Bull. Chem., Soc. Jpn.*, **48**, 2873 (1974); i) Y.Matsunaga, E.Osawa, and R.Osawa, *Bull. Chem., Soc. Jpn.*, **48**, 37 (1975).

21) J.Bernstein, H.Regev, and F.H.Herbstein, *Acta Crystallogr., Sect. B*, **36**., 1170(1980).

22) a) M.Tanaka, *Bull. Chem. Soc. Jpn.*, **50**, 3194 (1977); b) M.Tanaka, H.Matsui, J.Mizoguchi, and S.Kashino, *Bull. Chem. Soc. Jpn.*, **67**, 1572 (1994).

23) G.Saito and Y.Matsunaga, *Bull. Chem. Soc. Jpn.*, **46**, 1609 (1973); b) Y.Matsunaga and R.Osawa, *Bull. Chem. Soc. Jpn.*, **47**, 1589 (1974).

24) a) G.Saito and Y.Matsunaga, *Bull. Chem. Soc. Jpn.*, **45**, 2214(1972); b) G.Saito and T.Inukai, *J. Jpn. Association Cryst. Growth*, **16**, 2(1989).

25) a) T.Mitani, G.Saito, and H.Urayama, *Phys. Rev. Lett.*, **60**, 2299 (1988); b) K.Nakasuji, K.Sugiura, T.Kitagawa, J.Toyoda, H.Okamoto, T.Mitani, H.Yamamoto, I.Murata, A.Kawamoto, and J.Tanaka, *J. Am. Chem. Soc.*, **113**, 1862 (1991).

26) a) N.Hoshino, T.Inabe, T.Mitani, and Y.Maruyama, *Bull. Chem. Soc. Jpn.*, **61**, 4207 (1988); b) T.Inabe, N.Hoshino, T.Mitani, and Y.Maruyama, *Bull. Chem. Soc. Jpn.*, **62**, 2245 (1989); c)T.Inabe, I.Luneau, N.Hoshino, K.Okaniwa, H.Okamoto, T.Mitani, U.Ngashima, and Y.Maruyama, *Bull. Chem. Soc. Jpn.*, **64**, 801 (1991); d) T.Inabe, *New. J. Chem.*, **12**, 129 (1991); e) T.Inabe, I.Luneau, T.Mitani, Y.Maruyama, and S.Takeda, *Bull. Chem. Soc. Jpn.*, **67**, 612 (1994).

27) a) T.Mitani, H.Kitagawa, H.Okamoto, K.Nakasuji, and J.Toyoda, *Mol. Cryst. Liq. Cryst.*, **216**, 73 (1992); b)T.Ithoh, J.Toyoda, M.Tadokoro, H.Kitagawa, T.Mitani, and K.Nkasuji, *Chem. Lett.*, **41** (1995); c) H.Kitagawa, T.Mitani, T.Ithoh, J.Toyoda, and K.Nakasuji, *Synthetic Metals*, **71**, 1991 (1995).

28) F.H.Herbstein, "*In Perspectives in Structural Chemistry*" edited by J.D.Dunitz and J.A.Ibers, Vol. 4, N.Y., John Wiley.

29) a) J.B.Torrance, J.E.Vazquez, J.J.Mayerle, and V.Y.Lee, *Phys. Rev. Lett.*, **46**, 253 (1981); b) J.B.Torrance, A.Girlando, J.J.Mayerle, J.I.Crowley, V.Y.Lee, P.Batail, and S.J.LaPlaca, *Phys. Rev. Letts.*, **47**, 1747 (1981); c) P.Batail, S.J.Laplaca, J.J.Mayerle, and J.B.Torrance, *J. Am. Chem. Soc.*, **103**, 951 (1981); d) Y.Tokura, T.Koda, T.Mitani, and G.Saito, *Solid State Commun.*, **43**, 757 (1982); e) T.Mitani, G.Saito, Y.Tokura, and K.Kouda, *Phys. Rev. Lett.*, **53**, 842 (1984); f) R.M.Metzger and J.B.Torrance, *J. Am. Chem. Soc.*, **107**, 117 (1985); g) K.Takaoka, Y.Kaneko, H.Okamoto, Y.Tokura, T.Koda, T.Mitani, and G.Saito, *Phys. Rev., B*, **36**, 3884 (1987).

30) P.Pfeiffer, "*Organische Molekülverbindungen*", Aufl., 2, Verlag von F.Enke, Stuttgart, 341-346 (1927).

31) a) E.A.Braude and R.P.Linstead, *J. Chem. Soc.*, 3544 (1954); b) E.A.Braude L.M.Jackman, and R.P.Linstead, *J. Chem. Soc.*, 3548 (1954); c) E.A.Braude

L.M.Jackman, and R.P.Linstead, *J. Chem. Soc.*, 3564 (1954); d) E.A.Braude A.G.Brook, and R.P.Linstead, *J. Chem. Soc.*, 3569 (1954); e) E.A.Braude A.G.Brook, and R.P.Linstead, *J. Chem. Soc.*, 3574 (1954); f) E.A.Braude, R.P.Linstead, and P.W.D.Mitchell, *J. Chem. Soc.*, 3578 (1954); g) E.A.Braude, R.P.Linstead, and K.R.H.Wooldridge, *J. Chem. Soc.*, 3586 (1954); h) E.A.Braude, R.P.Linstead, P.W.D.Mitchell, and K.R.H.Wooldridge, *J. Chem. Soc.*, 3595 (1954).

32) a) G.Saito and A.K.Colter, *Tetrahedron Lett.*, 3325 (1977); b) A.K.Colter, P.Plank, J.P.Bergsam, R.Lahti, A.A.Quesnel, and A.G.Parsons, *Can. J. Chem.*, **62**, 1780 (1984); c) L.R.Melby, R.J.Harder, W.R.Hertler, W.Mahler, R.E.benson, and W.E.Mochel, *J. Am. Chem. Soc.*, **84**, 3374 (1962).

33) a) S.I.Bailey, I.M.Ritchie, and F.R.Hewgill, *J. Chem. Soc. Perkin Trans II.*, 645 (1983); b) J.Q.Chambers, "*The Chemistry of the Quinonoid Compounds*", Vol.2; edited by S.Patai, John Wiley & Sons, New York, 719-757 (1988).

34) T.Sakurai, *Acta Crystallogr., Sect. B*, **24**, 403 (1968).

35) a) G.Tollin, "*Molecular Associations in Biology*", edited by B.Pullman, Academic Press. New York, 393(1968); b) V.C.Flores, H.Keyzer. G.Varkey-Johnson, K.L.Young, "*Organic Conductors fundamentals and applications*", edited by J.-P.Farges, Marcel Dekker. New York, 691-734 (1994).

36) a) G.L.Gartland, G.R.Freeman, and C.E.Bugg, *Acta Crystallogr., Sect. B*, **30**, 1841 (1974); b) U.Thewalt and C.E.Bugg, *Acta Crystallogr., Sect. B*, **28**, 82 (1972).

37) a) A.G.MacDiarmid, and A.J.Epstein, *Lower-Dimenssional System and Molecular Electronics.*, 303 (1991).

38) F.Holmes, K.M.Jones, and E.G.Torrible, *J. Chem. Soc.*, 4790 (1961).

39) a) M.S.Haddad, E.N.Duesler, and D.N.Hendrickson, *Inorg. Chem.*, **18**, 141 (1979); b) B.F.Fiselmann, D.N.Hendrickson, and G.D.Stucky, *Inorg. Chem.*, **17**, 2078 (1978).

40) a) S.W.Kaiser, R.B.Saillant, W.H.Butler, and P.G.Rasmussen, *Inorg. Chem.*, **15**, 2681 (1976); b) S.W.Kaiser, R.B.Saillant, W.H.Butler, and P.G.Rasmussen, *Inorg. Chem.*, **15**, 2688 (1976).

41) R.Uson, J.Gimeno, L.A.Oro, J.M.M.Llarduya, J.A.Cabeza, A.Tiripicchio, and T.Camellini, *J. Chem. Soc., Dalton Trans.*, 1729 (1983).

42) M.Tadokoro, J.Toyoda, K.Isobe, T.Itoh, A.Miyazaki, T.Enoki, and K.Nakasuji, *Chem. Lett*, 613 (1995).

43) a) A.D.Mighell, C.W.Reimann, and F.A.Mauer, *Acta Crystallogr., Sect. B*, **25**, 60 (1969); b) C.Kirchner and B.Krebs, *Inorg. Chem.*, **26**, 3569 (1987).

44) D.T.Cromer, R.R.Ryan, and C.B.Storm, *Acta Crystallogr., Sect. C*, **43**, 1435 (1987).

45) M.Tamres, O.H.Bailey, J.E.Anderson, and P.G.Rasumussen, *Spectrochemica Acta*, **42A**, 741 (1986); b) P.G.Rasmussen, J.B.Kolowich, and J.C.Bayon, *J. Am. Chem. Soc.*, **110**, 7042 (1988); c) P.G.Rasmussen, J.E.Anderson, O.H.Bailey, and M.Tamres, *J. Am. Chem. Soc.*, **107**, 279 (1985); d) P.G.Rasmussen, O.C.Bayon, and J.C.Bayon, *Inorg. Chem.*, **23**, 338 (1984); e)P.G.Rasmussen, R.L.Hough, J.E.Anderson, O.H.Baiey, and J.C.Bayon, *J. Am. Chem. Soc.*, **104**, 6155 (1982).

46) a) J.H.M.Hill, *J. Org. Chem.*, **28**, 1931 (1963); b) S.G.Dedik, V.D.Orlov, A.S.Edzhinya, V.Y.Khodorkovskii, and O.Y.Neiland, *Khim. Geterotsikl. Soedin.*, **25**, 1421 (1989).

Chapter 2. Acid Dissociation Constants and Redox Properties of 2,2'-bi-1H-imidazole System in Solution.

Seven new states among the speculated 25 independent of 2,2'-1*H*-biimidazole (H2BIM) system were identified based on the study of their redox and acid dissociation properties. Isoelectronic substitution of four sulfur atoms of the dication state of tetrathiafulvalene (TTF^{2+}) by four imino groups was found to increase the stability of the dication state 2,2'-bi-1*H*-imidazolium ($H4BIM^{2+}$) with aromatic 6π - 6π character. The high PT character of $H3BIM^{+}$ (2-(2-1*H*-imidazolyl)-1*H*-imidazolium) and $H4BIM^{2+}$ compared with that of the corresponding hydroquinone system was clearly observed. The on-site Coulomb repulsion energy for electron-transfer (U_1^{CT}) was evaluated for various π-electron acceptor and donor systems. It was found that the U_1^{CT} values decrease linearly with increasing the length of a molecule, which can divide the molecular systems into two classifications, i.e. electron acceptors and dications. The on-site Coulomb repulsion energy for two step proton transfer processes (U_1^{PT}) was newly defined and evaluated for the H2BIM, $H4BIM^{2+}$, hydroquinone (H2Q), and bis(4-hydroxyphenyl) disulfide (HPDS) systems. The U_1^{PT} values become constant above a certain molecular length (r_c). Below r_c the U_1^{PT} values increase linearly with decreasing the distance r regardless of Würster and Weitz structures, approximately. The H2BIM ($H4BIM^{2+}$) system has large U_1^{PT} values in comparison with the H2Q and HPDS systems.

2-1 Introduction

The types of redox processes are classified into two typical cases: Weitz and Würster types, depending on whether the end groups of the redox system are ring members or external groups of a cyclic π-system, respectively.[1] According to this classification, the TTF and H4BIM systems have the redox character of the Weitz type and the p-benzoquinone (BQ), 7,7,8,8-tetracyanoquinodimethane (TCNQ) and p-

phenylenediamine (PPD) systems have that of the Würster one. The simultaneous CT and PT systems examined until now have been based on the BQs and diamines frameworks having Würster type redox natures (see section 1-2). The H2BIM is the first example having the Weitz type CT and PT character. Before the studies of the CT and PT complexes in the solid state, I first evaluate the most essential characters in such study; i.e. the CT and PT character of individual component, from the measurements of acid-base dissociation constants (pK_a) and redox potentials (E) in solution. I examine the redox character, especially the on-site Coulomb repulsion energy U_1^{CT}, which represents the repulsion energy between two electrons on the same site in the CT process and is an essential parameter, in the transport phenomena in the solid state, of these two types of molecular framework. I tried to find the differences of redox behavior between the Weitz (TTFs and H4BIM etc.) and Würster (BQ, p-diphenoquinone (DPQ), TCNQ, PPD, benzidine (Bz) systems, etc.) types with the magnitude of U_1^{CT} (Scheme 2-1)

$$M^0 \xrightarrow{e^-} M^{-\bullet} \xrightarrow{e^-} M^{2-}$$

$$U_1^{CT} = E(M^{2-}) + E(M^0) - 2E(M^{-\bullet})$$

Scheme 2-1

$$M^0 \xrightarrow{H^+} HM^+ \xrightarrow{H^+} H2M^{2+}$$

$$U_1^{PT} = E(H2M^{2+}) + E(M^0) - 2E(HM^+)$$

Scheme 2-2

where $E(M^{2-})$ represents the total energy of the M^{2-} molecule. Similarly, in the two-step PT processes (Scheme 2-2), I define the on-site Coulomb repulsion energy of the PT process, U_1^{PT}, which represents the repulsive energy between two charges on the same molecule in the PT process. The U_1^{PT} values are compared among the various types of molecular structures, Weitz ($H4BIM^{2+}$) and Würster (H2Q, bis(4-hydroxyphenyl) disulfide (HPDS) systems, etc.). I discuss the relationship between the U_1^{PT} values and the structural properties.

2-2 Experimental

Materials All solvents were distilled before use. TCNQ, 1*H*-imidazole, 2-methy-1*H*-limidazole, 4-nitro-1*H*-imidazole, 4,5-dichloro-1*H*-imidazole, 4,5-dicyano-1*H*-imidazole, H2Q, 2,3-dicyanohydroquinone (CN_2-H2Q), tetracyanoethylene (TCNE), BQ, 2,3-dichloro-5,6-dicyano-p-benzoquinone (DDQ), p-chloranil (Cl_4-BQ), 2,3,5,6-tetrafluoro-p-benzoquinone (F_4-BQ), 2,5-dimethyl-p-benzoquinone (Me_2-BQ), duroquinone (Me_4-BQ), 2,5-dichloro-p-benzoquinone (Cl_2-BQ), 1,4-naphthoquinone, Bz, 3,3'-dimethylbenzidine (o-tolidine), 3,3'-dimethoxybenzidine (o-dianisidine), 3,3'5,5'-tetramethylbenzidine (Me_4-Bz), *N,N,N',N'*-tetramethylbenzidine (N-TMB), PPD, and diaminodurene (DAD) were commercially obtained, and were purified by recrystallization and/or vacuum sublimation. 2,3,5,6-Tetrafluoro-7,7,8,8-tetracyanoquinodimethane (F_4-TCNQ),[2a] 2-fluoro-7,7,8,8-tetracyanoquinodimethane (F-TCNQ),[2b] 2,5-dimethyl-7,7,8,8-tetracyanoquinodimethane (Me_2-TCNQ),[2c] 2,5-diethyl-7,7,8,8-tetracyanoquinodimethane (Et_2-TCNQ),[2c] 2,5-dimethoxy-7,7,8,8-tetracyanoquinodimethane (MeO_2-TCNQ),[2c] 4,8-bis(dicyanomethylidene)-4,8-dihydrobenzo[1,2-c:4,5-c']bis[1,2,5]thiadiazole (BTDA-TCNQ),[2d] 2,5-dichlorohydroquinone (Cl_2-H2Q),[3a] 2,3,5,6-tetrachlorohydroquinone (Cl_4-H2Q),[3a] 2,3-dichloro-5,6-dicyanohydroquinone (H2DDQ),[3b] 2,3-dicyano-p-benzoquinone (CN_2-BQ),[3c] 2,3,5,6-tetrabromo-p-benzoquinone (Br_4-BQ),[20d] DPQ,[20e] 3,3',5,5'-tetramethyl-p-diphenoquinone (Me_4-DPQ),[3f] 3,3',5,5'-tetrachloro-p-diphenoquinone (Cl_4-DPQ),[3g] 3,3',5,5'-tetrabromo-p-diphenoquinone (Br_4-DPQ),[3g] TTF,[4a] (dimethyl)tetrathiafulvalene (DM-TTF),[4a] (tetramethyl)tetrathiafulvalene (TM-TTF),[4a] 2,3:6,7-bis(tetramethylene)tetrathiafulvalene (OM-TTF),[4a] 2,3:6,7-bis(trimethylene) tetrathiafulvalene (HM-TTF),[4a] 2,3:6,7-bis(ethylenedithio)tetrathiafulvalene (BEDT-TTF),[4d] 2,3:6,7-bis(ethylenedioxy)tetrathiafulvalene (BEDO-TTF),[4e] 2,3-(ethylenedithio)tetrathiafulvalene (EDT-TTF),[4f] tetrakis(methylthio)tetrathiafulvalene (TTC_1-TTF),[4d] 6,7-ethylenedithio-2,3-bis(methoxycarbonyl) tetrathiafulvalene ($(CO_2Me)_2$-EDT-TTF),[4g] 1,6-diaminopyrene (DAP),[5] 1,6-dithiapyrene (DTPY),[6]

and 5,6:11,12-bis(epidithio)naphthacene (TTT)[7] were prepared by the literature methods, and were purified by recrystallization and/or vacuum sublimation. All of 1,4-benzenedimalononitrile derivatives (F4-H2TCNQ, H2TCNQ, and Me2-H2TCNQ) were prepared by similar methods from the literature,[8] and were purified by recrystallization from MeOH - H_2O (6:4).

2,2'-Bi-1*H*-imidazole (H2BIM). The preparation of 2,2'-bi-1*H*-imidazole was done by the method of B. F. Fieselmann et al.[9] Anhydrous ammonia gas was slowly bubbled into 500 ml of a 20% solution of glyoxal at such a rate that the temperature was maintained about 50°C. After 10 h, the solution was filtered and washed with water, then acetone, to give 41.0 g of crude brown product with a yield of 35%. This was recrystallized from boiling ethylene glycol twice with charcoal. The cold filtrate was deposited as colorless needles, which were collected, washed with water, then acetone, and dried in a vacuum. Mp > 350°C. Found: C,53.78; H,4.40; N,41.90%. Calcd for $C_6H_6N_4$: C,53.72; H,4.51; N,41.77%. IR spectrum (KBr pellet; cm^{-1}) is in good agreement with the literature[9]: IR spectrum: 3333-2000(w,br); 3142, 3073, 3001, 2895, 2803, 2747, 2634; 1670(w,br); 1545(s); 1436(m); 1404(s); 1338(m); 1217(m); 1104(s); 939(s); 918(w); 887(s); 763(m); 748(s); 739(sh); 690(s).

4,4',5,5'-Tetramethyl-2,2'-bi-1*H*-imidazole (H2TMeBIM),[10a] 4,4',5,5'-tetrachloro- 2,2'-bi-1*H*-imidazole (H2TClBIM),[10b] 4,4',5,5'-tetrabromo-2,2'-bi-1*H*-imidazole (H2TBrBIM),[10b] and 4,4',5,5'-tetracyano-2,2'-bi-1*H*-imidazole (H2TCNBIM)[10c] were prepared by methods from the literatures, and were purified by recrystallization from 1,4-dioxane.

2-(2-1*H*-Imidazolyl)-1*H*-imidazolium iodide [H3BIM$^+$][I$^-$]. A mixture of 1 g (7.46 mmol) of H2BIM and 1.1 molar amount of aqueous hydroiodic acid (55%) in 30 ml of ethanol was stirred at room temperature for 30 min and left at -10°C overnight. The reaction mixture was filtered to provide 1.5 g (52%) of a white solid, which was washed with acetonitrile, then ether, and recrystallized from ethanol-water. Mp > 180°C (sublimation). Found: C,27.56; H,2.55; N,21.63; I,48.65%. Calcd for $C_6H_7N_4I$: C,27.51; H,2.67; N,21.39; I,48.44%. IR spectrum: 3322-2000(br); 3118, 3028, 2938,

2795; 1648(s); 1560(s); 1499(w); 1449(s); 1422(m); 1400(m); 1316(s); 1216(m); 1153(w); 1115(s); 1093(s); 927(s); 912(m); 871(m); 781(s); 754(s); 670(s); 474(s).

2-(2-1*H*-Imidazolyl)-1*H*-imidazolium tetrafluoroborate [H3BIM$^+$][BF_4^-]. Via the procedure described above for [H3BIM$^+$][I$^-$], 1 g (7.46 mmol) of H2BIM was treated with 1.1 molar amount of aqueous tetrafluoroboric acid solution in ethanol to provide 0.84 g (51%) of [H3BIM$^+$][BF_4^-], which was recrystallized from acetonitrile. Mp 210°C, as a white powder. Found: C,32.38; H,3.00; N,25.25%. Calcd for $C_6H_7N_4BF_4$: C,32.48; H,3.15; N,25.25%. IR spectrum: 3700-2200(br): 3349, 3227, 3168, 3035, 2940, 2805,2630; 1968(br); 1649(s); 1557(s); 1508(w); 1458(m); 1423(w); 1300(w); 1218(m); 1127(s); 1065(s); 932(m); 912(m); 877(m); 770(s); 733(m); 710(s); 686(s); 521(m).

2,2'-Bi-1*H*-imidazolium dichloride [H4BIM^{2+}][Cl$^-$]$_2$. A mixture of 1 g (7.46 mmol) of H2BIM and 3 molar amounts of hydrochloric acid solution in 200 ml of ethanol was refluxed for 3 h. After cooling, filtration provided 1.4 g (91%) of a white solid, which was washed well with water and recrystallized from ethanol-hydrochloric acid solution. Mp 320°C, as a white powder. Found: C,34.78;, H,3.67; N,27.30; Cl,34.02%. Calcd for $C_6H_8N_4Cl_2$: C,34.80; H,3.90; N,27.30; Cl,34.24%. IR spectrum: 3200-2000(br): 3127, 3103, 3029, 2923, 2771, 2714, 2649, 2539; 1686(s); 1586(s); 1436(s); 1334(m); 1218(m); 1124(s); 894(s); 794(s); 666(s).

2,2'-Bi-1*H*-imidazolium dibromide [H4BIM^{2+}][Br$^-$]$_2$. Via the procedure described above for [H4BIM^{2+}][Cl$^-$]$_2$, the treatment of aqueous hydrobromic acid provided [H4BIM^{2+}][Br$^-$]$_2$ with a yield of 83%, which was recrystallized from ethanol-hydrobromic acid solution. Mp 290°C, as a white powder. Found: C,24.35; H,2.80; N,18.87%. Calcd for $C_6H_8N_4Br_2$: C,24.36; H,2.70; N,18.94%. IR spectrum: 3200-2000(br): 3130, 3021, 2922, 2780, 2665; 1654(w); 1581(s); 1430(m); 1326(m); 1214(m); 1124(s); 1103(m); 920(w); 853(s); 788(s); 662(m).

2,2'-Bi-1*H*-imidazolium diiodide [H4BIM^{2+}][I$^-$]$_2$. Via the same procedure described above for [H4BIM^{2+}][Cl$^-$]$_2$, the treatment of aqueous hydroiodic acid solution provided [H4BIM^{2+}][I$^-$]$_2$ with a yield of 52%. Mp 280°C, as white needles. Found:

C,18.49; H,2.07; N,14.44%. Calcd for $C_6H_8I_2$: C,18.48; H,2.05; N,14.44%. IR spectrum: 3200-2000(br): 3126, 3020, 2922, 2778, 2680; 1579(s); 1430(w); 1319(m); 1206(m); 1098(s); 848(m); 821(m); 784(s); 654(m).

2,2'-Bi-1*H*-imidazolium bis(tetrafluoroborate) [H4BIM^{2+}]$_2$ [BF$_4^-$]$_4$[H$_2$O]$_3$. Via the procedure described above for [H4BIM^{2+}][Cl$^-$]$_2$. The treatment of aqueous tetrafluoroboric acid solution provided [H4BIM^{2+}]$_2$[BF$_4^-$]$_4$ [H$_2$O]$_3$ with a yield of 61%, which was washed with cold water, then ether. Mp 270°C, as a white powder. Found: C,21.15; H,3.52; N,16.74%. Calcd for $C_{12}H_{22}N_8O_3B_4F_{16}$: C,21.40; H,3.27; N,16.64%. IR spectrum: 3334(br); 3200-2450(br): 3130, 3023, 2923, 2787, 2658; 1584(br); 1432(s); 1328(s); 1084(br); 854(w); 787(m); 745(m); 522(s).

Measurements The infrared absorption spectra were taken on a Perkin-Elmer 1600 Series FT-IR spectrometer with a KBr pellet. Melting points were taken on a Yanaco MP-500D apparatus and are uncorrected.

pH Measurements. The instrument used for pH measurements was a Toa HM-5ES glass electrode. The pH meter was corrected using tetraborate (pH = 9.18 at 25°C), phosphate (pH = 6.86 at 25°C), and phthalate (pH = 4.01 at 25°C) pH standard solutions (Nacalai). The subsequent titrations were done by the addition of standard sodium hydroxide solution (0.1 M, Nacalai). All titrations were run at 22 ± 1°C, and the ion strengths fixed to a constant value (0.1 M) using sodium tetrafluoroborate. The low solubility of the 2,2'-bi-1*H*-imidazole derivatives in water necessitated the use of the 70% by volume dimethylformamide (DMF) - water solvent medium.

Cyclic Voltammetry Measurements. Redox potentials were measured on a Yanako Polarographic Analyzer P-1100 under argon. All measurements were done under the following conditions: solvent, DMF; supporting electrolyte, 0.1 M of tetrabutylammonium tetrafluoroborate (TBA-BF4); scan rate, 100 mVs^{-1}; reference electrode, Ag/AgCl; working and counter electrodes, Pt; temperature, 22 ± 1°C. The Ag/AgCl electrode was checked at the initial and the final points using reference compounds (TCNQ and ferrocene).

Molecular Orbital Calculations. Orbital eigenvalues and characters were calculated by the extended Hückel method (EHMO)[11] to examine the difference for TTF^{2+} and H4BIM^{2+}. A Pariser-Parr-Pople (PPP) self-consistent field (SCF) MO calculation[12] was also used to obtain the electron affinity (E_a), ionization potential (I_p) and π-electron density in Sections 2-3-1-4, 2-3-1-5, and 2-3-2-6. For the EHMO calculations, standard parameters were used for H, C, N, and S atoms.[11] For PPP calculations, atomic basis functions were used for all elements.[12] Bond lengths and angles were taken from the crystal structures of TTF[13] and H4BIM^{2+}.[14]

2-3 Results and Discussion

I examined the various molecular systems to clarify the PT and CT natures. Here, the representative molecular structures in Chapter 2 are summarized in Fig. 2-1. The neutral electron acceptors, BQ, DPQ, and TCNQ systems of the Würster type, are shown in Fig. 2-1a, and PPD, Bz, DAP, and 5,10-dimethyl-5,10-dihydrophenazine (Me$_2$PHz) also have a Würster type redox character (Fig. 2-1b). On the contrary, TTF, DTPY, and TTT, belonging to the Weitz type electron donors, are shown in Fig. 2-1c. These molecules are mainly discussed from the point of the CT properties. In the section on the PT properties, I did comparisons with the H2Q, H2TCNQ, and HPDS systems as shown in Fig. 2-1d.

a.

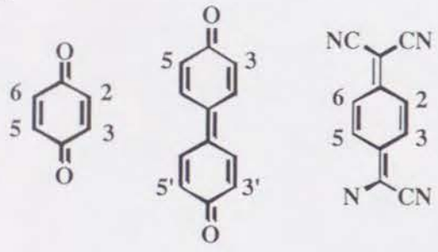

BQ DPQ TCNQ

b.

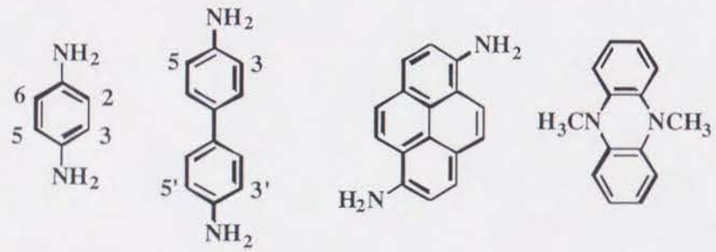

PPD Bz DAP Me_2PHz

c.

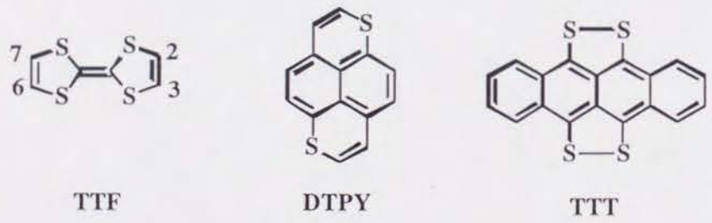

TTF DTPY TTT

d.

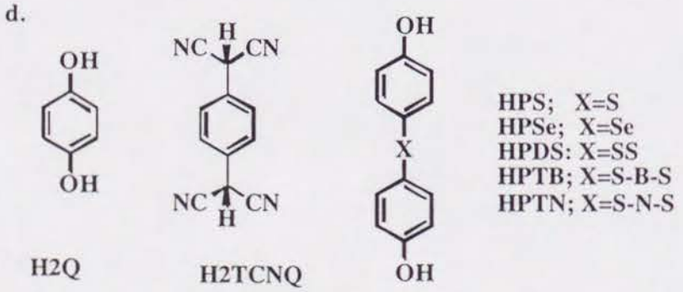

H2Q H2TCNQ

HPS; X=S
HPSe; X=Se
HPDS: X=SS
HPTB; X=S-B-S
HPTN; X=S-N-S

Fig. 2-1. The representative molecular structures appeared in this text. a) BQ, DPQ and TCNQ systems. b) PPD, Bz, DAP, and Me_2PHz systems. c) DTPY and TTT systems. d) H2Q, H2TCNQ and HPDS systems. In HPDS series, the bridging unit (X) is represented as S (HPS), Se (HPSe), SS (HPDS), 1,4-phenylenedithio (HPTB) and 1,5-naphthylenedithio (HPTN).

2-3-1. Electron-Transfer Properties in Solution.

The results of cyclic voltammetry studies of $H2BIM^0$, $H3BIM^+$, and $H4BIM^{2+}$, all of which have a 6π - 6π electronic structure (Scheme 2-3), are compared with those of related compounds in Table 2-1. All redox processes of biimidazole species are quasi- or irreversible ones even in a nonaqueous solvent (DMF).

6π-6π	E^r_{p1}	6π-7π	E^r_{p2}	7π-7π
$H4BIM^{2+}$	→	$H4BIM^{+\bullet}$	→	$H4BIM^0$
$H3BIM^+$	→	$H3BIM^\bullet$	→	$H3BIM^-$
$H2BIM^0$	→	$H2BIM^{-\bullet}$	→	$H2BIM^{2-}$
(TTF^{2+}	→	$TTF^{+\bullet}$	→	TTF^0)

Scheme 2-3

Table 2-1. Reduction (E^r_p) and oxidation (E^o_p) peak potentials of $H4BIM^{2+}$, $H3BIM^+$, $H2BIM^0$, and related compounds.[a]

E^o_{p1} V	Compounds	E^r_{p1} V	E^r_{p2} V
—	$H3BIM^+$	-0.84 [c]	—
—	*N*-$MeQn^+$ [d]	-0.94 [c]	—
—	*N*-$MeAc^+$ [e]	-0.44 [c]	—
—	HAc^+ [f]	-0.59 [c]	—
—	Me_4-BQ^0	-0.88	-1.70
1.22 [c]	$H2BIM^0$	-1.69 [c]	—
—	$Acridine^0$	-1.73 [b]	—
—	$Naphthacene^0$	-1.62	—
1.20 [c]	$H2Q^0$	—	—
1.42 [b]	$Anthracene^0$	—	—

a) Measured at a scan rate of 100 mV s^{-1} using Pt vs. Ag/AgCl in 0.1 M TBA-BF_4 / DMF. b) Quasi-irreversible process. c) Irreversible process. d) *N*-Methylquinolinium. e) *N*-Methylacridinium. f) Acridinium.

2-3-1-1 Dication state; $H4BIM^{2+}$

$H4BIM^{2+}$ shows two quasi-reversible reduction peaks at E^r_{p1} = -0.54 and E^r_{p2} = -0.77 V. These reduction peaks appear on the slightly negative side compared with

those of a weak electron acceptor; 2,4,7-trinitro-9H-fluoren-9-one (TNF^0): E^r_{p1} = -0.42 and E^r_{p2} = -0.69 V for $TNF^0 \rightarrow TNF^{-\bullet}$ and $TNF^{-\bullet} \rightarrow TNF^{2-}$ processes, respectively. And the E^r_{p1} value of $H4BIM^{2+}$ is the same as that of 2,5-dihydroxy-p-benzoquinone (DHQ^0): E^r_{p1} = -0.54 V for $DHQ^0 \rightarrow DHQ^{-\bullet}$ process. Therefore, the electron-accepting ability of $H4BIM^{2+}$ is very weak, approximately identical to that of DHQ^0, and is somewhat weaker than TNF^0. Under the same conditions, TTF^{2+} shows one-electron reduction processes at E^r_{p1} = +0.65 and E^r_{p2} = +0.41 V. This indicates that, despite their isoelectronic structures of TTF^0 and $H4BIM^0$, the dicationic species $H4BIM^{2+}$ and monocationic species $H4BIM^{+\bullet}$ gaine larger stability by 1.19 and 1.18 V than TTF^{2+} and $TTF^{+\bullet}$, respectively. This is the consequence of the replacement of four sulfur atoms of TTF^{2+} by four imino groups (sp^3-type) of $H4BIM^{2+}$, which is consistent with the observation that the isoelectronic substitutions of methylimino groups for sulfur atoms are considerably effective in increasing the electron-donating properties of neutral structures.[15] This is the most pronounced character of $H4BIM^{2+}$ species and the extremely strong electron-donating ability of $H4BIM^0$ is the reason why I was not able to isolate $H4BIM^0$ species in the solid state.

2-3-1-2 Monocation state; H3BIM$^+$

The reduction peak potential (E^r_{p1}) of $H3BIM^+$ is compared with typical nitrogen- containing monocations, which were frequently used in the study of highly conductive TCNQ anion radical salts, to evaluate the stability of the monocation state (Table 2-1). The first reduction of these monocations produces the neutral radicals, while the second reductive waves, which were not observed for all compounds examined, correspond to the generation of anion species. $H3BIM^+$ shows a reduction peak at -0.84 V, which is higher than that of *N*-methylquinolinium (*N*-$MeQn^+$; E^r_{p1} = -0.94 V) and lower than that of *N*-methylacridinium (*N*-$MeAc^+$; E^r_{p1} = -0.44 V). Thus the electron-accepting abilities of these monocations decrease in the following order: *N*-$MeAc^+$ (-0.44 V) > HAc^+ (-0.59 V) > $H3BIM^+$ (-0.84 V) > N-$MeQn^+$ (-0.94 V). The poor electron-accepting ability of $H3BIM^+$, which is comparable to that of Me_4-BQ

(E^r_{p1} = -0.88 V and E^r_{p2} = -1.70 V), suggests both the stable existence of the cation state ($H3BIM^+$) and the difficult accessibility of the neutral radical state ($H3BIM^{\bullet}$) in the solid state.

2-3-1-3 Neutral state; H2BIM^0

$H2BIM^0$, with a neutral 6π-6π electronic structure, shows both the irreversible reduction (E^r_{p1} = -1.69 V) and oxidation processes (E^o_{p1} = 1.22 V). The electron-accepting nature of $H2BIM^0$ is poor and is comparable to those of acridine^0 (E^r_{p1} = -1.73 V) and naphthacene^0 (E^r_{p1} = -1.62 V). On the other hand, the electron-donating character is very close to that of $H2Q^0$ (E^o_{p1} = 1.20 V) and is stronger than that of anthracene^0 (E^o_{p1} = 1.42 V). Thus it is said that $H2BIM^0$ is able to act as an electron donor rather than an electron acceptor in the solid state, though the electron-donating ability is not very strong.

2-3-1-4 The Substitution Effects of Imino and Nitrilo Groups for Sulfur Atoms of Tetrathiafulvalene

$H4BIM^0$ has only imino nitrogens, while BIM^0 has only nitrilo-nitrogens in the five-membered rings. $H2BIM^0$ has both kinds of nitrogens, so at first I discuss the substitution effects of imino and nitrilo groups on the electron transfer properties. It has been known that the insertion of nitrilo-nitrogen (sp^2-type) into an aromatic ring causes the enhancement of the electron-accepting ability. On the contrary, the isoelectronic substitution by imino-nitrogen (sp^3-type) increases the electron-donating character of neutral species. For example, the reduction peak potentials of neutral anthracene derivatives increase by increases of nitrilo-nitrogens (Scheme 2-4),

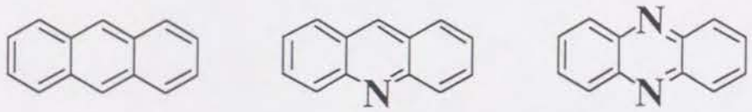

$E^r_p = -2.07$ < $E^r_p = -1.73$ < $E^r_p = -1.25$ (V)
$E_a = 0.67$ < $E_a = 1.11$ < $E_a = 1.56$ (eV)

Scheme 2-4

where E_a is the calculated electron affinity by the method of PPP calculation assuming Koopman's theorem. The E^r_p values of acridine and phenazine increase by 0.34 and 0.48 V per one nitrilo-nitrogen atom, respectively, and which has a linear relation with the calculated E_a values. For the TTF framework, the lowering of electron-donating abilities has been reported for tetrathiadiazafulvalene by the substitution of two nitrilo-nitrogens.[16]

Next the effects of the replacement of nitrilo groups by imino groups will be examined. For example, in the case of 4,4'-bipyridine (BPY^0) system (Scheme 2-5a),

a.

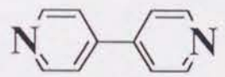

BPY^0

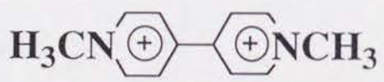

Me_2BPY^{2+}

$E^r_p(0 \longrightarrow -\bullet) = -2.05$ $E_a = 0.70$

$E^r_p(2+ \longrightarrow +\bullet) = -0.49$ (V) $E_a = 2.69$ (eV)

$E^r_p(0 \longrightarrow +\bullet) > 1.40$ $I_p = 9.10$

$E^r_p(+\bullet \longrightarrow 0) = -0.88$ (V) $I_p = 5.53$ (eV)

b.

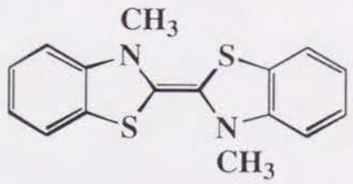

Scheme 2-5

where I_p is the calculated ionization potential. By the replacement of nitrilo with methylammonio groups, this system can change from neutral (BPY^0) to dication (Me_2BPY^{2+}), keeping the stable 6π - 6π electronic structure. BPY^0 has a quasi-reversible reduction peak at -2.05 V ($BPY^0 \rightarrow BPY^{-\bullet}$) but no oxidative peak ($BPY^0 \rightarrow BPY^{+\bullet}$) up to 1.4 V in DMF. The dication species (Me_2BPY^{2+}), which can be converted to the neutral 7π-7π structure by the use of magnesium as a reducing reagent,[17] show two reversible reduction peak potentials at -0.49 ($Me_2BPY^{2+} \rightarrow Me_2BPY^{+\bullet}$) and -0.88 V ($Me_2BPY^{+\bullet} \rightarrow Me_2BPY^0$). Therefore, Me_2BPY^{2+} is a stronger electron acceptor by 1.56 V than BPY^0. Concerning the electron-donating ability, the existence of a dication form at ambient condition is clear evidence of the enhancement of the electron-donating ability of Me_2BPY^0. The methylammonio groups increase the electron-donating ability of BPY^0 by at least 2.19 V. The enhancement of donor ability is also recognized by the replacement of sulfur atoms of the TTF moiety with methylimino groups as exemplified by the 3,3'-dimethyl-2,2'-bi(2,3-dihydrobenzothiazol-2-ylidene) molecule (Scheme 2-5b).[15]

The first reduction peak potentials of three biimidazole derivatives with 6π - 6π electronic structure increase in the following order: $H2BIM^0$ (E^r_p = -1.69 V) < $H3BIM^+$ (E^r_p = -0.84 V) < $H4BIM^{2+}$ (E^r_p = -0.54 V). The electron-accepting abilities increase by 0.85 and 0.30 V by the conversion of the first and second nitrilo groups to imino groups, respectively.

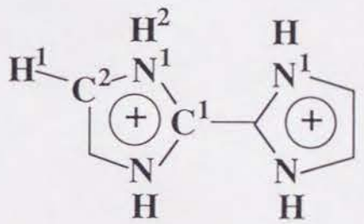

$H4BIM^{2+}$

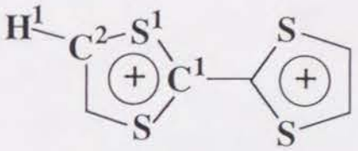

TTF^{2+}

Fig. 2-2. $H4BIM^{2+}$ and TTF^{2+} molecules with atomic numbering scheme.

Table 2-2. Extended Hückel molecular orbital calculations of TTF^{2+} and $H4BIM^{2+}$.

Atom	Orbital	Electron densities	Total[a)]	Net charge[b)]
TTF^{2+}				
C^1	s	1.156		
	$p_x + p_y$	1.712	3.694	0.306
	p_π	0.826		
C^2	s	1.162		
	$p_x + p_y$	1.829	3.998	0.002
	p_π	1.007		
S^1	s	1.481		
	$p_x + p_y$	2.650	5.711	0.289
	p_π	1.580		
H^1	s	0.944	0.944	0.056
$H4BIM^{2+}$				
C^1	s	1.053		
	$p_x + p_y$	1.532	3.442	0.558
	p_π	0.857		
C^2	s	1.146		
	$p_x + p_y$	1.699	3.902	0.098
	p_π	1.057		
N^1	s	1.338		
	$p_x + p_y$	2.289	5.141	-0.141
	p_π	1.514		
H^1	s	0.956	0.957	0.043
H^2	s	0.779	0.779	0.221

a) Total electron density (μ_t) is the sum of electron density of s, p_x, p_y and p_π orbitals.
b) Net charge is defined as the difference between the total charge and ideal number of the valence electron; N and S atoms has 5 and 6 valence electrons, respectively.

To clarify the differences of electronic states of TTF^{2+} and $H4BIM^{2+}$, the simple MO calculations (extended Hückel MO; EHMO) were done for these two cations. Table 2-2 summarizes the electron densities and the net charge (a polarization of the

charge distribution) of individual atoms for TTF^{2+} and $H4BIM^{2+}$ with the atomic numbering scheme in Fig. 2-2. The results indicate that π-electron densities (μ_π) of nitrogens in $H4BIM^{2+}$ ($\mu_\pi = 1.514$) are slightly low compared with those of sulfurs in TTF^{2+} ($\mu_\pi = 1.580$). Also the π-electron populations of carbon atoms (C^1 and C^2 atom sites) of $H4BIM^{2+}$ are slightly large in comparison with TTF^{2+}. The large difference exists in the sign of the net charge on hetero atoms. In the case of TTF^{2+}, the net charges of all atoms become the positive value and about 58 percent of the positive charge is localized at S^1 atom sites. For the $H4BIM^{2+}$ molecule, about 56 percent of the positive charge is localized at C^1 atom sites, and the net charge of nitrogen atoms (N^1) changes to the negative value which indicates that the N^1 sites have the negative charge. Furthermore, imino-proton (H^2) has less charge (0.779) by the polarization structure and about 45 percent of the positive charge is located at H^2 atom sites. Thus, $H4BIM^{2+}$ has a highly polarized structure represented as $N^{-0.221}$ — $H^{+0.221}$ and has the character of ion polarization structure.

2-3-1-5 On-site Coulomb Repulsion of Electron-Transfer

The effective on-site Coulomb energy (U_{eff}^{CT}) in solid CT-complexes has been simply approximated by the following equation,

$$U_{eff}^{CT} = U_1^{CT} - U_2^{CT} \qquad (2.1.1),$$

where U_1^{CT} (so called bare U) represents the repulsion between two electrons on the same site (disproportional energy for $2A^{-\bullet} \rightarrow A^0 + A^{2-}$ in the gas phase) and U_2^{CT} represents that between two electrons on neighboring sites. The value of U_{eff}^{CT} can be estimated from the optical or magnetic measurements,[18)] and the direct measurement of U_1^{CT} values has been done in special cases (some lanthanoid compounds).[19)] It has been known that half-wave redox potentials can be used to obtain information on the relative magnitude of U_1^{CT} for different molecules provided that the same conditions are used for comparative measurements.[18b)]

Table 2-3a. The first and second half-wave redox potentials ($E_{1/2}(1)$ and $E_{1/2}(2)$), ΔE ($E_{1/2}(1)$ - $E_{1/2}(2)$) and on-site Coulomb repulsion energy (U_1^{CT}) of the BQ, DPQ, and TCNQ systems.[a)]

Compounds[b)]	$E_{1/2}(1)$[c)] V	$E_{1/2}(2)$[c)] V	ΔE V	U_1^{CT} [d)] eV
BQ system				
a: 2,3-$(Cl)_2$-5,6-$(CN)_2$-BQ	0.50	-0.34	0.86	5.33
b: 2,3-$(CN)_2$-BQ	0.32	-0.62	0.94	5.32
c: 2,3,5,6-$(Cl)_4$-BQ	0.06	-0.82	0.88	5.31
d: 2,3,5,6-$(Br)_4$-BQ	0.03	-0.86	0.89	5.30
e: 2,3,5,6-$(F)_4$-BQ	0.03	-0.96	0.99	5.30
f: 2,5-$(Cl)_2$-BQ	-0.13	-1.08	0.95	5.29
g: BQ	-0.49	-1.44	0.95	5.27
h: 2,5-$(Me)_2$-BQ	-0.64	-1.50	0.86	5.26
i: 1,4-Naphthoquinone	-0.65	-1.45	0.80	5.26
j: 2,3,5,6-$(Me)_4$-BQ	-0.80	-1.60	0.80	5.25
DPQ system				
k: 3,3',5,5'-$(Cl)_4$-DPQ	0.27	-0.15	0.42	4.81
l: 3,3',5,5'-$(Br)_4$-DPQ	0.23	-0.12	0.35	4.81
m: DPQ	-0.20	-0.60	0.40	4.78
n: 3,3',5,5'-$(Me)_4$-DPQ	-0.41	-0.81	0.40	4.77
TCNQ system				
o: 2,3,5,6-$(F)_4$-TCNQ	0.62	0.07	0.55	4.99
p: 2-F-TCNQ	0.37	-0.23	0.60	4.97
q: TCNQ	0.28	-0.33	0.61	4.97
r: 2,5-$(Et)_2$-TCNQ	0.22	-0.36	0.58	4.96
s: 2,5-$(Me)_2$-TCNQ	0.21	-0.34	0.55	4.96
t: 2,5-$(MeO)_2$-TCNQ	0.10	-0.46	0.56	4.96
u: BTDA-TCNQ	0.04	-0.46	0.50	4.95

a) Measured at a scan rate of 100 mV s^{-1} using Pt vs. Ag/AgCl in 0.1 M TBA-BF_4 / DMF. b) Molecular structures and substituted positions were indicated in Fig. 2-1. c) $E_{1/2}(1)$ and $E_{1/2}(2)$ are the average values of reduction and oxidation peak potentials for the processes of $A + e^- \rightleftarrows A^{-\bullet}$ and $A^{-\bullet} + e^- \rightleftarrows A^{2-}$, respectively. d) ΔG_{sol} = -2.2 (eV) was used for the U_1^{CT} estimations.

Table 2-3b. The first and second half-wave redox potentials ($E_{1/2}(1)$ and $E_{1/2}(2)$), ΔE ($E_{1/2}(1)$ - $E_{1/2}(2)$), and on-site Coulomb repulsion energy (U_1^{CT}) of dication molecules.[a)]

Compounds[b)]	$E_{1/2}(1)$[c)] V	$E_{1/2}(2)$[c)] V	ΔE V	U_1^{CT} [d)] eV
TTF system				
a': HM-TTF	0.56	0.34	0.22	4.65
b': TM-TTF	0.58	0.32	0.26	4.65
c': TTF	0.59	0.36	0.23	4.65
d': EDT-TTF	0.60	0.42	0.18	4.54
e': BEDO-TTF	0.60	0.47	0.13	4.54
f': DM-TTF	0.61	0.35	0.26	4.65
g': OM-TTF	0.61	0.34	0.27	4.65
h': BEDT-TTF	0.68	0.56	0.12	4.54
i': TTC_1-TTF	0.70	0.57	0.13	4.55
j': $(CO_2Me)_2$-EDT-TTF	0.83	0.68	0.15	4.55
Bz system				
k': o-Dianisidine	0.54	0.42	0.12	4.57
l': Me_4-Bz	0.55	0.36	0.19	4.54
m': *N*-TMB	0.60	0.47	0.13	4.54
n': o-Tolidine	0.63	0.42	0.21	4.58
o': Bz	0.66	0.45	0.21	4.58
PPD system				
p': DAD	0.34	0.01	0.33	4.73
q': PPD	0.51	0.16	0.35	4.74
Another system				
r': TTT	0.44	0.20	0.24	4.64
s': DAP	0.45	0.21	0.24	4.64
t': DTPY	0.67	0.42	0.25	4.64
u': Me_2PHz	0.89	0.20	0.69	5.09
v': H4BIM	-0.54	-0.77	0.23	4.68

a) Measured at a scan rate of 100 mV s^{-1} using Pt vs. Ag/AgCl in 0.1 M TBA-BF_4 / DMF. b) All molecules are dication species and those neutral structures are illustrated in Fig. 2-1. c) $E_{1/2}(1)$ and $E_{1/2}(2)$ are the average values of reduction and oxidation peak potentials for the processes of $D^{2+} + e^- \rightleftarrows D^{+\bullet}$ and $D^{+\bullet} + e^- \rightleftarrows D^0$, respectively. d) ΔG_{sol} = -2.2 (eV) was used for the U_1^{CT} estimations.

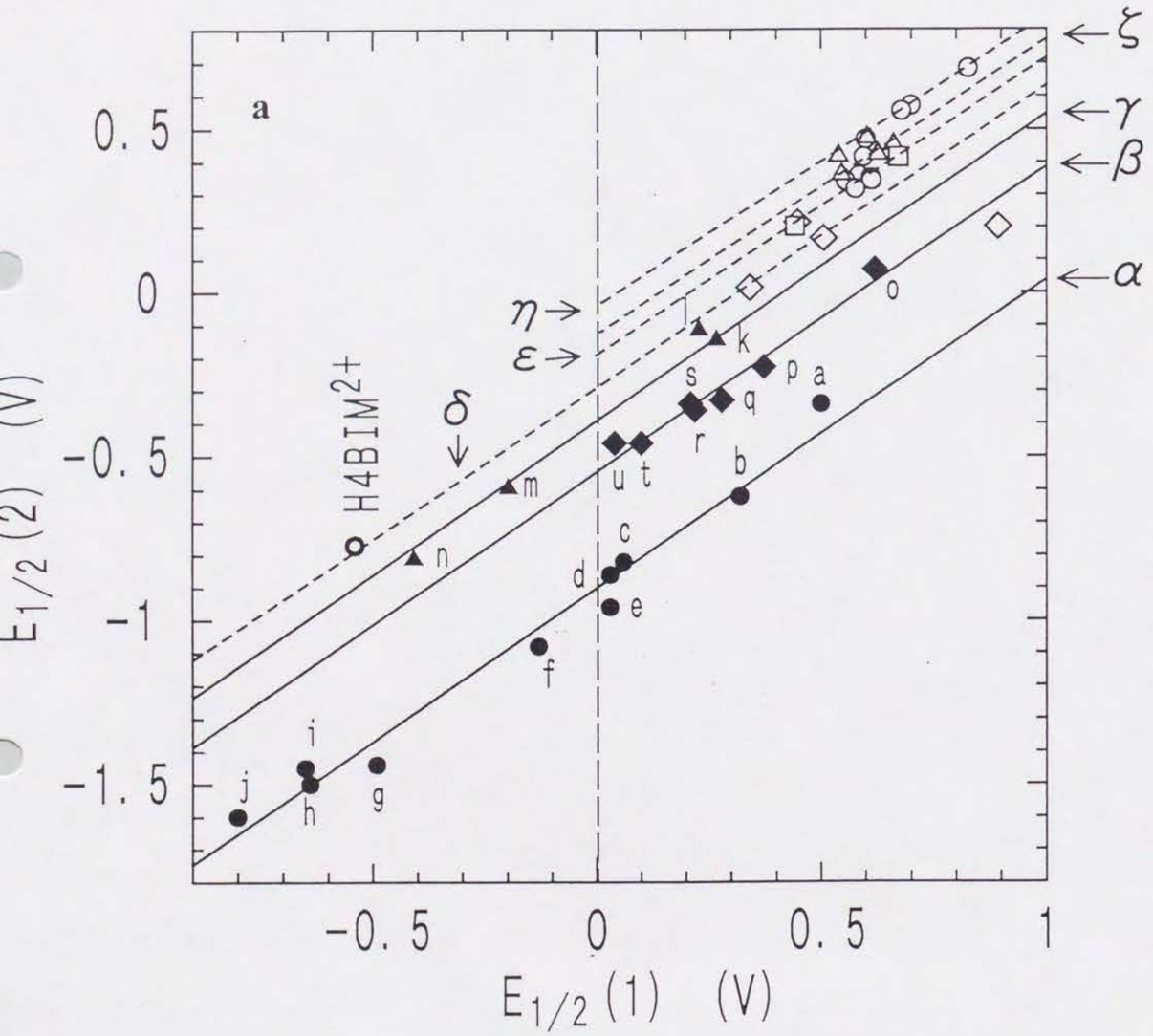

Fig. 2-3. The plots of $E_{1/2}(1)$ vs. $E_{1/2}(2)$ for α; BQ(O), β; TCNQ(◊), γ; DPQ(Δ), δ; PPD(◊), ε; TTF(O), ζ; Bz(Δ) and η; BEDT-TTF systems. About the lines, see text. a) The numbering of BQ (a-j), TCNQ (o-u) and DPQ (k-n) systems correspond to those listed in Table 2-3a. b) The expanded figure of a) to clarify δ, ε, ζ and η systems. The numberings correspond to those listed in Table 2-3b.

No quantitative comparison has been attempted between the two extreme classifications of redox properties of organic molecule, namely the Weitz or Würster type. Here, I examine the redox potentials to evaluate U_1^{CT} values of various types of molecules and try to find the differences, if any, between these two types.

The half-wave redox potentials ($E_{1/2} = (E^r_p + E^o_p) / 2$) of reduction processes, ΔE ($E_{1/2}(1) - E_{1/2}(2)$) and the estimated U_1^{CT} values (described later) for the BQ, DPQ, and TCNQ systems are summarized in Table 2-3a. The results show that similar kinds of molecules give the same extent of ΔE values. The ΔE values of the BQ system amount in the ΔE range from 0.80 to 0.99 V, and those of the TCNQ system are in the ΔE range from 0.50 to 0.61 V. The plots of $E_{1/2}(1)$ and $E_{1/2}(2)$ values for two redox processes, $A^0 + e^- \rightleftarrows A^{-\bullet}$ and $A^{-\bullet} + e^- \rightleftarrows A^{2-}$, indicate the good linear correlation of these two redox processes for the BQ (a-j, line α) and TCNQ (o-u, line β) systems as shown in Fig. 2-3. By a least-squares method, the following equations were obtained.

$$\text{BQ system; } E_{1/2}(2) = 0.941E_{1/2}(1) - 0.901 \qquad (2.1.2),$$

and

$$\text{TCNQ system; } E_{1/2}(2) = 0.935E_{1/2}(1) - 0.547 \qquad (2.1.3).$$

The slopes of equations 2.1.2 and 2.1.3 are less than unity [20] and are equal to 0.94 within experimental error. A linear relation with the slope of 0.94 fits well with the data of the DPQ system (k-n, line γ in Fig. 2-3a),

$$\text{DPQ system; } E_{1/2}(2) = 0.94E_{1/2}(1) - 0.391 \qquad (2.1.4).$$

The values of intercept decrease in the order of the DPQ, TCNQ, and BQ systems, which suggests that the U_1^{CT} values increase in this sequence. The observed linear relationships between $E_{1/2}(1)$ and $E_{1/2}(2)$ values are expressed as

$$E_{1/2}(2) = \alpha E_{1/2}(1) - \beta \qquad (2.1.5).$$

In the gas phase, the energy change for the reaction $A^0 + e^- \rightarrow A^{-\bullet}$ corresponds to $E^t_1 - E^t_0$, where E^t_0 and E^t_1 indicate the total energies of A^0 and $A^{-\bullet}$ species, respectively. On the other hands, in solution I need to consider the term of solvation energy as shown in equation 2.1.6,

$$E^t_1 - E^t_0 = -E_{1/2}(1) - \Delta G_{sol} + C \qquad (2.1.6),$$

where ΔG_{sol} is the difference in solvation energies for A^0 and $A^{-\bullet}$ molecules, and C is a constant which depends upon the reference electrode.[21] In the same manner, the energy change between $A^{-\bullet}$ and A^{2-} species can be related to the $E_{1/2}(2)$ value as shown in equation 2.1.7,

$$E^t_2 - E^t_1 = -E_{1/2}(2) - \Delta F_{sol} + C \qquad (2.1.7),$$

where E^t_2 means the total energy of A^{2-} molecule and ΔF_{sol} is the difference in solvation energies for $A^{-\bullet}$ and A^{2-} molecules. From equations 2.1.6 and 2.1.7, the relation of $E_{1/2}(1)$ and $E_{1/2}(2)$ is described as

$$-E_{1/2}(2) = -E_{1/2}(1) + (E^t_2 + E^t_0 - 2E^t_1) - \Delta G_{sol} + \Delta F_{sol} \qquad (2.1.8).$$

ΔF_{sol} was roughly approximated as $3\Delta G_{sol}$ by Hedges and Matsen,[22] and the term in the parenthesis is equal to U_1^{CT}, so equations 2.1.5 and 2.1.8 give

$$U_1^{CT} = (1-\alpha)E_{1/2}(1) + \beta - 2\Delta G_{sol} \qquad (2.1.9).$$

Kebarle et al. estimated the ΔG_{sol} values for various sizes and shapes of p-benzoquinone derivatives based on the measured electron affinities and half-wave redox potentials.[21a] For example, the estimated ΔG_{sol} values are -2.13 eV (p-chloranil; c in Table 2-3a),

-2.36 eV (9,10-anthraquinone), and -2.45 eV (2,5-dimethyl-p-benzoquinone; h in Table 2-3a) in DMF. While, in acetonitrile, the $|\Delta G_{sol}|$ decreases slightly, 2.09 eV for p-chloranil and 2.23 eV for 9,10-anthraquinone. They derived these ΔG_{sol} as a function of $E_{1/2}(1)$ values. However, the $E_{1/2}(1)$ dependence in ΔG_{sol} and ΔF_{sol} is already included in equation 2.1.5 and the deviation from unity in the observed α is the consequence of the $E_{1/2}(1)$ dependence. The constant term in ΔG_{sol} ($E_{1/2}(1) = 0$) is evaluated as 2.196 eV by using the ΔG_{sol} values in Ref. 21a and $E_{1/2}(1)$ values in Table 2-3a for the BQ system. Assuming that ΔG_{sol} ($E_{1/2}(1) = 0$) is not much different among the systems (the difference of ΔG between BQ and TCNQ system is within the difference of ΔG in the BQ system), sizes, and shapes of molecules under examination, I can represent the relationship between the U_1^{CT} and the $E_{1/2}(1)$ values.

$$\text{line } \alpha;\quad U_1^{CT}(\text{BQ}) = 0.06E_{1/2}(1) + 5.30 \qquad (2.1.10),$$

$$\text{line } \beta;\quad U_1^{CT}(\text{TCNQ}) = 0.06E_{1/2}(1) + 4.95 \qquad (2.1.11),$$

and

$$\text{line } \gamma;\quad U^1{}_{CT}(\text{DPQ}) = 0.06E_{1/2}(1) + 4.79 \qquad (2.1.12).$$

The estimated $U^1{}_{CT}$ values decrease in the order of the BQ, TCNQ, and DPQ systems. In the BQ system, the strongest acceptor, DDQ (a in Table 2-3a), has the highest U_1^{CT} of 5.33 eV and the weakest one, Me4-BQ (j in Table 2-3a), has the lowest U_1^{CT} of 5.25 eV within my experimental data. So all BQs in Table 2-3a are included within the change of U_1^{CT} of 0.08 eV. For the TCNQ system, the change of U_1^{CT} is much less amount; 0.04 eV.

The MO calculations on the U_1^{CT} values have been done by several groups for TCNQ, and it is between 2.33 and 5.44 eV.[18a, 23] The estimated value for TCNQ (U_1^{CT} = 4.97 eV) is within this range.

The half-wave redox potentials ($E_{1/2}$) for the process $D^{2+} + e^- \rightleftarrows D^{+\bullet}$ and $D^{+\bullet} + e^- \rightleftarrows D^0$, ΔE ($E_{1/2}(1) - E_{1/2}(2)$) and the estimated U_1^{CT} for dication systems

are summarized in Table 2-3b. The ΔE values of dication molecules are somewhat smaller than those of the BQ, TCNQ, and DPQ systems.

The ΔE values of the TTF system exist within the ΔE range from 0.12 to 0.27 V, and those of the Bz system have the ΔE range from 0.12 to 0.21 V. There are some molecular series on the same line having the slope of 0.94 just as the BQ, TCNQ, and DPQ systems do, so I classified these dications into four representative groups (Fig. 2-3b): i) the PPD system; DAD^{2+} (p') and PPD^{2+} (q') are on the line δ having an intercept at -0.31 V. In TTF derivatives, there are two classes of molecules: ii) TTF and alkyl substituted TTF; HM-TTF^{2+} (a'), TM-TTF^{2+} (b'), TTF^{2+} (c'), DM-TTF^{2+} (f') and OM-TTF^{2+} (g') belong to the line ε with an intercept at -0.19 V, on which TTT^{2+} (r'), DAP^{2+} (s') and $DTPY^{2+}$ (t') are located. iii) the BEDT-TTF system (alkylthio substituted TTF); BEDO-TTF^{2+} (e'), BEDT-TTF^{2+} (h'), TTC_1-TTF^{2+} (i') and $(CO_2Me)_2$-EDT-TTF^{2+} (j') in addition to two Bz^{2+} derivatives (o-dianisidine^{2+} (k') and N-TMB^{2+} (m')) are on the line η with an intercept at -0.09 V. iv) Benzidine system; Me_4-Bz^{2+} (l'), o-tolidine^{2+} (n') and Bz^{2+} (o') are on the line ζ with an intercept at -0.16 V, on which EDT-TTF^{2+} (d') resides. In addition to these classifications, Me_2PHz^{2+} (u') and $H4BIM^{2+}$ (v') are also shown in Fig. 2-3.

Roughly speaking, molecules on one line in Fig. 2-3 have almost the same U_1^{CT} value. Furthermore, molecules on the upper line have smaller U_1^{CT} values than those on the lower one and the difference of U_1^{CT} between them is approximately the difference in the intercepts; β in equation 2.1.5. Therefore, the molecules on lines $\alpha - \eta$ have the U_1^{CT} values in the following order, line α ($\beta = 0.90$) > line β ($\beta = 0.55$) > line γ ($\beta = 0.39$) > line δ ($\beta = 0.31$) > line ε ($\beta = 0.19$) > line ζ ($\beta = 0.16$) > line η ($\beta = 0.09$).

For the case of diamine molecules, since DAP^{2+} (s') is on the line ε and Me_2PHz^{2+} (u') is below the line β, the estimated U_1^{CT} values decrease in the order of Me_2PHz^{2+}, PPD^{2+} (line δ), DAP^{2+} (line ε), and Bz^{2+} (line ζ). This order suggests the existence of a correlation between the values of U_1^{CT} and the distances of two nitrogen atoms for these Würster's dication species (described later). For the case of the

TTF system, there is a slight difference between the alkyl substituted TTF^{2+}; line ε, and the alkylthio-substituted TTF^{2+}; line η, the latter group has a smaller U_1^{CT} value than that of the former one and EDT-TTF^{2+} is between them.

Table 2-4. r^{-1} and estimated U_1^{CT} of acceptors and dications.

Compounds	r^{-1} a) Å^{-1}	U_1^{CT} b) eV
Acceptors		
a:BCDT[c)]	0.127	4.61
b:TCNDQ[d)]	0.128	4.55
c:TNAP[d)]	0.133	4.77
d:TCNP[e)]	0.145	4.74
e:TCNT[d)]	0.180	5.00
f:TCNQ	0.183	4.97
g:DPQ	0.187	4.78
h:CNQI[f)]	0.219	4.91
i:HCBD	0.247	4.94
j:DCNQI[g)]	0.270	5.03
k:BQ	0.327	5.29
l:TCNE	0.476	5.20
Dications		
m:DTPY	0.177	4.64
n:BEDT-TTF	0.178	4.55
o:Bz	0.179	4.57
p:Me_4-Bz	0.179	4.54
q:TTT	0.189	4.64
r:DAP	0.190	1.64
s:TTF	0.258	4.65
t:H4BIM	0.283	4.68
u:PPD	0.315	4.74
v:Me_2PHz	0.482	5.09

a) The r values are defined as $\Sigma\mu_{\pi i}r_i / \Sigma\mu_{\pi i}$ in a half unit of molecules divided by a mirror plane at a center of inversion. The $\mu_{\pi i}$ (π-electron density) was obtained for the dianions and neutral donors by PPP molecular orbital calculation. b) U_1^{CT} were estimated from equation 1.9 taking the α as 0.94. Redox potentials in c) Ref. 24e, d) Ref. 24c, e) Ref. 24d, f) Ref. 24a and g) Ref. 24b were used in the estimation of U_1^{CT}.

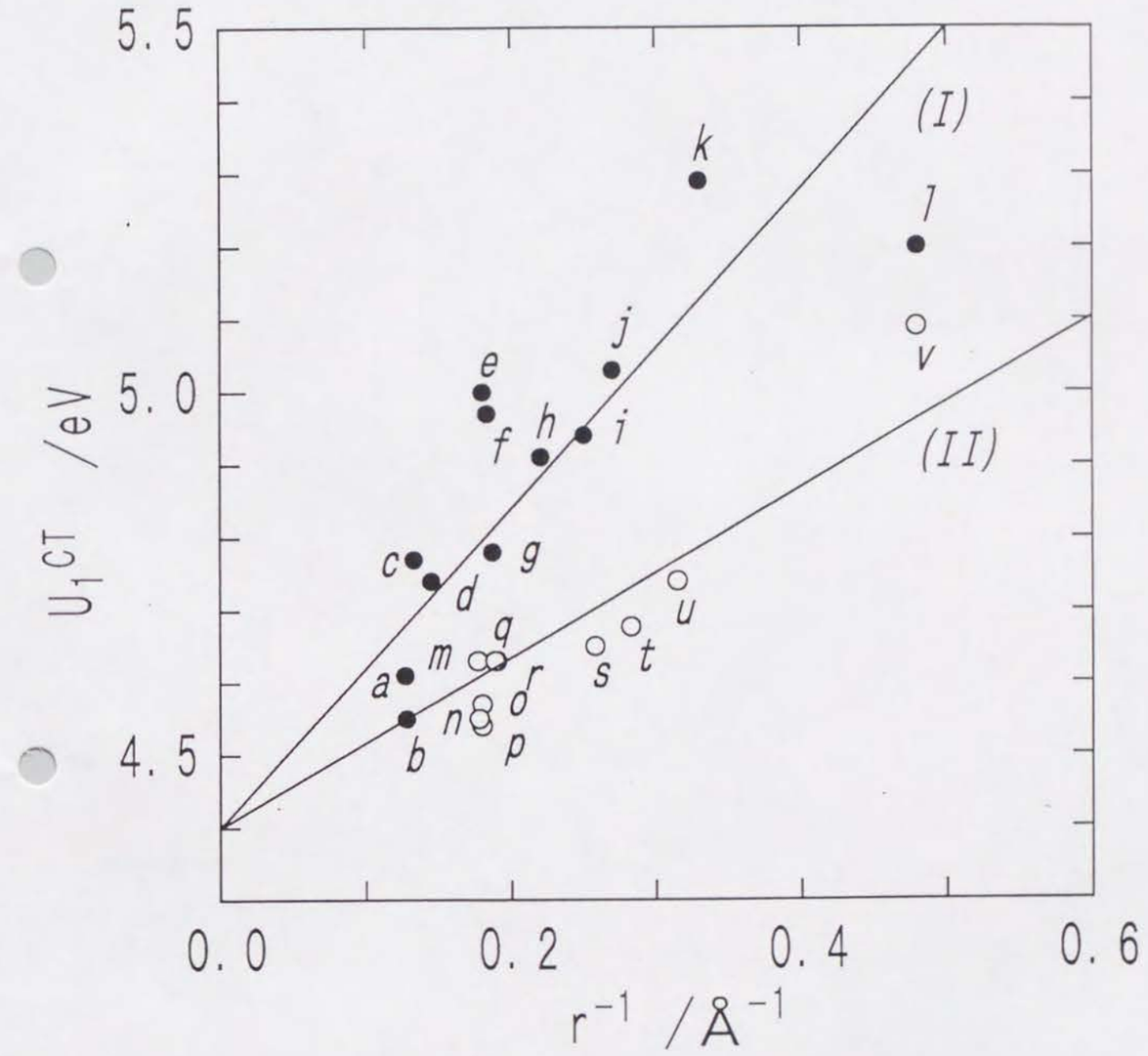

Fig. 2-4. The relation between U_1^{CT} (eV) and r^{-1} (Å^{-1}) for (I); electron acceptors (closed circles), II) dications (open circles). Two straight lines were obtained by the method of the least-squares. The numberings correspond to these listed in Table 2-4.

The Weitz type dication $H4BIM^{2+}$ is close to line δ and its U_1^{CT} value is higher than TTF^{2+} and lower than PPD^{2+}. Reflecting the low electron-accepting ability of $H4BIM^{2+}$, its position is far from the usual TTF^{2+} system in Fig. 2-3.

Table 2-4 summarizes the r^{-1} and the estimated U_1^{CT} values. Here the structural parameter r value is the distance between the centers of gravities of π-electron density for a half unit of molecule, which is caluculated for neutral donor and dianion states of acceptor based on PPP MO calculations. To make the relation between the U_1^{CT} and r values clear, I added data from the literatures for the following molecules; *N,N'*-dicyano-p-benzoquinonediimine (DCNQI),[24a] 7,7-dicyano-p-benzoquinone methide (CNQI),[24b] 9,9,10,10-tetracyano-2,6-naphthoquinodimethane (TNAP),[24c] 13,13,14,14-tetracyanodiphenoquinodimethane (TCNDQ),[24c] 2,5-bis (dicyanomethylidene)-2,5-dihydrothiophene (TCNT),[24c] 11,11,12,12-tetracyano-2,7-pyrenoquinodimethane (TCNP)[24d], and 2,5-bis(4-oxo-2,5-cyclohexadien-1-ylidene)-2,5-dihydrothiophene (BCDT).[24e]

The relation between the estimated U_1^{CT} and r^{-1} values (Fig. 2-4) clearly divided the examined molecules into two classes: I, electron acceptors (closed circles) and II, dications (open circles). The roughly linear relationship is observed for these two classes, though there are some exceptions, for example, TCNDQ (b) is near class II and BCDT (a) and TCNE (l) are between classes I and II. Two straight lines, I and II in Fig. 2-4 the intercepts of which are fixed to 4.4 eV ($= -2\Delta G_{sol}$), are the guides to eyes to distinguish the two classes. For the electron acceptors (line I), all of them belong to the Würster type, while both the Würster and Weitz types are on the same line II for dication molecules. So there are no differences between the Würster and Weitz types for U_1^{CT}. However, it should be noted that a distinct difference exists in the correlation of U_1^{CT} and 1/r between electron acceptors (line I) and donors (line II) and the U_1^{CT} values of the dications are insensitive to the change in the r compared with those of electron acceptors.

2-3-2. Proton-Transfer Properties in Solution

2-3-2-1 General Scope

Since the pK_a values of the H2BIM system extend for a wide pH range due to the large influence of the substitution effects, I was only able to measure part of the acid dissociation constants experimentally. To get insight into the structural information for the pK_a values, the estimation of the pK_a values not measured was done by the following procedure. Based on the pK_a values of 1*H*-imidazoles (HIM) having a half unit of the H2BIM molecule, the linear relationship between the pK_a values and the sum of Hammett's constants ($\Sigma\sigma_i$) was derived. By using this relation and the pK_a values of the H2BIM system, the σ_p values of 2-1*H*-imidazolyls were estimated. Using the estimated σ_p values of 2-1*H*-imidazolyls, the pK_a values not measured for the H2BIM system were obtained, and the linear relationship between pK_a values and $\Sigma\sigma_i$ was compared with those of other representative PT and CT systems, H2Q and H2TCNQ systems with the Würster type molecular framework. The PT processes of the H2Q system have extensively been examined, but almost none of the H2TCNQ one have been reported, no matter what a good component of the CT and PT system it is. Some examples of CT complex formation using the PT process of the H2TCNQ molecule, which requires hydride transfer, have been reported by Melby et al.[25a] and Saito and Colter (see Section 1-2).[25b] Against these two-step PT systems, I describe the procedure of the estimation of U_1^{PT} values based on the pK_a values in solution. Finally, the correlation will be described between the degree of U_1^{PT} values and the structural characteristics, namely the distance r in Section 2-3-1-5.

2-3-2-2 Acid Dissociation Constants (pK_a) of the H2BIM System

Table 2-5 summarizes the pK_a data of H2TMBIM, H2BIM, H2TClBIM, H2TBrBIM, and H2TCNBIM, together with the $\Sigma\sigma_i$[26] based on 2,2'-bi-1*H*-imidazole ($\Sigma\sigma_i = 2\sigma_p + 2\sigma_m = 0$). The values in parenthesis correspond to the estimated ones described later. The second acid dissociation constant (pK_{a2}) for the process of

$H3BIM^+ \rightarrow H2BIM + H^+$ was measured as 4.60 (Scheme 2-6), while no further protonation of $H3BIM^+$ was observed below pH = 1.50 ($pK_{a1} < 1.50$) and no deprotonation of H2BIM was detected up to the range of pH = 12.0 indicating that pK_{a3} and pK_{a4} of H2BIM are larger than 12.0.

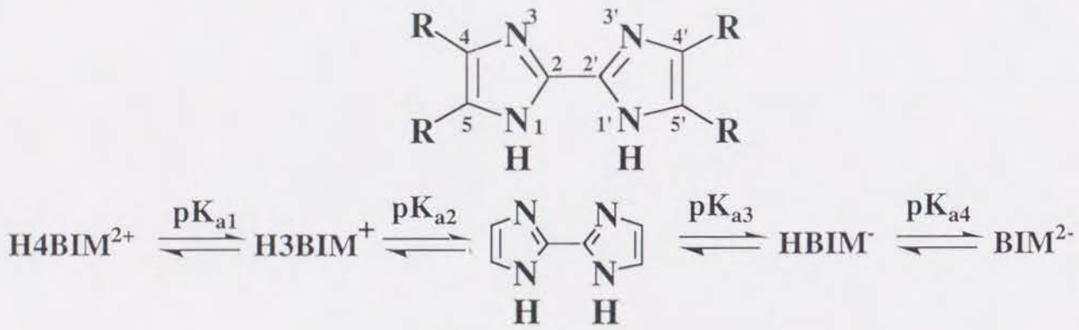

Scheme 2-6

Table 2-5. $\Sigma\sigma_i$ and pK_a values of 2,2'-1*H*-biimidazole derivatives and the data in parenthesis are the estimated pK_a values.

Compounds[a]	$\Sigma\sigma_i$[b]	pK_{a1}	pK_{a2}	pK_{a3}	pK_{a4}
R = Me	-0.48	1.60[c]	6.30	(14.15)	(18.17)
R = H	0.00	(-0.24)	4.60	(12.31)	(16.33)
R = Cl	1.20	(-5.52)	(-0.94)	7.45	11.40
R = Br	1.24	(-5.52)	(-0.94)	7.44	11.50
R = CN	2.44	(-9.68)	(-5.10)	2.99	7.60

a) Molecular structures are shown in Scheme 2-6. b) $\Sigma\sigma_i = 2\sigma_p + 2\sigma_m$. c) Determined by the spectrometry.

The H2TMBIM system ($\Sigma\sigma_i$ = -0.48) had the dissociation constants at pK_{a1} = 1.60, pK_{a2} = 6.30 and pK_{a3}, pK_{a4} > 12.0. Consequently, both H2BIM and H2TMBIM molecules behave as bases and are usable as a source of cation species from pH 1.50 to 12.0, while H2TClBIM ($\Sigma\sigma_i$ = 1.20), H2TBrBIM ($\Sigma\sigma_i$ = 1.24), and H2TCNBIM ($\Sigma\sigma_i$ = 2.44) molecules had two-step acid dissociation processes, pK_{a3} and pK_{a4} as shown in Table 2-5. Consequently, H2TBrBIM, H2TClBIM, and H2TCNBIM molecules behave as acids and are a source of anion species in the pH range from 1.5 to 12.0.

2-3-2-3 Linear Correlation between $\Sigma\sigma_i$ and pK_a of 1H-Imidazoliums

The acid dissociation processes of various simple 1*H*-imidazolium compounds (Scheme 2-7) were compared with the H2BIM system to have a deeper insight into H2BIM framework.

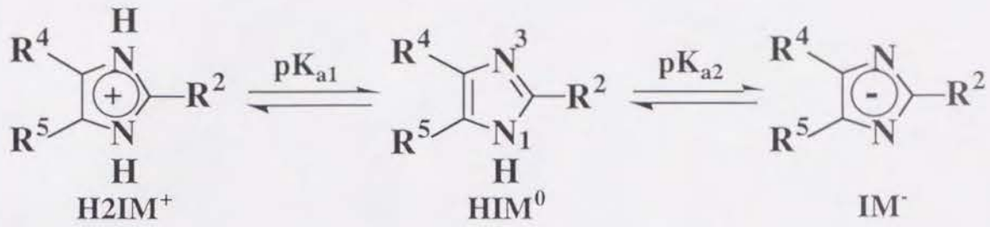

Scheme 2-7

The shift of equilibrium constant (pK_a) in different solvent systems has been ascribed to the change of solvation energy, which depends mainly on the electrostatic interaction of solvents.[27] For the case of the complete dissociation of charged species, Born's equation can be used for the derivation of the solvation energy, especially for solvents with high dielectric constants. For the acid dissociation process; HA (HA^+) $\rightarrow$ A^- (A^0) + H^+, the change of pK_a ($\Delta pK_a = pK_a(II) - pK_a(I)$) in two different solvents (I and II) can be described as,[27]

$$\Delta pK_a = 0.217Ne^2/(RT)(1/r_H + z_A^2/r_A - z_{HA}^2/r_{HA})(1/\varepsilon_{II} - 1/\varepsilon_I) \qquad (2.2.1),$$

where N is Avogadro's number, r and z are the radius and the charge of respective chemical species, e is the charge of electron, R is the gas constant, T is the temperature, and ε is the dielectric constant. The ΔpK_a value is a linear function of ($1/\varepsilon_{II} - 1/\varepsilon_I$) and the slope depends on the type of dissociation processes, i.e. the slope in the $HA^+ \rightarrow A + H^+$ process is smaller than that in the $HA \rightarrow A^- + H^+$ one.

Table 2-6. $\Sigma\sigma_i$ and pK_a of 1*H*-imidazolium.

Compounds[a]	$\Sigma\sigma_i$[b]	pK_{a1}[c]	pK_{a2}[c]
a: R_2=R_4=R_5=Me	-0.41	8.92	
b: R_2=R_4=Me, R_5=H	-0.24	8.50	
c: R_2=Me, R_4=R_5=H	-0.17	7.85	15.10
d: R_2=Me, R_4=R_5=H[d]	-0.17	7.66	
e: R_2=Et, R_4=R_5=H	-0.15	8.00	
f: R_2=H, R_4=Me, R_5=H	-0.07	7.56	15.10
g: R_2=R_4=R_5=H	0.00	7.00	14.90
h: R_2=R_4=R_5=H[d]	0.00	7.10	
i: R_2=H, R_4=CH_2OH, R_5=H	0.00	5.54	
j: R_2=H, R_4=CH_2O_2Ac, R_5=H	0.05	6.20	
k: R_2=Br, R_4=R_5=H	0.23	3.85	11.03
l: R_2=H, R_4=F, R_5=H	0.34	2.44	11.92
m: R_2=H, R_4=CO_2Et, R_5=H	0.37	3.66	
n: R_2=H, R_4=Br, R_5=H	0.39	3.88	12.32
o: R_2=H, R_4=CHO, R_5=H	0.42	2.90	10.70
p: R_2=H, R_4=CF_3, R_5=H	0.43	2.28	
q: R_2=Me, R_4=NO_2, R_5=H	0.54	0.5	
r: R2=H, R4=R5=Cl[d]	0.60		9.70
s: R_2=H, R_4=NO_2, R_5=H	0.71	0.0	9.30
t: R_2=H, R_4=NO_2, R_5=H[d]	0.71		9.50
u: R_2=Me, R_4=NO_2, R_5=Br	0.77	-0.55	
v: R_2=NO_2, R_4=R_5=H	0.78	-0.81	
w: R_2=I, R_4=NO_2, R_5=H	0.89	-0.85	
x: R_2=H, R_4=Cl, R_5=NO_2	1.22		5.2
z: R_2=H, R_4=R_5=CN[d]	1.22		5.53

a) Molecular structures and substituted positions are shown in Scheme 2-7.
b) $\Sigma\sigma_i = 2\sigma_p + \sigma_m$. c) pK_{a1} and pK_{a2} corresponds to $H2IM^+ \rightleftarrows HIM^0 + H^+$ and $HIM^0 \rightleftarrows IM^- + H^+$, respectively. d) This work in DMF-H_2O (7:3), others are in water (Ref. 28).

Table 2-6 summarizes the $\Sigma\sigma_i$ and the pK_a values together with data from Ref. 28. I used a σ_p for 2- and 5-substituted groups and a σ_m for 4-substitution (Scheme 2-7). The pK_{a1} values of 1*H*-imidazolium (h; pK_{a1} = 7.10) and 2-methyl-1*H*-imidazolium (d; pK_{a1} = 7.66) in DMF-H_2O (7:3) are close to those in water (g; pK_{a1} = 7.00, ΔpK_a = -0.10. c; pK_{a1} = 7.85, ΔpK_a = +0.19.). The ε of H_2O and DMF-H_2O

(7:3) are known to be 78.5 and 49.2, respectively.[29] The difference of pK_a in these two solvents was obtained from equation 2.1 as + 0.24 pK_a unit in the case of T = 295 K, r_H = 1.4 and $r_{HA} = r_A$ = 10 Å. The influence of the lengths of r_{HA} and r_A was small, for example, the ΔpK_a value of + 0.26 pK_a unit is obtained if using $r_{HA} = r_A$ = 20 Å. Therefore, the observed ΔpK_a value is within the range of the difference in the solvent used, and my pK_{a1} values measured in a mixed solvent agree with those in water within + 0.20 in pK_a units.

The second acid dissociation constant (pK_{a2}) of 4-nitro-1*H*-imidazolium (t; pK_{a2} = 9.50) and 4,5-dicyano-1*H*-imidazolium (z; pK_{a2} = 5.53) in DMF-H_2O (7:3) are also comparable to those in water (s: pK_{a2} = 9.30, y: pK_{a2} = 5.20.). The pK_{a2} values in DMF-H_2O are larger by 0.2 - 0.3 in pK_a units than those in water. The shift of pK_{a2} values is explained similarly using equation 2.1; the degree of ΔpK_a was derived as + 0.32 pK_a unit for $r_{HA} = r_A$ = 10 Å and + 0.30 pK_a unit for $r_{HA} = r_A$ = 20 Å, which is compatible with the observed one. Accordingly, I treat the pK_{a2} values as the same in these two solvents.

Hammett's equation can be written,

$$pK_a = pK_{a0} - \rho\Sigma\sigma_i \qquad (2.2.2),$$

where K_{a0} and K_a are the equibrium constants for unsubstituted and substituted molecules, respectively, ρ is the constant for a given reaction under a given set of conditions, and the value of ρ is set at 1.00 for the ionization of the benzoic acid system.[30] The ρ value is a characteristic constant for the molecular framework and implies the sensitivity of the substitution effects.

The correlations of the pK_a and $\Sigma\sigma_i$ for imidazole compounds can be represented by two straight lines, (1) and (2) in Fig. 2-5, assuming the same slopes (ρ) by the least-squares method,

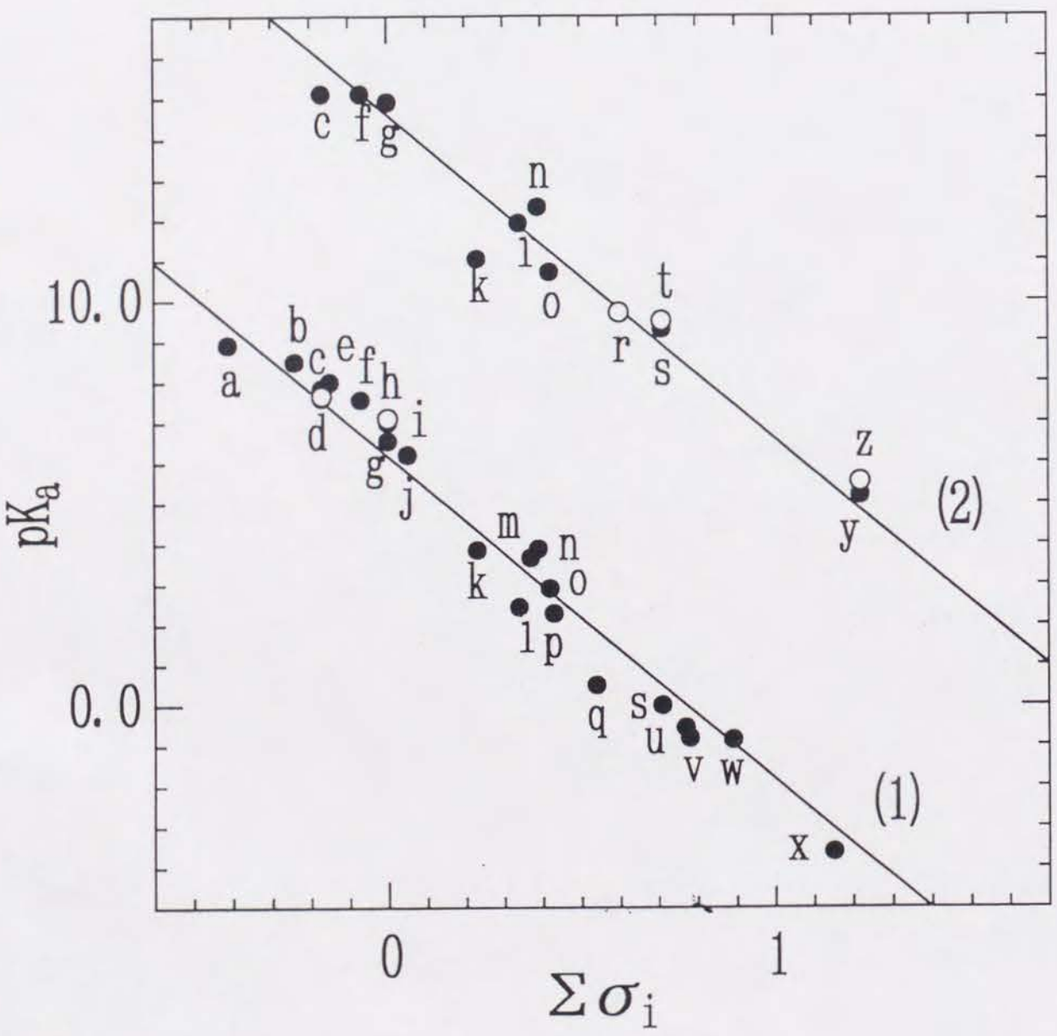

Fig. 2-5. $\Sigma\sigma_i$ vs. pK_a of 1*H*-imidazoles (compounds a-z in Table 2-6). Two straight lines, (1) and (2), correspond to the PT process of $H2IM^+ \rightarrow HIM^0 + H^+$ and $HIM^0 \rightarrow IM^- + H^+$, respectively. My measurements in DMF-H_2O (7:3) are represented as open circles and closed circles are corresponded to the data from Ref.28.

$$pK_{a1}\ (H2IM^+) = 6.26 - 8.00\Sigma\sigma_i \qquad (2.2.3)$$

and

$$pK_{a2}\ (H2IM^+) = 14.23 - 8.00\Sigma\sigma_i \qquad (2.2.4),$$

for the two acid dissociation processes (Scheme 2-7), respectively. A good linear relationship is ascertained as a standard deviation of 0.98 for equation 2.2.3 and 0.97 for equation 2.2.4, respectively. The large ρ value for the imidazole framework suggests that the electron density on nitrogen atoms is more sensitive to the substitution effects than the benzoic acid (ρ = 1.00), anilinium (ρ = 2.77 in H_2O at 25°C), or pyridinium (ρ = 6.11 in H_2O at 25°C) systems.[31] Thus, the acidity of the imidazoles and imidazoliums has the great susceptibility to substitution effects of any acid-base equilibrium series.

2-3-2-4 Derivation of Hammett's Constant (σ_p)

About the nitrogen-containing ring membered groups, the σ_p values of 2-pyridinyl, 3-pyridinyl, 5-pyrimidinyl, and 1-phenyl-1*H*-benzoimidazol-2-yl have been calculated as 0.17, 0.25, 0.39, and 0.21, respectively.[26, 32] For 2-1*H*-imidazolyl, the σ_I value, which represents the contribution from the field or inductive effects caused by the polarization through the bond and space due to the difference of the electronegativities ($X^{\delta+}$ — $Y^{\delta-}$), has been obtained as 0.27,[26] however its σ_p value has not been measured. Furthermore, there are no reported σ_p values of 4,5-disubstituted 2-1*H*-imidazolyls, 2-imidazolide, and 2-imidazolio.

Based on equations 2.2.3 and 2.2.4 and the pK_a values of H2BIM derivatives, I can evaluate Hammett's constant of 2-1*H*-imidazolyl, 2-imidazolio, and 2-imidazolide groups (Table 2-7). The evaluated σ_p of 2-1*H*-imidazolyl groups (0.19 ~ 0.25) are similar to those of chloro (σ_p = 0.23) and bromo (σ_p = 0.23) groups[26] and not much different from those of the nitrogen containing rings above mentioned. These results indicate that the substitutions of 4- and 5-positions on 2-1*H*-imidazolyl group with either electron-donating or -accepting substituents have a minor influence on the σ_p values. It

is concluded that the resonance effect, which stabilizes the conjugated acid by the contribution of certain resonance structures ($X^- — Y \rightleftarrows X — Y^-$), of the 2-1*H*-imidazolyl group makes the major contribution to the σ_p value, because 2-1*H*-imidazolyl has several kinds of resonance structures.

Table 2-7. Estimated Hammett's constant (σ_p) of 2-1*H*-imidazolyl, 2-imidazolio, and 2-imidazolide groups together with related ones.

R_2	σ_p	R_2	σ_p
2-imidazolyl	0.24	4,5-dimethyl-2-imidazolio	0.82
4,5-dimethy-2-limidazolyl	0.25	4,5-dibromo-2-imidazolide	-0.28
4,5-dibromo-2-imidazolyl	0.23	4,5-dichloro-2-imidazolide	-0.26
4,5-dichloro-2-imidazolyl	0.25	4,5-dicyano-2-imidazolide	-0.39
4,5-dicyano-2-imidazolyl	0.19	$-N(CH_3)_3^+$	0.82[a]
-Cl	0.23[a]	$-NO_2$	0.75[a]
-Br	0.23[a]	$-OCH_2O-$	-0.17[a]
		-O-	-0.81[a]
		-OH	-0.37[a]
2-pyridinyl	0.17[a]	3-pyridinyl	0.25[a]
5-pyrimidinyl	0.39[a]	1-phenyl-1*H*-benzoimidazol-2-yl	0.21[a]

a) Cited from Ref. 26.

The equation 2.2.3 and pK_{a1} of $H4TMBIM^{2+}$ give a σ_p of 4,5-dimethyl-2-imidazolio (σ_p = 0.82) which is the same as that of trimethylammonium (σ_p = 0.82) and slightly higher than that of a nitro group (σ_p = 0.75).[26] The σ_p values of 2-imidazolide groups (σ_p = -0.26 ~ -0.39) deduced from equation 2.4 and pK_{a4} of H2BIM derivatives is between those of $-OCH_2O-$ (σ_p = -0.17) and -O- (σ_p = -0.81), and are close to that of hydroxy group (σ_p = -0.37).[26]

The pK_{a1} of the H2BIM framework, which is a deprotonation at the 1-position, is governed by the field and inductive effects at 4- and 5- substituted groups and the resonance one of the remaining imidazolium (σ_p ~ 0.8) at the 2-position. The pK_{a2}, which is a deprotonation on the remaining imidazolium ring, is affected by the 4'- and 5'-substituted groups and the imidazolyl (σ_p ~ 0.2) at 2'-position. The pK_{a3}, where the deprotonation occurs in one of two 1*H*-imiadzolyl rings, say at the 3'-position, is

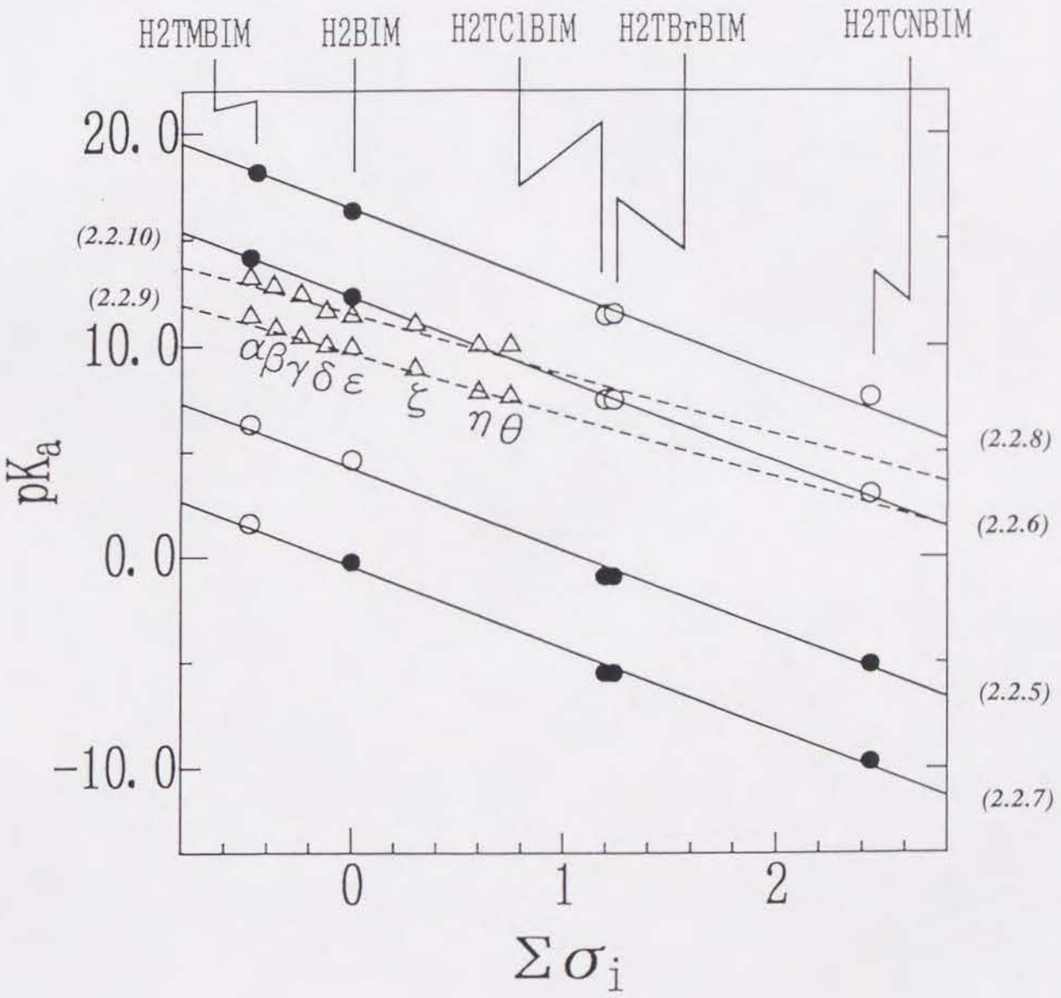

Fig. 2-6. $\Sigma\sigma_i$ vs. pK_a of 2,2'-bi-1*H*-imidazole and hydroquinone systems. The lines are represented by the equation number in text. The open and closed circles correspond to the measured and estimated pK_a values, respectively. For dotted lines, the pK_{a1} and pK_{a2} data (triangular circles); α, Me_4-H2Q; β, Me_3-H2Q; γ, 2,5-Me_2-H2Q; δ, Me-H2Q; ε, H2Q; ζ, Cl-H2Q; η, 2,5-Cl_2-H2Q; θ, 2-NO_2-H2Q in water were cited from Ref. 33.

influenced by the effects at 4'-, 5'-substituted groups and the 1*H*-imidazolyl (σ_p ~ 0.2) at the 2'-position. So the pK_{a2} and pK_{a3} have similar field, inductive, and resonance effects. Finally the pK_{a4}, say the last proton is on the 3-position, is governed by the effects at 4- and 5-substituted groups and the neighboring 2-imidazolide (σ_p ~ -0.3) at the 2-position.

2-3-2-5 pK_a Prediction for H2BIM System and Comparison with Another System

The predicted pK_{a2} and pK_{a3} indicated in parenthesis in Table 2-5 were obtained from equations 2.2.3 and 2.2.4 using the σ_p values in Section 2-3-2-4. For example, the pK_{a3} of $H4TMBIM^{2+}$ was estimated by Hammett's constants for methyl (σ_m and σ_p) and 4,5-dimethyl-2-1*H*-imidazolyl (σ_p) groups having been determined as -0.07, -0.17, and 0.25, respectively. So the $\Sigma\sigma_i$ was obtained as 0.01, which leads to the pK_{a3} as 14.15 (pK_{a3} = 14.23 - 8.00 x 0.01 = 14.15).

Figure 2-6 shows the plots of pK_a and $\Sigma\sigma_i$ based on the H2BIM framework; The open and closed circles correspond to the observed and the predicted pK_a values, respectively. Two equations, 2.2.5 and 2.2.6, assuming the same slope,

$$pK_{a2} = 4.20 - 3.88\Sigma\sigma_i \qquad (2.2.5)$$

and

$$pK_{a3} = 12.28 - 3.88\Sigma\sigma_i \qquad (2.2.6),$$

were obtained by the least-squares method based on the pK_{a2} and pK_{a3} data in Table 2-5. Even though the confidence of estimated pK_{a1} and pK_{a4} values are not high owing to the restricted experimental data, I can get two equations,

$$pK_{a1} = -0.46 - 3.88\Sigma\sigma_i \qquad (2.2.7)$$

and

$$pK_{a4} = 16.44 - 3.88\Sigma\sigma_i \qquad (2.2.8).$$

Here the slope was adjusted to 3.88, just as in the previous equations. By the replacement of the molecular framework of $H2IM^{+}$ by $H4BIM^{2+}$, the dissociation sites are increased twice. As a result, the susceptibility to substitution effects in equations 2.2.5 ~ 2.2.8 for the H2BIM system are reduced to approximately one-half of that of simple 1*H*-imidazoles. The triangular points in Fig. 2-6 show the pK_a of hydroquinone (H2Q) system measured in water (Scheme 2-8).[33]

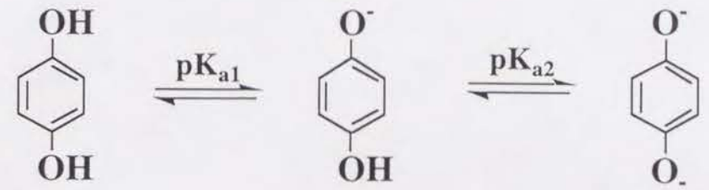

Scheme 2-8

Two dotted straight lines for the H2Q system,

$$pK_{a1} = 9.96 - 2.38\Sigma\sigma_i \qquad (2.2.9)$$

and

$$pK_{a2} = 11.67 - 2.38\Sigma\sigma_i \qquad (2.2.10),$$

are obtained by the least-squares method assuming the same slope. The ρ value of H2Q system (ρ = 2.38) is smaller than for the H2BIM system (ρ = 3.88) indicating that the electron density of nitrogen atoms of H2BIM framework has a higher sensitivity than that of the oxygen atoms of H2Q system toward the substitution. The comparison of acidity between H2BIM and H2Q systems was done under the same measurement conditions. Since the pK_{a1} value of H2Q (pK_{a1} = 9.85 and pK_{a2} = 11.39 in water[33]) is higher than 12.0 in DMF-H_2O (7:3), I examined the pK_a values of more acidic H2Q derivatives; polychloro- and polycyano-substituted hydroquinones. Cl_4-H2Q (pK_{a1} = 6.43 and pK_{a2} = 8.21) has the acidity as strong as CN_2-H2Q (pK_{a1} = 6.54 and pK_{a2} = 8.32), and H2DDQ (pK_{a1} = 5.14 and pK_{a2} = 7.46) is the most acidic one in our study

of the H2Q system. It turned out that $H3BIM^+$ (pK_{a2} = 4.60) is a stronger acid than H2DDQ. Consequently, it is expected that the proton-donating nature of $H4BIM^{2+}$ is considerably superior to the H2Q system. Even the pK_{a3} values of H2TClBIM and H2TBrBIM are slightly lower than Cl_4-H2Q and CN_2-H2Q.

The two-step reduction process of $TCNQ^0$ gives the dianion species $TCNQ^{2-}$, which is also obtained by the two-step acid dissociation processes of the $H2TCNQ^0$, $H2TCNQ^0 \rightarrow HTCNQ^- + H^+$ and $HTCNQ^- \rightarrow TCNQ^{2-} + H^+$. Since TCNQ has proven its excellency in electron-accepting ability in the CT process, it is of significance to examine the pK_a values of the H2TCNQ system. However no pK_a data for H2TCNQ derivatives and other typical electron acceptors have been reported except for BTDA-H2TCNQ (pK_{a2} = -0.2 in water)[34] and H2TCNE (pK_{a1} = 3.6 in water).[35] The pK_a values of H2TCNQ, Me_2-H2TCNQ, and F_4-H2TCNQ in DMF-H_2O (7:3) indicate that F_4-H2TCNQ has the highest acidity (pK_{a1} = 4.01 and pK_{a2} = 7.20), more than H2TCNQ (pK_{a1} = 7.10 and pK_{a2} = 10.30) and Me_2-H2TCNQ (pK_{a1} = 7.60 and pK_{a2} = 11.30). The dianion state is stabilized in the case of strong electron acceptors (A^0); for example, 2,3,5,6-tetracyano-7,7,8,8-tetracyanoquinodimethane (CN_4-TCNQ) can be isolated only as dianion species (A^{2-}),[2a] and this implies that $H2A^0$ is a very strong proton donor. Consequently, in general, there is a correlation between electron-accepting abilities ($E_{1/2}(1)$ and $E_{1/2}(2)$) of A^0 states and proton-donating abilities (pK_{a1} and pK_{a2}) of $H2A^0$ states among the structurally related molecules. Therefore, the extremely strong proton-donating ability of BTDA-H2TCNQ cannot be expected from its moderate electron-accepting ability of BTDA-TCNQ, suggesting that the anomalous enhancement of the proton-donating ability of BTDA-H2TCNQ may be structurally caused.

Scheme 2-9 compares the pK_a values necessary for the reaction between the H2BIM and TCNQ derivatives

$$H4BIM^{2+} \xrightarrow[-0.24]{pK_{a1}} H3BIM^+ \xrightarrow[4.60]{pK_{a2}} H2BIM \xrightarrow[12.31]{pK_{a3}} HBIM^-$$

$$F_4\text{-}H2TCNQ^0 \xrightarrow[4.01]{pK_{a1}} F_4\text{-}HTCNQ^- \xrightarrow[7.20]{pK_{a2}} F_4\text{-}TCNQ^{2-}$$

$$H2TCNQ^0 \xrightarrow[7.10]{} HTCNQ^- \xrightarrow[10.30]{} TCNQ^{2-}$$

$$Me_2\text{-}H2TCNQ^0 \xrightarrow[7.60]{} Me_2\text{-}HTCNQ^- \xrightarrow[11.30]{} Me_2\text{-}TCNQ^{2-}$$

Scheme 2-9

$H3BIM^+$ is a weaker proton donor than F_4-H2TCNQ by 0.6 pK_a unit, but is stronger than H2TCNQ and Me_2-H2TCNQ by 2.50 - 3.00 pK_a units. Therefore, the following reaction, H2BIM + H2TCNQ (Me_2-H2TCNQ) $\rightarrow$ $H3BIM^+$ + $HTCNQ^-$ (Me_2-$HTCNQ^-$), is entirely negligible, but the reverse PT reaction, $H3BIM^+$ + $HTCNQ^-$ (Me_2-$HTCNQ^-$) $\rightarrow$ H2BIM + H2TCNQ (Me_2-H2TCNQ), will easily occur. About the solid CT complex formation between the H2BIM and H2TCNQ systems, the difference of pK_a in the component molecules is one of the parameters that govern the physical properties and structures of the solid.

2-3-2-6 On-site Coulomb Repulsion of Proton-Transfer

In the case of dibase or diacid compounds, the charges of molecules vary from neutral, monovalent, to divalent states or vice versa by two-step PT processes; $H2D^0 \rightarrow HD^- + H^+$ ($H2A^{2+} \rightarrow HA^+ + H^+$) and $HD^- \rightarrow D^{2-} + H^+$ ($HA^+ \rightarrow A^0 + H^+$). The two-step PT processes are similar to the two-step CT ones and the parameters of PT processes are expressed by the acid dissociation constants (pK_a) instead of the half-wave redox potentials ($E_{1/2}$) in CT processes. The exact ability for a PT process relates to the proton affinity in the gas phase,[36] since the value of pK_a in solution is appreciably influenced by the solvation energy. For large numbers of organic molecules, however,

the pK_a values are available only in solution. I try here to evaluate the electrostatic energy for the PT process, namely the on-site Coulomb repulsion energy (U_1^{PT}) of the divalent state ($H2A^{2+}$ and D^{2-}) from the pK_a values in solution based on the same approaches at Section 2-3-1-5. The evaluations of U_1^{PT} value were done for H2BIM ($H4BIM^{2+}$), H2Q, H2TCNQ, and HPDS[37] systems (Table 2-8).

Table 2-8. Acid dissociation constants and estimated U_1^{CT} of H2BIM ($H4BIM^{2+}$), H2Q, H2TCNQ, and HPDS systems.

Compounds	pK_{a1} or pK_{a3}[a]	pK_{a2} or pK_{a4}[a]	ΔpK_a[b]	U_1^{PT}(eV)
H2BIM (H4BIM^{2+})	***system***			
a: $H4TMBIM^{2+}$	1.60	6.30	4.70	4.27
b: $H4BIM^{2+}$	-0.24	4.60	4.84	4.26
c: $H4TClBIM^{2+}$	-5.52	-0.94	4.58	4.25
d: $H4TBrBIM^{2+}$	-9.68	-0.94	4.58	4.25
e: $H4TCNBIM^{2+}$	14.15	-5.10	4.58	4.25
f: H2TMBIM	12.31	18.17	4.02	4.29
g: H2BIM	12.31	16.33	4.02	4.29
h: H2TClBIM	7.45	11.40	3.95	4.28
i: H2TBrBIM	7.44	11.50	4.06	4.28
j: H2TCNBIM	2.99	7.60	4.61	4.27
H2Q system				
k: 2,5-$(NO_2)_2$-DHQ[c]	-3.00	-0.50	2.50	4.13
l: 2,5-$(Cl)_2$-DHQ[c]	1.09	2.42	1.33	4.14
m: DHQ[c]	2.71	5.18	2.47	4.14
n: H2DDQ	5.14	7.46	2.32	4.14
o: $(Cl)_4$-H2Q	6.43	8.21	1.78	4.15
p: 2,3-$(CN)_2$-H2Q	6.54	8.31	1.77	4.15
q: 2,6-$(Cl)_2$-H2Q[c]	7.30	9.99	2.69	4.15
r: 2,5-$(Cl)_2$-H2Q[c]	7.90	10.00	2.10	4.15
s: Cl-H2Q[c]	8.90	11.90	3.00	4.15
t: H2Q[c]	9.85	11.39	1.54	4.15
u: (MeO)-H2Q[c]	9.91	11.90	1.99	4.15
v: (Me)-H2Q[c]	10.05	11.62	1.57	4.15
w: 2,5-$(Me)_2$-H2Q[c]	10.35	12.40	2.05	4.15
x: $(Me)_3$-H2Q[c]	10.80	12.90	2.10	4.15
y: $(Me)_4$-H2Q[c]	11.25	13.20	1.95	4.15
H2TCNQ system				
A: F_4-H2TCNQ	4.01	7.20	3.19	4.22
B: H2TCNQ	7.10	10.30	3.20	4.22
C: Me_2-H2TCNQ	7.60	11.30	3.70	4.22
HPDS system				
D: HPS[d]	12.30	13.10	0.80	4.08
E: HPSe[d]	12.50	13.00	0.50	4.08
F: HPDS[d]	11.90	12.50	0.60	4.08
G: HPTB[d]	12.00	12.60	0.60	4.08
H: HPTN[d]	11.90	12.50	0.60	4.08

a) pK_{a3} is for $H2BIM \rightarrow HBIM^- + H^+$. pK_{a4} is for $HBIM^- \rightarrow BIM^{2-} + H^+$. b) ΔpK_a = pK_{a2} or pK_{a4} - pK_{a1} or pK_{a3}. c) Cited from Ref. 33. d) Cited from Ref. 37 and the molecular structures are shown in Fig. 2-1d.

In the case of the H2Q system, the values of ΔpK_a are within the ΔpK_a range from 1.33 to 3.00, while those of the $H4BIM^{2+}$ (H2BIM) system range from 3.95 to 4.84, which is larger than the former system. The compounds with similar molecular frameworks have the same extent of ΔpK_a values, which suggests the correlation of pK_{a1} or pK_{a3} and pK_{a2} or pK_{a4} (Fig. 2-7). By the method of the least-squares, the relation is expressed as

$$H4BIM^{2+}\ (H2BIM)\ \text{system};\ pK_{a2}\ \text{or}\ pK_{a4} = 0.972pK_{a1}\ \text{or}\ pK_{a3} + 4.476 \qquad (2.2.11),$$

where the slope and intercept of $H4BIM^{2+}$ and H2BIM systems are the same, respectively, within the experimental error (line i). A linearity is also observed for the H2Q (line iii) system.

$$H2Q\ \text{system};\ pK_{a2} = 0.974pK_{a1} + 2.288 \qquad (2.2.12).$$

Similarly for the case of H2TCNQ (line ii) and HPDS (line iv) systems, equations 2.2.13 and 2.2.14 are obtained, though the numbers of observed data are limited, assuming the same slope as 0.97.

H2TCNQ system; $pK_{a2} = 0.97pK_{a1} + 3.550$ (2.2.13),

and

HPDS system; $pK_{a2} = 0.97pK_{a1} + 0.984$ (2.2.14).

The values of the intercept increase in the order of the HPDS, H2Q, H2TCNQ, and H2BIM ($H4BIM^{2+}$) systems. This order corresponds to the degree of ΔpK_a, which relates to the value of U^1_{PT} as following.

The experimental relation between pK_{a1} or pK_{a3} and pK_{a2} or pK_{a4} is represented as the form of

$$pK_{a2} \text{ or } pK_{a4} = \alpha(pK_{a1} \text{ or } pK_{a3}) + \beta \quad (2.2.15).$$

In the gas phase, the total energy change for the first acid dissociation process, $H2D^0 \rightarrow HD^- + H^+$ corresponds to $E^t_1 - E^t_0$, where E^t_0 and E^t_1 are the total energies of $H2D^0$ and HD^- species, respectively. In solution, it is needed to add the term of solvation, so the energy difference of two states is represented as the following equation,

$$E^t_1 - E^t_0 = 2.303RT(pK_{a1} \text{ or } pK_{a3}) - \Delta G'_{sol} + C_1 \quad (2.2.16),$$

where $\Delta G'_{sol}$ is the change of the solvation energies for $H2D^0$ and HD^- species, C_1 is a constant which depends on the glass electrode.[38] Similarly for the second (or fourth for the H2BIM system) acid dissociation process of $HD^- \rightarrow D^{2-} + H^+$, the change of total energy is expressed by

$$E^t_2 - E^t_1 = 2.303RT(pK_{a2} \text{ or } pK_{a4}) - \Delta F'_{sol} + C_1 \quad (2.2.17),$$

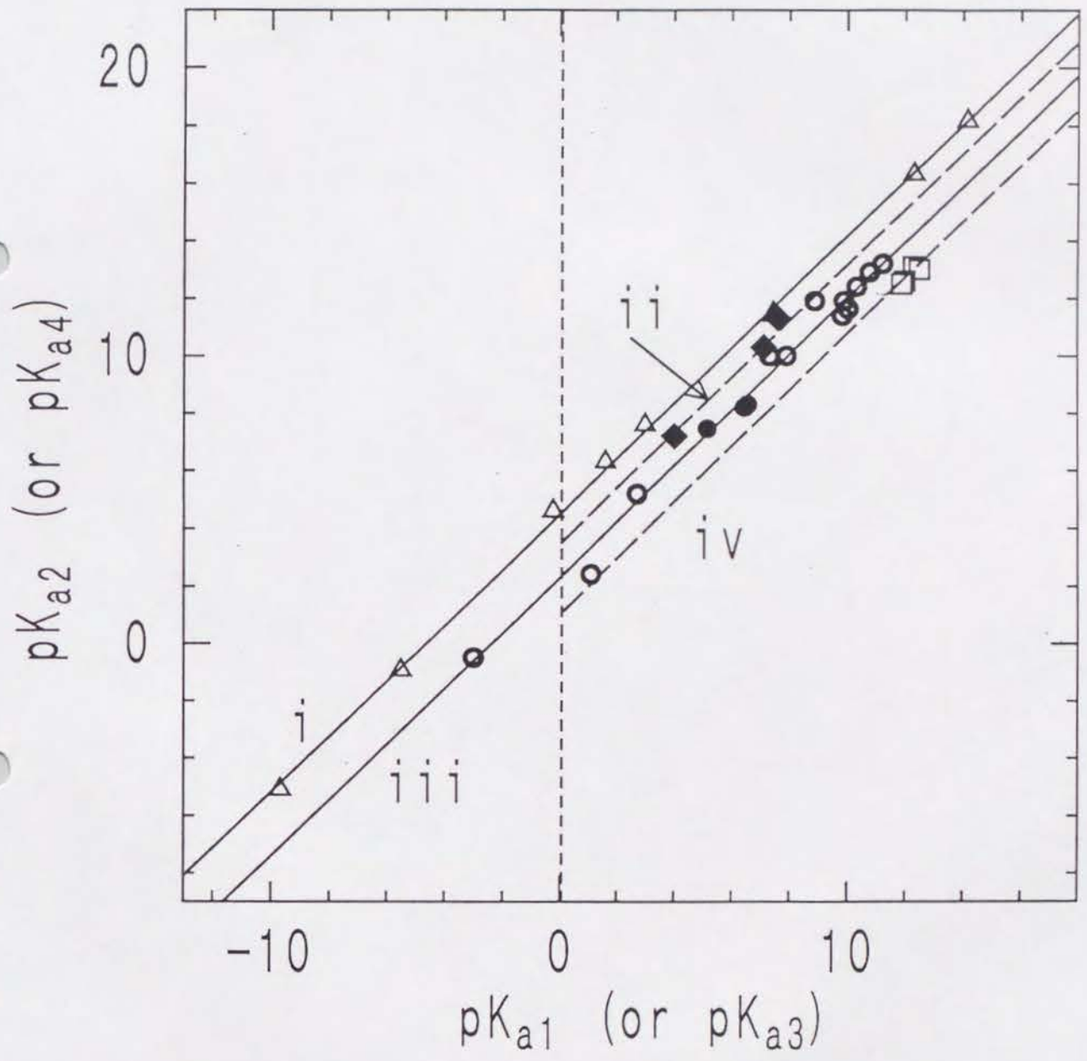

Fig. 2-7. The linear relationship between pK_{a1} (pK_{a3}) vs. pK_{a2} (pK_{a4}) of i) $H4BIM^{2+}$ (H2BIM) system (triangular circles), ii) H2TCNQ (closed squares), iii) H2Q (open and closed circles) and iv) HPDS (open squares) systems. The open and closed circles in H2Q system correspond to pK_a values of our measurement and these of Ref. 33, respectively.

where E^t_2 is the total energy of the D^{2-} molecule and $\Delta F'_{sol}$ is the difference of solvation energies for HD^- and D^{2-} species. The equations 2.2.16 and 2.2.17 will give the equation 2.2.18.

$$2.303RT(pK_{a2} \text{ or } pK_{a4}) = 2.303RT(pK_{a1} \text{ or } pK_{a3}) + (E^t_2 + E^t_0 - 2E^t_1) - \Delta G'_{sol} + \Delta F'_{sol} \quad (2.2.18)$$

The U_1^{PT} value can be defined as the disproportional energy for the process of $2HD^- \rightarrow H2D^0 + D^{2-}$, which is equal to the term within the parenthesis in equation 2.2.18. The term of solvation energy is deduced as $2\Delta G'_{sol}$ assuming the same procedure at Section 2-3-1-5.

$$2.303RT(pK_{a2} \text{ or } pK_{a4}) = 2.303RT(pK_{a1} \text{ or } pK_{a3}) + U_1^{PT} + 2\Delta G'_{sol} \quad (2.2.19).$$

Similarly for the PT processes of $H2A^{2+} \rightarrow HA^+ + H^+$ and $HA^+ \rightarrow A^0 + H^+$, namely the first and second dissociation steps of $H4BIM^{2+}$, the following equation can be derived,

$$2.303RTpK_{a2} = 2.303RTpK_{a1} + U_1^{PT} - 2\Delta G''_{sol} \quad (2.2.20),$$

where U_1^{PT} ($= E'^t_2 + E'^t_0 - 2E'^t_1$ and E'^t_2 is the total energy of $H2A^{2+}$ and so on) is the on-site Coulomb repulsion energy of $H2A^{2+}$. $\Delta G''_{sol}$ is the difference of solvation energies of HA^+ and A^0 species and is approximated as $-\Delta G'_{sol}$. The equations 2.2.15 and 2.2.19 lead to the following formula,

$$U_1^{PT} = -2.303RT(1-\alpha)(pK_{a1} \text{ or } pK_{a3}) + 2.303RT\beta - 2\Delta G'_{sol} \quad (2.2.21).$$

No precise values of $\Delta G'_{sol}$ for the systems under examination have been measured, unfortunately, so I roughly approximated it by the value for aromatic hydrocarbons (-2.0 eV).[22] As a result, the individual values of U_1^{PT} at 295 K for the H2BIM ($H4BIM^{2+}$), H2TCNQ, H2Q, and HPDS systems can be represented as the following equations,

H2BIM ($H4BIM^{2+}$) system; $U_1^{PT} = -0.00176(pK_{a1} \text{ or } pK_{a3}) + 4.26$ (2.2.22),

H2TCNQ system; $U_1^{PT} = -0.00176pK_{a1} + 4.21$ (2.2.23),

H2Q system; $U_1^{PT} = -0.00176pK_{a1} + 4.13$ (2.2.24),

and

HPDS system; $U_1^{PT} = -0.00176pK_{a1} + 4.06$ (2.2.25).

The estimated U_1^{PT} values decrease in the order of H2BIM ($H4BIM^{2+}$), H2TCNQ, H2Q, and HPDS systems (Table 2-8). In each system, the differences of U_1^{PT} value are less than 0.02 eV because of its insensitivity to the pK_{a1} or pK_{a3} value.

ΔpK_a, r^{-1}, and the estimated U_1^{PT} are summarized in Table 2-9, where the data for dicarboxylic acid ($HOOC(CH_2)_nCOOH$; DCAR),[39] 4,4'-biphenyldiol (BPH),[29] Bz,[29] and terephthalic acid (PHTH)[29] are compared. The distance r is derived as the same procedure in Section 2-3-1-5. The correlations between the estimated U_1^{PT} and r^{-1} for these systems are shown in Fig. 2-8.

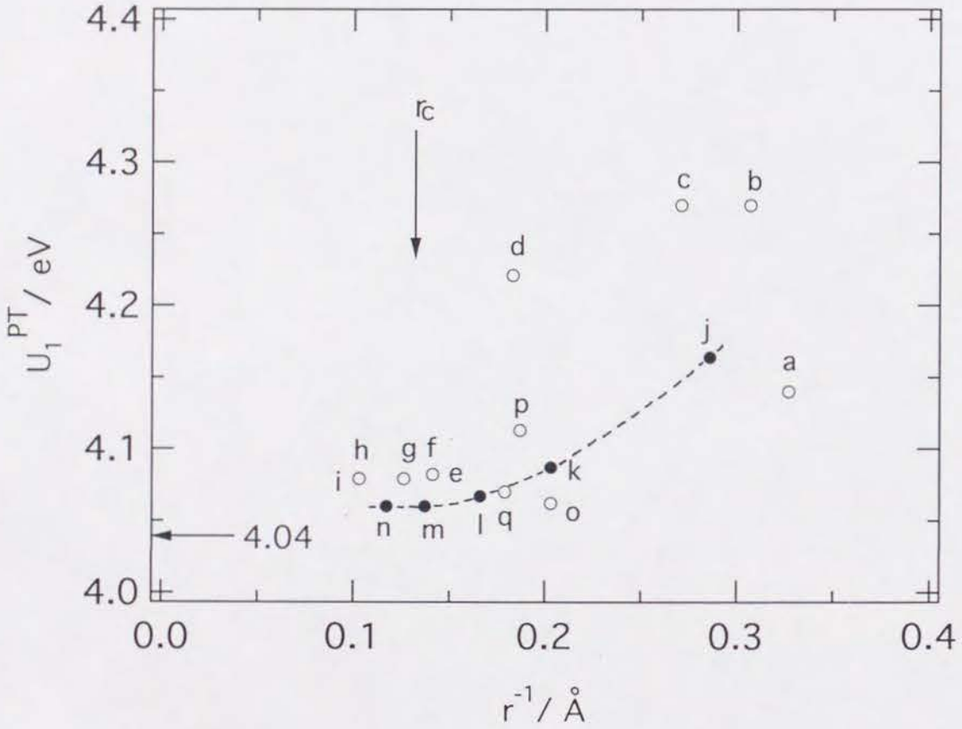

Fig. 2-8. The relation of U_1^{PT} (eV) and r^{-1} ($Å^{-1}$) for H2BIM, H2Q, H2TCNQ, HPDS (open circles), and DCAR (closed circles) systems. The respective species of HPDS system are depicted in Fig. 2-1d. r_c is the critical length for U_1^{PT} values. The dotted line is a guide for eye of DCAR system.

Table 2-9. ΔpK_a, r^{-1}, and estimated U_1^{PT} of related molecules.

Compounds	ΔpK_a [a]	r^{-1} [b] $Å^{-1}$	U_1^{PT} [c] eV
a:H2Q	1.54	0.327	4.140
b:H4BIM	4.84	0.307	4.270
c:H2BIM	4.02	0.271	4.270
d:H2TCNQ	3.20	0.183	4.221
HPDS system [d]			
e:HPS	0.80	0.141	4.082
f:HPSe	0.50	0.141	4.082
g:HPDS	0.60	0.126	4.079
h:HPTB	0.60	0.103	4.079
i:HPTN	0.60	0.103	4.079
DCAR system [e]			
j:n=1	2.63	0.286	4.164
k:n=2	1.24	0.203	4.087
l:n=3	0.90	0.166	4.067
m:n=4	0.77	0.137	4.060
n:n=5	0.77	0.117	4.060
Another system			
o:PHTH[f]	0.84	0.203	4.062
p:BPH[f]	1.30	0.187	4.113
q:Bz[f]	1.10	0.179	4.077

a) ΔpK_a is the same as Table 2-8. b) r is the same as Table 2-4. c) U_1^{PT} is estimated from equation 2.2.15 assuming the α as 0.97. d) Measured in DMF-H_2O (7:3) from Ref. 39. e) DCAR is $HOOC(CH_2)_nCOOH$ series and n is the number of methylenes. f) pK_a data of PHTH (terephthalic acid), BPH (4,4'-biphenyldiol), and Bz are cited from Ref. 29.

The values of U_1^{PT} of DCAR system show a linear decrease against the value of r^{-1} in the small r range and tend to saturate in the large r range (r_c > 7 Å). For this system, if two dissociation sites of diacidic base are perfectly independent of each other, for example n = ∞ in $HOOC(CH_2)_nCOOH$ molecules, the difference of pK_{a1} and pK_{a2} is equal to 0.6 (= log 4) from a statistical reason,[39] namely the equilibriium constant of the first dissociation process (K_{a1}) is four times larger than that of the second one (K_{a2}). In the short r region, the ratio of K_{a1}/K_{a2} becomes larger than 4 due to the electrostatic

repulsion of the two sites. From equation 2.2.19, the U_1^{PT} (1/r = 0) is estimated as 4.04 eV from the relation of $pK_{a2} = pK_{a1} + 0.6$. Approximately, the same feature of U_1^{PT} vs. 1/r is seen among H2BIM ($H4BIM^{2+}$), H2Q, HPDS, PHTH, BPH, and Bz systems, though the U_1^{PT} value of H2TCNQ system is rather out of the expected point. In the course of my titration measurements of H2TCNQs in DMF-H_2O (7:3), the colorless solution changes to a slightly green one in the second acid dissociation process which may suggest instability of the $TCNQ^{2-}$ species. At this moment, I do not have confidence whether the deviation of H2TCNQ data is intrinsic or not. The general features of Fig. 2-8 are as follows. The value of U_1^{PT} increases as the decreasing of r value with a weak correlation with the topological molecular structure, either Weitz or Würster type. And the U_1^{PT} values emerge within 4.06 ± 0.02 eV in the region r > 7 Å, while in the r < 7 Å region the U_1^{PT} values are dominated by the distance r.

2-4 Summary

I examined the proton-transfer and electron (charge)-transfer properties of the H2BIM system in solution. This system belongs to a new CT and PT system that has a Weitz's type molecular structure. Furthermore the evaluations of on-site Coulomb repulsion of the CT process (U_1^{CT}) were done for various types of molecules, including $H4BIM^{2+}$, and I discussed the relation with the molecular structures (Würster and Weitz types). At the same time, the concept of U_1^{PT} was proposed for the two-step PT process. The value of U_1^{PT} of H2BIM system was estimated and compared with those of the H2Q, H2TCNQ, and HPDS systems.

Seven new species; $H4BIM^0$, $H4BIM^{+\bullet}$, $H4BIM^{2+}$, $H3BIM^+$, $H3BIM^\bullet$, $H2BIM^{-\bullet}$, and $H2BIM^{+\bullet}$, in addition to known five species; $H2BIM^0$, $HBIM^-$, BIM^{2-}, $BIM^{-\bullet}$, and BIM^0 were confirmed among the twenty-five ideal ones in solution. Despite the isoelectronic structure of $H4BIM^{2+}$ and TTF^{2+}, the reduction peak potential of $H4BIM^{2+}$ was largely suppressed (about -1.2 V) by the isoelectronic substitution of four sulfur atoms of TTF by four imino groups. However, the value of U_1^{CT} in

$H4BIM^{2+}$ becomes on the same order of that in TTF^{2+}. From the results of EHMO calculation, the ionic polarization structure was found to be essential for the stabilization of $H4BIM^{2+}$ state. The high stability of the monoprotonated state of $H3BIM^+$ is confirmed by its low electron-accepting ability as its reduction potential is comparable to that of the stable cation *N*-methylquinolinium. The neutral species of $H2BIM^0$ is a weak electron donor rather than acceptor.

The plots of the first and second reduction potentials for 43 kinds of molecules indicated that each type of molecular system, for example BQ, DPQ, and TCNQ systems, has an individual linear correlation, with the same slope but different intercepts between these potentials. I discussed the conventional procedure to estimate the value of U_1^{CT} from the redox properties and find interesting correlations between the estimated U_1^{CT} and the distances r between the centers of gravities of π-electron at a half unit of a molecule. As a result, two types of classification can be made, I) electron acceptors and II) dications. For electron acceptors, the degree of change in U_1^{CT} against the r values is bigger than dications. The value of U_1^{CT} in dication molecule is found to be insensitive to the molecular size.

The H2BIM framework has an essentially amphoteric acid-base character, so neutral H2BIM derivatives can change the PT characters from a base (H2TMBIM and H2BIM) to an acid (H2TClBIM, H2TBrBIM, and H2TCNBIM) according to the substituted groups covering the pH range from 1.5 to 12.0. I confirmed the linear relationship between pK_a and $\Sigma\sigma_i$ and the high sensitivity of substitution effects for 1*H*-imidazole framework. The σ_p values of 2-1*H*-imidazolyls are not influenced by the substituted groups at the 4'- and 5'-position, but the pKa values of H2BIM derivatives are influenced by the resonance contribution of the 2-1*H*-imidazolyl group. The acidity of $H3BIM^+$ was comparable to the first dissociation of H2DDQ, and that of $H4BIM^{2+}$ was further enhanced. The plots of the first acid dissociation constants and the second ones indicated a linear relationship for H2BIM and H2Q systems. From this linearity, the estimation of U_1^{PT} was done for H2BIM ($H4BIM^{2+}$), H2Q, H2TCNQ, and HPDS systems. The values of U_1^{PT} are related with the distances r regardless of whether the

molecule is the Würster or Weitz type, and show saturation in the U_1^{PT} values in the big r region ($r > 7$ Å).

1) K.Deuchert and S.Hünig, *Angew. Chem. Int. Ed. Engl.*, **17**, 875 (1978); b) S.Hünig and H.Berneth, *Top. Curr. Chem.*, **92**, 1 (1980).

2) a) R.C.Wheland and E.L.Martin, *J. Org. Chem.*, **40**, 3101 (1975); b) J.P.Ferraris and G.Saito, *J. Chem. Soc., Chem. Commun.*, 902 (1978); c) M.Uno, K.Seto, M.Masuda, W.Ueda, and S.Takahashi, *Tetrahedron Lett.*, **26**, 1553 (1985); d) Y.Yamashita, T.Suzuki, T.Mukai, and G.Saito, *J. Chem. Soc., Chem. Commun.* 1044 (1985).

3) a) O.Dimroth, E.Eber, and K.Wehr, *Justus Liebigs Ann. Chem.*, **446**, 132 (1926); b) A.G.Brok and R.P.Linsteud, *J. Chem. Soc.*, 3569 (1954); c) J.Thiele and F.Gunther, *Justus Liebigs Ann. Chem.*, **349**, 45 (1906); d) H.A.Torrey and W.H.Hunter, *J. Am. Chem. Soc.*, **34**, 702 (1912); e) J.William and H.Harold, *J. Am. Chem. Soc.*, **74**, 5215 (1952); f) C.R.H.Jouge, H.M.Dort, and L.Vollbracht, *Tetrahedron Lett.*, 1881 (1970); g) L.M.Jackman, *Adv. Org. Chem.*, **2**, 329 (1960).

4) The locations of substituents for TTF derivatives are shown in Fig. 2-1c. a) For leading references in 4b and 4c; b) M.Narita and C.U.Pittman Jr, *Synthesis*, 489 (1976); c) A.Krief, *Tetrahedron.*, **42**, 1209 (1986); d) G.Saito, *Pure & Appl. Chem.*, **59**, 999(1987); e) F.Wudl, H.Yamochi, T.Suzuki, H.Isotaro, C.Fite, H.Kasmani, K.Lious, G.Srdanov, P.Coppens, K.Maly, and A.F.Jensen, *J. Am. Chem. Soc.*, **112**, 2461(1990); f) H.Tatemitsu, E.Nishikawa, Y.Sakata, and S.Misumi, *J. Chem. Soc., Chem. Commun.*, 106 (1985); g) C.Gemmell, J.D.Kilburn, H.Veck, and A.E.Underhill, *Tetrahedron Lett.*, **33**, 3923 (1992).

5) H.Vollman, H.Becker, M.Corell, H.Streek, and G.Langbein, *Justus Liebigs Ann. Chem.*, **531**, 1 (1937).

6) a) N.Thorup, G.Rindorf, C.S.Jacobsen, K.Bechgaard, I.Johannsen, and K.Mortensen, *Mol, Cryst, Liq, Cryst.*, **120**, 349 (1985); b) K.Nakasuji, H.Kubota, T.Kotani, I.Murata, G.Saito, T.Enoki, K.Imaeda, H.Inokuchi, M.Honda, C.Katayama, and J.Tanaka, *J. Am. Chem. Soc.*, **108**, 3460 (1986).

7) C.Marschall and C.Stumm, *Bull. Soc. Chim. Fr.*, 418 (1948).

8) D.S.Acker and W.R.Hertler, *J. Am. Chem. Soc.*, **84**, 3370 (1962).

9) B.F.Fieselmann, D.N.Hendrickson, and G.D.Stucky., *Inorg. Chem.*, **17**, 2078 (1978).

10) a) E.E.Bernarducci, P.K.Bharadwaj, R.A.Lalancette, K.K.Jespersen, J.H.Potenza, and H.J.Schugar, *Inorg. Chem.*, **22**, 3911 (1983); b) K.Lehmstedt and H.Rolker, *Ber.*, **76**, 879 (1943); c) P.G.Apen and P.G.Rasmussen, *J. Am. Chem. Soc.*, **113**, 6178 (1991).

11) a) R.Hoffman and W.N.Lipscomb, *J. Chem. Phys.*, **36**, 2179 (1962); b) R.Hoffman and W.N.Lipscomb, *J. Chem. Phys.*, **37**, 2872 (1962); c) R.Hoffman, *J. Chem. Phys.*, **39**, 1367 (1963).

12) a) R.Pariser and R.G.Parr, *J. Chem. Phys.*, **21**, 466 (1953): b) N.Mataga and K.Nishimoto, *Z. Phys. Chem. Neue Folge*, **13**, 140 (1957); c) D.A.Lowitz, *J. Chem. Phys.*, **46**, 4698 (1967); d) K.Nisimoto and L.S.Forster, *Theoret. Chim. Acta*, **3**, 407(1965); e) K.Nishimoto and L.S.Forster, *Theoret. Chim. Acta.*, **4**, 155 (1966).

13) a) W.F.Cooper, N.C.Kenny, J.W.Edomonds, A.Nagel, F.Wudl, and P.Coppens, *J. Chem. Soc., Chem. Commun.*, 889 (1971).

14) See Chapter 3.

15) a) J.Metzger, H.Larive, R.Dennilauler, R.Baralle, and C.Gaurat, *Bull. Soc. Chim. Fr.*, **11**, 2857 (1964); b) M.R.Bryce, E.Fleckenstein, and S.Hünig, *J. Chem. Soc., Perkin Trans 2*, 1777(1990); c) V.Goulle, S.Chirayil, and R.P.Thummel, *Tetrahedron Lett.*, **31**, 1539 (1990); d) G.V.Tormos, O.J.Neilands, and M.P.Cava, *J. Org. Chem.*, **57**, 1008 (1992).

16) a) R.T.Oakely, J.F.Richardson, and R.E.H.Spencel, *J. Chem. Soc.. Chem. Commun.*, 1226 (1993); b) R.T.Oakely, J.F.Richardson, and R.E.H.Spencel, *J. Org. Chem.*, **59**, 2997 (1994).

17) M.Mohammad, *J. Org. Chem.*, **52**, 2779 (1987).

18) a) S.Hiroma, H.Kuroda, and H.Akamatu, *Bull. Chem. Soc. Jpn.*, **44**, 9 (1971); b) A.J.Epstein, S.Etemad, A.F.Garito, and A.J.Heeger, *Phys. Rev., B*, **5**, 952 (1972); c) J.B.Torrance, Y.Tomkiewicz, and B.D.Silverman, *Phys. Rev., B*, **15**, 4738 (1977).

19) P.A.Cox, "*The Electronic Structure and Chemistry of Solids*", Oxford Press, New York (1987).

20) E.C.M.Chen and W.E.Wentworth, *Mol. Cryst. Liq. Cryst.*, **171**, 271 (1989).

21) a) E.P.Grimsrud, G.Caldwell, S.Chowdhury, and P.Kebarle, *J. Am. Chem. Soc.*, **107**, 4627 (1985); b) P.Kebarle and S.Chowdhury, *Chem. Revs.*, **87**, 513 (1987); c) T. Heinis, S.Chowdhury, S.L.Scott, and P.Kebarle, *J. Am. Chem. Soc.*, **88**, 400 (1988).

22) R.M.Hedges and F.A.Matsen, *J. Chem. Phys.*, **28**, 950 (1958).

23) a) H.T.Jonkman and J.Kommandeur, *Chem. Phys. Lett.*, **15**, 496 (1972); b) H.T.Jonkman, G.A.V.Velde, and W.C.Nieuwpoort, *Chem. Phys. Lett.*, **25**, 62 (1974); c) J.Ladik, A.Karpfen, G.Stollhoff, and P.Fulde, *Chem. Phys.*, **7**, 267 (1975); d) A.Karpfen, J.Ladik, G.Stollhoff, and P.Fulde, *Chem. Phys. Lett.*, **31**, 291 (1975); e) A.J.Epstein, N.O.Lipari, D.J.Sandman, and P.Nielsen., *Phys. Rev., B*, **13**, 1569 (1976).

24) a) A.Aumuller and S.Hünig, *Liebigs Ann. Chem.*, 165 (1986); b) S.Iwatsuki, T.Itoh, and H.Itoh, *Chem. Lett.*, 1187 (1988); c) M.L.Kaplan, R.C.Haddon, F.B.Bramwell, F.Wudl, J.H.Marshall, D.O.Cowan, and S.Gronowitz, *J. Phys. Chem.*, **84**, 427 (1980); d) M.Maxfield, R.Heckendorn, D.O.Cowan, A.M.Kini, and M.Maxfield, *J. Am. Chem. Soc.*, **105**, 7017 (1983); e) K.Takahasi and T.Sakai, *Chem. Lett*, 157 (1993).

25) a) L.R.Melby, R.J.Harder, W.R.Hertler, W.Mahler, R.E.Benson, and W.E.Mochel, *J. Am. Chem. Soc.*, **84**, 3374 (1962); b) G.Saito and A.K.Colter, *Tetrahedron Lett.*, 3325 (1977).

26) C.Hansch, A.Leo, and R.W.Taft, *Chem. Revs.*, **91**, 165 (1991).

27) a) M.Paabo, R.G.Bates, and R.A.Robinson, *J. Phys. Chem.*, **70**, 247 (1966); b) H.Ohtaki, *Bull. Chem. Soc. Jpn.*, **42**, 1573 (1969).

28) M.R.Grimmett, "*Comprehensive Heterocyclic Chemistry*" Vol.5, edited by A.R.Katritzky and C.W.Rees, Pergamon press, New York, 345-456 (1984).

29) a) H.S.Harned and B.B.Owen, "*The Physical Chemistry of Electrolyte Solution*", 3rd ed, Reinhold Publishing Corp., New York (1958); b) J.A.Riddick and W.B.Bunger, "*Organic Solvents*", 3rd ed, Interscience (1970).

30) J.March, "*Advanced Organic Chemistry*" 4th ed, John Willy & Sons, Inc. 248-286 (1992).

31) a) H.H.Jaffe, *Chem. Revs.*, **53**, 191 (1953); b) P.P.Wells, *Chem. Revs.*, **63**, 171 (1963).

32) P.Tomasik and C.D.Johnson, *Adv. Heterocyclic Chem.*, **20**, 1 (1976).

33) a) L.Sacconi, *J. Phys. Chem.*, **54**, 829 (1950); b) C.A.Bishop and L.K.J.Tong, *J. Am. Chem. Soc.*, **87**, 501 (1965); c) P.J.Pearce and R.J.J.Simkins, *Can. J. Chem.*, **46**, 241 (1968).

34) Y.Yamashita, T.Suzuki, and T.Mukai, *J. Chem. Soc., Chem. Commun.*, 1184 (1987).

35) W.J.Middleton, R.E.Heckert, E.L.Little, and C.G.Krespan, *J. Am. Chem. Soc.*, **80**, 2783 (1958).

36) P.L.Huyskens, W.A.P.Luck, and T.Z.Huyskens, "*Intermolecular Forces*" Spring-Verlag, New York (1991).

37) K.Sugiura, J.Toyoda, H.Okamoto, K.Okaniwa, T.Mitani, A.Kawamoto, J.Tanaka, and K.Nakasuji, *Angew. Chem. Int. Engl*, **31**, 852 (1992); b) K.Sugiura, Doctoral Dissertation, The Graduate University for Advanced Studies and Institute for Molecular Science.

38) M.J.S.Dewar and T.Morita, *J. Am. Chem. Soc.*, **91**, 802 (1969).

39) P.G.Bonhomme, *Bull. Soc. Chim. Fr.*, **11**, 60 (1968).

Chapter 3. Crystal Structures and Charge-Transfer Complexes of 2,2'-Bi-1*H*-imidazole System

Studies of the crystal structures and formation of a charge-transfer (CT) complex proved that 2,2'-bi-1*H*-imidazole ($H2BIM^0$) forms a new system concerned with the interplay of proton - transfer (PT) and electron - transfer (or CT)) interactions. X-ray crystal analyses of newly isolated species, 2-(2-1*H*-imidazolyl)-1*H*-imidazolium ($H3BIM^+$) and 2,2'-bi-1*H*-imidazolium ($H4BIM^{2+}$), revealed the formation of strong hydrogen bonds along the side-by-side direction of the molecular plane. CT complexes of $H3BIM^+$ and $H4BIM^{2+}$ with the 7,7,8,8-tetracyanoquinodimethane derivatives (TCNQs) were synthesized by a method of metathesis, and the crystal structure of $(H3BIM^+)_2(TCNQ^-)_2(TCNQ^0)$ was determined.* During CT complex formation, the initial simple protonated states of $[H3BIM^+]$ or $[H4BIM^{2+}]$ changed to different ones, for example, $[H4BIM^{2+}]_x[H3BIM^+]_{1-x}$, $[H3BIM^+]_x[H2BIM^0]_{1-x}$, and $H2BIM^0$. According to the protonated states of the H2BIM system, the formal charge of the TCNQs in the CT complexes varies from completely ionic, partial CT, to neutral. The mechanism of these complex formations was explained by differences in the acidities between the TCNQ anion radicals ($TCNQs^{-\bullet}$) and $H3BIM^+$ or $H4BIM^{2+}$. Higher acidities of $H3BIM^+$ and $H4BIM^{2+}$ than the $TCNQs^{-\bullet}$ induce the following PT reaction: $H3BIM^+$ (or $H4BIM^{2+}$) + $TCNQs^{-\bullet} \rightarrow H2BIM^0$ (or $H3BIM^+$) + $HTCNQ^\bullet$. The isolation of $HTCNQ^\bullet$ was a failure due to the following disproportional reaction: $2HTCNQ^\bullet \rightarrow TCNQ^0 + H2TCNQ^0$. However, the formation of the 1,4-benzenedimalononitrile ($H2TCNQ^0$) was confirmed by an analysis of the residual compounds after complex formation. Although the electronic absorptions of TCNQ complexes indicated both the partial CT state of TCNQ and a segregated stacking manner, semiconductive characters were observed. In a crystal of $(H3BIM^+)_2(TCNQ^-)_2(TCNQ^0)$, the $H3BIM^+$ formed a planar dimer connected by two N-H•••N hydrogen bonds, and TCNQ molecules existed as a charge-separated state with segregated trimer stacks. These dimers and TCNQ stacks were tightly connected by both the N-H•••N≡C

hydrogen bonds, which spread into the overall crystal, and by the CT interaction. For the PT and CT system, I propose a synthetic strategy based on the redox potentials and acid dissociation constants.

* The tentative and the real chemical formulas are represented in parenthesis and brackets, respectively.

3-1 Introduction

Using the differences in the redox potentials ($\Delta E_{1/2} = E_{1/2}$(D or DH) - $E_{1/2}$(A or AH)), the synthetic strategy of the organic metal has been proposed by Wheland [1a] and Saito and Ferraris.[1b] For the PT process, the differences in the pK_a values ($\Delta pK_a = pK_a$ (DH or AH) - pK_a (D or A)) determine whether the proton is moved from DH (AH) to A (D) (DH or AH + A or D $\rightarrow$ D^- or A^- + AH^+ or DH^+) or not. Here, D and A are electron donor and acceptor molecules having proton-accepting ability, and HD and AH are electron donor and acceptor molecules having proton-donating ability. In some polynitrophenol - amine complexes, Saito and Inukai described the interconversion point from the CT to PT one.[2] To construct the CT and PT system, the acid-dissociation constants (pK_a) and half-wave redox potentials ($E_{1/2}$) of the component molecules are appropriate parameters.

From the viewpoints of a PT and CT system, I have been studying the 2,2'-bi-1*H*-imidazole (H2BIM) system (see Chapter 2). Figure 3-1 illustrates a part of the species within the 25 independent states, showing the known redox peak potentials (E_p) and acid-dissociation constants (pK_a). The acidic characters of 2-(2-1*H*-imidazolyl)-1*H*-imidazolium ($H3BIM^+$, pK_a = 4.60) and 2,2'-bi-1*H*-imidazolium ($H4BIM^{2+}$, pK_a = -0.24) are expected to be much higher than that of H2Q (pK_a = 10.5) or 2,3-dichloro-5,6-dicyanohydroquinone (pK_{a1} = 5.14 and pK_{a2} = 7.46) in an *N,N*-dimethylformamide (DMF) - H_2O (7:3) media. The electron-accepting abilities of the $H3BIM^+$ (reduction peak potential; E^r_p = - 0.84 V) and $H4BIM^{2+}$ (E^r_p = - 0.54 V) species are comparable

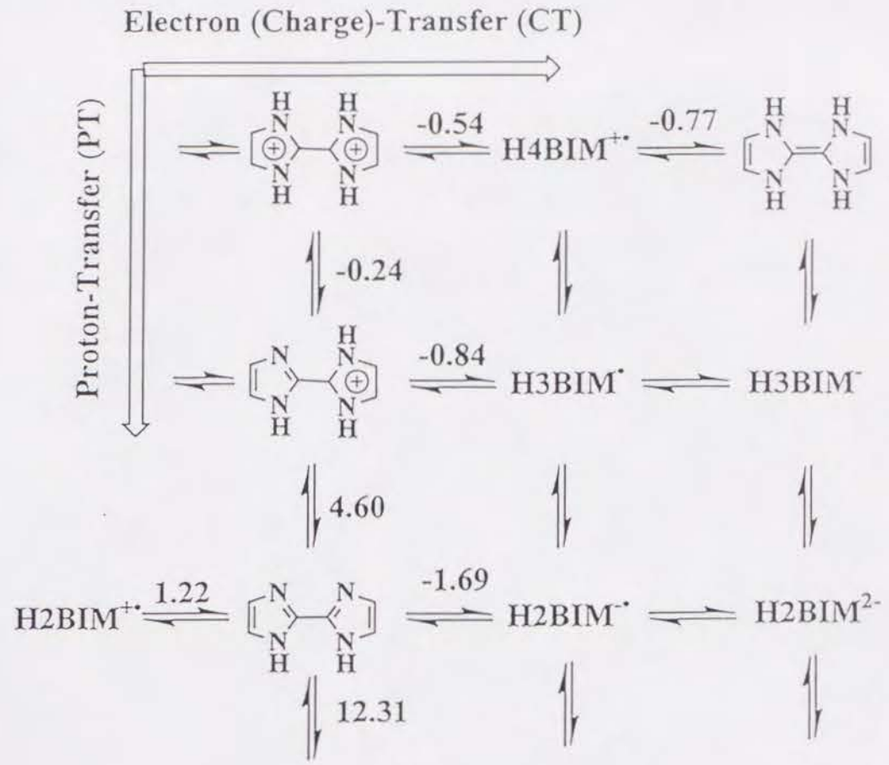

Fig. 3-1. Proton - transfer (PT) and electron (charge) - transfer (CT) diagram of 2,2'-bi-1*H*-imidazole system. Two step PT and CT processes of $H2BIM^0$ - $H4BIM^0$ system are drawn and part of species (BIM^0 - $H2BIM^0$) are omitted to clarify the figure. Each vertical and horizontal line corresponds to the PT and CT process, respectively. The reduction and oxidation peak potentials (E^r_p and E^o_p) and acid dissociation constants (pK_a) are cited from Chapter 2.

to that of 2,3,5,6,-tetramethyl-p-benzoquinone (E^r_p = -0.88 V) and 2,4,7-trinitro-9*H*-fluoren-9-one (E^r_p = -0.42 V), respectively. As a result, I expect that the CT ability of the H2BIM system is not very high, but that a high acidic character of $H3BIM^+$ and $H4BIM^{2+}$ influences the CT complex formations. To clarify the complicated protonated states of the H2BIM system, I prepared a variety of complexes of $H2BIM^0$, $H3BIM^+$, and $H4BIM^{2+}$ and examined the crystal structures, molecular vibrational spectra, electronic absorption spectra, and electric properties. The tentative chemical formula of the CT complex in parentheses was deduced only from an elemental analysis, and is represented by the initial components of complex formation. The real states of the component molecules in the complex, i.e. the valence states of TCNQs and the protonated states of the H2BIM system, deduced by spectroscopic, structural, and elemental analyses, are represented in brackets. The mechanism of these complex formations is discussed on the basis of the differences in the acidity (ΔpK_a) and redox potential ($\Delta E_{1/2}$) between $H3BIM^+$ or $H4BIM^{2+}$ and the anion radical of the TCNQ derivatives. The representative molecular structures in Chapter 3 are shown in Fig. 3-2.

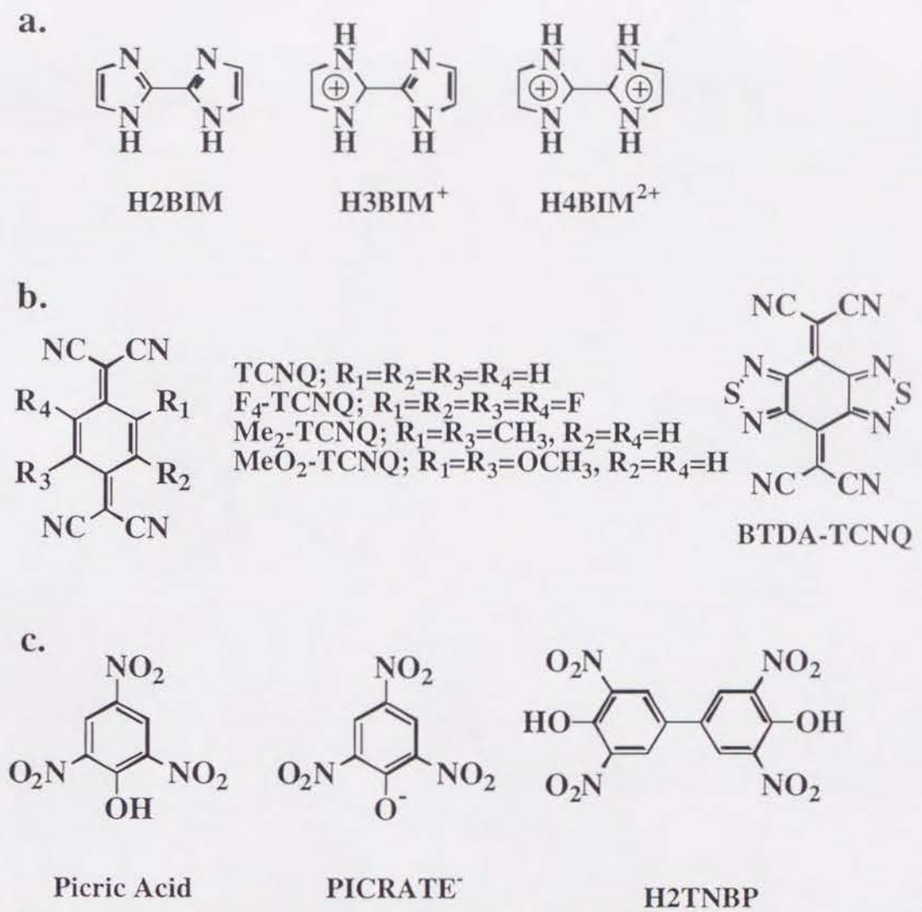

Fig. 3-2. The representative molecular structures appeared in this text. a) H2BIM series. b) TCNQ series. c) Picric acid, $PICRATE^-$, and 3,3',5,5'-tetranitrobiphenyl-4,4'-diol (H2TNBP).

3-2 Experimental

Materials. In Chapter 3, the compounds are described as the entry number of the underline. The preparations of 2,2'-bi-1*H*-imidazole ($H2BIM^0$) (**1**), 2-(2-imidazolyl)-1*H*-imizazolium iodide ($[H3BIM^+][I^-]$) (**2**), 2,2'-bi-1*H*-imidazolium diiodide ($[H4BIM^{2+}][I^-]_2$) (**3**), other closed shell cations (Cl^-, Br^-, and BF_4^- salts), and all of TCNQ derivatives were described in Chapter 2.

[H3BIM$^+$][PICRATE$^-$] (**4**): To a saturated solution of 0.5 mmol of (**2**) in 30 ml of methanol was added a solution of 0.5 mmol of $[Na^+][PICRATE^-]$ in 20 ml of methanol. After it was stirred for 3 h, the precipitates were collected and washed with water, then

methanol. Mp. 287°C (dec), yellow powder. Found: C,39.51; H,2.35; N,27.08%. Calcd for $C_{12}H_9N_7O_7$: C,39.69; H,2.48; N,27.00%.

[H4BIM^{2+}][PICRATE$^-$]$_2$ (**5**) and **[H4BIM^{2+}][TNBP^{2-}]** (**6**): To a suspended solution of 0.5 mmol of (**1**) in 300 ml of ethanol was added a solution of 1.0 mmol of picric acid in 50 ml of ethanol or a solution of 0.5 mmol of 3,3',5,5'-tetranitrobiphenyl-4,4'-diol ($H2TNBP^0$) in 100 ml of ethanol. It was refluxed for 3 h and cooled to room temperature; the precipitates were then collected and washed with ethanol. Single crystals were obtained by recrystallization from methanol for (**5**). (**5**); Mp. 258°C (dec), yellow needles. Found: C,36.69; H,1.99; N,23.63%. Calcd for $C_{18}H_{12}N_7O_{14}$: C,36.50; H,2.03; N,23.65%. (**6**); Mp. > 350°C, orange powder. Found: C,43.50; H,2.69; N,22.60%. Calcd for $C_{18}H_{12}N_8O_{10}$: C,43.22; H,2.40; N,22.40%.

[H2BIM^0]$_3$[H3BIM$^+$]$_2$[I$^-$]$_2$ (**7**): Recrystallization of (**2**) from acetonitrile gave single crystals of (**7**). Then, white needles were collected and washed with acetonitrile. Mp. 380°C. Found: C,39.20; H,3.53; N,30.44; I,27.40%. Calcd for $C_{30}H_{32}N_{20}I_2$: C,38.90; H,3.46; N,30.24; I,27.40%.

Preparation of Charge-Transfer Complexes

$H2BIM^0$ complexes: It was not possible to prepare the $H2BIM^0$ complexes in solution due to the low solubility of (**1**) in most organic solvents. Thus, the complex formations were prepared by the cosublimation method. There was no complex formation for the F_4-TCNQ, TCNQ, and BTDA-TCNQ cases. The infrared (IR) spectra and elemental analysis of the Me_2-TCNQ and MeO_2-TCNQ complexes deduced these complexes as $[H2BIM^{+\delta}][TCNQs^{-\delta}]$ with $\delta \approx 0$.

$H3BIM^+$ and $H4BIM^{2+}$ complexes: A preparation of CT complexes of $H3BIM^+$ and $H4BIM^{2+}$ was achieved by the method of metathesis[3] between lithium or sodium salts of $TCNQs^{-\bullet}$ and (**2**) and/or (**3**). Each anion radical salt of TCNQs was prepared by the reaction of neutral TCNQs and three molar amounts of anhydrous lithium iodide or sodium iodide in acetonitrile. The metathesis of the equimolar solution of Li salt of TCNQs and (**2**) gave 1:1 CT complexes. The 2:1 complex was prepared only with the combination of Me_2-TCNQ and $H3BIM^+$ by the use of a twice excess of (**2**); no other

stoichiometries other than 1:1 were realized for the combination of $H3BIM^+$ and other TCNQs, even using a wide range of concentrations of the components in the metathesis. However, the recrystallization of ($H3BIM^+$)($TCNQ^-$) (**11**) or ($H4BIM^{2+}$)($TCNQ^-$)$_2$ (**18**) from acetonitrile or methanol yields the 2:3 complex, ($H3BIM^+$)$_2$($TCNQ^-$)$_2$ ($TCNQ^0$) (**12**), as well-developed single crystals. The chemical formulas of the complexes are summarized in Table 3-1 in addition to the results of the elemental analysis, decomposition points (d.p.), and colour of the obtained CT complexes. The transition peaks of the ultra violet, visible and near-infrared (UV-VIS-NIR) spectra of these CT complexes are tabulated in Table 3-2.

($H2BIM^0$)(Me_2-$TCNQ^0$) (8) and ($H2BIM^0$)(MeO_2-$TCNQ^0$) (9): The equimolar component molecules (0.25 mmol of (**1**) and 0.25 mmol of TCNQs) were heated under a vacuum condition (200°C / 0.3 Torr) using an H-shaped cell to give (**8**) and (**9**).

($H3BIM^+$)(F_4-$TCNQ^-$)(10), ($H3BIM^+$)($TCNQ^-$) (11), ($H3BIM^+$)(BTDA-$TCNQ^-$) (13), ($H3BIM^+$)(Me_2-$TCNQ^-$) (14), and ($H3BIM^+$)(MeO_2-$TCNQ^-$) (16): To a saturated solution of 0.5 mmol of [Li^+][$TCNQs^{-\bullet}$], though [Na^+][F_4-$TCNQ^{-\bullet}$] was used for the (**10**) case, in absolute methanol was added a solution of 0.5 mmol of (**2**) in 10 ml of methanol; the mixture was stirred at room temperature for 30 min and left standing at -10°C overnight. The precipitates were collected and washed with cold methanol, then ether.

($H3BIM^+$)$_2$($TCNQ^-$)$_2$($TCNQ^0$) (12): Recrystallization of (**11**) or ($H4BIM^{2+}$)($TCNQ^-$)$_2$ (**18**) from methanol and/or acetonitrile gave single crystals of (**12**). Then, black blocks were collected and washed with cold methanol. The composition was changed from 1:1 or 1:2 to 2:3 after recrystallization.

($H3BIM^+$)$_2$(Me_2-$TCNQ^-$) (15): To a saturated solution of 0.5 mmol of [Li^+][Me_2-$TCNQ^{-\bullet}$] in methanol was added a solution of 1 mmol of (**2**) in 20 ml of methanol; the mixture was stirred at room temperature for 30 min and left standing at -10°C overnight. Green precipitates were collected and washed with cold methanol, then ether.

($H4BIM^{2+}$)(F_4-$TCNQ^-$)$_2$(H_2O)$_2$(17), ($H4BIM^{2+}$)($TCNQ^-$)$_2$(18), ($H4BIM^{2+}$)(BTDA-$TCNQ^-$)$_2$ (19), and **($H4BIM^{2+}$)$_3$(Me_2-$TCNQ^-$)$_4$(H_2O)$_2$ (20)**:

Table 3-1. Real Chemical Formula, Elemental Analysis, Decomposition Points (°C), and Crystal Colour of TCNQs CT Complexes.

Entry	Tentative formula[a)]	Real formula[b)]	Elemental analysis (%)[c)]	d.p.	Colour
8	$(H2BIM^0)(Me_2\text{-}TCNQ)$	$[H2BIM^{\sim 0}][Me_2\text{-}TCNQ^{\sim 0}]$	Found: C,65.76; H,3.92; N,30.66	280	Brown
		$C_{20}H_{14}N_8$	Calcd.: C,65.58; H,3.82; N,30.59		
9	$(H2BIM^0)(MeO_2\text{-}TCNQ)$	$[H2BIM^{\sim 0}][MeO_2\text{-}TCNQ^{\sim 0}]$	Found: C,60.27; H,3.42; N,27.98	310	Red
		$C_{20}H_{14}N_8O_2$	Calcd.: C,60.31; H,3.52; N,28.14		
10	$(H3BIM^+)(F_4\text{-}TCNQ^-)$	$[H3BIM^+][F_4\text{-}TCNQ^{-\bullet}]$	Found: C,52.06; H,2.33; N,27.22	280	Blue
		$C_{18}H_7N_8F_4$	Calcd.: C,52.57; H,1.70; N,27.25		
11	$(H3BIM^+)(TCNQ^-)$	$[H3BIM^+]_x[H2BIM^0]_{1-x}[TCNQ^{-\bullet}]_x[TCNQ^0]_{1-x}$	Found: C,63.50; H,3.07; N,33.38	250	Black
		$C_{18}H_{11}N_8$	Calcd.: C,63.73; H,3.24; N,33.03		
12	$(H3BIM^+)_2(TCNQ^-)_2(TCNQ^0)$	$[H3BIM^+]_2[TCNQ^{-\bullet}]_2[TCNQ^0]$	Found: C,65.62; H,2.79 N,31.65	285	Black
		$C_{48}H_{26}N_{20}$	Calcd.: C,65.32; H,2.95; N,31.73		
13	$(H3BIM^+)(BTDA\text{-}TCNQ^-)$	$[H3BIM^+][BTDA\text{-}TCNQ^{-\bullet}]$	Found: C,47.62; H,1.76; N,36.39; S,14.23.	255	Brown
		$C_{18}H_7N_{12}S_2$	Calcd.: C,47.47; H,1.54; N,36.91; S,14.08		
14	$(H3BIM^+)(Me_2\text{-}TCNQ^-)$	$[H2BIM^{\sim 0}][Me_2\text{-}TCNQ^{\sim 0}]$	Found: C,64.96; H,4.07; N,31.10	250	Brown
		$C_{20}H_{15}N_8$	Calcd.: C,65.41; H,4.08; N,30.51		
15	$(H3BIM^+)_2(Me_2\text{-}TCNQ^-)$	$[H2BIM^{\sim 0}]_2[Me_2\text{-}TCNQ^{\sim 0}]$	Found: C,62.78; H,4.11 N,33.43	240	Green
		$C_{26}H_{22}N_{12}$	Calcd.: C,62.16; H,4.38; N,33.46		
16	$(H3BIM^+)(MeO_2\text{-}TCNQ^-)$	$[H2BIM^{\sim 0}][MeO_2\text{-}TCNQ^{\sim 0}]$	Found: C,60.28; H,3.46; N,28.11; O,8.24	267	Red
		$C_{20}H_{15}N_8O_2$	Calcd.: C,60.16; H,3.76; N,28.07; O,8.01		

To a saturated solution of 0.5 mmol of $[Li^+][TCNQs^{-\bullet}]$, though $[Na^+][F4\text{-}TCNQ^{-\bullet}]$ was used for the complex formation of (**17**), in water was added a solution of 0.25 mmol of (**3**) in 10 ml of methanol; the mixture was stirred at room temperature for 30 min and left standing at 0°C overnight. The precipitates were collected and washed with water, then ether.

Stoichiometric Relation of CT Complex Formation Table 3-3 summarizes the tentative chemical formula, mole amount of the initial components for a metathesis reaction (A and B), the mole amount of the obtained CT complexes (C), yield (%), and the residual compounds recovered by the addition of excess water in mother liquor. Identification of the residual compounds was achieved by infrared (IR) measurements.

Measurements The IR and the UV-VIS-NIR absorption spectra were measured by a method of Chapter 2.

X-Ray Structural Analyses An automatic Rigaku AFC-4 diffractometer with $CuK\alpha$ radiation (λ = 1.54178 Å: 40 kV, 200 mA) was used for the data collection of $[H4BIM^{2+}][PICRATE^-]_2$ (**5**) and $(H3BIM^+)_2(TCNQ^-)_2(TCNQ^0)$ (**12**). Intensity data of $[H2BIM^0]_3[H3BIM^+]_2[I^-]_2$ (**7**) were collected using $MoK\alpha$ radiation (λ = 0.71069 Å: 40 kV, 200 mA) of an automatic Rigaku AFC-4. A summary of the crystal parameters is given in Table 3-4. Twenty reflections with $40^o < 2\theta < 60^o$ were used to determine the lattice parameters. The intensity data were collected in the $2\theta < 125^o$ region for (**5**) and (**12**), and $2\theta < 60^o$ for (**7**) in the 2θ-ϖ mode at a scan rate of 4^o min^{-1}. The background counts were 4 s. The intensities of three standards, monitored every 100 data measurements, showed no significant variation. I used 1386, 1631, and 2562 independent reflections with $|F_\sigma| > 3\sigma(F_0)$ for a structural analysis of (**5**), (**12**), and (**7**), respectively. The crystal structures were solved by a direct method,[4)] and all hydrogen atoms, except for (**7**), were determined from difference synthesis maps. A block-diagonal least-squares technique with anisotropic thermal parameters for non-hydrogen atoms and isotropic for hydrogen atoms were employed for structure refinements.[5)]

Table 3-2. Absorption Energy (x 10^3 cm^{-1}) of UV-VIS-NIR Spectra of TCNQ Complexes in KBr pellet.

Compounds	A[a]	B[b]	I[c]	C[d]	D[e]	E[f]	F[g]	F'[g]	G[h]	H[i]
F_4-TCNQ Complex										
$[Li^+][F_4\text{-}TCNQ^{-\bullet}]$ [j]				11.7, 13.3				24.3		
$[Na^+][F_4\text{-}TCNQ^{-\bullet}]$		8.07			15.6			27.2		
$[TTF^{+\bullet}][F_4\text{-}TCNQ^{-\bullet}]$		6.50		10.8	13.9			25.7		
$(H3BIM^+)(F_4\text{-}TCNQ^-)$		6.90			15.4			26.7		33.5
$(H4BIM^{2+})(F_4\text{-}TCNQ^-)_2(H_2O)_2$				10.6	14.5			26.5		33.5
TCNQ Complex										
$[Li^+][TCNQ^{-\bullet}]$ [j]				11.9,13.5			23.8	24.5		
$[K^+][TCNQ^{-\bullet}]$		8.19		11.6	16.6		25.3	27.6		
$(H3BIM^+)(TCNQ^-)$	5.06			11.5	16.2		25.3	27.6		34.5
$(H4BIM^{2+})(TCNQ^-)_2$	4.75			11.5	16.2		24.9	27.7		35.1
$(H3BIM^+)_2(TCNQ^-)_2(TCNQ^0)$	4.90			11.5	16.2		24.9	27.7		35.2
BTDA-TCNQ Complex										
$[Li^+][BTDA\text{-}TCNQ^{-\bullet}]$ [j]				15.9,17.4			26.2	28.8		
$[Li^+][BTDA\text{-}TCNQ^{-\bullet}]$		5.23	8.35	18.7			21.8	28.9		
$(H3BIM^+)(BTDA\text{-}TCNQ^-)$		5.23	9.66	17.2			23.6	28.4		33.5
$(H4BIM^{2+})(BTDA\text{-}TCNQ^-)_2$	3.26		9.17	17.1			23.6	28.4		33.2
$(TEA^+)_2(BTDA\text{-}TCNQ)_3$ [k]	3.40		9.66	16.9			23.6	28.4		
Me_2-TCNQ and MeO_2-TCNQ Complexes										
$[K^+][Me_2\text{-}TCNQ^{-\bullet}]$		6.38			16.2		26.0			

17	$(H4BIM^{2+})(F_4\text{-}TCNQ^-)_2(H_2O)_2$	$[H3BIM^+]_{0.1}[H4BIM^{2+}]_{0.9}[F_4\text{-}TCNQ^{-\bullet}]_{1.9}[H_2O]_2$	Found: C,49.76; H,1.78; N,23.41	>35	Blue
		$C_{28.8}H_{12}N_{11.6}O_2F_8$	Calcd.: C,49.65; H,1.72; N,23.32	0	
18	$(H4BIM^{2+})(TCNQ^-)_2$	$[H4BIM^{2+}]_x[H3BIM^+]_{1-x}[TCNQ^{-\bullet}]_{1+x}[TCNQ^0]_{1-x}$	Found: C,66.10; H,3.19; N,30.59	290	Green
		$C_{30}H_{16}N_{12}$	Calcd.: C,66.19; H,2.94; N,30.87		
19	$(H4BIM^{2+})(BTDA\text{-}TCNQ^-)_2$	$[H4BIM^{2+}]_x[H3BIM^+]_{1-x}[BTDA\text{-}TCNQ^{\sim 0}]_x[BTDA\text{-}TCNQ^{-\bullet}]_{2-x}$	Found: C,46.28; H,0.73; N,35.87; S,16.24	300	Brown
		$C_{30}H_8N_{20}S_4$	Calcd.: C,46.39; H,1.03; N,36.07; S,16.51		
20	$(H4BIM^{2+})_3$	$[H2BIM^{\sim\delta}]_3[Me_2\text{-}TCNQ^{\sim 3\delta/(4-x)}]_{4-x}[H2Me_2\text{-}TCNQ]_x[H_2O]_2$	Found: C,64.98; H,4.37; N,28.49	188	Green
	$(Me_2\text{-}TCNQ^-)_4(H_2O)_2$	$C_{74}H_{60}N_{28}O_2$	Calcd.: C,64.73; H,4.37; N,28.57		

a) Tentative formula is described as an initial component of metathesis reaction. b) Real formula is based on the spectroscopic measurements. c) Calculation of elemental analysis is based on the tentative formula.

Table 3-3. Stoichiometric Relation of CT Complex Formation.

Entry	Composition [a]	A	B	C	(Yield) [b]	Residual Compounds [c]
		mmol				
8	$(H2BIM^0)(Me_2\text{-}TCNQ^0)$	0.206	0.210	0.200	(97)	No [f]
9	$(H2BIM^0)(MeO_2\text{-}TCNQ^0)$	0.149	0.153	0.145	(97)	No [f]
11	$(H3BIM^+)(TCNQ^-)$	0.946	0.930	0.830	(88)	$H2TCNQ^0$, $TCNQ^{-\bullet}$, $H2BIM^0$
14	$(H3BIM^+)(Me_2\text{-}TCNQ^-)$	0.477	0.400	0.242	(51)	$H2Me_2\text{-}TCNQ^0$, $H2BIM^0$
16	$(H3BIM^+)(MeO_2\text{-}TCNQ^-)$	0.664	0.632	0.345	(52)	— [e]
17	$(H4BIM^{2+})(F_4\text{-}TCNQ^-)_2(H_2O)$	0.376	0.770	0.201	(54)	$H2F_4\text{-}TCNQ^0$, $F_4\text{-}TCNQ^{-\bullet}$, $H2BIM^0$
18	$(H4BIM^{2+})(TCNQ^-)_2$	0.420	0.851	0.302	(72)	$H2TCNQ^0$, $TCNQ^{-\bullet}$
19	$(H4BIM^{2+})(BTDA\text{-}TCNQ^-)_2$	0.191	0.380	0.120	(63)	? [d]

a) The compositions are tentative chemical formula. b) The compounds; A, B, and C, correspond to those of the following reaction, $A = [HxBIM^{(x-2)+}][I^-] + B = [Li^+][TCNQs^{-\bullet}] \rightarrow C = [HxBIM^{(x-2)+}][TCNQs^{-\bullet}] + [Li^+][I^-]$. The yields (%) correspond to the obtained complexes: $[HxBIM^{(x-2)+}][TCNQs^{-\bullet}]$. c) $H2TCNQ^0$ is the 1,4-benzenedimalononitrile. Residual compounds except for lithium iodide and sodium iodide were collected from the mother liquor and were identified by the IR spectra. d) Not identified due to the complicated spectrum. e) Not determined. f) No residual compounds.

$(H2BIM^0)(Me_2\text{-}TCNQ^0)$		~15.5		22.9	36.0
$(H3BIM^+)(Me_2\text{-}TCNQ^-)$		~15.5		23.7	36.2
$(H3BIM^+)_2(Me_2\text{-}TCNQ^-)$		~15.5		23.3	36.2
$(H4BIM^{2+})_3(Me_2\text{-}TCNQ^-)_4(H_2O)_2$		~15.3		24.5	36.2
$[Li^+][MeO_2\text{-}TCNQ^{-\bullet}]$	6.45	15.8	25.5		
$(H2BIM^0)(MeO_2\text{-}TCNQ^0)$		~18.0		23.3	36.1
$(H3BIM^+)(MeO_2\text{-}TCNQ^-)$		~18.0		23.2	36.0

These bands are ascribed to a) A-band; intracolumn ($A^{-\bullet} + A^0 \rightarrow A^0 + A^{-\bullet}$) absorption, b) B-band; intracolumn ($A^{-\bullet} + A^{-\bullet} \rightarrow A^0 + A^{2-}$) absorption, c) I-band; unidentified, d) C-band; isolated monomer of $A^{-\bullet}$, e) D-band; intra- or interdimer of $A^{-\bullet}$, f) E-band; intermolecular ($A^0 + H2BIM^0 \rightarrow A^{-\bullet} + H2BIM^{+\bullet}$), g) F- and F'-band; intramolecular of $A^{-\bullet}$, h) G-band; intramolecular of A^0, i) H-band; intramolecular of $H2BIM^0$, $H3BIM^+$, or $H4BIM^{2+}$. j) in acetonitrile (~ 10^{-5} M). k) TEA^+ is tetraethylammonium.

Table 3-4. Crystal Data of $[H4BIM^{2+}][PICRATE^{-}]_2$ (**5**), $[H2BIM]_3[H3BIM^{+}]_2[I^{-}]_2$ (**7**), and $(H3BIM^{+})_2(TCNQ^{-})_2(TCNQ^{0})$ (**12**).

	5	**7**	**12**
Chemical formula	$C_{18}H_{12}N_{10}O_{14}$	$C_{30}H_{32}N_{20}I_2$	$C_{48}H_{26}N_{20}$
Crystal colour	yellow	white	black
Crystal size / mm^3	0.6x0.03x0.02	0.5x0.02x0.02	0.3x0.2x0.2
Crystal system	Monoclinic	Monoclinic	Triclinic
Space group	$P2_1$	$P2_1$	$P\bar{1}$
a / Å	25.522(3)	29.422(8)	10.411(9)
b / Å	5.459(3)	12.304(3)	13.998(8)
c / Å	8.781(4)	5.071(1)	7.822(7)
α / deg			79.15(9)
β / deg	96.66(7)	94.06(3)	68.62(3)
γ / deg			83.37(2)
V / $Å^3$	1120.0(8)	1831.1(8)	1041.4(3)
Z	2	2	1
D_c / gcm^{-3} a)	1.756	1.680	1.408
R	4.02	5.28	8.38

a) D_c is the calculated density.

pH and Cyclic Voltammetry (CV) Measurements The measurement procedures of the acid-dissociation constants and redox potentials were described in Chapter 2. The basic pK_a values of $TCNQs^{-\bullet}$ ($HTCNQ^{\bullet} \rightleftarrows TCNQ^{-\bullet} + H^{+}$ process) are not so precise due to the occurrence of a disproportionation reaction ($2TCNQ^{-\bullet} + 2H^{+} \rightarrow TCNQ^{0} + H2TCNQ^{0}$) during titration.

Electrical Conductivity Measurements The electrical conductivities were measured on a compressed pellet by a two-probe method, except for (**12**); a single crystal, which was measured by the standard four-prove one. Electrical contacts were made using gold paste (Tokuriki 8560).

3-3-1. Structural and Optical Properties of H2BIM System

I have prepared several simple salts of $H4BIM^{2+}$ with Cl^{-}, Br^{-}, I^{-}, BF_4^{-}, $PICRATE^{-}$, $TNBP^{2-}$ and $H3BIM^{+}$ with Cl^{-}, Br^{-}, I^{-}, BF_4^{-}, $PICRATE^{-}$, and a complex salt of $[H2BIM^{0}]_3[H3BIM^{+}]_2[I^{-}]_2$. To characterize the electronic states of the CT complexes and to understand the nature of the intermolecular contacts and the hydrogen bonds in the H2BIM system, I first elucidated the crystal structures and spectroscopic features of the H2BIM compounds with the counter anions of the close shell electronic structure.

3-3-1-1 Crystal Structure of $[H2BIM^{0}]_3[H3BIM^{+}]_2[I^{-}]_2$ (7)

Three crystallographically independent $H2BIM^{0}$, two $H3BIM^{+}$ molecules, and two iodide ions (I^{-}) exist within a unit cell. Figure 3-3b illustrates a unit cell viewed along the c-axis. The crystal consists of a hydrogen bond $H3BIM^{+}(1)$ ••• $H2BIM^{0}(2)$••• $H2BIM^{0}(1)$ ••• $H3BIM^{+}(2)$ tetramer unit, a $H2BIM^{0}(3)$ molecule, and two kinds of iodide (I(1) and I(2)), where the numbers in parentheses correspond to those in Fig. 3-3a. Two molecules located at both ends of a tetramer were deduced as being $H3BIM^{+}$ species from the concept of ice-rule based on the hydrogen bond pattern.[6] Six N-H•••N hydrogen bonds within a tetramer unit link four molecules, and each dihedral angle of the $H2BIM^{0}$ and $H3BIM^{+}$ molecules at the central C - C bond decreased according to the following order:

$$H3BIM^{+}(2);\ 10.07^{o} > H3BIM^{+}(1);\ 5.37^{o} > H2BIM^{0}(3);\ 4.63^{o}$$
$$\approx H2BIM^{0}(1);\ 4.62^{o} \approx H2BIM^{0}(2);\ 4.41^{o}.$$

The low planarity of the $H3BIM^{+}(2)$ molecule implies the existence of a molecular strain due to strong hydrogen bonds within the tetramer unit. The dihedral angle of $H3BIM^{+}(2)$ is larger than that of $H3BIM^{+}(1)$ which is probably due to the existence of

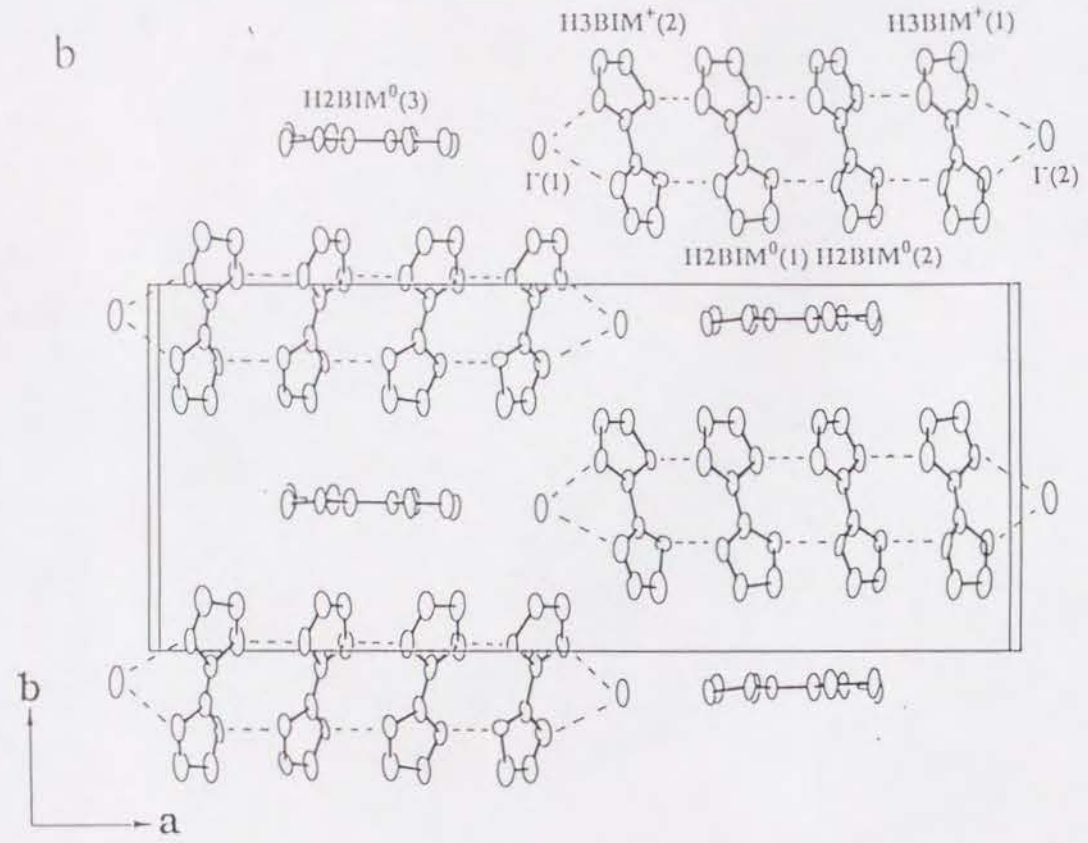

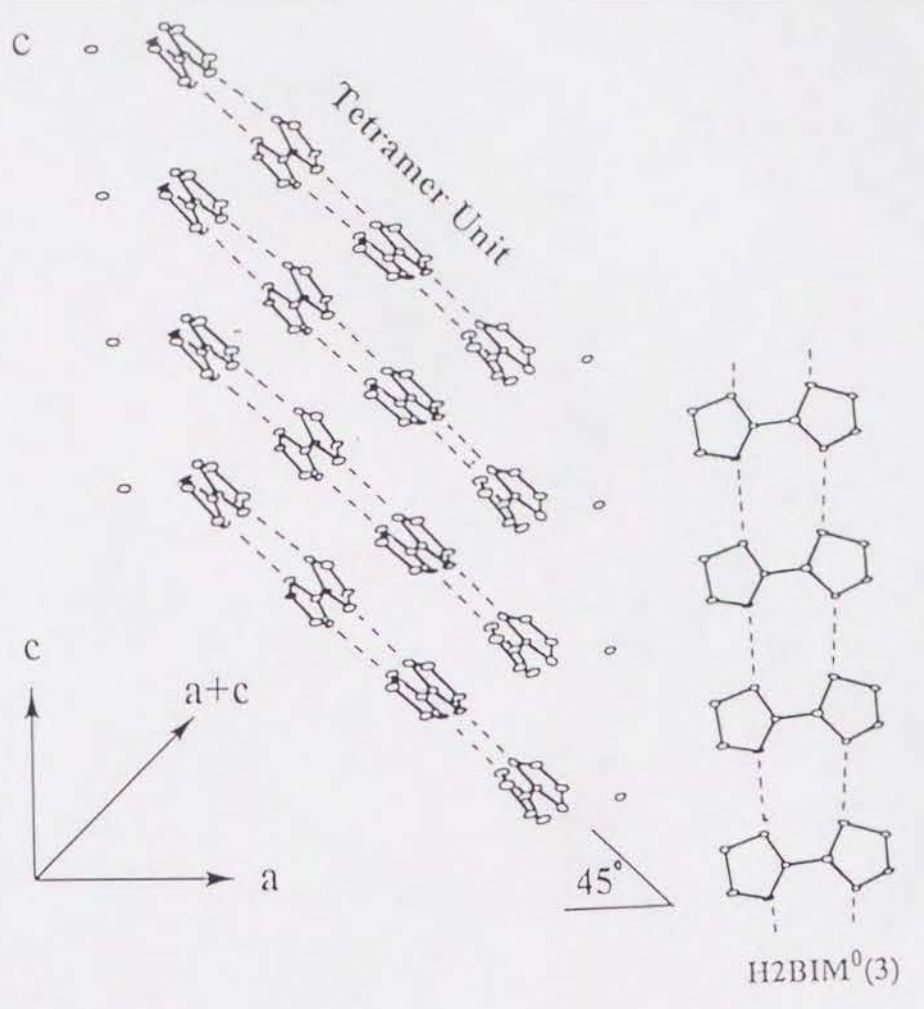

Fig. 3-3. Crystal structure of $[H2BIM^0]_3[H3BIM^+]_2[I^-]_2$ (7). a) Hydrogen bond tetramer unit, $H3BIM^+(1)$ ••• $H2BIM^0(2)$ ••• $H2BIM^0(1)$ ••• $H3BIM^+(2)$, and $H2BIM^0(3)$ showing the atom numbering scheme. Dashed lines correspond to the N-H•••N and N-H•••I^- hydrogen bonds (Å). b) Unit cell viewed along the c-axis. c) Stacking pattern of tetramer units and $H2BIM^0(3)$ viewed along the b-axis. $H2BIM^0(3)$ is connected by the hydrogen bonds (dashed lines) along the c-axis. The I^- ions are located at the lateral position of the tetramer.

a

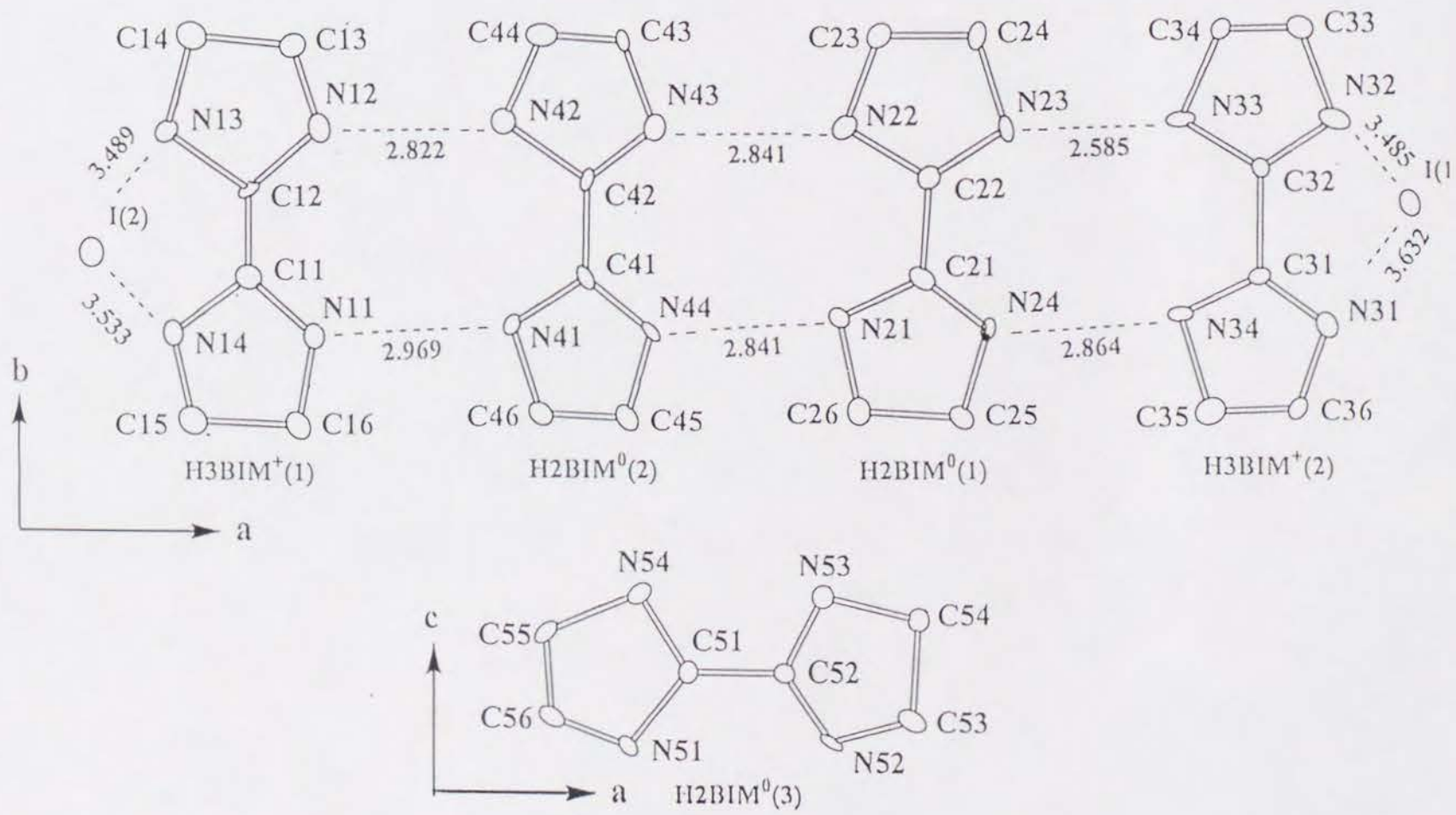

an extremely strong hydrogen bond, N_{23}•••N_{33}. The deviations from a tetramer plane, which were calculated from the individual forty atoms (N and C) within the tetramer, are less than 0.27 Å, and are larger at the $H2BIM^0$(2) molecule (N42 (-0.27Å), C43 (-0.25Å), and N44 (0.22Å)).

On the other hand, $H2BIM^0$(3) molecules are aligned in the perpendicular direction to the tetramer plane; the long axis of the molecule corresponds to the a-axis. Two I^- ions are allocated at the lateral position of the tetramer plane, and form N-H•••I^- type hydrogen bonds between $H3BIM^+$ and I^-.

Every tetramer unit stacks to form a segregated column along the c-axis (Fig. 3-3c). The average interplanar distance of the tetramer unit (3.34 Å) is shorter than the sum of the van der Waals radius of the carbon atom (3.40 Å).[7] The tetramer plane inclines by an angle of 45° toward the long axis of $H2BIM^0$(3). The I^- ions are not on the tetramer planes, but between them. Short contacts between terminal $H3BIM^+$ molecules of the tetramer and I^- ions exist along the a-axis. Along the c-axis, there are no interatomic contacts of I^- ions within the sum of the ion radius, and each tetramer is piled up together along the stacking direction (c-axis). Since no meaningfully short atomic contacts exist between $H2BIM^0$(3) and the I^- ions, the hydrogen bond chain of $H2BIM^0$(3) is isolated from the stack of tetramers. Two kinds of N-H•••N type hydrogen bonds (one is finite within a tetramer unit along the a - c direction and the other is infinite among the $H2BIM^0$(3) molecules along the c-axis) are observed simultaneously.

Table 3-5. Hydrogen bond distances (Å) of $[H2BIM^0]_3[H3BIM^+]_2[I^-]_2$ (7).[a]

N-H•••N type [b]	N-H•••I type [c]
N_{11} ••• N_{41} = 2.969(12)	N_{31} ••• I(1) = 3.632(8)
N_{12} ••• N_{42} = 2.822(13)	N_{32} ••• I(1) = 3.485(9)
N_{21} ••• N_{44} = 2.841(13)	N_{13} ••• I(2) = 3.489(9)
N_{22} ••• N_{43} = 2.841(13)	N_{14} ••• I(2) = 3.533(9)
N_{23} ••• N_{33} = 2.585(12)	
N_{24} ••• N_{34} = 2.864(13)	
N_{51} ••• N_{54}' = 2.816(12)	
N_{52} ••• N_{53}' = 2.888(13)	

a) Standard deviations are shown in parenthesis. b) Interatomic distance of two nitrogens. c) Interatomic distance between the nitrogen and iodide ion (I^-).

Table 3-5 summarizes all of the hydrogen bond distances observed in this crystal. Within a tetramer unit, an alternating sequence of the lengths of the hydrogen bonds is observed (Fig. 3-3b), that is, short (N_{12}•••N_{42} = 2.822Å) ••• long (N_{43}•••N_{22} = 2.841Å) ••• short (N_{23}•••N_{33} = 2.585Å) and long (N_{11}•••N_{41} = 2.969Å) ••• short (N_{44}•••N_{21} = 2.841Å) ••• long (N_{24}•••N_{34} = 2.864Å); also all of the N•••N distances can be found within 2.97 Å, which is shorter by about 0.13 Å compared with the sum of the van der Waals radius of nitrogen (3.10 Å).[7] It should be emphasized that an extremely short N•••N distance among them, 2.585(12) Å, is detected at N_{23}•••N_{33}, which is comparable to the N•••N distance of 2.59 Å observed in $H_3Co(CN)_6$ (a symmetric single minimum potential of the N•••H•••N type of hydrogen bond has been postulated.[8]). Other hydrogen bond distances are indicative of the formation of an unsymmetric potential. For $H2BIM^0$(3), two kinds of hydrogen bond distances along the c-axis, N_{51}•••N'54 = 2.816(12) and N_{52}•••N'53 = 2.888(13) Å, where the prime symbol indicates the atoms generated by the translation along the c-axis, are nearly identical to those of free $H2BIM^0$.[9] In the N-H•••I^- hydrogen bonds, three N•••I^- distances (N_{32}•••I(1) = 3.485, N_{13}•••I(2) = 3.489, and N_{14}•••I(2) = 3.533 Å) are shorter than the sum of the van der Waals radius of the nitrogen and the ion radius of the I^- ions (3.61 Å).[7]

The stacks of I^- ions are elongated uniformly along the c-axis (5.07 Å interval), which is longer than the sum of the ion radius of I^- ions (4.12 Å),[7b] and the minimum distance between I^- ions in the ab-plane is obtained as 6.454 Å along the b-axis (Fig. 3-3b). Thus, there are no effective interatomic contacts of I^- ions in the zig zag arrangement of I^- ions, which gives rise to the isolation of the I^- ions from each other. There are also no effective overlaps between the tetramer and $H2BIM(3)^0$; the shortest contact between them is $N_{51}\cdots C_{45}$ (3.45 Å), which is longer than the sum of the van der Waals radius (3.25 Å).[7] Thus, the respective units (tetramer, $H2BIM(3)^0$, and I^-) are isolated from each other in the ab-plane, except for the N-H•••I^- hydrogen bonds.

It should be emphasized that the crystal of (7) contains two kinds of protonated species, i.e., both $H2BIM^0$ and $H3BIM^+$ coexist in the crystal. I call this states a mixed PT state; a further confirmation was made by IR measurements (Section 3-3-1-3).

3-3-1-2 Crystal Structure of [H4BIM^{2+}][PICRATE$^-$]$_2$ (5)

Here, I examined the crystal structure of the 1:2 complex (5), which belongs to a simple salt with no CT interaction (see section 3-3-1-4), in order to evaluate the characteristics of the hydrogen bond and stacking pattern in the solid state.

Within a unit cell, there are two crystallographically independent $PICRATE^-$ and one $H4BIM^{2+}$ molecules. Figure 3-4a shows a stereoview of the packing pattern for (5) viewed along the c-axis. A fundamental unit of crystal structure consists of a hydrogen bond trimer: $PICRATE^-(1)$ ••• $H4BIM^{2+}$ ••• $PICRATE^-(2)$. The spiral arrangement of the trimer unit elongates along the direction of the a-axis, and there are no effective intermolecular contacts between the trimer units.

a

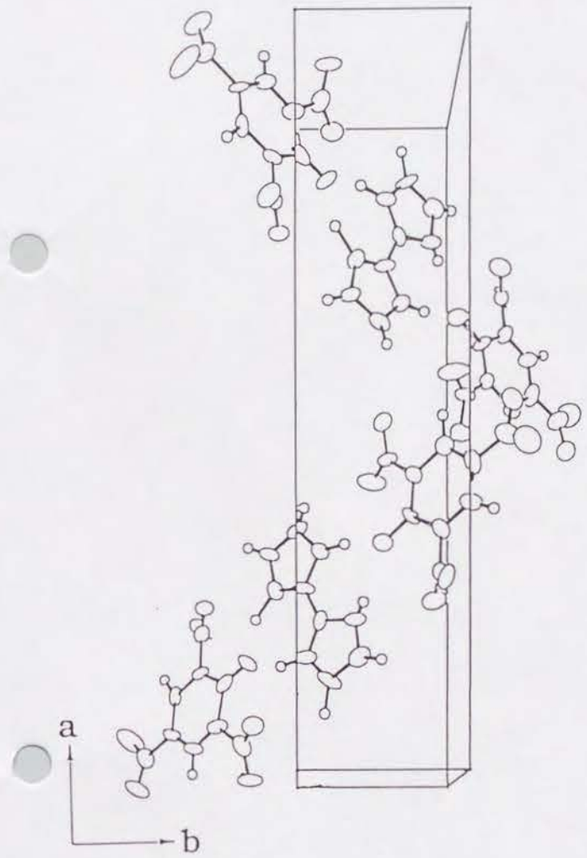

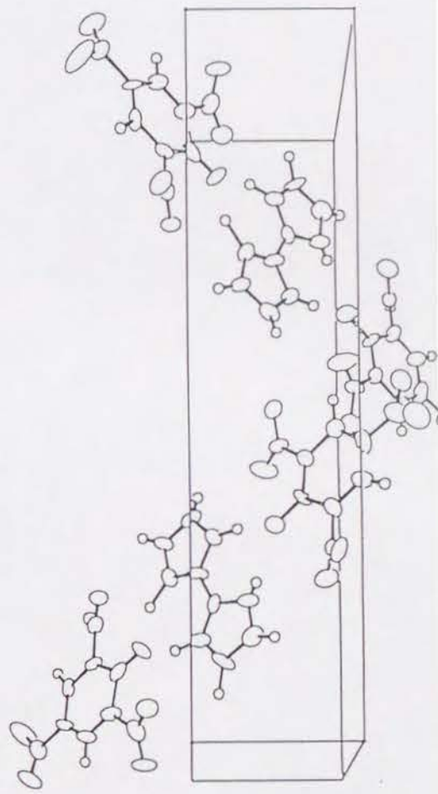

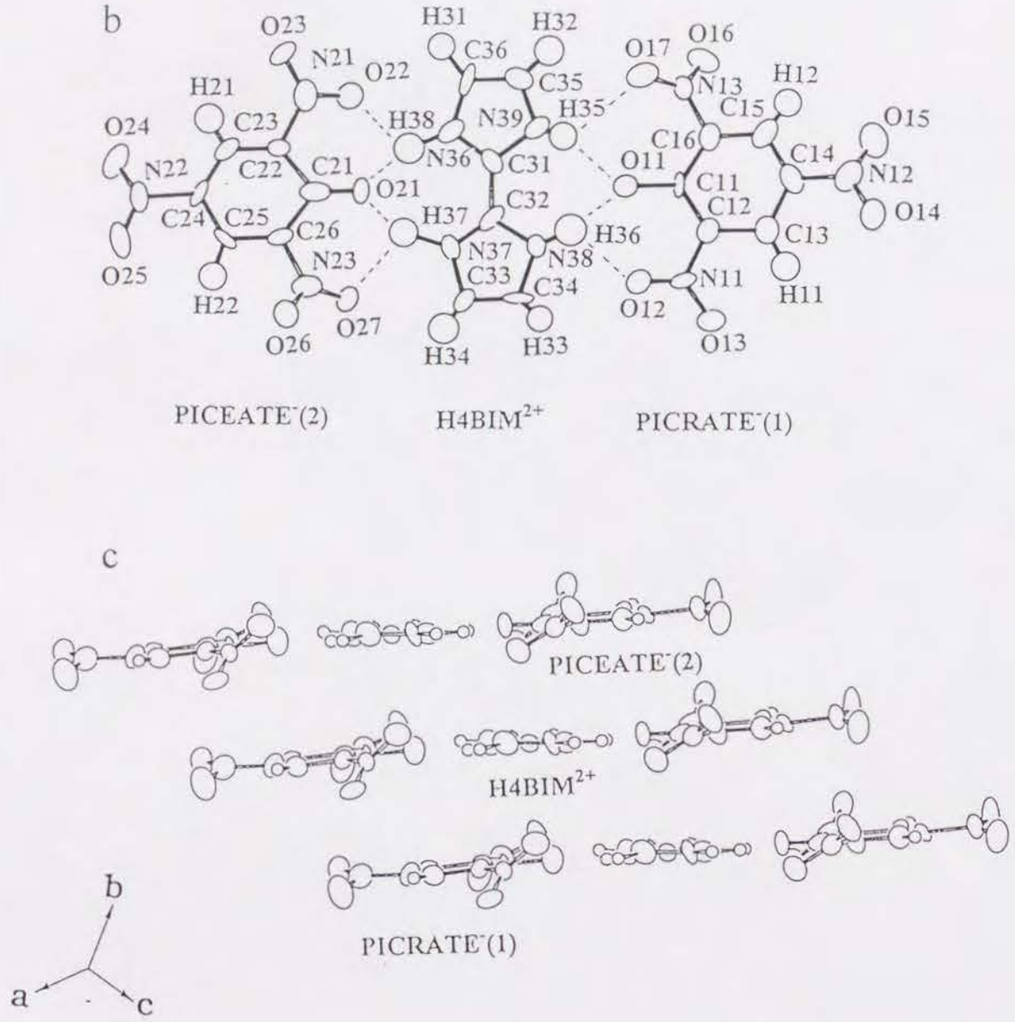

Fig. 3-4. Crystal structure of $[H4BIM^{2+}][PICRATE^-]_2$ (**5**). a) Unit cell viewed along the c-axis (stereoview). Spiral configuration is elongated along the a-axis. b) Hydrogen bond trimer unit, $PICRATE^-(2)$ ••• $H4BIM^{2+}$ ••• $PICRATE^-(1)$, showing the atom numbering scheme. Dashed lines indicate the N-H•••O hydrogen bond. c) Stacking pattern of trimer units viewed along the long axis of $H4BIM^{2+}$. Each molecule stacks in the order of $PICRATE^-(1)$, $H4BIM^{2+}$, and $PICRATE^-(2)$ along the b-axis.

Table 3-6. Hydrogen bond distances (Å) for $PICRATE^-(1)$ ••• $H4BIM^{2+}$ ••• $PICRATE^-(2)$ unit of $[H4BIM^{2+}][PICRATE^-]_2$ (**5**).[a)]

N-H•••O (Phenolate) [b)]	N-H•••O (Nitro) [c)]
$N37•••O21 = 2.700(8)$	$N37•••O27 = 2.917(8)$
$N38•••O11 = 2.668(9)$	$N38•••O12 = 2.865(8)$
$N39•••O11 = 2.681(9)$	$N39•••O17 = 2.937(9)$
$N40•••O21 = 2.704(8)$	$N40•••O22 = 2.885(8)$

a) Atomic numbering scheme is shown in Fig. 3-4b. b) N-H•••O hydrogen bond between $H4BIM^{2+}$ and phenolate-oxygen of $PICRATE^-$. c) N-H•••O hydrogen bonds between $H4BIM^{2+}$ and nitro-oxygens of $PICRATE^-$.

Figure 3-4b illustrates the trimer unit, showing the atom numbering scheme. Four strong N-H•••O^- hydrogen bonds between $H4BIM^{2+}$ and the phenolate oxygen atom of $PICRATE^-$ link each molecule to form a trimer; four different N-H•••O hydrogen bonds between $H4BIM^{2+}$ and the nitro groups of $PICRATE^-$ support its trimer structure. Table 3-6 summarizes the N•••O distances of the N-H•••O hydrogen bond. Four N•••O (phenolate) distances within the trimer plane (2.668 ~ 2.704 Å) are contracted by about 0.2 Å compared with the sum of the van der Waals radius (2.90 Å), [7)] and are shorter than the standard hydrogen bond distance of the N-H•••O system (2.88 Å).[10)] Since the maximum deviation from the trimer plane, which is defined by one $H4BIM^{2+}$ and two $PICRATE^-$ except for the nitro-oxygens and hydrogens, is within 0.13 Å, the trimer unit is nearly coplanar. Two hydrogen bond nitro-oxygens, O_{12} (+ 0.57 Å) and O_{17} (+ 0.66 Å), exist above the trimer plane; on the contrary, O_{22} (- 0.67 Å) and O_{27} (- 0.60 Å) atoms exist below the plane.

Each hydrogen bond trimer unit stacks along the b-axis in the order of $PICRATE^-(1)$, $H4BIM^{2+}$, and $PICRATE^-(2)$, as shown in Fig. 3-4c, which is viewed along the long axis of $H4BIM^{2+}$. The average intertrimer distance (3.65 Å) is longer than the sum of the van der Waals radius of the carbon atom (3.40 Å).[7)]

3-3-1-3 IR and UV-VIS Spectra of H2BIM System in Solid

Figure 3-5 shows the vibration spectra of $H2BIM^0$, $[H3BIM^+][I^-]$, and $[H4BIM^{2+}][Cl^-]_2$ at the frequency range from 4000 to 400 cm^{-1}. Although the

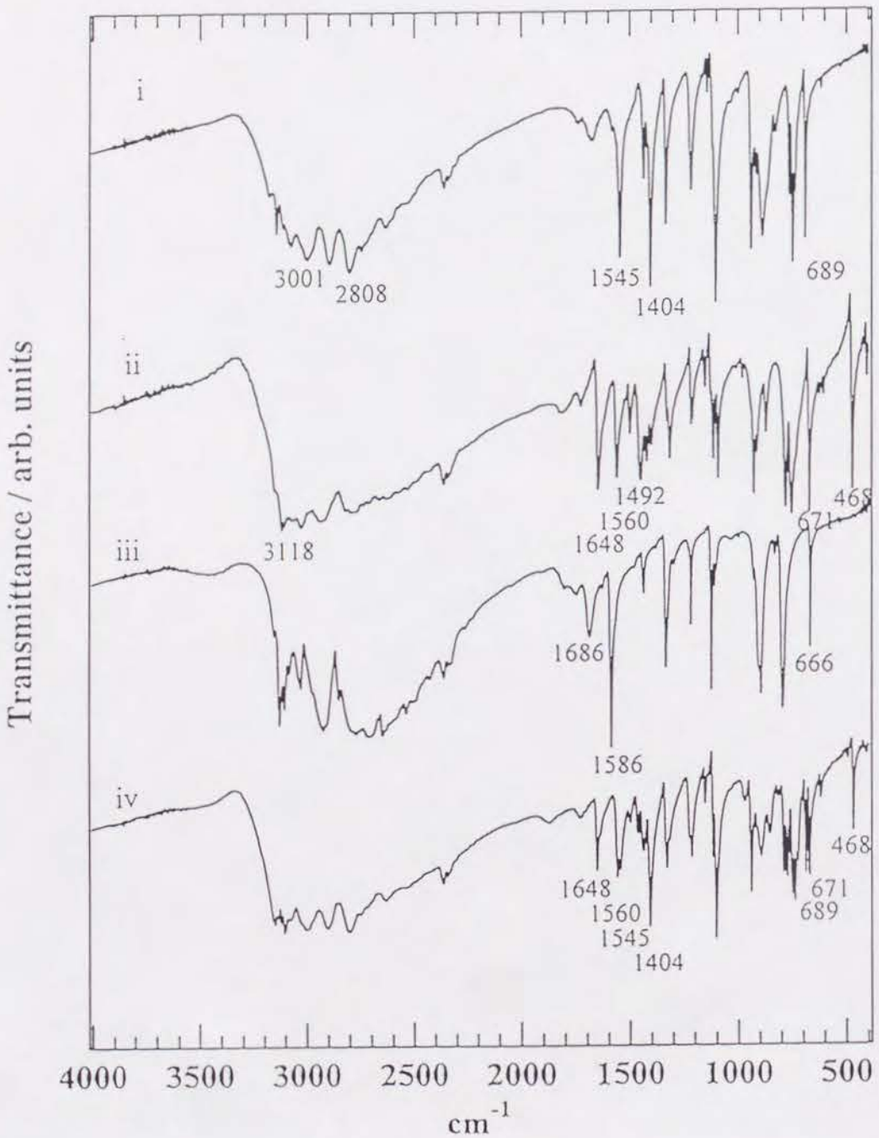

Fig. 3-5. Vibration spectra of each protonated species of i) $H2BIM^0$ (1), ii) $[H3BIM^+][I^-]$ (2), iii) $[H4BIM^{2+}][Cl^-]_2$, and iv) $[H2BIM^0]_3[H3BIM^+]_2[I^-]_2$ (7) at the frequency range of 4000 ~ 400 cm^{-1}.

replacement of the counter anions (Cl^-, Br^-, and I^-) did not change the observable spectra of the N-H in-plane bending ($\nu^b_{N\text{-}H}$) and the ring-torsion modes (ν^t) of H2BIM system, a slight change of the N-H stretching ($\nu^s_{N\text{-}H}$) mode was observed. The structural simplicity of the spectra of $H4BIM^{2+}$ and $H2BIM^0$ indicates that the molecular symmetry increases according to the following order

$$H4BIM^{2+}\,(D_{2h}) > H2BIM^0\,(C_{2h}) > H3BIM^+\,(C_s).$$

One finds a broad stretching absorption spread out from ca. 3200 to 2200 cm^{-1} which is characteristic of the hydrogen bond intramolecular N-H stretching bands ($\nu^s_{N\text{-}H}$).[11] In addition, multiple structures of $\nu^s_{N\text{-}H}$, which greatly resemble that of 1*H*-imidazole,[12] are also observed in all of the protonated species. In the case of a very strong N-H•••N hydrogen bond system, the single minimum potential of the position of the proton, that is, a proton locates at the center of two nitrogens (N•••H•••N), causes a large red shift of the $\nu^s_{N\text{-}H}$ mode.[13] For the imidazole system, the absorption range of the $\nu^s_{N\text{-}H}$ mode indicates no existence of a single minimum potential for the proton position, which has also been confirmed by the neutron-diffraction method for 1*H*-imidazole.[14] In the H2BIM system, other characteristic absorptions, which are assigned to the $\nu^b_{N\text{-}H}$ (1700 ~ 1500 cm^{-1}) and ν^t (600 ~ 700 cm^{-1}) modes, respectively, are useful guides to identify the protonated state of the H2BIM system.

The vibration spectrum of $[H2BIM^0]_3[H3BIM^+]_2[I^-]_2$ (7) is compared with those of $H2BIM^0$, $H3BIM^+$, and $H4BIM^{2+}$ in the frequency ranges of 1750 - 1350 cm^{-1} and 750 - 420 cm^{-1}. The $\nu^b_{N\text{-}H}$ of $H2BIM^0$ is observed at 1545 cm^{-1}, and the imidazole ring stretching frequency locates at 1404 cm^{-1}.[11] Two nearby bands of $H3BIM^+$, observed at 1648 and 1560 cm^{-1}, should be assigned to $\nu^b_{N^+\text{-}H}$ and $\nu^b_{N\text{-}H}$, while the $\nu^b_{N^+\text{-}H}$ of $H4BIM^{2+}$ is assigned to the 1586 cm^{-1} band. In the case of (7), both the $\nu^b_{N\text{-}H}$ and $\nu^b_{N^+\text{-}H}$ of $H3BIM^+$, together with the $\nu^b_{N\text{-}H}$ ascribable to $H2BIM^0$, are found at 1648, 1560, and 1545 cm^{-1}, respectively.

A single band observed at 689 cm^{-1} is assigned to the ν^t of $H2BIM^0$.[11] For the case of $H3BIM^+$, the corresponding band appears at 671 cm^{-1}. Further, the occurrence of the 468 cm^{-1} band in $H3BIM^+$ is particularly noteworthy. The band observed at 468 cm^{-1} disappears again in the fully protonated form of $H4BIM^{2+}$. In the case of (7), three absorptions ascribable to $H2BIM^0$ and $H3BIM^+$ emerge at 689, 671, and 468 cm^{-1} simultaneously. Above mentioned spectral features strongly support the coexistence of the $H2BIM^0$ and $H3BIM^+$ species in complex (7), which is in excellent agreement with the result of the afore-mentioned X-ray crystal analysis.

The $H2BIM^0$, $[H3BIM^+][BF_4^-]$, and $[H4BIM^{2+}][BF_4^-]_2$ show a broad absorption in the solid state with the absorption maxima located at 34.4 x 10^3 cm^{-1} ($H2BIM^0$), 33.6 x 10^3 cm^{-1} ($H3BIM^+$), and 32.2 x 10^3 cm^{-1} ($H4BIM^{2+}$), respectively. The absorption maxima of these are slightly shifted by protonation, and there is no well-defined change in the electronic absorption spectra in the UV-VIS-NIR region by protonation in a solid.

3-3-1-4 IR and UV-VIS-NIR Spectra of PICRATE and TNBP Complexes

I describe here three complexes: ($H3BIM^+$)($PICRATE^-$) (4), ($H2BIM^0$)(Picric acid)$_2$ (5), and ($H2BIM^0$)($H2TNBP^0$) (6). The compounds in parenthesis are the initial components of complex formations.

For the complex of (4), three absorptions (Fig. 3-6: 1652, 1567, and 1492 cm^{-1}), which are assumed to the $\nu^b_{N\text{-}H}$ modes of the $H3BIM^+$ species, and no absorptions ascribable to those of $H2BIM^0$ and $H4BIM^{2+}$, were observed. These results afford the real state of the H2BIM species of this complex as being $H3BIM^+$. Since the absorptions at 1586 cm^{-1} observed in (5) and (6) are consistent with the $\nu^b_{N+\text{-}H}$ of $[H4BIM^{2+}][Cl^-]_2$, the protonated states of the H2BIM species are assigned to the fully protonated form of $H4BIM^{2+}$.

The UV-VIS spectrum of (5) has an electronic absorption band at 25.0 x 10^3 cm^{-1}, which is consistent with that of $[Na^+][PICRATE^-]$ (24.7 x 10^3 cm^{-1}). This indicates that Picric acid, which has an absorption maximum at 29.1 x10^3 cm^{-1}, is

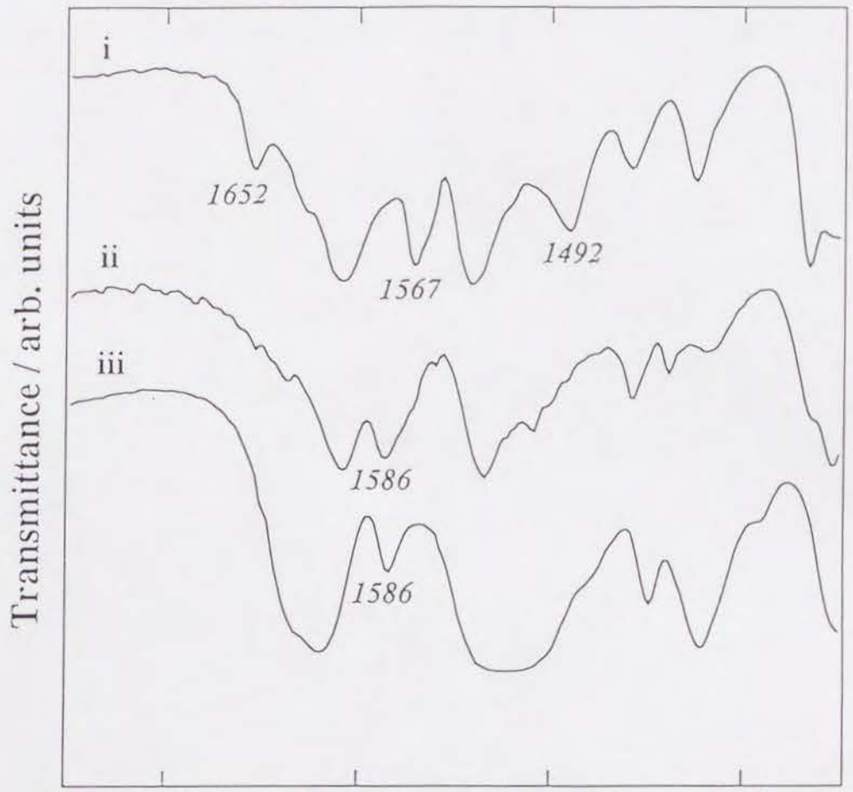

Fig. 3-6. The N-H in plane bending mode ($\nu^b_{N\text{-}H}$) at 1750 ~ 1350 cm^{-1} of PT salts, i) $[H3BIM^+][PICRATE^-]$ (4), ii) $[H4BIM^{2+}][PICRATE^-]_2$ (5), and iii) $[H4BIM^{2+}][TNBP^{2-}]$ (6).

changed to PICRATE$^-$ by the intermolecular PT process in solution, 2 Picric acid + H2BIM^0 → 2PICRATE$^-$ + H4BIM^{2+}; also, there is no evidence of a CT interaction. A similar UV-VIS spectral character was also observed for (**4**) and (**5**). Thus, the real chemical formulas of (**4**) and (**5**) were deduced as to be [H3BIM$^+$][PICRATE$^-$] and [H4BIM^{2+}][PICRATE$^-$]$_2$.

The UV-VIS spectrum of the fully protonated H2TNBP^0 shows an absorption at 26.3 x 10^3 cm^{-1}; also, [Na$^+$]$_2$[TNBP^{2-}] has an absorption maximum at 21.6 x 10^3 cm^{-1} in the solid state.[15] The absorption maximum of (**6**), located at 22.9 x 10^3 cm^{-1}, with a shoulder near to 19.5 x 10^3 cm^{-1} was observed. This spectral feature is very similar to the case of the 1:1 diamines - H2TNBP complexes, where the diamines are p-phenylenediamine, 1,5-naphthalenediamine, 1,6-pyrenediamine, and 3,3'-dimethylbenzidine. All of these complexes have an electronic absorption band located in the energy range from 22.5 x 10^3 to 23.6 x 10^3 cm^{-1}, and is classified into PT type with no CT interaction.[15] The absorption maxima of (**6**), in addition to IR measurements, indicate the real chemical formula as being [H4BIM^{2+}][TNBP^{2-}].

3-3-2. Charge-Transfer Complexes with TCNQ Derivative

Table 3-7 summarizes the compositions, electrical resistivities at room temperature (ρ_{RT}), activation energies for conduction (E_a), CT energies ($h\nu_{CT}$), and nitrile stretching frequencies (ν_{CN}) of the obtained complexes by employing H3BIM$^+$ and H4BIM^{2+}. I obtained three types of CT, namely, complete ionic, neutral and mixed CT.

3-3-2-1 Completely Ionic CT Complex: (10), (13), and (17)

The complexes; [H3BIM$^+$][F4-TCNQ$^{-\bullet}$] (**10**), [H4BIM^{2+}]$_{0.9}$[H3BIM$^+$]$_{0.1}$[F4-TCNQ$^{-\bullet}$]$_{1.9}$[H$_2$O]$_2$ (**17**), and [H3BIM$^+$][BTDA-TCNQ$^{-\bullet}$] (**13**), belong to a completely ionic CT complex. (**10**) and (**17**) exhibit high resistivity (4.2 x 10^6 and 8.0 x 10^8 Ωcm) and a CT band at high energy (6.90 x 10^3 and 10.6 x 10^3 cm^{-1}). The last one (**13**) will be described in section 3-3-2-3b.

The UV-VIS-NIR spectra of two F4-TCNQ complexes are compared with those of [Na$^+$][F4-TCNQ$^{-\bullet}$] and [TTF$^{+\bullet}$][F4-TCNQ$^{-\bullet}$], which comprise of the fully ionized components (Fig. 3-7).[16] The main transitions in a crystal comprising a segregated column of F4-TCNQ$^{-\bullet}$ are known to be observed at three positions:[16] 6 ~ 8 x 10^3 cm^{-1}, due to the intermolecular (intracolumn: B-band) one; 14 ~ 15 x 10^3 cm^{-1}, due to the inter- or intradimer (D-band); and 25 ~ 27 x 10^3 cm^{-1}, due to the intramolecular (F-band) transitions in F4-TCNQ$^{-\bullet}$. [Li$^+$][F4-TCNQ$^{-\bullet}$] shows absorptions of 11.7, 13.3, and 24.3 x 10^3 cm^{-1} in an acetonitrile solution. Sometimes the former two transitions, attributable to the isolated monomeric F4-TCNQ$^{-\bullet}$, appear in the solid spectra due to the formation of defects (C-band).

It is evident that the spectrum of the H3BIM$^+$ complex is almost identical to that of [Na$^+$][F4-TCNQ$^{-\bullet}$], suggesting a segregated stacking of a completely ionized state of F4-TCNQ. The spectrum of the H4BIM^{2+} complex, however, is very similar to that of [TTF$^{+\bullet}$][F4-TCNQ$^{-\bullet}$], except for the loss of the lowest energy absorption at 6.50 x 10^3 cm^{-1} in the TTF complex. There is no absorptions around 6 ~ 8 x 10^3 and below 5 x 10^3 cm^{-1}, which are usually ascribed to the intermolecular transition of the completely

Table 3-7. CT complexes of H3BIM$^+$ and H4BIM^{2+} with TCNQs.

Entry	Acceptor [a]	ρ_{RT} [b] Ωcm	E_a eV	$h\nu_{CT}$ [c] x10^{3}cm^{-1}	ν_{CN} [c] cm^{-1}
	H3BIM$^+$ Complexes				
10	F_4-TCNQ	4.2x10^6	0.16	6.90	2212
11	TCNQ	1.7x10^7	0.37	5.06	2213, 2219
12	TCNQ	1.2x10^6	0.33	4.75	2213, 2219
13	BTDA-TCNQ	3.4x10^5	0.30	5.23	2220
14	Me_2-TCNQ	2.4x10^9	0.39	~15.5	2219
15	Me_2-TCNQ	6.4x10^9	— [d]	~15.5	2222
16	MeO_2-TCNQ	2.9x10^9	0.39	~18.0	2222
	H4BIM^{2+} Complexes				
17	F_4-TCNQ	8.0x10^8	0.40	10.6	2201
18	TCNQ	6.2x10^6	0.41	4.90	2213, 2190
19	BTDA-TCNQ	3.3x10^4	0.16	3.26	2185
20	Me_2-TCNQ	8.8x10^7	— [d]	~15.5	2258[e], 2222

a) The moleculare structures are shown in Fig. 3-2 b) Measured by two-probe method on compressed pellet. c) Measured on KBr disks. d) Not determined. e) This peak is ascribed to the ν_{CN} mode of Me_2-H2TCNQ^0 species.

Fig. 3-7. UV-VIS-NIR spectra of F_4-TCNQ complexes. i) [Na$^+$][F_4-TCNQ$^{\bullet}$], ii) [TTF$^{+\bullet}$][F_4-TCNQ$^{\bullet}$], iii) (H3BIM$^+$)(F_4-TCNQ$^{\bullet}$) (**10**), and iv) (H4BIM^{2+})(F_4-TCNQ$^{\bullet}$)$_2$(H_2O)$_2$ (**17**). The origin of each band is denoted in Table 3-2.

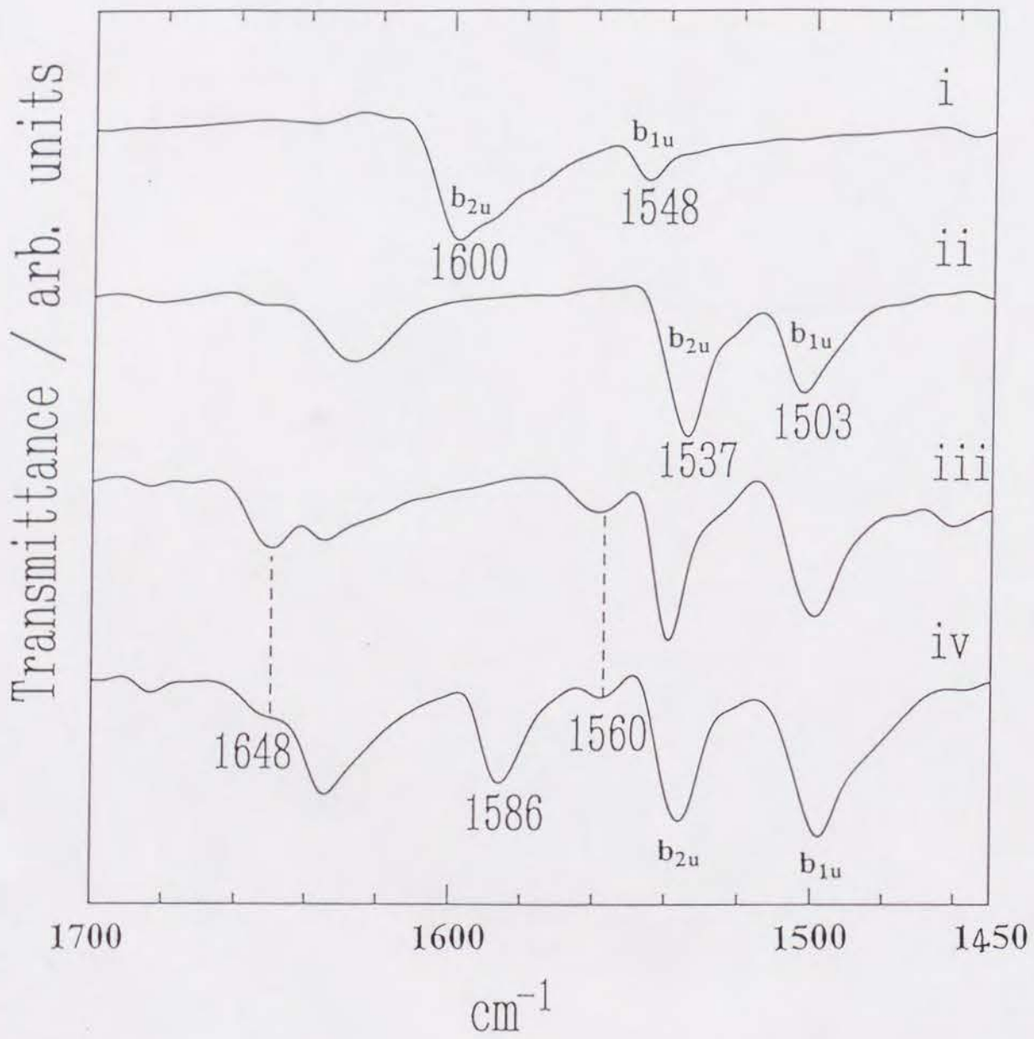

Fig. 3-8. Vibration spectra of F_4-TCNQ complexes at the frequency range 1700 ~ 1450 cm^{-1}, i) F_4-TCNQ^0, ii) [Na^+][F_4-TCNQ$^{-\bullet}$], iii) ($H3BIM^+$)(F_4-TCNQ$^-$) (**10**), and iv) ($H4BIM^{2+}$)(F_4-TCNQ$^-$)$_2$(H_2O)$_2$ (**17**).

and partially ionic acceptor molecules in the segregated stacking, respectively. It is therefore suggested that F_4-TCNQ is a completely ionized monovalent state, and that the intermolecular interactions among the F_4-TCNQ anion radical are prohibited by a special stacking manner in complex (**17**).

Figure 3-8 shows the IR spectrum of F_4-TCNQ^0, [Na^+][F_4-TCNQ$^{-\bullet}$], (**10**) and (**17**) in the frequency range of 1700 ~ 1350 cm^{-1}. It has been reported that the b_{1u} (ν_{19}) and b_{2u} (ν_{23}) modes display the highest ionization shifts, and are almost insensitive to environmental perturbations.[17] The b_{1u} (1548 cm^{-1}) and b_{2u} (1600 cm^{-1}) modes of F_4-TCNQ^0 shifted to lower frequencies at 1503 (b_{1u}) and 1537 cm^{-1} (b_{2u}) for F_4-TCNQ$^{-\bullet}$, respectively. These two modes of $H3BIM^+$ and $H4BIM^{2+}$ complexes with F_4-TCNQ indicate the completely ionized state of the F_4-TCNQ molecule, in agreement with the result of the UV-VIS-NIR spectra. Curve **iii** in Fig. 3-8 clearly indicates that $H3BIM^+$ is the only species of the biimidazole molecule, confirming the real state of the complex as being [$H3BIM^+$][F_4-TCNQ$^{-\bullet}$]. On the other hand, I can see both absorptions due to $H3BIM^+$ (1648 and 1560 cm^{-1}) and $H4BIM^{2+}$ (1586 cm^{-1}) in the spectrum of (**18**). As a result, I must conclude that some of $H4BIM^{2+}$ molecules changed to $H3BIM^+$ owing to the deprotonation process of $H4BIM^{2+}$ ($H4BIM^{2+} \rightarrow xH4BIM^{2+} + (1-x)H3BIM^+ + H^+$). This conclusion predicts that one of the following chemical formulas is the real one for this complex:

i) $[H4BIM^{2+}]_x[H3BIM^+]_{1-x}[F_4\text{-}TCNQ^{-\bullet}]_{1+x}[H_2O]_2$,

ii) $[H4BIM^{2+}]_x[H3BIM^+]_{1-x}[F_4\text{-}TCNQ^{-\bullet}]_{1+x}[H2F_4\text{-}TCNQ^0]_{1-x}[H_2O]_2$,

or

iii) $[H4BIM^{2+}]_x[H3BIM^+]_{1-x}[F_4\text{-}TCNQ^{-\bullet}]_{1+x}[F_4\text{-}TCNQ^0]_{1-x}[H_2O]_2$.

The IR spectrum of the complex in a solid shows no evidence of the existence of either F_4-TCNQ^0 or $H2F_4$-TCNQ^0 ($H2F_4$-TCNQ^0 has a strong $\nu^S_{C\text{-}H}$ absorption at 2911 cm^{-1} accompanying by the disappearance of $\nu_{C\text{-}H}$ (b_{2u}) mode at 1600 cm^{-1} of F_4-TCNQ^0). Therefore, it is most plausible that the chemical formula of the complex is $[H4BIM^{2+}]_x[H3BIM^+]_{1-x}[F_4\text{-}TCNQ^{-\bullet}]_{1+x}[H_2O]_2$ with x = 0.9, which is assumed

from an elemental analysis. This complex should be designated as a fully CT and mixed PT complex.

3-3-2-2 Neutral CT Complex: (8), (9), (14), (15), (16), and (20)

The CT complexes of $H3BIM^+$ and $H4BIM^{2+}$ with Me_2-TCNQ and MeO_2-TCNQ ((**14**), (**15**), and (**20**)) have high resistivity ($8.8 \times 10^7 \sim 6.4 \times 10^9$ Ωcm) with high E_a values. Figure 3-9 shows the UV-VIS-NIR spectra of $[K^+][Me_2\text{-}TCNQ^{-\bullet}]$ and biimidazole complexes. The main transition in the solid state, comprising a segregated column of $Me_2\text{-}TCNQ^{-\bullet}$, has three distinguishable bands, 6.38×10^3 cm^{-1}, due to the intermolecular (intracolumn; B-band) one, 16.2×10^3 cm^{-1} (D-band), and 26.0×10^3 cm^{-1} to the intramolecular transition (F-band) for the case of $[K^+][Me_2\text{-}TCNQ^{-\bullet}]$. The D-band was assigned to the CT from next HOMO of $TCNQ^{-\bullet}$ to the LUMO of $TCNQ^0$ in the lowest triplet excited state in the case of $(Cs^+)_2(TCNQ)_3$, but the explanation in the 1 : 1 completely ionic salt is not present.

$(H3BIM^+)(Me_2\text{-}TCNQ^-)$ (**14**): The IR spectrum of (**14**) complex is completely represented by a superposition of those of neutral $H2BIM^0$ and $Me_2\text{-}TCNQ^0$. There are no vibration bands ascribable to $H3BIM^+$, $Me_2\text{-}TCNQ^{-\bullet}$, and $H2Me_2\text{-}TCNQ^0$. None of electronic absorptions ascribable to $Me_2\text{-}TCNQ^{-\bullet}$ were observed for (**14**) in curve **iii** of Fig. 3-9. $Me_2\text{-}TCNQ^0$ and $H2BIM^0$ exhibit intramolecular transitions in the regions of 23 - 25 x 10^3 (G-band) and 36 x 10^3 cm^{-1} (H-band), respectively. The origin of the additional transition at the lower energy side (~ 15.5 x 10^3 cm^{-1}: E-band) observed in this complex is conceivable to the CT interaction between $H2BIM^0$ and $Me_2\text{-}TCNQ^0$ for the process of $H2BIM^0 + Me_2\text{-}TCNQ^0 \rightarrow H2BIM^{+\bullet} + Me_2\text{-}TCNQ^{-\bullet}$.[18] In order to verify this idea, I tried to determine the CT transition between $H2BIM^0$ and Me_2-TCNQ in solution, and to compare the CT transition energies. However, the low solubility of the $H2BIM^0$ species in an organic solvent prevents such experiments. I thus prepared the $[H2BIM^0][Me_2\text{-}TCNQ^0]$ (**8**) complex by a direct reaction in the gas phase.

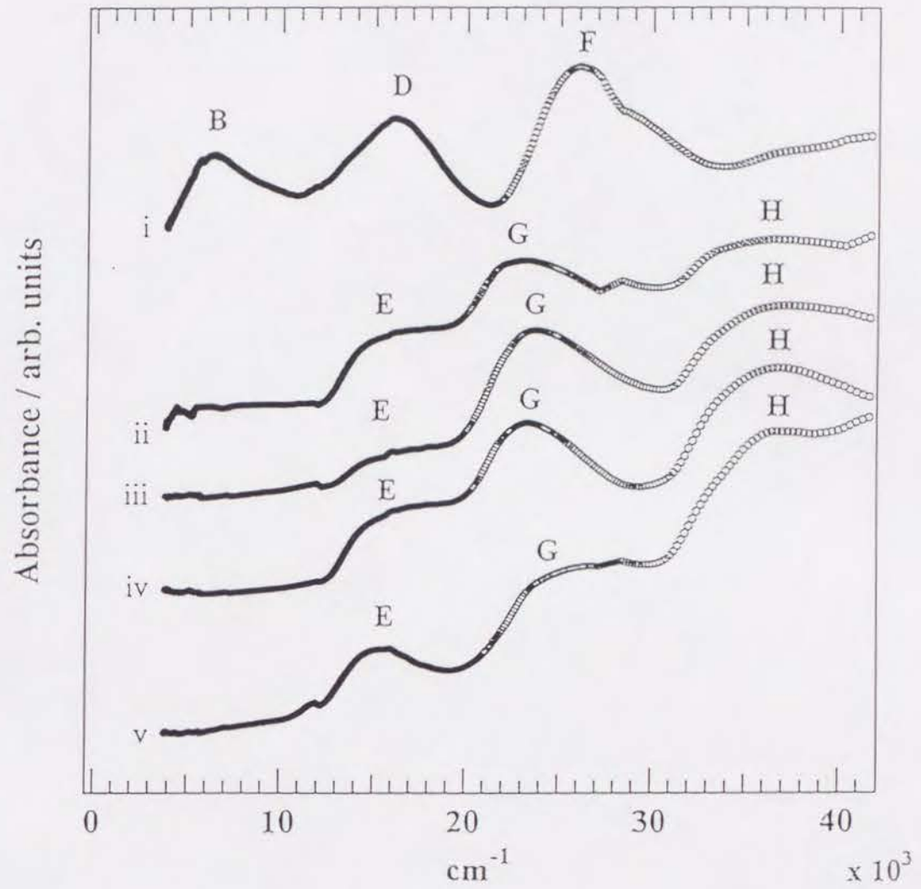

Fig. 3-9. UV-VIS-NIR spectra of Me_2-TCNQ complexes, i) $[K^+][Me_2\text{-}TCNQ^{-\bullet}]$, ii) $[H2BIM^0][Me_2\text{-}TCNQ^0]$ (**8**), iii) $(H3BIM^+)(Me_2\text{-}TCNQ^-)$ (**14**), iv) $(H3BIM^+)_2(Me_2\text{-}TCNQ^-)$ (**15**), and v) $(H4BIM^{2+})_3(Me_2\text{-}TCNQ^-)_4(H_2O)_2$ (**20**). The origin of each band is denoted in Table 3-2.

The IR spectra of (**8**) was completely represented by a superposition of those of $H2BIM^0$ and Me_2-$TCNQ^0$. There was no change found in the protonated states of the $H2BIM^0$ species. The overall feature of the UV-VIS-NIR spectrum of (**8**) (curve **ii** in Fig. 3-9) greatly resembles that of (**14**). Thus, the E-band (~ 15.5 x 10^3 cm^{-1}) can be ascribed to the CT transition between $H2BIM^0$ and Me_2-$TCNQ^0$. Therefore, complex (**14**) should be designated as a $[H2BIM^{+\delta}][Me_2\text{-}TCNQ^{-\delta}]$ with $\delta \sim 0$.

The donor ability of $H2BIM^0$ is estimated to be as follows. The CT absorption energy of the Me_2-TCNQ complex with pyrene is observed at 13.7 x 10^3 cm^{-1} in chloroform. Usually, the CT energy in a solid shows a red shift by 2 ~ 3 x 10^3 cm^{-1} due to the crystal field interaction. Therefore, $H2BIM^0$ is a weaker donor by about 4 ~ 5 x 10^3 cm^{-1} (0.5 ~ 0.6 eV) than pyrene, and is comparable to naphthalene or phenanthrene.

$(H3BIM^+)_2(Me_2\text{-}TCNQ^-)$ (**15**): The 2:1 complex of (**15**) shows an IR spectrum similar to that of the 1:1 complex (**14**), except for a decreased intensity of the absorptions assigned to Me_2-$TCNQ^0$. The UV-VIS-NIR spectrum of the 2:1 complex (curve **iv** in Fig. 3-9) is almost identical to that of the 1:1 complex. These results indicate the real chemical formula of this complex to be $[H2BIM^{+\delta}]_2[Me_2\text{-}TCNQ^{-2\delta}]$ with $\delta \sim 0$.

$(H4BIM^{2+})_3(Me_2\text{-}TCNQ^-)_4(H_2O)_2$ (**20**): This complex exhibits somewhat different features. No absorptions ascribable to $H4BIM^{2+}$ and $H3BIM^+$ have been observed in the IR spectrum. Instead, all of the absorptions of $H2BIM^0$ have been detected, and the inclusion of water molecules has been identified by the broad bands at around 3450 and 1718 cm^{-1}. Several peaks due to neutral Me_2-$TCNQ^0$ were observed, though their intensities are very weak. However, the strong peak at 2913 cm^{-1} and the complicated ν_{CN} (2258, 2222, 2211, and 2177 cm^{-1}) can only be explained by the coexistence of Me_2-$TCNQ^0$ and $H2Me_2$-$TCNQ^0$, which have absorptions at 2913 (ν_{CH}) and 2258 (ν_{CN}) cm^{-1}. Thus, the IR spectrum of (**20**) is represented by a superposition of those of $H2BIM^0$, Me_2-$TCNQ^0$, $H2Me_2$-$TCNQ^0$, and H_2O. Since the UV-VIS-NIR spectrum of this 3:4 complex (curve **v** in Fig. 3-9) is almost identical

to that of a 1:1 complex of $[H2BIM^{0+\delta}][Me_2\text{-}TCNQ^{-\delta}]$ ($\delta \sim 0$), the electronic transition at the low-energy side (E-band) is attributed to the CT transition between the $H2BIM^0$ and Me_2-$TCNQ^0$ molecules. Consequently, the complex is formulated as $[H2BIM^{+\delta}]_3[Me_2\text{-}TCNQ^{-3\delta/(4-x)}]_{(4-x)}[H2Me_2\text{-}TCNQ^0]_x[H_2O]_2$ with $\delta \sim 0$; x ($\neq$0, 1) is unknown.

$(H3BIM^+)(MeO_2\text{-}TCNQ^-)$ (**16**): The IR spectrum of (**16**) is a superposition of those of the neutral $H2BIM^0$ and MeO_2-$TCNQ^0$, and no absorptions due to $H4BIM^{2+}$ and $H3BIM^+$ have been detected. The complex shows a broad electronic absorption band above 36.0 x 10^3 cm^{-1} due to $H2BIM^0$, and at around 23.2 x 10^3 cm^{-1} due to MeO_2-$TCNQ^0$. A broad shoulder near to 18 x 10^3 cm^{-1} should have originated from the CT transition from $H2BIM^0$ to MeO_2-$TCNQ^0$. This was confirmed by direct complex formation between $H2BIM^0$ and MeO_2-$TCNQ^0$ in the gas phase, to yield a 1:1 complex, $[H2BIM^0][MeO_2\text{-}TCNQ^0]$ (**9**), which has a broad shoulder near to 18 x 10^3 cm^{-1}, and its IR spectrum is completely represented by a superposition of the neutral $H2BIM^0$ and Me_2-$TCNQ^0$. This complex is represented as $[H2BIM^{+\delta}][MeO_2\text{-}TCNQ^{-\delta}]$ with $\delta \sim 0$.

For these neutral complexes, since the recombinational PT processes of the H2BIM system, $H4BIM^{2+} \rightarrow H2BIM^0 + 2H^+$, have occurred completely, these complexes are designated as weak CT complexes, where $H2BIM^0$ is an electron donor and Me_2-$TCNQ^0$ and MeO_2-$TCNQ^0$ are electron acceptors. The low degree of CT for these Me_2-TCNQ and MeO_2-TCNQ complexes, and their low conductivities may indicate an alternating stack of H2BIM and Me_2-TCNQ (or MeO_2-TCNQ) molecules in the crystal.

3-3-2-3 Mixed CT and PT Complex

3-3-2-3a TCNQ Complex: (11), (12), and (18)

The TCNQ complexes show resistivities of 10^6 ~ 10^7 Ωcm with the CT absorption below 5.2 x 10^3 cm^{-1}, which is usually ascribed to a transition among the

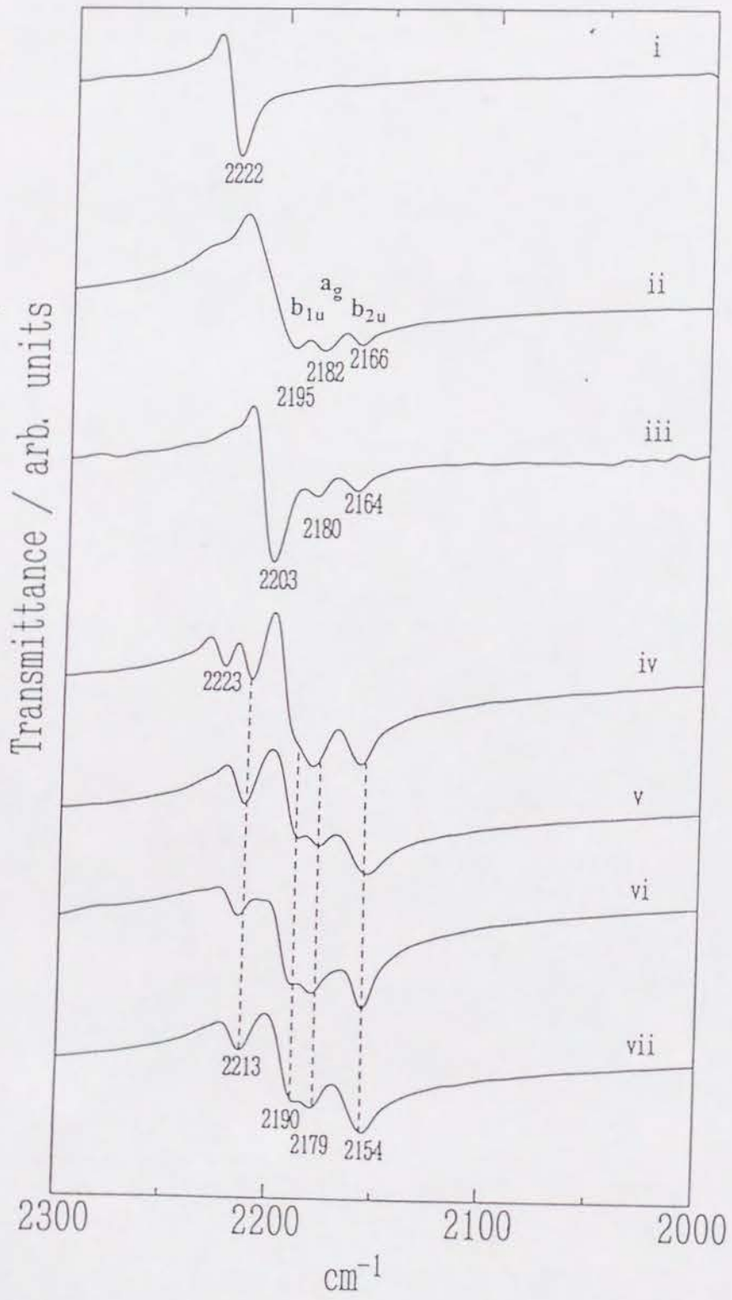

Fig. 3-11. Nitrile stretching frequencies (ν_{CN}) of TCNQ complexes, i) $TCNQ^0$, ii) $[K^+][TCNQ^{-\bullet}]$, iii) $[TTF^{+0.59}][TCNQ^{-0.59}]$, iv) $[Cs^+]_2[TCNQ^{-\bullet}]_2[TCNQ^0]$, v) $(H3BIM^+)(TCNQ^-)$, vi) $(H4BIM^{2+})(TCNQ^-)_2$, and vii) $(H3BIM^+)_2(TCNQ^-)_3$.

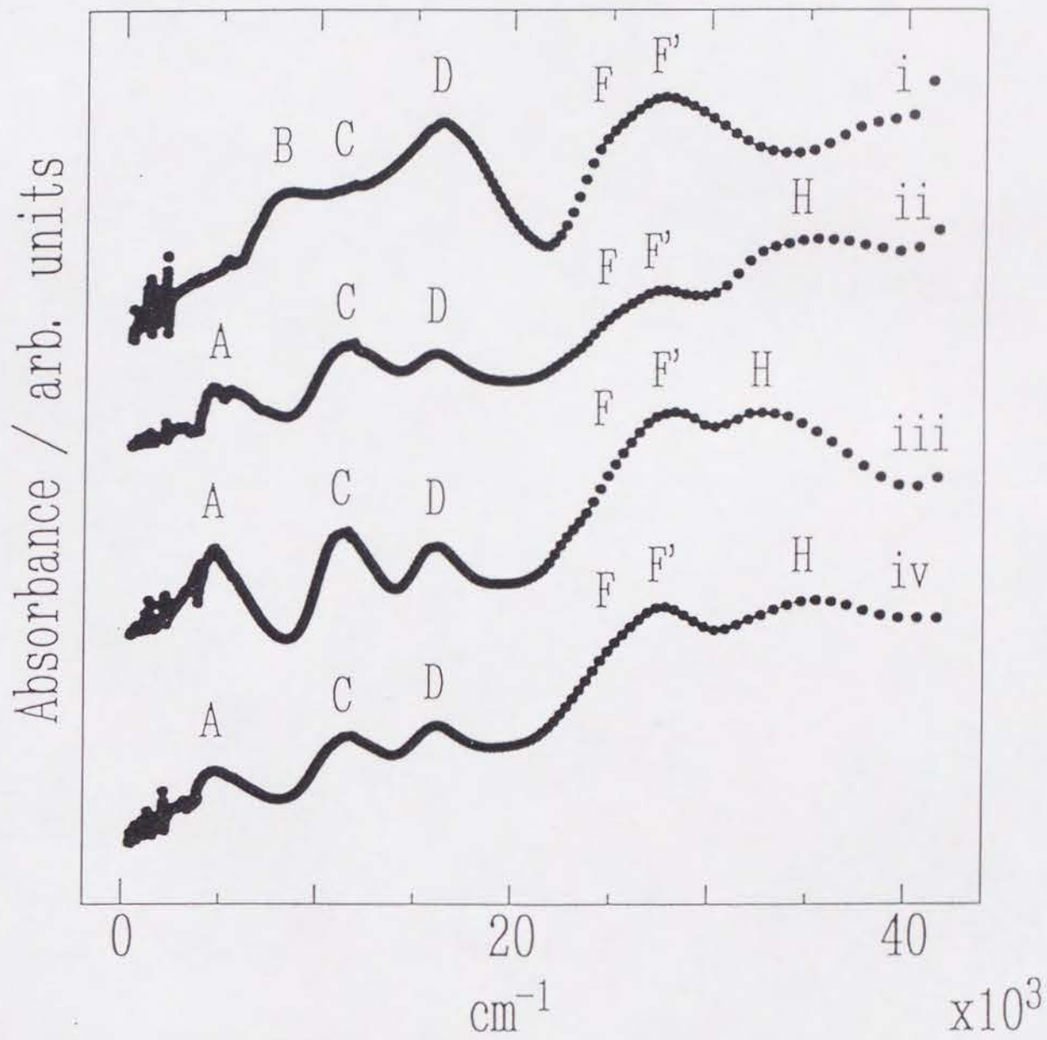

Fig. 3-10. UV-VIS-NIR spectra of TCNQ complexes, i) $[K^+][TCNQ^{-\bullet}]$, ii) $(H3BIM^+)(TCNQ^-)$ (**11**), iii) $(H4BIM^{2+})(TCNQ^-)_2$ (**18**), and iv) $(H3BIM^+)_2(TCNQ^-)_3$ (**12**). The origin of each band is denoted in Table 3-2.

segregated column of partially ionized or charge-separated TCNQ molecules. All of the TCNQ complexes have two kinds of ν_{CN} modes.

Figure 3-10 displays the UV-VIS-NIR spectra of TCNQ complexes. The completely ionized salt $[K^+][TCNQ^{-\bullet}]$, which contains dimerized non-uniform segregated TCNQ columns, reveals the B-band (intradimer transition) at 8.19 $x10^3 cm^{-1}$, the C-band (interdimer + monomer) at 11.6 x 10^3 cm^{-1}, the D-band at 16.6 x 10^3 cm^{-1} (the CT from next HOMO of $TCNQ^{-\bullet}$ to the LUMO of $TCNQ^0$ in the lowest triplet excited state), and the F- and F'-bands (intramolecular transition) at 25.3 (shoulder) and 27.6 x 10^3 cm^{-1}.[19] The UV-VIS-NIR spectra of $(H3BIM^+)(TCNQ^-)$ (**11**), $(H3BIM^+)_2$ $(TCNQ^-)_2(TCNQ^0)$ (**12**), and $(H4BIM^{2+})(TCNQ^-)_2$ (**18**) all bear a general resemblance to each other. The differences from $[K^+][TCNQ^{-\bullet}]$ represent the appearance of the H-band due to the $H2BIM^0$, $H3BIM^+$, and/or $H4BIM^{2+}$ species at 34 ~ 35 x 10^3 cm^{-1}, the increment of the intensity of the C-band, and especially the appearance of a new A-band below 5.0 x 10^3 cm^{-1}. The appearance of the A-band requires the incomplete CT state of TCNQ molecules in these complexes.[19] The distinct C-band may indicate: i) charge separation among the TCNQ molecules in a uniform segregated stacking; ii) a uniform charge, but non-uniform segregated stacking; or iii) a non-uniform charge in a non-uniform segregated stacking. The X-ray crystal analysis given in the Section 3-3-2-4 indicates the formation of non-uniform segregated stacking, which is also suggested by the spectral feature of the ν_{CN} mode.

Figure 3-11 shows the ν_{CN} of $TCNQ^0$, $[K^+][TCNQ^{-\bullet}]$, $[TTF^{+0.59}][TCNQ^{-0.59}]$, $(Cs^+)_2(TCNQ^-)_2(TCNQ^0)$, (**11**), (**12**), and (**18**). The $TCNQ^0$ has a single absorption at 2222 cm^{-1}, and $[K^+][TCNQ^{-\bullet}]$ has three distinguishable modes at 2195 (b_{1u}), 2182 (a_g), and 2166 cm^{-1} (b_{2u}).[20] The ν_{CN} of $[TTF^{+0.59}][TCNQ^{-0.59}]$ having uniform segregated stacks, shows a strong b_{1u} mode at 2203 cm^{-1}, a weak a_g (2180 cm^{-1}), and b_{2u} (2164 cm^{-1}) modes. On the contrary, the ν_{CN} of $[Cs^+]_2[TCNQ^{-\bullet}]_2[TCNQ^0]$, which has charge-separated TCNQ molecules in non-uniform stacks,[21] displays absorption due to $TCNQ^0$ (2223 cm^{-1}) and $TCNQ^{-\bullet}$ (2190, 2179, and 2154 cm^{-1}) in addition to the band at 2213 cm^{-1}. The ν_{CN} of three TCNQ complexes of (**11**), (**12**),

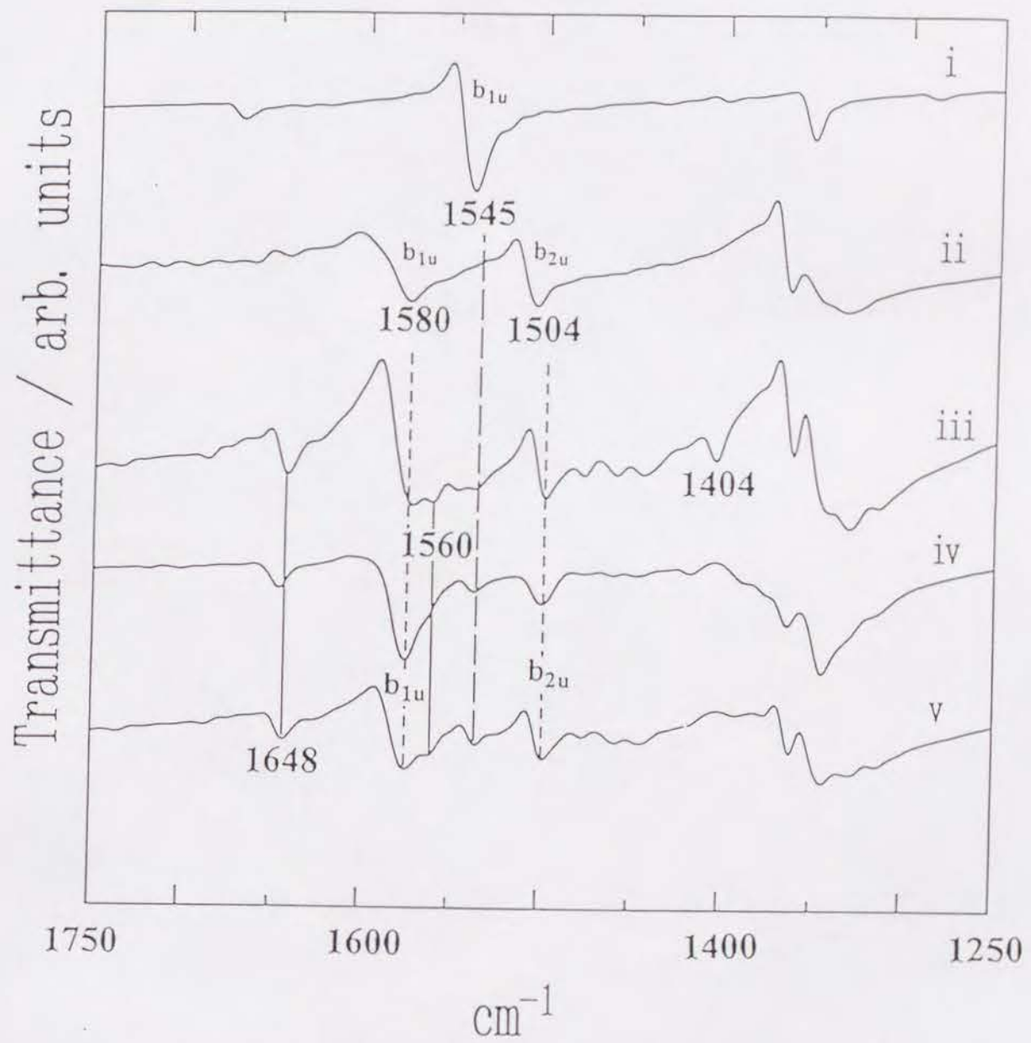

Fig. 3-12. Vibration spectra of TCNQ complexes in the frequency region 1750 ~ 1250 cm^{-1}. i) $TCNQ^0$, ii) $[K^+][TCNQ^{-\bullet}]$, iii) $(H3BIM^+)(TCNQ^-)$ (**11**), iv) $(H4BIM^{2+})(TCNQ^-)_2$ (**18**), and v) $(H3BIM^+)_2(TCNQ^-)_3$ (**12**).

and (**18**), which have four distinguishable bands at 2213, 2190, 2179, and 2154 cm^{-1}, greatly resemble each other and $(Cs^+)_2(TCNQ)_2(TCNQ^0)$, except for the disappearance of absorption at 2223 cm^{-1}. Three absorptions located at 2190, 2179, and 2154 cm^{-1} suggest the existence of $TCNQ^{-\bullet}$ species. The strong intensity of the a_g mode at 2179 cm^{-1} indicates dimerized non-uniform stacking.

Figure 3-12 shows the vibration spectra of $TCNQ^0$, $[K^+][TCNQ^{-\bullet}]$, (**11**), (**12**), and (**18**) in the frequency range of 1750 ~ 1250 cm^{-1}. The $TCNQ^0$ has a b_{1u} mode at 1545 cm^{-1}, and that of $TCNQ^{-\bullet}$ is observed at 1580 cm^{-1} in addition to the appearance of the b_{2u} mode at 1504 cm^{-1}.[20] Two kinds of b_{1u} (ν_{20}) modes due to $TCNQ^0$ and $TCNQ^{-\bullet}$ are observed at 1580 and 1545 cm^{-1} in my three TCNQ complexes (curves **iii**, **iv**, and **v** in Fig. 3-12). It is thus concluded that the existence of both $TCNQ^0$ and $TCNQ^{-\bullet}$ leads to a partial CT state having charge-separated TCNQ molecules in CT complexes.

Complex (**11**) has two additional absorptions at 1648 and 1560 cm^{-1} due to the existence of $H3BIM^+$, and a weak band at 1404 cm^{-1}, which has been identified to be the $\nu^b_{N\text{-}H}$ mode of $H2BIM^0$ (curve **iii** of Fig. 3-12. see Section 3-3-1-4). It is thus concluded that the mixed PT state is attained, and that the real chemical formula of this can be deduced as $[H3BIM^+]_x[H2BIM^0]_{1-x}[TCNQ^{-\bullet}]_x[TCNQ^0]_{1-x}$.

In the case of (**12**), the vibration spectrum is almost completely explained by the $TCNQ^0$, $TCNQ^{-\bullet}$, and $H3BIM^+$ species. The disappearance of the band at 1404 cm^{-1} indicates the absence of the $H2BIM^0$ species in (**12**). Thus, the spectral evidence for the complex deduces the real chemical formula as being $[H3BIM^+]_2[TCNQ^{-\bullet}]_2[TCNQ^0]$. Complex (**18**) exhibits the $\nu^s_{N\text{-}H}$ modes assignable to both $H3BIM^+$ (1648 and 1560 cm^{-1}) and $H4BIM^{2+}$ (1586 cm^{-1}), though the latter band overlaps with the b_{1u} mode of $TCNQ^{-\bullet}$. However, the absorption at 666 cm^{-1} clearly indicates the presence of the $H4BIM^{2+}$ species. These spectral features deduce the real chemical formula as being $[H4BIM^{2+}]_x[H3BIM^+]_{1-x}[TCNQ^{-\bullet}]_{1+x}[TCNQ^0]_{1-x}$.

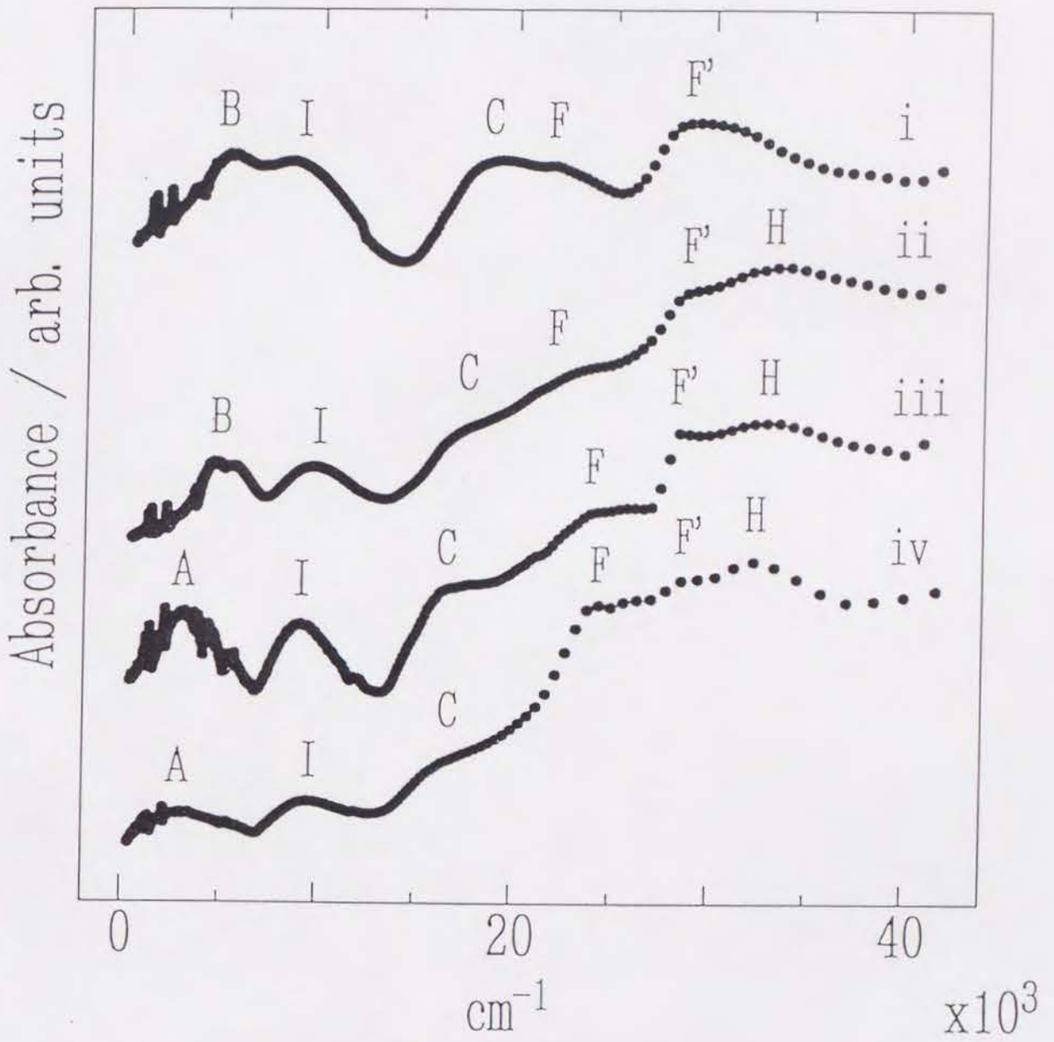

Fig. 3-13. UV-VIS-NIR spectra of BTDA-TCNQ complexes. i) $[Li^+][BTDA\text{-}TCNQ^{-\bullet}]$, ii) $(H3BIM^+)(BTDA\text{-}TCNQ^-)$ (**13**), iii) $(H4BIM^{2+})(BTDA\text{-}TCNQ^-)_2$ (**19**), and iv) $(triethylammonium^+)_2(BTDA\text{-}TCNQ)_3$. The origin of each band is denoted in Table 3-2.

It is concluded that these TCNQ complexes have segregated stacking, but lack the requirements for a low-dimensional organic metal, namely a uniform charge distribution with uniform stacking.

3-3-2-3b BTDA-TCNQ Complex: (13) and (19)

$(H4BIM^{2+})(BTDA\text{-}TCNQ^{-})_2$ (**19**) was the most conductive one (3.3×10^4 Ωcm) with the lowest E_a (0.16 eV) and $h\nu_{CT}$ (3.26×10^3 cm^{-1}) values among the complexes studied here. The UV-VIS-NIR spectra of the BTDA-TCNQ complexes are compared with those of $[Li^+][BTDA\text{-}TCNQ^{-\bullet}]$ and $(triethylammonium^+)_2(BTDA\text{-}TCNQ^{-})_2(BTDA\text{-}TCNQ^0)$ [22] in Fig. 3-13.

$(H3BIM^+)(BTDA\text{-}TCNQ^{-})$ (**13**) exhibits a similar spectrum to that of the Li salt. The first B-band at 5.23×10^3 cm^{-1} is ascribed to the CT transition in the segregated column of $BTDA\text{-}TCNQ^{-\bullet}$, i.e., $2BTDA\text{-}TCNQ^{-\bullet} \rightarrow BTDA\text{-}TCNQ^0 + BTDA\text{-}TCNQ^{2-}$, which is also observed in the Li salt at 5.23×10^3 cm^{-1}, indicating the small effective on-site Coulomb repulsion in $BTDA\text{-}TCNQ^{2-}$. The I-band at 9.66×10^3 cm^{-1} has the same origin to that of 8.35×10^3 cm^{-1} of the Li salt, and the assignment of this one is not clear. Since $[Li^+][BTDA\text{-}TCNQ^{-\bullet}]$ displays absorptions at 15.9, 17.4, 26.2, 28.8, and 32.8×10^3 cm^{-1} in acetonitrile, the C-band originates from the isolated monomer of $BTDA\text{-}TCNQ^{-\bullet}$. The F and F' bands are intramolecular ones in $BTDA\text{-}TCNQ^{-\bullet}$, and the H-band is assigned to the biimidazole species. The IR spectrum of (**13**) has a strong resemblance to those of 1 : 1 BTDA-TCNQ salts of Li^+, *N*-methylpyridinium, and ethyltrimethylammonium. Although the absorptions ascribable to those of $H4BIM^{2+}$, $H3BIM^+$, or $H2BIM^0$ could not be identified in the IR spectrum, the above results together with those of an elemental analysis and conductivity measurements indicate the real chemical formula of this complex to be $[H3BIM^+][BTDA\text{-}TCNQ^{-\bullet}]$ with segregated non-uniform stacking.

The most conductive complex in this study (**19**) clearly affords evidence of a mixed CT state in the UV-VIS-NIR spectrum, namely, the lowest energy A-band at 3.26×10^3 cm^{-1}, which originates from the intermolecular CT transition between charge-

separated species ($BTDA\text{-}TCNQ^0$ and $BTDA\text{-}TCNQ^{-\bullet}$ molecules) or partially ionized BTDA-TCNQ molecules (intraband transition). This kind of transition is also observed in $(triethylammonium^+)_2(BTDA\text{-}TCNQ)_3$ at 3.40×10^3 cm^{-1}. The other bands correspond to those observed in (**13**). The vibration spectrum of this complex is rather featureless, as usual for the mixed CT complex, due to an overlap of the electronic transition of the A-band. The total feature is more similar to that of $(triethylammonium^+)_2(BTDA\text{-}TCNQ)$ than $[Li^+][BTDA\text{-}TCNQ^{-\bullet}]$. The triethylammonium salt exhibits distinct absorptions assignable to $BTDA\text{-}TCNQ^0$ at 1203, 1165, 1026, 845, 831, 585, and 490 cm^{-1}, almost all of which are identified in (**19**), though their intensities are very weak. I have examined whether the cation species is $H4BIM^{2+}$, $H3BIM^+$, or a mixture of them. The vibration bands ascribable to $H2BIM^0$ were not present at all, but weak bands characteristic of $H3BIM^+$ and $H4BIM^{2+}$ were observed together with those unidentified. Taking into account these spectral features and the resistivity of 3.3×10^3 Ωcm, the complex is represented as $[H3BIM^+]_x[H4BIM^{2+}]_{1-x}[BTDA\text{-}TCNQ^{-\delta}]_y[BTDA\text{-}TCNQ^{-(1-\delta)}]_{2-y}$ with $\delta \sim 1$, $0 < x < 1$ and $y = \frac{2\delta - x}{2\delta - 1}$, and segregated non-uniform stacking.

3-3-2-4 Crystal Structure of $[H3BIM^+]_2[TCNQ^{-\bullet}]_2[TCNQ^0]$ (12)

Some of the TCNQ complexes with a 2 : 3 composition have already been prepared. Among them, the common crystal characteristics have been observed for $(TMA^+)_2(TCNQ^-)_2(TCNQ^0)$, $(Cs^+)_2(TCNQ)_2(TCNQ^0)$, and $(Mor^+)_2(TCNQ)_2(TCNQ^0)$, where TMA^+ and Mor^+ are tetramethylammonium and morpholinium, respectively[21, 23, 24] All of these reference complexes have two $TCNQ^{-\bullet}$ molecules and one $TCNQ^0$ molecule in the crystal. Table 3-8 compares the natures of the intermolecular contacts, that is, the mean interplanar distance in the TCNQ columns ($A^{-\bullet}$ ••• $A^{-\bullet}$ and $A^{-\bullet}$ ••• A^0, where $A^{-\bullet}$ and A^0 are $TCNQ^{-\bullet}$ and $TCNQ^0$, respectively), interatomic contacts ($A^{-\bullet}$ ••• D^+, where D^+ is the counter cation), and selected intramolecular distances of the 2 : 3 TCNQ complexes with those of $(H3BIM^+)_2(TCNQ^-)_2(TCNQ^0)$ (**12**).

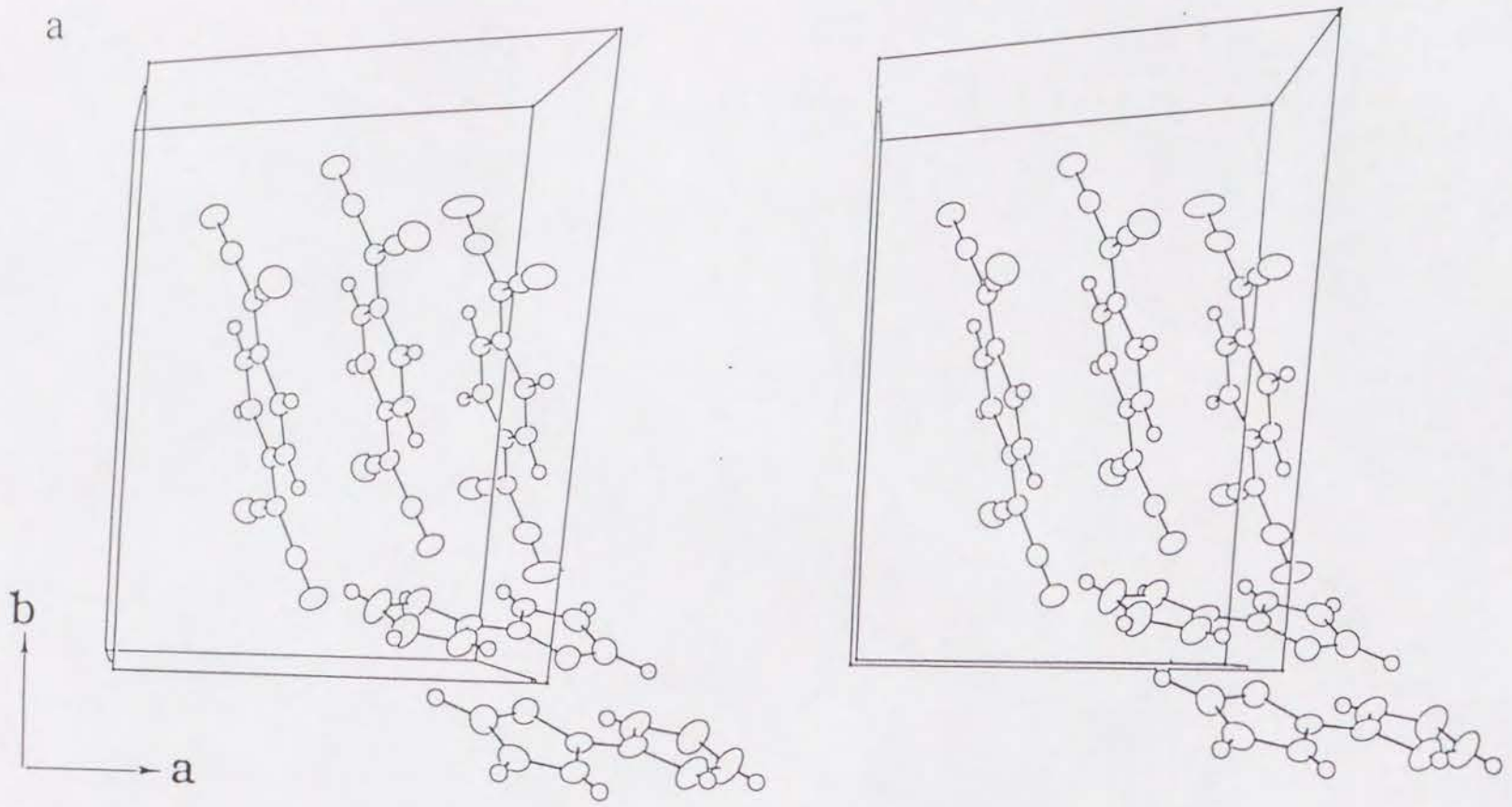

Table 3-8. Mean Interplanar Distances (Å), Intermolecular Contacts (Å), and Selected Intramolecular Distances (Å) of Some TCNQ Complexes with the Composition of 2 : 3.

Real composition [a]	$A^{-\bullet}\cdots A^{-\bullet}$ [b]	$A^{-\bullet}\cdots A^{0}$ [c]	$A^{-\bullet}\cdots D^{+}$ [d]	**b** [e] $A^{-\bullet} : A^{0}$ [c]	**c** [e] $A^{-\bullet} : A^{0}$ [c]	**d** [e] $A^{-\bullet} : A^{0}$ [c]
$[TMA^{+}]_2[TCNQ^{-\bullet}]_2[TCNQ^{0}]$	3.26	No contact[f]	N-H$^{+}\cdots$N≡C = 3.031	1.419 : 1.447	1.421 : 1.338	1.423 : 1.433
$[Cs^{+}]_2[TCNQ^{-\bullet}]_2[TCNQ^{0}]$	3.26	3.22	Cs$^{+}\cdots$N≡C = 3.07	1.427 : 1.444	1.410 : 1.371	1.419 : 1.428
$[Mor^{+}]_2[TCNQ^{-\bullet}]_2[TCNQ^{0}]$	3.24	3.25	N-H$^{+}\cdots$N≡C = 2.945	1.419 : 1.432	1.416 : 1.391	1.414 : 1.426
$[H3BIM^{+}]_2[TCNQ^{-\bullet}]_2[TCNQ^{0}]$	3.28	3.27	N-H$^{+}\cdots$N≡C = 2.903	1.428 : 1.449	1.407 : 1.360	1.432 : 1.449

a) TMA^{+} and Mor^{+} are tetramethylammonium and morpholinium, respectively. b) Interplanar distance between two $TCNQ^{-\bullet}$ ($A^{-\bullet}$). Overlap mode is the ring - ring type. c) Interplanar distance between $TCNQ^{-\bullet}$ ($A^{-\bullet}$) and $TCNQ^{0}$ (A^{0}). Overlap mode is ring - external bond type. d) Intermolecular contacts between $TCNQ^{-\bullet}$ ($A^{-\bullet}$) and counter cation (D^{+}). e) Bond lengths **b**, **c**, and **d** are shown in Fig. 3-14b, where TCNQ(1) and TCNQ(2) correspond to the $TCNQ^{0}$ and $TCNQ^{-\bullet}$, respectively. f) $[TMA^{+}]_2[TCNQ^{-\bullet}]_2[TCNQ^{0}]$ has no effective intermolecular contacts within the sum of the van der Waals redius.

b

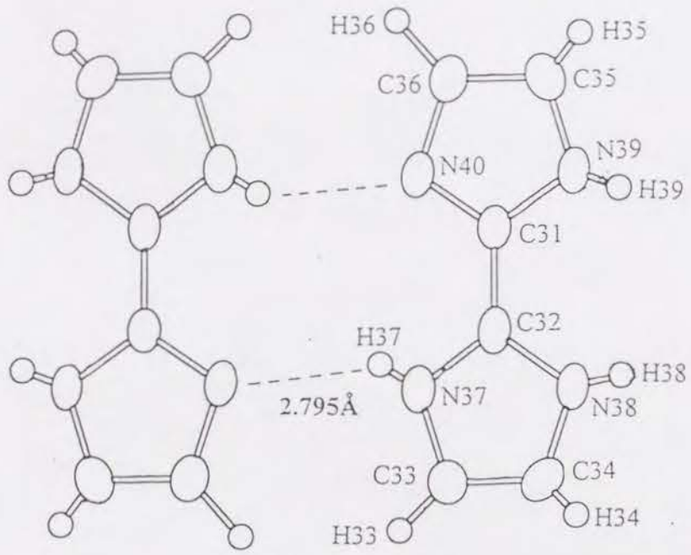

H3BIM$^+$ Dimer

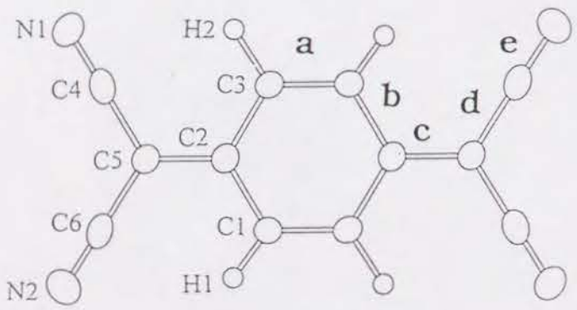

TCNQ(1)

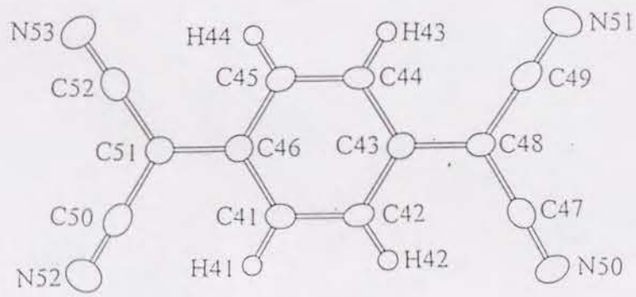

TCNQ(2)

Fig. 3-14. Crystal structure of $(H3BIM^+)_2(TCNQ^-)_3$ (**12**). a) Unit cell of $(H3BIM^+)_2(TCNQ^-)_3$ viewed along the c-axis (stereoview). b) Hydrogen bond $H3BIM^+$ dimer, TCNQ(1), and TCNQ(2) showing the atom numbering scheme. Dashed lines indicate N-H•••N hydrogen bond (2.795Å).

Figure 3-14a shows a stereoview of the crystal packing of $(H3BIM^+)_2(TCNQ^-)_2(TCNQ^0)$ viewed along the c-axis. Fig. 3-14b illustrates the crystallographically independent $H3BIM^+$, which is drawn as a dimer, and two kinds of TCNQ molecules (TCNQ(1) and TCNQ(2)) with an atomic-numbering scheme. The TCNQ(1) lies on a center of inversion. The TCNQ molecules stack in a segregated pattern parallel to the a-axis. The $H3BIM^+$ molecules are connected by two intermolecular N-H•••N hydrogen bonds, so as to form a nearly planar dimer. The $H3BIM^+$ dimer is located essentially perpendicular to the TCNQ column with the molecular long axis along the TCNQ column. The N•••N bond length of 2.795(7) Å in the $H3BIM^+$ dimer is contracted by 0.305 Å compared with the sum of the van der Waals radius of nitrogen (3.10 Å).[7] This distance can be comparable to the N•••N distance of 2.75(1) Å observed in [pyridine][pyridinium$^+$][I^-], which has unsymmetric N-H•••N hydrogen bonds.[25] In the N-H•••N system reported here, the hydrogen atoms are unsymmetrically located in the hydrogen bonds within the accuracy of structural analysis. Therefore, two $H3BIM^+$ molecules are related by short and unsymmetric hydrogen bonds at ambient pressure in the crystal.

The mean bond lengths (**b**, **c**, and **d** as shown in Fig. 3-14b) were used to estimate the charged state of the TCNQ molecules,[26] where I assume an inversion center at the center of the TCNQ(2) molecule; some deviations were detected in three reference complexes. The **b** value of 1.449Å of TCNQ(1) is similar to those of $TCNQ^0$ (1.432Å) in the TMA and Cs salts, and that of TCNQ(2) (1.428Å) is similar to that of $TCNQ^{-\bullet}$ in the Cs salt (1.427Å). The bond length **c** in the TCNQ molecule is known to elongate by the addition of an electron. The changes in the **c** values of TCNQ(1) and TCNQ(2) in complex (**12**) have quantitatively the same tendency as those of $TCNQ^0$ and $TCNQ^{-\bullet}$ in the Cs salt, respectively. Although bond length **d** increases to some extent, the overall feature is similar to those of the reference complexes. It is thus said that TCNQ(1) is nearly neutral and TCNQ(2) is completely charged:

$$TCNQ(1) = TCNQ^0$$

$$TCNQ(2) = TCNQ^{-\bullet}$$

As a result, the real chemical formula is deduced to be $[H3BIM^+]_2[TCNQ^{-\bullet}]_2[TCNQ^0]$, which is consistent with that one derived from the spectroscopic results.

In the case of (**12**), the order of stacking of the TCNQ molecules within a column is represented as $TCNQ(2)^{-\bullet}$ ~ $TCNQ(1)^0$ ~ $TCNQ(2)^{-\bullet}$ in Fig. 3-15a. This indicates that the TCNQ column consists of a timer unit, and two types of overlap modes are observed: the ring - external bond for $TCNQ(2)^{-\bullet}$ ~ $TCNQ(1)^0$ and the ring - ring for $TCNQ(2)^{-\bullet}$ ~ $TCNQ(2)^{-\bullet}$. The mean intratrimer separation ($TCNQ(2)^{-\bullet}$ ~ $TCNQ(1)^0$ = 3.27 Å) is comparable to the intertrimer separation ($TCNQ(2)^{-\bullet}$ ~ $TCNQ(2)^{-\bullet}$ = 3.28 Å). The effective overlap mode exists between two $TCNQ(2)^{-\bullet}$ molecules, and $TCNQ(2)^{-\bullet}$ is connected to $H3BIM^+$ by a N-H•••N≡C hydrogen bond. For all of 2 : 3 complexes in Table 3-8, the overlap modes of the TCNQ molecule within the column are the ring-over-ring ($TCNQ^{-\bullet}$ ~ $TCNQ^{-\bullet}$) and ring-over-bond ($TCNQ^0$ ~ $TCNQ^{-\bullet}$) types.[24b)]

All of the complexes listed in Table 3-8 have short atomic contacts, N-H•••N≡C hydrogen bonds or a Cs^+•••N≡C contact, between the monovalent $TCNQ^{-\bullet}$ and the cations. Figure 3-15a shows the cations and TCNQ columns of $(H3BIM^+)_2$ $(TCNQ^-)_2$ $(TCNQ^0)$ viewed along the molecular long axis of TCNQ. Each $TCNQ(2)^{-\bullet}$ is connected by N-H•••N≡C hydrogen bonds, where the N•••N distance (2.903(7) Å) is shorter than those of $(TMA^+)_2(TCNQ^-)_2(TCNQ^0)$ (3.031 Å) and $(Mor^+)_2$ $(TCNQ^-)_2(TCNQ^0)$ (2.945 Å). This result indicates the formation of a strong hydrogen bond in (**12**). The local structure of (**12**) comprises the hydrogen bond unit, $TCNQ(2)^{-\bullet}$ ••• $H3BIM^+$ ••• $H3BIM^+$ ••• $TCNQ(2)^{-\bullet}$, and $TCNQ(2)^{-\bullet}$ makes dimeric pairs by an effective overlap within the TCNQ column.

Figure 3-15b illustrates the overall crystal packing viewed along the perpendicular direction of the TCNQ plane. The TCNQ stacks are represented by $TCNQ(2)^{-\bullet}$ ~ $TCNQ(2)^{-\bullet}$ pairs, and the hydrogen bond networks are indicated by the dotted lines. Along the c-axis, there are no intermolecular side-by-side contacts of the TCNQ molecules, which are shorter than the sum of the van der Waals contacts. The $H3BIM^+$ dimer is located at a parallel position to the TCNQ column. The mean interplanar

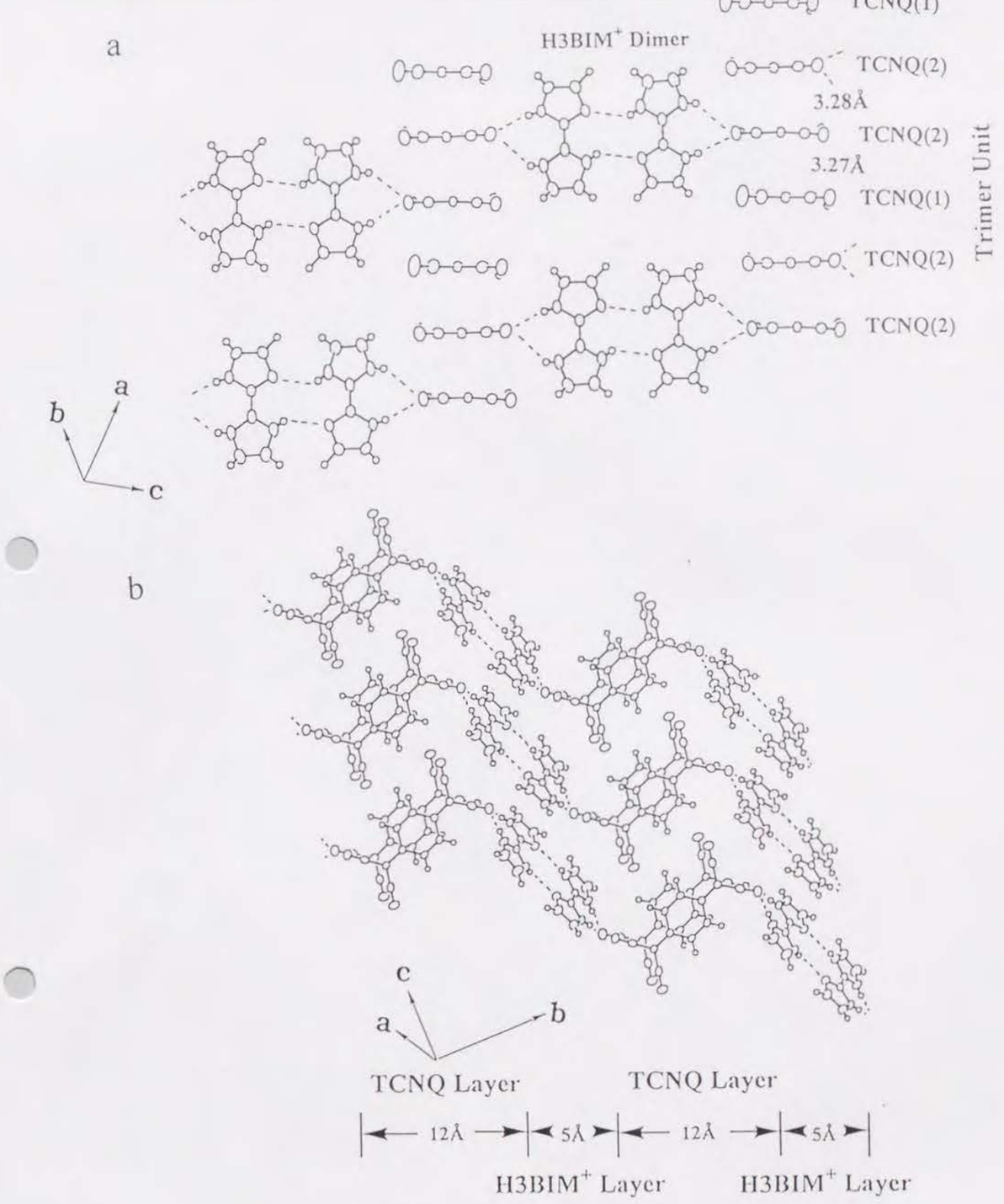

Fig. 3-15. Intermolecular contacts of $(H3BIM^+)_2(TCNQ^-)_3$ (**12**). a) N-H•••N and N-H•••N≡C hydrogen bond structures viewed along the molecular long axis of TCNQ. The TCNQ column is composed of trimer unit (TCNQ(2) ~ TCNQ(1) ~ TCNQ(2)) and the mean interplaner distances of TCNQ(1) ~ TCNQ(2) and TCNQ(2) ~ TCNQ(2) are 3.27 and 3.28Å, respectively. Dashed lines show the hydrogen bonds. b) Overall crystal packing viewed along the perpendicular direction of the TCNQ plane. Dashed lines indicate the hydrogen bonds. The crystal is constructed by two-dimensional TCNQ layer (12Å) and $H3BIM^+$ dimer layer (5Å).

distance between the $H3BIM^+$ molecules, which overlaps at the five-membered ring moiety of $H3BIM^+$, was obtained as 3.17 Å; the thickness of cation layers was thus estimated to be about 5.0 Å. Along the b-axis, the TCNQ (about 12 Å) and $H3BIM^+$ layers (about 5 Å) stack in an alternating fashion and form a two-dimensional layered structure. The hydrogen bond unit relays in the crystal by the CT interactions (Scheme 3-1), and the neutral $TCNQ(1)^0$ incorporates into these hydrogen bond and CT networks.

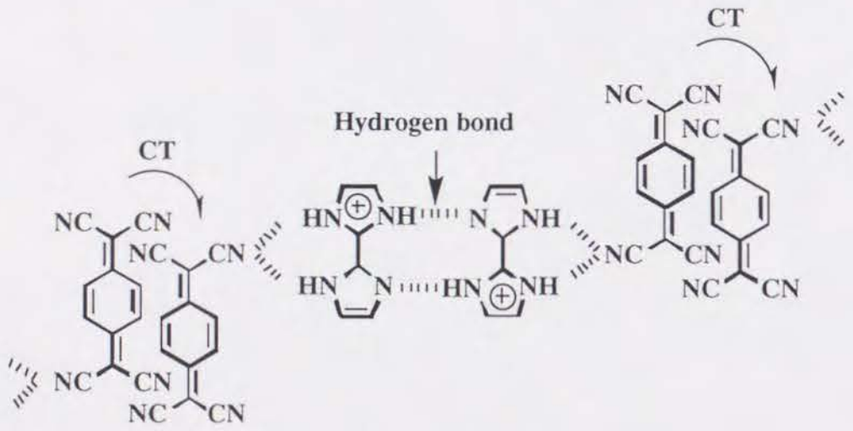

Scheme 3-1

3-3-3 Mechanism of Complex Formation Regarding with PT and CT

In the metathesis reaction, the complex formation accompanies with a charge redistribution and recombination among the initial components. Thus, both of the protonated state of the H2BIM system and the valence state of the TCNQs are expected to change from the initial condition to the real one. The types of obtained complexes vary according to the kinds of TCNQ derivatives; for example, F_4-TCNQ and Me_2-TCNQ gave completely ionic and neutral complexes, respectively, in the metathesis reaction. For the neutral complexes, the protonated states of the H2BIM system changed from $H3BIM^+$ or $H4BIM^{2+}$ to the $H2BIM^0$ species.

Here, I defined the complete PT reaction, such as $H4BIM^{2+} \rightarrow H3BIM^+ + H^+$. For most partial CT complexes, the protonated states of H2BIM system contain two kinds of species, that is, $[H2BIM^0]_x[H3BIM^+]_{1-x}$ and $[H3BIM^+]_x$

$[H4BIM^{2+}]_{1-x}$, which is called mixed PT.

Complete PT; $H4BIM^{2+}$ (or $H3BIM^+$) $\rightarrow$ $H3BIM^+$ (or $H2BIM^0$) + H^+

Mixed PT; $H4BIM^{2+} \rightarrow [H4BIM^{2+}]_{1-x}[H3BIM^+]_x + xH^+$

$H3BIM^+ \rightarrow [H3BIM^+]_{1-x}[H2BIM^0]_x + xH^+$

No PT; $H4BIM^{2+}$ (or $H3BIM^+$) $\not\rightarrow$ $H3BIM^+$ (or $H2BIM^0$) + H^+

In order to gain a deeper insight into the mechanism of the protonation and deprotonations on the complex formation of the H2BIM system, I examined the CT and PT natures of the TCNQs and H2TCNQs molecules.

Nine independent species can also be speculated for the H2TCNQs - TCNQs system (see Section 1-2). Table 3-9 summarizes the oxidation and reduction peak potentials of $TCNQs^{-\bullet}$ (E^o_{p1} or E^r_{p2}) together with pK_{a1}, pK_{a2}, and pK_{a3}, as shown in Fig. 1-5. At the same time, the differences in the reduction potentials of $TCNQs^{-\bullet}$ and $H3BIM^+$ or $H4BIM^{2+}$ (ΔE_{p1} or ΔE_{p2}) are summarized, where ΔE_{p1} and ΔEp_2 are defined as $E^o_{p1}(TCNQs^{-\bullet})$ - $E^r_{p1}(H3BIM^+)$ and E^o_{p1} $(TCNQs^{-\bullet})$ - $E^r_{p1}(H4BIM^{2+})$, respectively. Also, the differences in the pK_a values for TCNQ-• and $H3BIM^+$ or $H4BIM^{2+}$ (ΔpK_{a1} and ΔpK_{a2}) are listed in the table, where ΔpK_{a1} and ΔpK_{a2} correspond to $pK_a(H3BIM^+)$ - $pK_{a3}(TCNQ^{-\bullet})$ and $pK_a(H4BIM^{2+})$ - $pK_{a3}(TCNQ^{-\bullet})$, respectively. The oxidation peak potentials of $TCNQs^{-\bullet}$ decrease in the following order:

F_4-$TCNQ^{-\bullet}$ (0.66 V) > $TCNQ^{-\bullet}$ (0.31 V) > Me_2-$TCNQ^{-\bullet}$ (0.24 V) >

BTDA-$TCNQ^{-\bullet}$ (0.13 V vs. Ag / AgCl).

Thus, the electron-donating abilities of $TCNQs^{-\bullet}$ increase in the above order, and the electron-accepting ones are the inverse order from the E^r_{p2} values. In addition to the previously reported pK_{a1} and pK_{a2} of H2TCNQs, I obtained the acidity of $TCNQs^{-\bullet}$ (pK_{a3}) in the $HTCNQs^{\bullet} \rightleftarrows TCNQs^{-\bullet} + H^+$ process. However, the following

Table 3-9. Redox Peak Potentials (V) [a] and pK_a Values [b] of $TCNQs^{-\bullet}$ System.

Compounds	E^o_{p1}	Er_{p2}	pK_{a1}	pK_{a2}	pK_{a3}	ΔE^1_p [c]	ΔE^2_p [d]	ΔpK_{a1} [e]	ΔpK_{a2} [f]
F_4-$TCNQ^{-\bullet}$	0.66	0.02	4.01	4.20	~ 0	1.50	1.20	~ 4.6	~ -0.2
$TCNQ^{-\bullet}$	0.31	-0.36	7.10	10.30	~ 2.0	1.15	0.85	~ 2.6	~ -2.2
Me_2-$TCNQ^{-\bullet}$	0.24	-0.38	7.60	11.30	~ 5.0	1.08	0.78	~ -0.4	~ -5.2
BTDA-$TCNQ^{-\bullet}$	0.13	-0.51	—	—	~ 1.0	0.97	0.67	~ 3.6	~ -1.2

a) Measured in DMF, Ag / AgCl, $TBA{\bullet}BF_4$ (0.1 M), scan rate 100 mVs^{-1}, and Pt electrode. E^o_{p1} and Er_{p2} correspond to the processes; $TCNQs^{-\bullet} \rightarrow TCNQ^0 + e^-$ and $TCNQ^{-\bullet} + e^- \rightarrow TCNQ^{2-}$, respectively. b) Measured in DMF - H_2O (7:3). pK_{a1} and pK_{a2} indicate the following acid dissociation processes, $H2TCNQs^0 \rightleftarrows TCNQs^{-\bullet} + H^+$ (pK_{a2}). pK_{a3} is the basic acidity of $TCNQs^{-\bullet}$ species, $TCNQs^{-\bullet} + H^+ \rightleftarrows HTCNQ^{\bullet}$. c) $\Delta E^1_p = E^o_{p1}$ ($TCNQs^{-\bullet}$) - Er_{p1} ($H3BIM^+$). Er_{p1} ($H3BIM^+$) is -0.84V. d) $\Delta E^2_p = E^o_{p1}$ ($TCNQs^{-\bullet}$) - Er_{p1} ($H4BIM^{2+}$). Er_{p1} ($H4BIM^{2+}$) is -0.54V. e) ΔpK_{a1} = $pK_a(H3BIM^+)$ - pK_{a3} ($TCNQs^{-\bullet}$). f) $\Delta pK_{a2} = pK_a(H4BIM^{2+})$ - pK_{a3} ($TCNQs^{-\bullet}$).

disproportionation reaction (equation 3-1) caused some ambiguity in the determination of the pK_{a3} values:

$$TCNQs^{-\bullet} + H^+ \overset{pK_{a3}}{\rightleftarrows} HTCNQs^{\bullet} \rightarrow 0.5TCNQs^0 + 0.5H2TCNQs^0. \quad (3\text{-}1)$$

The pK_{a3} values of $TCNQs^{-\bullet}$ increase in the order F_4-$TCNQ^{-\bullet}$, $TCNQ^{-\bullet}$, and Me_2-$TCNQ^{-\bullet}$, and an unexpected high pK_{a3} was observed for BTDA-$TCNQ^{-\bullet}$. The obtained order of the acidity (pK_{a3}) was as follows:

Me_2-$TCNQ^{-\bullet}$ (pK_{a3} ~5) > $TCNQ^{-\bullet}$ (~2) > BTDA-$TCNQ^{-\bullet}$ (~1) > F_4-$TCNQ^{-\bullet}$ (~0).

The anomalously high acidity of BTDA-$TCNQ^{-\bullet}$ influences CT complex formation in the metathesis reaction.

I now examine the individual complex formation processes. The initial species in the metathesis complex formation are $TCNQs^{-\bullet}$ and $H3BIM^+$ or $H4BIM^{2+}$. Consequently, the first step reaction of complex formation is the electron-transfer (CT), proton-transfer (PT), or hydrogen-transfer (HT) processes between the initial species:

$H3BIM^+$(or $H4BIM^{2+}$) + $TCNQs^{-\bullet}$ → $H3BIM^{\bullet}$(or $H4BIM^{+\bullet}$) + $TCNQ^0$ ••• *CT*

$H3BIM^+$(or $H4BIM^{2+}$) + $TCNQs^{-\bullet}$ → $H2BIM^0$(or $H3BIM^+$) + $HTCNQ^{\bullet}$ ••• *PT*

$H3BIM^+$(or $H4BIM^{2+}$) + $TCNQs^{-\bullet}$ → $H2BIM^{+\bullet}$(or $H3BIM^{2+\bullet}$) + $HTCNQ^-$ ••• *HT*

At first, I consider the possibilities of CT from an electron donor, $TCNQs^{-\bullet}$, to an electron acceptor, $H3BIM^+$ or $H4BIM^{2+}$. I can predict the CT state of the obtained complexes using the difference in the oxidation potentials of the donor and the reduction potentials of the acceptor (ΔE_p).[1b] The equation proposed by Saito and Ferraris,

Ionic ≤ Mixed valence ≤ Neutral

$-0.02 \leq \Delta E^{1 \text{ or } 2}{}_p = E_p(\text{Donor}) - E_p(\text{Acceptor}) \leq 0.34$,

is examined to predict the CT state for the TCNQ system. I can obtain the following ΔE_p values for the combination of $TCNQs^{-\bullet}$ - $H3BIM^+$ and $TCNQ^{-\bullet}$ - $H4BIM^{2+}$ (see Table 3-9):

$$0.97 \leq \Delta E^1{}_p = E^o{}_{p1}(TCNQs^{-\bullet}) - E^r{}_{p1}(H3BIM^+) \leq 1.50$$

and

$$0.67 \leq \Delta E^2{}_p = E^o{}_{p1}(TCNQs^{-\bullet}) - E^r{}_{p1}(H4BIM^{2+}) \leq 1.20.$$

For the $H3BIM^+$ and $H4BIM^{2+}$ complexes, the ΔE_p values greatly shifted to the positive side, which indicates that the CT from $TCNQ^{-\bullet}$ to $H3BIM^+$ or $H4BIM^{2+}$ is very unrealistic, due both to the low electron-accepting abilities of the $H3BIM^+$ and $H4BIM^{2+}$ species, and the loss of the Madelung energy in the CT process.

I next consider the possibility of the HT processes. Since the energetically unstable species $H3BIM^{2+\bullet}$ was formed by the HT reaction of the $H4BIM^{2+}$ species, the possibility of the HT process is very low. As a result, the first-step reaction of the complex formation is highly expected to be the PT process from $H3BIM^+$ or $H4BIM^{2+}$ to $TCNQs^{-\bullet}$. Although the equilibrium of $H^+ + I^- \rightleftarrows HI$ also exists during the metathesis reaction, I neglect this process in order to simplify the mechanism of complex formations.

It was expected that the differences in the acidity (ΔpK_a) between $H4BIM^{2+}$ (or $H3BIM^+$) and $TCNQs^{-\bullet}$ determine whether the PT reaction occurs or not. In the case of a negative ΔpK_a value, the $H4BIM^{2+}$ (or $H3BIM^+$) $\rightarrow$ $H3BIM^+$ (or $H2BIM^0$) process occurs, while there is no contribution from the PT process in the case of a positive ΔpK_a value. In the region of $\Delta pK_a \approx 0$, the mixed PT states are attained. In the following, the mechanism of CT complex formation is discussed in detail. Table 3-10 summarizes the PT and CT states, type of obtained complexes, ΔpK_a between

Table 3-10. Entry Number, Type of Complexes, ΔpK_a between HxBIM (x = 2 ~ 4) and TCNQs, and the Degree of PT (%) for the Obtained TCNQ Complexes

Entry [a]	Type [b]		ΔpK_a [c]	% of PT species [d]
H2BIM⁰ Complex	***PT***	***CT***		***% of HBIM⁻***
8	No	No	7.3	0
9	No	No	~7	0
H3BIM⁺ Complex				***% of H2BIM⁰***
10	No	Complete	~4.6	0
11	Mixed	Mixed	2.6	11
12	No	Mixed	2.6	0
13	No	Complete	3.6	0
14	Complete	No	-0.4	100
15	Complete	No	-0.4	100
16	Complete	No	~ -0.4	100
H4BIM²⁺ Complex				***% of H3BIM⁺***
17	Mixed	Complete	~0	10
18	Mixed	Mixed	-2.2	40
19	Mixed	Mixed	-1.2	—
20	Complete	No	-5.2	100

a) Entry number and real chemical formula are corresponding to those in Table 3-1. b) The classification of the protonated and electronic states of H2BIM and TCNQ systems, respectively. c) $\Delta pK_a = pK_a(H2BIM^0, H3BIM^+, \text{or } H4BIM^{2+}) - pK_a(TCNQs^{-\bullet})$. The $pK_a(TCNQ^{-\bullet})$ is the acid dissociation process as shown in Fig. 1-5. d) The contents of PT species in the complexes, % of $HBIM^- = [HBIM^-] / \{[H2BIM^0] + [HBIM^-]\}$, % of $H2BIM^0 = [H3BIM^+] / \{[H2BIM^0] + [H3BIM^+]\}$, and % of $H3BIM^+ = [H4BIM^{2+}] / \{[H4BIM^{2+}] + [H3BIM^+]\}$.

$H4BIM^{2+}$ (or $H3BIM^{+}$) and $TCNQs^{-\bullet}$, and the degree of PT species (%) based on the discussion given in the Sections 3-3-3-1 ~ 3-3-3-3.

3-3-3-1 Completely Ionic Complex: (10), (13), and (17)

The complexes of $[H3BIM^{+}][F_4\text{-}TCNQ^{-\bullet}]$ (**10**) and $[H3BIM^{+}][BTDA\text{-}TCNQ^{-\bullet}]$ (**13**) belong to the completely ionic CT with a non-mixed PT complex; $[H3BIM^{+}]_{0.1}[H4BIM^{2+}]_{0.9}[F_4\text{-}TCNQ^{-\bullet}]_{1.9}[H_2O]_2$ (**17**) is classified as a completely ionic CT with a mixed PT complex. The acidity of $H3BIM^{+}$ ($pK_{a2} = 4.60$) is fairly lower than the acidity (pK_{a3}) of $F_4\text{-}TCNQ^{-\bullet}$ ($pK_{a3} < 0$) and $BTDA\text{-}TCNQ^{-\bullet}$ ($pK_{a3} \sim 1$). This means that the PT from $H3BIM^{+}$ to $F_4\text{-}TCNQ^{-\bullet}$ and $BTDA\text{-}TCNQ^{-\bullet}$,

$$H3BIM^{+} + F_4\text{-}TCNQ^{-\bullet} \not\rightarrow H2BIM^{0} + HF_4\text{-}TCNQ^{\bullet}$$

and

$$H3BIM^{+} + BTDA\text{-}TCNQ^{-\bullet} \not\rightarrow H2BIM^{0} + HBTDA\text{-}TCNQ^{\bullet},$$

are negligible for these two acceptors. Consequently, the complexes of completely ionic CT with a non-mixed PT were formed directly by the cation exchange reactions from $[Li^{+}][TCNQs^{-\bullet}]$ to $[H3BIM^{+}][TCNQs^{-\bullet}]$ lacking an intermediate PT state, i.e. $HF_4\text{-}TCNQ^{\bullet}$ and $HBTDA\text{-}TCNQ^{\bullet}$ species.

For $[H3BIM^{+}]_{0.1}[H4BIM^{2+}]_{0.9}[F_4\text{-}TCNQ^{-\bullet}]_{1.9}[H_2O]_2$ (**17**), the results of elemental and spectroscopic analyses indicate the following PT-assisted reaction scheme, $H4D^{2+} + A^{-\bullet} \rightarrow H3D^{+} + HA^{\bullet}$:

$$H4D^{2+} + 2A^{-\bullet} \rightarrow 0.9H4D^{2+} + 0.1H3D^{+} + 1.9A^{-\bullet} + 0.1\,HA^{\bullet}$$
$$\xrightarrow[H_2O]{} [H4D^{2+}]_{0.9}[H3D^{+}]_{0.1}[A^{-\bullet}]_{1.9}[H_2O]_2\downarrow + 0.1HA^{\bullet}, \quad (3\text{-}2)$$

where D and A represent BIM and F_4-TCNQ, respectively. The low stability of the monoprotonated neutral radical state, $HTCNQs^{\bullet}$, easily gives rise to a disproportionation

reaction as shown in equation 3-1. I confirmed the formation of $F_4\text{-}H2TCNQ^{0}$, which has a strong absorption of ν_{CH} at 2911 cm^{-1}, by an analysis of the residual compounds (Table 3-3).

The occurrence of the PT process of $H4BIM^{2+} + F_4\text{-}TCNQ^{-\bullet} \rightarrow H3BIM^{+} + HF_4\text{-}TCNQ^{\bullet}$ is explained by the acidity of the $H4BIM^{2+}$ species, which is higher than that of $F_4\text{-}TCNQ^{-\bullet}$. From the titration data, the pK_{a3} of $F_4\text{-}TCNQ^{-\bullet}$ was expected to be below 0. If I assume that pK_{a3} of $F_4\text{-}TCNQ^{-\bullet}$ is 0, the ΔpK_a value between $H3BIM^{+}$ and $F_4\text{-}TCNQ^{-\bullet}$ is a large positive value (+4.60), which is consistent with no contribution of the PT process from $H3BIM^{+}$ to $F_4\text{-}TCNQ^{-\bullet}$. In the case of the $H4BIM^{2+}$ complex, the formation of mixed PT salts with $[H3BIM^{+}]_{0.1}[H4BIM^{2+}]_{0.9}[F_4\text{-}TCNQ^{-\bullet}]_{1.9}[H_2O]_2$ is explained by a slightly negative ΔpK_a (-0.2) value.

3-3-3-2 Mixed CT and/or PT Complex: (11), (12), (18), and (19)

The complexes of i) $[H3BIM^{+}]_x[H2BIM^{0}]_{1-x}[TCNQ^{-\bullet}]_x[TCNQ^{0}]_{1-x}$ (**11**), ii) $[H4BIM^{2+}]_x[H3BIM^{+}]_{1-x}[TCNQ^{-\bullet}]_{1+x}[TCNQ^{0}]_{1-x}$ (**18**), and iii) $[H4BIM^{2+}]_x[H3BIM^{+}]_{1-x}[BTDA\text{-}TCNQ^{-\delta}]_y\,[BTDA\text{-}TCNQ^{-(1-\delta)}]_{2-y}$ (**19**) belong to this class, while iv) $[H3BIM^{+}]_2[TCNQ^{-\bullet}]_2[TCNQ^{0}]$ (**12**) is classified as a mixed CT with a non-mixed PT type. The acidity of $TCNQ^{-\bullet}$ ($pK_{a3} \sim 2.0$) locates at the intermediate point between $H3BIM^{+}$ ($pK_{a2} = 4.60$) and $H4BIM^{2+}$ ($pK_{a1} = -0.24$), which makes the occurrence of the PT possible.

i) $[H3BIM^{+}]_x[H2BIM^{0}]_{1-x}[TCNQ^{-\bullet}]_x[TCNQ^{0}]_{1-x}$ (**11**): The following scheme can be derived for the 1:1 complex formation:

$$H3D^{+} + A^{-\bullet} \rightarrow \alpha H3D^{+} + (1\text{-}\alpha)H2D^{0} + \alpha A^{-\bullet} + (1\text{-}\alpha)HA^{\bullet}$$
$$(1\text{-}\alpha)HA^{\bullet} \rightarrow 0.5(1\text{-}\alpha)H2A^{0} + 0.5(1\text{-}\alpha)A^{0}$$

$$H3D^{+} + A^{-\bullet} \rightarrow [H3D^{+}]_{\alpha}[H2D^{0}]_{0.5(1-\alpha)}[A^{-\bullet}]_{\alpha}[A^{0}]_{0.5(1-\alpha)}\downarrow$$
$$+ 0.5(1\text{-}\alpha)\,H2A^{0} + 0.5(1\text{-}\alpha)\,H2D^{0}, \quad (3\text{-}3)$$

where A and D represent TCNQ and BIM, respectively. The ratio for $H3BIM^+$ and $H2BIM^0$ (α / (1-α)) of the first step in solution is changed according to the pH of the reaction solvents. There exists equimolar amounts of $H3BIM^+$ and $H2BIM^0$ species in a solvent of pH = 4.60. In solution, the $H3BIM^+$ and $H2BIM^0$ species coexist in the pH range from about 1 to about 8; it is thus possible to control the degree of the PT reaction from $H3BIM^+$ to $TCNQ^{-\bullet}$, depending on the pH of the solution of the metathesis reaction. The stoichiometric relationship of the reaction products indicates the recovery of 0.88 equivalents of the CT complex (Table 3-3) in the experiment, which assumes α = 0.76 from the equation of α + (1-α) / 2 = 0.88. Consequently, I can represent the real chemical formula of this complex as $[H3BIM^+]_{0.86}[H2BIM^0]_{0.14}$ $[TCNQ^{-\bullet}]_{0.86}[TCNQ^0]_{0.14}$, and the degree of CT is estimated to be 0.86 based on this formula. The residual products, except for $[Li^+][I^-]$, indicate a strong absorption at 2980 cm^{-1}, which is ascribed to ν_{CN} of the $H2TCNQ^0$ species in addition to $H2BIM^0$. The formation of $H2TCNQ^0$ supports the validity of both the above-mentioned reaction scheme and the partial PT state of the H2BIM system as well as the mixed CT state of TCNQ.

ii) $[H4BIM^{2+}]_x[H3BIM^+]_{1-x}[TCNQ^{-\bullet}]_{1+x}[TCNQ^0]_{1-x}$ (**18**): If there exists a completely recombinational PT process from $H4BIM^{2+}$ to $TCNQ^{-\bullet}$, and no contribution from the PT process of $H3BIM^+$ ($H3BIM^+ \rightarrow H2BIM^0 + H^+$), the stoichiometry and charge balance can be fulfilled by the following equation 3-4 of this complex:

$$H4D^{2+} + 2A^{-\bullet} \rightarrow H3D^+ + A^{-\bullet} + 0.5H2A + 0.5A^0$$
$$0.5H3D^+ + 0.5A^{-\bullet} \rightarrow 0.5H2D^0 + 0.5HA^\bullet$$
$$\rightarrow 0.5H2D^0 + 0.25H2A^0 + 0.25A^0$$

$$H4D^{2+} + 2A^{-\bullet} \rightarrow 0.5H3D^+ + 0.5A^{-\bullet} + 0.5H2A^0 + 0.5A^0 + 0.5H2D^0 + 0.25H2A^0 + 0.25A^0$$
$$\rightarrow [H3D^+]_{0.5}[A^{-\bullet}]_{0.5}[A^0]_{0.5}\downarrow + 0.25A^0 + 0.5H2D^0 + 0.75H2A^0. \quad (3\text{-}4)$$

The residual products after complex formation showed strong absorption at 2980 cm^{-1} due to $H2TCNQ^0$, in addition to a weak band ascribable to $TCNQ^{-\bullet}$. However, there is no evidence for the formation of $H2BIM^0$ in the residual compounds. Furthermore, since the experimental yield (0.72 equivalents) of the complex exceeded the expected maximum yield (0.50 equivalents), equation 3-4 is not adequate. As a result, I must consider the partial PT mechanism according to the following equation 3-5:

$$H4D^{2+} + 2A^{-\bullet} \rightarrow xH4D^{2+} + (1-x)H3D^+ + (1+x)A^{-\bullet} + 0.5(1-x)H2A^0 + 0.5(1-x)A^0. \quad (3\text{-}5).$$

From the 72 % recovery of the obtained complex, the real chemical formula against the initial composition ($[H4BIM^{2+}]$ + $2[TCNQ^{-\bullet}]$) is represented by $[H4BIM^{2+}]_x[H3BIM^+]_{0.72-x}[TCNQ^{-\bullet}]_x + 0.72[TCNQ^0]_{0.72-x}$ to fulfil both the stoichiometry and charge balance. The ratio of $TCNQ^{-\bullet}$ and $TCNQ^0$ was determined from a spectrometrical calibration curve using the synthetic mixture of $[Li^+][TCNQ^{-\bullet}]$ and $TCNQ^0$.[27] The mole ratio of $[Li^+][TCNQ^{-\bullet}]$ and $TCNQ^0$ changes the ratio of the absorption intensities at 842 nm ($TCNQ^{-\bullet}$) and 395 nm ($TCNQ^0$) in acetonitrile. In the case of $(H4BIM^{2+})(TCNQ^-)_2$, this intensity ratio was found to be 0.82 in acetonitrile, which leads to a mole ratio of 4 : 1 ($TCNQ^{-\bullet}$: $TCNQ^0$). Thus, the value of x in

equation 3-5 was determined to be 0.43 (x+0.72 : 0.72-x = 4 : 1), and equation 3-5 is represented as follows:

$$H4D^{2+} + 2A^{-\bullet} \rightarrow 0.43H4D^{2+} + 0.57H3D^{+} + 1.43A^{-\bullet} + 0.29H2A^{0} + 0.29A^{0}.$$

$$\rightarrow [H4D^{2+}]_{0.43}[H3D^{+}]_{0.29}[A^{-\bullet}]_{1.15}[A^{0}]_{0.29} + 0.28H3D^{+} + 0.28A^{-\bullet} + 0.29H2A^{0} \quad (3\text{-}5)'.$$

Based on the above real chemical formula, the degree of CT is 0.78.

iii) $[H4BIM^{2+}]_x[H3BIM^{+}]_{1-x}[BTDA\text{-}TCNQ^{-\delta}]_y[BTDA\text{-}TCNQ^{-(1-\delta)}]_{2-y}$ (**19**): In the case of BTDA-TCNQ, since 0.64 equivalents of the complex were recovered directly, the real chemical formula of this complex is deduced to be: $[H4BIM^{2+}]_x[H3BIM^{+}]_{0.64-x}[BTDA\text{-}TCNQ^{-\bullet}]_{x+0.64}[BTDA\text{-}TCNQ^{0}]_{0.64-x}$ and $0.64 > x > 0$. The residual products are very complicated, and the precise value of x is unknown.

iv) $[H3BIM^{+}]_2[TCNQ^{-\bullet}]_2[TCNQ^{0}]$ (**12**): Recrystallization of $(H4BIM^{2+})(TCNQ)_2$ causes the subtraction of $H4BIM^{2+}$ and a part of $TCNQ^{-\bullet}$, giving a 2 : 3 complex of single crystals (**12**). The degree of CT was obtained to be 0.67 based on this formula. Furthermore, the intensity ratio of UV-VIS absorptions at 842 and 395 nm is 1.5 in acetonitrile, which is consistent with a mole ratio for 2 : 1 of $TCNQ^{-\bullet}$ and $TCNQ^{0}$.[27]

The complex formation of mixed CT and PT types can be ascribed to the high acidity of $H4BIM^{2+}$ ($pK_{a1} = -0.24$) compared with those of $TCNQ^{-\bullet}$ ($pK_{a3} \sim 2.0$) and BTDA-$TCNQ^{-\bullet}$ ($pK_{a3} \sim 1$). The differences in acidity ($\Delta pK_a = pK_{a1}(H4BIM^{2+}) - pK_{a3}(TCNQs^{-\bullet})$) for the TCNQ and BTDA-TCNQ complexes are negative, -2.24 and ~ -1.24, respectively. Based on the acidity of $H3BIM^{+}$ ($pK_a = 4.60$), the values of ΔpK_a ($4.6 - pK_a(TCNQs^{-\bullet})$) of the F_4-TCNQ and BTDA-TCNQ complexes are positive (4.6 and 3.6, respectively); thus, there is no contribution of the PT reaction $H3BIM^{+} \rightarrow H2BIM^{0} + H^{+}$. The formation of the $H2BIM^{0}$ species according to the above PT reaction is observable in the case of ΔpK_a below 3.6. The formation of a neutral CT complex is expected from the redox potential of BTDA-$TCNQ^{-\bullet}$. However, the high acidity of BTDA-$TCNQ^{-\bullet}$ ($pK_{a3} \sim 1$) interferes with the occurrence of a PT reaction from $H3BIM^{+}$ to BTDA-$TCNQ^{-\bullet}$. From these results, I can also confirm that the first step is the charge-redistribution process of PT from $H3BIM^{+}$ or $H4BIM^{2+}$ to $TCNQ^{-\bullet}$.

3-3-3-3 Neutral CT Complex: (8), (9), (14), (15), (16), and (20)

All of the Me_2-TCNQ ((**8**), (**14**), (**15**), and (**20**)) and MeO_2-TCNQ ((**9**) and (**16**)) complexes belong to a neutral CT with a completely PT complex. The acid-dissociation constant of Me_2-$TCNQ^{-\bullet}$ ($pK_a \sim 5.0$) is higher than the acidity of $H4BIM^{2+}$ and $H3BIM^{+}$. That of MeO_2-$TCNQ^{-\bullet}$ is expected to be of the same order, due to the similar value of the Hammett's constant between methyl (σ_p=-0.17 and σ_m=-0.07) and methoxy (σ_p=-0.27 and σ_m=0.12).[28] Since the ΔpK_a value between $H4BIM^{2+}$ (or $H3BIM^{+}$) and Me_2-$TCNQ^{-\bullet}$ is negative, -0.4 (or -5.2), it is expected that the PT process easily takes place, as follows:

$$H4BIM^{2+} + 2Me_2\text{-}TCNQ^{-\bullet} \rightarrow H3BIM^{+} + HMe_2\text{-}TCNQ^{\bullet} + Me_2\text{-}TCNQ^{-\bullet},$$
$$\rightarrow H2BIM^{0} + 2HMe_2\text{-}TCNQ^{\bullet}$$
$$\rightarrow H2BIM^{0} + Me_2\text{-}TCNQ^{0} + H2Me_2\text{-}TCNQ^{0}, \quad (3\text{-}6)$$

and

$$H3BIM^{+} + Me_2\text{-}TCNQ^{-\bullet} \rightarrow H2BIM^{0} + HMe_2\text{-}TCNQ^{\bullet}.$$
$$\rightarrow H2BIM^{0} + 0.5Me_2\text{-}TCNQ^{0} + 0.5H2Me_2\text{-}TCNQ^{0} \quad (3\text{-}7)$$

For the complex formation of $(H3BIM^{+})(Me_2\text{-}TCNQ^{-})$ (**14**), I can derive the following equation 3-8:

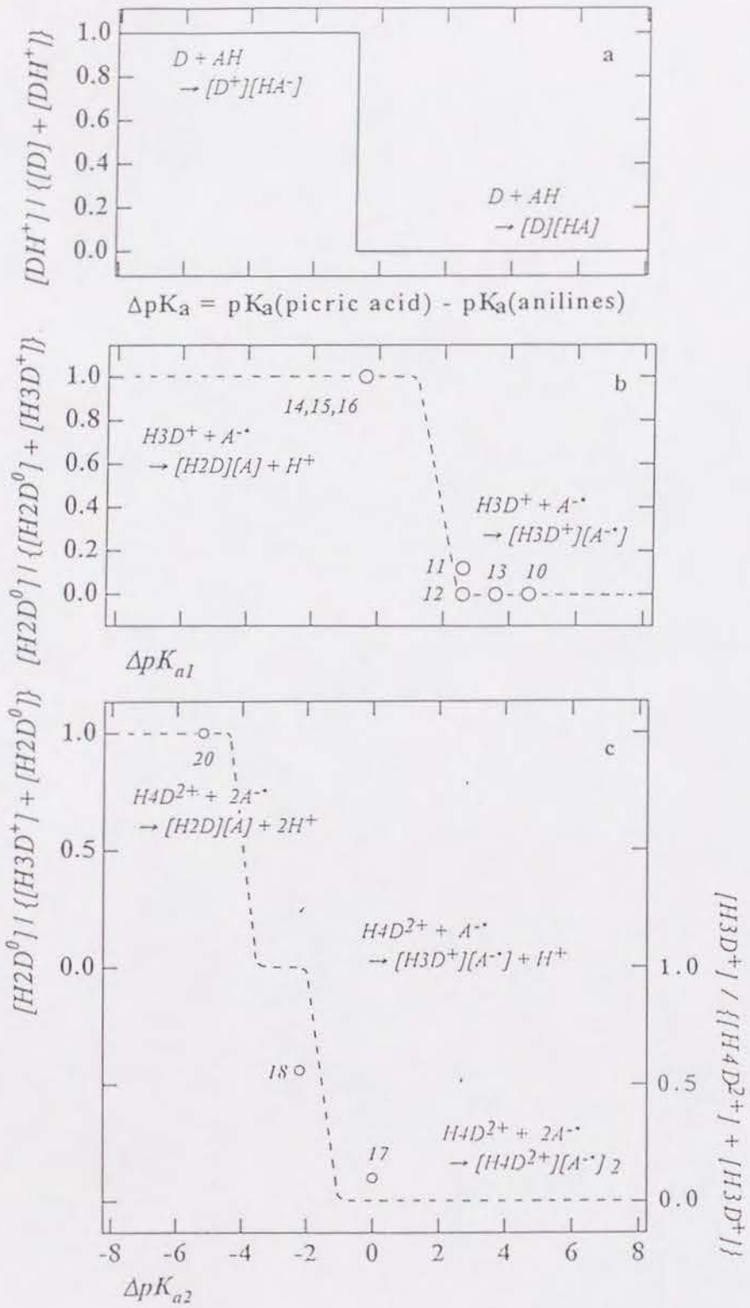

Fig. 3-16. The degree of PT vs. ΔpK_a of a) anilines - Picric acid, b) $H3BIM^+$ - $TCNQs^{-\bullet}$, and c) $H4BIM^{2+}$ - $TCNQs^{-\bullet}$ systems. The vertical axis is the ratio of the PT species, and horizontal one is the differences of pK_a. The numbers of complexes correspond to the entry number in Table 3-1. The dashed lines are the guide for eye.

$$2H3D^+ + 2A^{-\bullet} \rightarrow 2H2D^0 + 2HA^\bullet \rightarrow 2H2D^0 + H2A^0 + A^0$$
$$\rightarrow [H2D^{+\delta}][A^{-\delta}]\downarrow + H2D^0 + H2A^0 \qquad (3\text{-}8)$$

where A and D represent Me_2-TCNQ and BIM, respectively. The above reaction scheme gives the maximum yield of 50 % (Table 3-3). The yield of (**14**) is 51 %, and the residual compounds show a strong absorption at 2908 cm^{-1}, which is assigned to νCH of $H2Me_2\text{-}TCNQ^0$ in addition to the bands ascribable to $H2BIM^0$. A similar stoichiometric relationship was observed for the case of $(H3BIM^+)(MeO_2\text{-}TCNQ^-)$ (**16**).

In the gas phase, the recovery of $(H2BIM^0)(Me_2\text{-}TCNQ^0)$ (**8**) was attained to be 100 %, due to the absence of the PT process (Table 3-3),

$$H2BIM^0 + Me_2\text{-}TCNQ^0 \rightarrow [H2BIM^{+\delta}][Me_2\text{-}TCNQ^{-\delta}]$$
$$H2BIM^0 + Me_2\text{-}TCNQ^0 \not\rightarrow HBIM^- + HMe_2\text{-}TCNQ^+.$$

The pK_a3 of $H4BIM^{2+}$, that is $H2BIM^0 \rightleftarrows HBIM^- + H^+$, is estimated to be 12.3; and since ΔpK_a is 7.3, no recombinational PT process is expected during complex formation. The complex formation of (**9**) gives a similar stoichiometric relationship (Table 3-3).

In the case of $(H4BIM^{2+})_3(Me_2\text{-}TCNQ^-)_4(H_2O)_2$ (**20**), the reaction scheme is similar to equation 3-6. The real chemical formula of the obtained complex can be described as $[H2BIM^{\sim 0}][Me_2\text{-}TCNQ^{\sim 0}][H2Me_2\text{-}TCNQ^0]_{0.33}$.

3-3-3-4 Relation Between ΔpK_a and ΔE_p

According to the differences between pK_a of polynitrophenol and pK_b of amines, it is possible to classify the solid complexes of the PT type ([anilinium$^+$][PICRATE$^-$] form) and of the CT one ([aniline][Picric acid] form). For the PT and CT system, the types of obtained complexes relate to the magnitude of two parameters, which are the

acid dissociation constants (pK_a) and the redox potentials (E_p).[29] I first consider the relationship between the protonated states of the H2BIM system and the ΔpK_a values.

Figure 3-16 shows a correlation between the ΔpK_a values of a) amines - Picric acid systems measured in water, b) $H3BIM^+$ - $TCNQs^{-\bullet}$, and c) $H4BIM^{2+}$ - $TCNQs^{-\bullet}$ in water - DMF (7 : 3) media and the degree of PT of the solid complexes for the H2BIM system based on the real chemical formula (Table 3-1), where ΔpK_{a1} and ΔpK_{a2} are defined as

$$\Delta pK_{a1} = pK_a(H3BIM^+) - pK_a(TCNQs^{-\bullet}), \text{ Fig. 3-16b}$$

and

$$\Delta pK_{a2} = pK_a(H4BIM^{2+}) - pK_a(TCNQs^{-\bullet}), \text{ Fig. 3-16c,}$$

respectively. In the combinations of Picric acid and aromatic amines, the proton of Picric acid transfers to the amines at the interconversion point of $\Delta pK_a = -0.7$. A sharp boundary from the [D][AH] type to the $[DH^+][A^-]$ one was observed (Fig. 3-16a), where D, DH^+, AH, and A^- are amine, anilinium, Picric acid, and $PICRATE^-$, respectively.[2] Some complexes near to the boundary show complex isomerism either enantiotropically or monotropically: namely, a transformation from the $[HD^+][A^-]$ type complex to the [D][AH] one by a heating process in a solid or melt, or the precipitation of both the $[HD^+][A^-]$ and [D][AH] complexes separately, or simultaneously, depending on the crystal-growth conditions.

In contrast, the protonated states of the $H3BIM^+$ complexes (Fig. 3-16b) vary from $H3BIM^+$, $(H3BIM^+)_x(H2BIM^0)_{1-x}$, to $H2BIM^0$ according to the ΔpK_{a1} values. Only the $H3BIM^+$ species can exist for $\Delta pK_a \geq 3.6$ (the F_4-TCNQ (**10**) and BTDA-TCNQ (**13**) complexes), and the condition of $\Delta pK_a = -0.4$ (the Me_2-TCNQ complex (**14**, **15**) and MeO_2-TCNQ (**16**)) gave completely PT complexes due to the full participation of the $H3BIM^+ \rightarrow H2BIM^0 + H^+$ process. In the intermediate range of ΔpK_a, a mixed PT complex with TCNQ ((**11**); $\Delta pK_a = 2.6$) was obtained. This mixed PT character was also observed in (1-naphthylamine)(pyridine)(Picric acid) and

$(benzidine)_3(Picric\ acid)_2$. Approximately, the CT - PT mixed valence state is speculated to be located within a ΔpK_a range of 0 ~ 3 for the $H3BIM^+$ complexes.

All of the $H4BIM^{2+}$ complexes, except for Me_2-TCNQ, require a partial transformation of the H2BIM system from $H4BIM^{2+}$ to $H3BIM^+$, $H4BIM^{2+} \rightarrow \alpha H4BIM^{2+} + (1-\alpha)H3BIM^+ + \alpha H^+$, due to the high acidic character of the $H4BIM^{2+}$ species. This process makes the mixed PT state of $[H4BIM^{2+}]_x[H3BIM^+]_{1-x}$ for the F_4-TCNQ (**17**), TCNQ (**18**), and BTDA-TCNQ (**19**) complexes. In the BTDA-TCNQ complex, the precise content of the $H3BIM^+$ species is unknown. In the Me_2-TCNQ complex ((**20**); $\Delta pK_a = -5.2$), the complete doublet PT process of $H4BIM^{2+} \rightarrow H2BIM^0 + 2H^+$ gives only the $H2BIM^0$ species. The CT - PT mixed valence state may exist in the ΔpK_a range of -3 ~ 0, based on an extrapolation of the experimental data; this has a somewhat broad regime compared with the $H3BIM^+$ complexes, because this regime includes the transfer of two protons ($H4BIM^{2+} \rightarrow H3BIM^+ + H^+ \rightarrow H2BIM^0 + 2H^+$).

Based on the above-mentioned mixed PT boundary, I can estimate the PT and CT natures of the H2BIM - TCNQs system. Here, the mixed CT boundary, $-0.02 < \Delta E_p < 0.34$, was used for predicting the CT state.[1] Similar to the CT boundary, the PT state can also vary from neutral or mixed, to ionic PT, according to the degree of ΔpK_a.

Since all of the $H4BIM^{2+}$ (and $H3BIM^+$) - TCNQs system is located at the largely positive side of the ΔE_p region (Table 3-9), the occurrence of the following CT reactions is energetically unfavorable:

$$TCNQ^{-\bullet} + H3BIM^+ \text{ (or } H4BIM^{2+}\text{)}$$
$$\rightarrow TCNQ^0 + H3BIM^{\bullet} \text{ (or } H4BIM^{+\bullet}\text{).}$$

On the other hand, the value of ΔpK_a crosses the mixed-PT region, where two kinds of H2BIM species coexist in the TCNQs complexes. The degree of the PT reaction in solid complexes is defined by the following equations:

% of $H_nBIM^{n-3} = [H_nBIM^{3-n}] / [\{[H_{n+1}BIM^{n-3}] + [H_nBIM^{n-3}]\}]$,

% of $HBIM^- = [HBIM^-] / \{[H2BIM^0] + [HBIM^-]\}$,

% of $H2BIM^0 = [H2BIM^0] / \{[H3BIM^+] + [H2BIM^0]\}$,

% of $H3BIM^+ = [H3BIM^+] / \{[H4BIM^{2+}] + [H3BIM^+]\}$.

The control of the PT state of the H2BIM system induces a change in the band-filling of the conducting acceptor column. A continuous change in the degree of PT produces a variable band-filling of the electron acceptor chain, that is, from completely ionic, mixed valence, to neutral ground states. For example, it may be possible that the completely ionic 1 : 1 TCNQ complex with $H3BIM^+$ varies to the mixed valent CT complex induced by the mixed PT state of $[H2BIM^0]_x[H3BIM^+]_{1-x}$; finally, it can be converted to the neutral CT complex of $[H2BIM^{\sim 0}][TCNQ^{\sim 0}]$.

For the BQ - H2Q system, ΔpK_a and ΔE_p are derived as 16.9 (pK_a (H2Q) = 9.9 and pK_a (BQ) = -7) and 1.89 (E^o_p (H2Q) = 1.20 and E^r_p (BQ) = - 0.69 V vs. Ag / AgCl in DMF), respectively.[30] These parameters make the BQ - H2Q complex to be a weak CT with a weak PT regime. In Picric acid - aromatic amine complexes, the PT interactions cross from the ionic (PT type) regime to the neutral (CT type) regime (Fig. 3-16a). Since this system has large ΔE_p values, the CT state is a neutral one. For the H2BIM - TCNQs system, the ΔE_p values are located nearly at the regime between the mixed CT and neutral CT types. Searches for complexes in the special regime, where $-0.02 < \Delta E_p < 0.34$ and $0 < \Delta pK_a < 3$, are the next targets for the development of a new PT and CT system.

3-4 Summary

The properties of proton-transfer (PT) and electron-transfer (charge-transfer (CT)) in CT complexes were investigated for 2,2'-bi-1*H* -imidazole (H2BIM) derivatives. The crystal structures of a mixed PT salt ($[H2BIM^0]_3[H3BIM^+]_2[I^-]_2$) and a simple salt

($[H4BIM^{2+}][PICRATE^-]_2$) were determined in this work. The common structural character of the H2BIM system is the formation of strong hydrogen bonds in the side-by-side direction of the molecular planes.

The electronic state of the TCNQs among the CT complexes of $H3BIM^+$ and $H4BIM^{2+}$ changed from completely ionic, mixed valent, to neutral state according to the PT character of the $TCNQs^{-\bullet}$. F_4-$TCNQ^{-\bullet}$ gave completely ionic CT complexes, and the BTDA-TCNQ gave completely ionic CT with the non-mixed PT and the mixed CT and PT types. All of the valence states for the TCNQ complexes were classified as the mixed CT type. The protonated states were different for each complex: mixed PT for the 1 : 1 and 1 : 2 complexes and non-mixed PT for the 2 : 3 type. For the Me_2-TCNQ and MeO_2-TCNQ complexes, neutral CT complexes were obtained by the participation of complete PT process: $H4BIM^{2+} \rightarrow H3BIM^+ \rightarrow H2BIM^0$. Here, $H2BIM^0$ behaves as a weak electron donor. The crystal of $[H3BIM^+]_2[TCNQ^-]_2[TCNQ^0]$ contains a segregated non-uniform TCNQ column, which is connected by N-H•••N≡C hydrogen bonds between the $H3BIM^+$ dimer and $TCNQ^{-\bullet}$.

The kinds of complex formations are related to the acidic character between $TCNQs^{-\bullet}$ and $H3BIM^+$ or $H4BIM^{2+}$. It is concluded that the PT from $H3BIM^+$ or $H4BIM^{2+}$ to $TCNQs^{-\bullet}$ during metathesis leads to a variation of the protonated states of the H2BIM system and the electronic states of TCNQs. The diagram of ΔE_p and ΔpK_a shows that the H2BIM - TCNQs system belongs to the neutral CT with a crossing at the PT - CT interconversion point. For a comparison with the previously reported systems, H2BIM system is close to the mixed PT and CT regime.

In the H2BIM system, the term mixed PT states has a key role in constructing the CT complex. Since the charged states of TCNQs depend upon the PT states of the H2BIM system, it is necessary to control the PT state by a novel approach.

1) a) R.C.Wheland, *J. Am. Chem. Soc.*, **98**, 3926 (1976); b) G.Saito and J.P.Ferraris, *Bull. Chem. Soc. Jpn.*, **53**, 2141 (1980).

2) G.Saito and T.Inukai, *J. Jpn. Association Cryst. Growth,* **16**, 2 (1989).

3) D.S.Acker and W.R.Hertler, *J. Am. Chem. Soc.*, **84**, 3370 (1962).

4) G.M.Sheldrick, "SHELXS-86", Program for Crystal Structure Determination," Univ. of Göttingen, Federal Republic Germany.

5) The lists of atomic coordinates, structure factors, and anisotropic thermal parameters for non-hydrogen atoms are summarized at Chapter 6.

6) R.Blinc, *J. Phys. Chem. Solid.*, **13**, 204 (1960).

7) a) A.Bondi, *J. Phys. Chem.*, **68**, 441 (1964); b) R.D.Shannon, *Acta Crystallogr., Sect. A*, **32**, 751 (1976).

8) R.Huser, B.Bonnet, and J.Roziere, *J. Mol. Struct.*, **40**, 117 (1977).

9) D.T.Cromer, R.R.Ryan, and C.B.Storm, *Acta Crystallogr., Sect. C*, **43**, 1435 (1987).

10) a) G.C.Pimentel and A.L.McClellan, "*The Hydrogen Bond*", W.H.Freeman, San Francisco (1960); b) W.C.Hamilton and J.A.Ibers, " *Hydrogen Bonding in Solids*", W.A.Benjamin, New York (1968).

11) D.Boinnard, P.Cassoux, V.Petrouleas, J.M.Savariault, and J.P.Tuchagues, *Inorg. Chem.*, **29**, 4114 (1990).

12) C.Perchard and A.Novak, *J. Chem. Phys.*, **48**, 3079 (1968).

13) J.Roziere, C.Belin, and M.S.Lehman, *J. Chem. Soc., Chem. Commun.*, **1982**, 388.

14) B.M.Craren, R.K.McMullan, J.D.Bell, and H.C.Freeman, *Acta Crystallogr., Sect. B*, **33**, 2585 (1977).

15) G.Saito and Y.Matsunaga, *Bull. Chem. Soc. Jpn.*, **46**, 1609 (1973).

16) F.M.Wiygul, T.J.Emge, and T.J.Kistenmacher, *Mol. Cryst. Liq. Cryst.*, **90**, 163 (1982).

17) M.Meneghetti and C.Pecile, *J. Chem. Phys.*, **84**, 4149 (1986).

18) R.Foster, "*Organic Charge-Transfer Complexes*", Academic Press, London (1969).

19) a) J.B.Torrance, B.A.Scott, B.Welber, F.B.Kaufman, and P.E.Seiden., *Phys. Rev., B*, **19**, 730 (1979); b) E.M.Conwell, I.A.Howard, J.P.Pouget, C.S.Jacobsen, J.C.Scott, and L.Zuppiroli, "*Semiconductors and Semimetals*" Vol.27, edited by E.M.Conwell, Academic Press, Inc., New York (1988); c) J.Tanaka, M.Tanaka, T.Kawai, T.Takabe, and O.Maki, *Bull. Chem. Soc. Jpn.*, **49**, 2358 (1976).

20) a) Z.Iqbal, C.W.Christoe, and D.K.Dawson, *J. Chem. Phys.*, **63**, 4485 (1975); b) M.Meneghetti, A.Girlando, and C.Pecile, *J. Chem. Phys.*, **83**, 3134 (1985).

21) a) C.J.Fritchie, and P.Arthur, *Acta Crystallogr., Sect. B*, **21**, 139 (1966); b) K.D.Cummings, D.B.Tanner, and J.S.Miller, *Phys. Rev., B*, **24**, 4142 (1981).

22) T.Suzuki, C.Kabuto, Y.Yamashita, T.Mukai, T.Miyashi, and G.Saito, *Bull. Chem. Soc. Jpn.*, **61**, 483 (1988).

23) T.Sundaresan, and S.C.Wallwork, *Acta Crystallogr., Sect. B*, **28**, 491 (1972).

24) H.Kobayashi, T.Danno, and Y.Saito, *Acta Crystallogr., Sect. B*, **29**, 2693 (1973).

25) J.Roziere, J.M.Williams, E.Grech, Z.Malarski, and L.Sobcyzk, *J. Chem. Phys.*, **72**, 6117 (1980).

26) a) P.S.Flandrois, and D.Chasseau, *Acta Crystallogr., Sect. B*, **33**, 2744 (1977); b) T.J.Kistenmacher, T.J.Emge, A.N.Bloch, and D.O.Cowan, *Acta Crystallogr., Sect. B*, **38**, 1193 (1982).

27) A.Rembaum, V.Hadek, and S.P.S.Yen, *J. Am. Chem. Soc.*, **93**, 2532 (1971).

28) C.Hanasch, A.Leo, and R.W.Taft, *Chem. Rev*, **91**, 165 (1991).

29) Strictly speaking, the differences of lattice energy (Madelung energy) between the PT and CT type complexes are also paid attentions for the classifications.

30) J.Q.Chambers, "*The Chemistry of the Quinonoid Compounds*", Vol. 2; edited by S.Patai, John Wiley & Sons, New York, 719-757 (1988).

Chapter 4. Crystal Structure and Electrical Conductivity of Mixed Proton-Transfer and Charge-Transfer Complex of 2,2'-Bi-1H-benzoimidazole System and 7,7,8,8-Tetracyanoquinodimethane

The 2,2'-bi-1*H*-benzoimidazole (H2BBIM) system can utilize the component system of the multiplex proton-transfer (PT) and charge-transfer (CT) interactions. The 2-(2-1*H*-benzoimidazolyl)-1*H*-benzoimidazolium ($H3BBIM^+$) has higher acidity and electron accepting ability than that of parent 2-(2-1*H*-imidazolyl)-1*H*-imidazolium ($H3BIM^+$). The crystal structures of close shell species; H2BBIM and [2,2'-bi-1*H*-benzoimidazolium ($H4BBIM^{2+}$)][BF_4^-]$_2$, indicated the formations of the infinite hydrogen bond network of N-H•••N and N-H•••BF_4^-. The charge transfer (CT) complex of $H3BBIM^+$ with 7,7,8,8-tetracyanoquinodimethane (TCNQ) was prepared by a novel electrocrystallization method. Since the monocation species $H3BBIM^+$ was unstable in dry acetonitrile solution due to the occurrence of deprotonation reaction of $H3BBIM^+ \rightleftarrows H2BBIM + H^+$, the electrocrystallization was carried out in the mixed solvent system of the buffer solution (KCl - HCl with pH = 1.20) and acetonitrile. The obtained single crystals had a composition of $(H3BBIM^+)(TCNQ)(Cl^-)_{0.7}(H_2O)_{0.7}$, and the crystal structure was composed of the segregated uniform stacks of TCNQ and $H3BBIM^+$. The degree of CT (δ) of TCNQ was estimated as 0.7 from the analysis of bond length of TCNQ. The electrical conductivity at room temperature was 4 ~ 20 Scm^{-1} with the semiconduting temperature dependence, which changed to the insulator at around 100 K, and the temperature dependence of molar magnetic susceptibility indicated a broad maxima at around 80 K. Both of the mixed CT state $[TCNQ^{-\bullet}]_x[TCNQ^0]_{1-x}$ and the mixed PT state $[H3BBIM^+]_x[H4BBIM^{2+}]_{1-x}$ were confirmed by the optical measurements. The real chemical formula of this complex was deduced as $[H3BBIM^+]_{0.6}[H4BBIM^{2+}]_{0.4}[TCNQ^{-0.7}][Cl^-]_{0.7}[H_2O]_{0.7}$ from the result of structural analysis.

4-1. Introduction

From the redox and acid dissociation properties of H2BIM system, highly PT abilities of the 2-(2-1*H*-imidazolyl)-1*H*-imidazolium ($H3BIM^+$) and 2,2'-bi-1*H*-imidazolium ($H4BIM^{2+}$) were confirmed as shown in Chapter 2. I examined the CT complex formation between the $H3BIM^+$ (or $H4BIM^{2+}$) and anion radical of 7,7,8,8-tetracyanoquinodimethane ($TCNQ^{-\bullet}$) in Chapter 3. The characteristic feature of H2BIM system within the CT complex was the formation of the mixed PT states ($[H2BIM^0]_x[H3BIM^+]_{1-x}$ and $[H3BIM^+]_x[H4BIM^{2+}]_{1-x}$), which also provided the electronic state of TCNQ with the mixed CT state to compensate the total charge balance in the solid state. The mixed PT state was closely related to the difference of acid dissociation constants (pK_a) between the initial component molecules in the CT complex formation.

Although the mixed CT state was confirmed in the TCNQ complexes, the electrical conducting behaviour of these was the semiconducting or insulating due to the charge separated state of TCNQ molecules. The crystal of $(H3BIM^+)_2(TCNQ^-)_3$ was composed of the segregated non-uniform stack of TCNQ with charge separation, and real chemical formula was deduced as the $[H3BIM^+]_2[TCNQ^{-\bullet}]_2[TCNQ^0]$. The $H3BIM^+$ molecule existed as the hydrogen bond dimer unit with non stacking structure, which distorted the TCNQ stack by the formation of the strong hydrogen bond between the imino proton of $H3BIM^+$ and nitrile group of TCNQ. I focus on the 2,2'-bi-1*H*-benzoimidazole (H2BBIM) system, which has the extended π-electron system, to construct the stacking structure of H2BBIM system in the CT complex.

The H2BBIM system has the multiplex PT and CT nature as well as the H2BIM system (Fig. 4-1). By the stepwise protonations, the neutral H2BBIM changes to monocation, 2-(2-1*H*-benzoimidazolyl)-1*H*-benzoimidazolium ($H3BBIM^+$), and dication, 2,2'-bi-1*H*-benzoimidazolium ($H4BBIM^{2+}$). The reduction of the $H4BBIM^{2+}$ forms the cation radical of $H4BBIM^{+\bullet}$, and further reduction generates the neutral

H4BBIM, which has the same electronic structure of dibenzotetrathiafulvalene. On the other hand, the reduction of $H3BBIM^+$ produces the neutral radical state of $H3BBIM^{\bullet}$.

At first, I examined the acid dissociation and redox properties of close shell H2BBIM system (H2BBIM, $H3BBIM^+$, and $H4BBIM^{2+}$) and the character of hydrogen bond in the solid state. Then, I tried to prepare the highly conducting TCNQ salt having the mixed PT state of $[H2BBIM]_X[H3BBIM^+]_{1-x}$ or $[H3BBIM^+]_X[H4BBIM^{2+}]_{1-x}$. The crystal preparation, crystal structure, electrical conducting behaviour, magnetic, and optical properties of obtained TCNQ salt are examined, and I discussed the CT and PT states in the complex.

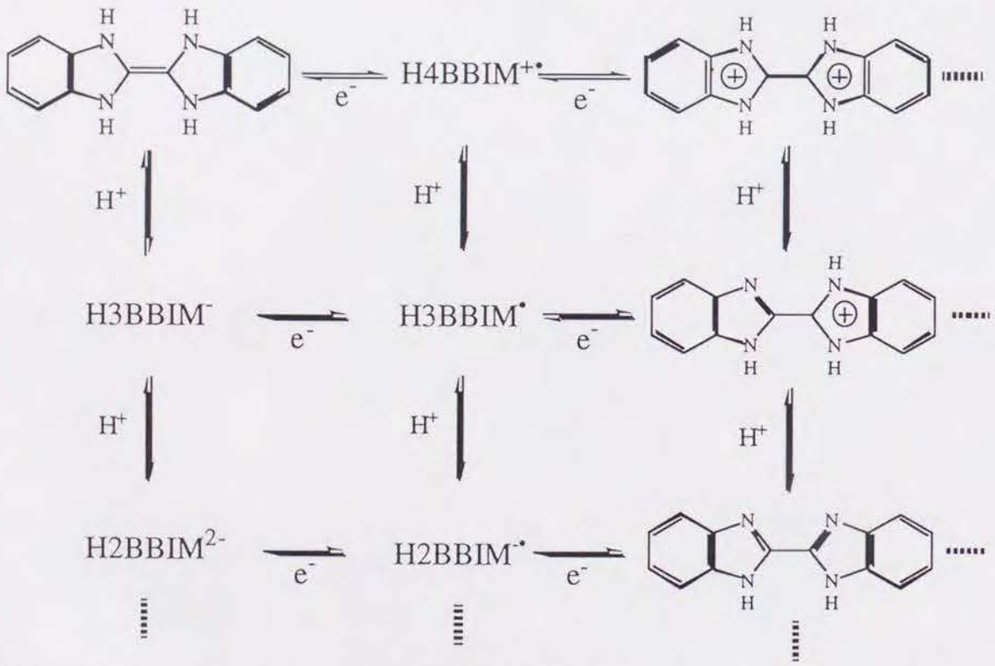

Fig. 4-1 Proton - transfer (PT) and electron (charge) - transfer (CT) diagram of H2BBIM system. Two step PT and CT processes of H2BBIM - H4BBIM system are drawn and part of species (BBIM - H2BBIM) are omitted to clarify the figure. Each vertical and horizontal line corresponds to the PT and CT process, respectively.

4-2. Experimental

2,2'-bi-1*H*-benzoimidazole H2BBIM (1) The preparation of (**1**) was done by the method of Fieselmann.[1] The 0.1 molar amount of oxamide and 0.2 molar amount of o-phenylenediamine were refluxed for 24 h in ethyleneglycol (20 ml). It was added to the 400 ml of hot water and collect the yellow crude products, which were recrystallized from ethylenglycol twice using charcol. The yellow colored fine needles were obtained with the yield of 50%. M.p. > 350°C. Found: C, 71.49; H, 4.47; N, 23.99. Calcd for $C_{14}H_{10}N_4$: C, 71.80; H, 4.27; N, 23.93.

2-(2-1*H*-benzoimidazolyl)-1*H*-benzoimidazolium iodide [H3BBIM$^+$][I$^-$] (2) A mixture of 0.1mol of (**1**) and 1.1 molar amount of aqueous hydroiodic acid (55%) in 50 ml of ethanol was stirred at room temperature for 30 min and left at 0°C overnight. The reaction mixture was filtered to provide 0.8 mol of a yellow solid, which was washed with ether, then recrystallized from ethanol - water. Mp. > 350°C. Found: C,45.15; H,3.06; N,14.69. Calcd for $C_{14}H_{11}N_4I$: C,45.19; H,2.96; N,15.06.

2-(2-1*H*-benzoimidazolyl)-1*H*-benzoimidazolium tetrafluoroborate [H3BBIM$^+$][BF$_4^-$][H$_2$O] (3) A mixture of 0.1mol of (**1**) and 1.1 molar amount of aqueous hydrogen tetrafluoroborate (HBF_4) solution in 50 ml of ethanol was stirred at room temperature for 30 min and left at 0°C overnight. The reaction mixture was filtered to provide 0.08 mol of a yellow solid, which was washed with ether, then recrystallized from ethanol - water. Mp. 320°C. Found: C,49.30; H,3.90; N,16.50. Calcd for $C_{14}H_{13}N_4OBF_4$: C,49.46; H,3.82; N,16.47.

2,2'-bi-1*H*-benzoimidazolium ditetrafluoroborate [H4BBIM^{2+}][BF$_4^-$]$_2$ (4) A mixture of 0.1 molar amount of (**1**) and 2.4 molar amount of aqueous HBF_4 solution in 50 ml of ethanol was stirred at room temperature for 30 min and left at 0°C overnight. The reaction mixture was filtered to provide 0.09 mol of yellow single crystals, which were washed with ether, then recrystallized from acetonitrile. Mp. 380°C. Found: C,41.03; H,3.13; N,13.76. Calcd for $C_{14}H_{12}N_4B_2F_8$: C,41.03; H,2.93; N,13.67.

Preparation of CT Complex with TCNQ A preparation of TCNQ complex was done by the electrocrystallization method. TCNQ (12mg) and [H3BBIM$^+$][I$^-$] (60mg) were inserted into the H-shaped cell (20 ml). The 4 (acetonitrile) : 1 (Clark-Lubus's buffer solution with pH = 1.20) volume ratio of solution, where buffer solution was prepared by mixing of 0.2 M HCl (6.45 ml) and 0.2 M KCl (6.45 ml) solution in 8.55 ml of H_2O,[2] was used as the electrocrystallization solvent to suppress the deprotonation process of H3BBIM$^+$ $\rightleftarrows$ H2BBIM + H$^+$. The current value was the constant (1μA). After the period of two weeks, black coloured single crystals were obtained as typical dimension of 2.0 x 0.1 x 0.1 mm^3. The insertion of the chlorine and oxygen atoms was confirmed by the elemental analysis. The tentative chemical formula of (H3BBIM$^+$)(TCNQ)(Cl$^-$)$_{0.7}$(H_2O)$_{0.7}$ (**5**) was best fitted to the result of elemental analysis (Table 4-1).

Table 4-1. Results of elemental analysis of (H3BBIM$^+$)(TCNQ)(Cl$^-$)$_x$(H_2O)$_y$

		C	H	N	O	Cl
Found(%)						
		65.68	3.51	23.31	2.48	5.00
Calcd.(%)						
x=0.5	y=0.5	67.00	3.43	24.04	1.72	3.81
x=1.0	y=0.5	65.73	3.58	23.59	2.79	3.73
x=0.7	y=0.7	65.50	3.44	23.50	2.35	5.21
x=0.7	y=0.8	65.01	3.41	23.32	2.33	5.91

Measurements The infrared (IR) and the ultra-violet, visible and near-infrared (UV-VIS-NIR) absorption spectra were measured by the method of Chapter 2.

X-Ray Structural Analyses An automatic Rigaku AFC-4 diffractometer with CuKα radiation (λ = 1.54178 Å: 40 kV, 200 mA) was used for data collection of H2BBIM (**1**), [H4BBIM$^+$][BF_4^-]$_2$ (**4**), and (H3BBIM$^+$)(TCNQ)(Cl$^-$)$_{0.7}$(H_2O)$_{0.7}$ (**5**). A summary of crystal parameters was given in Table 4-2. Twenty reflections with $40^o < 2\theta < 60^o$ were used to determine the lattice parameters. The intensity data were collected in the region $2\theta < 125^o$ for (**1**), (**4**), and (**5**) in the 2θ-ϖ mode at a scan rate of 4^o min^{-1}.

Background counts were 4 s. The intensities of three standards, monitored every 100 data measurements, showed no significant variation. The 1130 independent reflections with $|F_\sigma| > 3\sigma(F_0)$ were used for a structural analysis of (**1**), and the 1353 independent reflections with $|F_0| > 3\sigma(F_0)$ were used for (**4**). While, the 1605 independent reflections with $|F_0| > 3\sigma(F_0)$ were used for a structural analysis of (**5**). The crystal structures were solved by a direct method[3] and all hydrogen atoms, except for a part of (**5**), were determined from the difference synthesis maps. A block-diagonal least-squares technique with anisotropic thermal parameters for non-hydrogen atoms and isotropic for hydrogen atoms was employed for the structure refinements.[4]

Table 4-2. Crystal data of H2BBIM (**1**), [H4BBIM^{2+}][BF_4^-]$_2$ (**4**), and (H3BBIM$^+$)(TCNQ)(Cl$^-$)$_{0.7}$(H_2O)$_{0.7}$ (**5**).

	(**1**)	(**4**)	(**5**)
Chemical formula	$C_{14}H_{10}N_4$	$C_{14}H_{12}N_4B_2F_8$	$C_{26}H_{16.4}N_8O_{0.7}Cl_{0.7}$
Crystal colour	yellow	yellow	black
Crystal size / mm^3	0.9x0.06x0.06	0.5x0.02x0.02	0.3x0.2x0.2
Crystal system	Orthorhombic	Monoclinic	Triclinic
Space group	$Pca2_1$	$P2_1/c$	P1
a / Å	10.165(8)	17.603(2)	7.664(7)
b / Å	11.380(9)	8.150(2)	19.090(4)
c / Å	9.902(7)	13.113(2)	3.883(5)
α / deg			88.710(9)
β / deg		120.72(3)	85.12(9)
γ / deg			88.35(8)
V / Å^3	1145(2)	1617(2)	565.7(12)
Z	4	4	1
D_c / gcm^{-3} a)	1.354	1.680	1.40
R	3.73	4.76	6.60

a) D_c is the calculated density.

pH and Cyclic Voltammetry (CV) Measurements The measurement procedures of acid dissociation constants (pK_a) and redox potentials (E_p) were described in Chapter 2. All titrations were run at 22 ± 1°C, and the ion strengths were fixed at 0.1 M using sodium tetrafluoroborate in *N,N'*-dimethylformamide (DMF) - H_2O (7:3). The

measurement condition of CV is as follows, solvent; DMF, supporting electrolyte; 0.1 M of tetrabutylammonium tetrafluoroborate (TBA•BF_4), reference electrode; Ag / AgCl, working and counter electrodes; Pt, temperature; 22 ± 1 ^oC.

Electrical Conductivity Measurements Electrical conductivities were measured on a single crystal with the standard four-prove method. Electrical contacts were done by the gold paste (Tokuriki 8560). The pressure measurements up to 18 x 10^3 bar were made using a Be-Cu clamp cell using Daphne oil (Idemitu #7373) as pressure medium.

Magnetization Measurements Magnetic DC susceptibilities were measured at the temperature range from 2 to 300 K by the aid of a superconducting quantum interference device (SQUID) magnetometer (Quantum Design MPMS). 12 mg of a sample in polyethylene film was used for the measurement. The measured susceptibility was corrected for polyethylene and sample diamagnetism using a compilation of blank and Pascal's constant, respectively. I used the diamagnetic susceptibility correction of 2.73 x 10^{-4} emu mol^{-1} for (H3BBIM)(TCNQ)$(Cl^-)_{0.7}(H_2O)_{0.7}$.

4-3 Results and Discussion

4-3-1. Redox and Acid Dissociation Properties of H2BBIM System

Since the CT and PT nature of H2BBIM system in solution is an indispensable parameter to decide the types of the obtained CT complex, both of the redox potentials (E_{redox}) and acid dissociation constants (pK_a) of the H2BBIM, $H3BBIM^+$, and $H4BBIM^{2+}$ species are measured.

Table 4-3. Reduction peak potentials (E^r_p) of H2BBIM system[a].

Initial Form	E^r_p / V	Reduced Form
H2BBIM	-1.20	$H2BBIM^{-\bullet}$
$H3BBIM^+$	-0.68	$H3BBIM^\bullet$
$H4BBIM^{2+}$	-0.47	$H4BBIM^{+\bullet}$
$Acridinium^+$	-0.59	$Acridinium^\bullet$
N-$methylacridinium^+$	-0.44	*N*-$methylacridinium^\bullet$

a) Measured at a scan rate of 100 mV s^{-1} using Pt vs. Ag/AgCl in 0.1 M TBA•BF_4 / DMF.

Table 4-3 summarizes the reduction peak potentials (E^r_p) of H2BBIM system and related cations (Scheme 4-1). All of reduction processes of H2BBIM system were irreversible one. The E^r_p value of H2BBIM appeared at -1.20 V, which was 0.49 V larger than that of H2BIM (E^r_p = -1.69 V). The reductions of $H3BBIM^+$ and $H4BBIM^{2+}$ correspond to the generations of the $H3BBIM^\bullet$ and $H4BBIM^{+\bullet}$, and E^r_p of these appeared at -0.68 and -0.47 V, respectively. The E^r_p of $H3BBIM^+$ and $H4BBIM^{2+}$ increased 0.16 and 0.07 V compared with those of $H3BIM^+$ (-0.84 V) and $H4BIM^{2+}$ (-0.54 V). Thus the expansion of π-electron system to the parent $H3BIM^+$ and $H4BIM^{2+}$ enhances the electron-accepting abilities. To evaluate the stabilities of $H3BBIM^+$ and $H4BBIM^{2+}$, the E^r_p of *N*-methylacridinium (*N*-Ac) and acridinium (Ac) were measured at the same condition. The cation state of *N*-Ac^+ and Ac^+ are known to be stable compared with opene shell state *N*-$Ac^\bullet$ and $Ac^\bullet$, and the E^r_p of *N*-Ac and Ac were -0.44 and -0.59 V, respectively. Since the electron-accepting ability of

$H3BBIM^+$ and $H4BBIM^{2+}$ are lower than that of the Ac^+ and *N*-Ac^+, the cation states, $H3BBIM^+$ and $H4BBIM^{2+}$, are inert to the CT processes as well as H2BIM system.

$$H2BBIM + e^- \xrightarrow{-1.20} H2BBIM^{-\bullet}$$

$$H3BBIM^+ + e^- \xrightarrow{-0.68} H3BBIM^{\bullet}$$

$$H4BBIM^{2+} + e^- \xrightarrow{-0.47} H4BBIM^{+\bullet}$$

$$acridinium^+ + e^- \xrightarrow{-0.59} acridinium^{\bullet}$$

$$N\text{-methylacridinium}^+ + e^- \xrightarrow{-0.44\ V} N\text{-methylacridinium}^{\bullet}$$

Scheme 4-1

The CT state in the complex can predict from the difference of redox potential (ΔE_p) between the electron donor and electron acceptor.[5] It is known that the mixed CT state appears at the following ΔE_p equation;

$$\text{Completely Ionic} \leq \quad \text{Mixed CT} \quad \leq \text{Neutral}$$

$$-0.02 \leq \Delta E_p \ (= E_p(\text{Donor}) - E_p(\text{Acceptor})) \leq 0.34.$$

I consider the case of complex formation between the $TCNQ^{-\bullet}$ and $H3BBIM^+$ or $H4BBIM^{2+}$, here electron donor is the $TCNQ^{-\bullet}$ and electron acceptor is $H3BBIM^+$ or $H4BBIM^{2+}$. Since the oxidation peak potential of $TCNQ^{-\bullet}$ appears at 0.32 V, the ΔE_p values of $H3BBIM^+$ - $TCNQ^{-\bullet}$ and $H4BBIM^{2+}$ - $TCNQ^{-\bullet}$ systems were 1.15 and 0.85 V, respectively. The largely positive ΔE_p values exist at the neutral CT region according to the above equation, thus the CT from $TCNQ^{-\bullet}$ to $H3BBIM^+$ or $H4BBIM^{2+}$ are negligible amount.

Next, I consider the possibility of PT from $H3BBIM^+$ or $H4BBIM^{2+}$ to $TCNQ^{-\bullet}$. The pK_a value of $H3BBIM^+$ ($H3BBIM^+ \rightleftarrows H2BBIM + H^+$, pK_a = 2.32) was determined by the standard titration method, but no observable change of titration curve below pH of 1.0 was found (Scheme 4-2). The pK_{a1} or pK_{a2} values of $H4BIM^{2+}$, $H4BBIM^{2+}$, $HTCNQ^{\bullet}$, and H2TCNQ are summarized in Table 4-4.

$$H4BBIM^{2+} \overset{pK_a < 1}{\rightleftarrows} H3BBIM^+ + H^+ \overset{2.32}{\rightleftarrows} H2BBIM + H^+$$

$$H4BIM^{2+} \overset{-0.24}{\rightleftarrows} H3BIM^+ + H^+ \overset{4.60}{\rightleftarrows} H2BIM + H^+$$

Scheme 4-2

The pK_{a1} and pK_{a2} values of $H4BIM^{2+}$ were determined as -0.24 and 4.60, respectively, at the same condition (see Chapter 2). The pK_a of $H3BBIM^+$ increased about 2.3 pK_a unit by the expansion of π-electron system to the parent H2BIM molecule. The pK_a value of $HTCNQ^{\bullet}$ was estimated as ca. 2.3, and pK_{a1} and pK_{a2} of H2TCNQ (1,4-benzenedimalononitrile) were 7.10 and 10.30, respectively.

Table 4-4. Acid dissociation constants of $H4BIM^{2+}$, $H4BBIM^{2+}$, and TCNQs.[a]

Compounds	pK_{a1}	pK_{a2}
$H4BIM^{2+}$	-0.24	4.60
$H4BBIM^{2+}$	< 1	2.32
$HTCNQ^{\bullet}$	ca. 2.3	—
H2TCNQ	7.10	10.30

a) Measured at DMF-H_2O (7 : 3) condition.

The difference of pK_a ($\Delta pK_a = pK_a(HA) - pK_a(HD^+)$) between proton donor (HA) and acceptor (D) can utilize as the parameter whether the obtained complex classifies to the CT type ($[D^{+\delta}][HA^{-\delta}]$), PT ($[HD^+][A^-]$) type, or mixed type. In the case of aromatic amine (D) - picric acid (HA) system, the sharp transformation from the CT

type to PT one was observed at ΔpK_a boundary of -0.7 (i of Scheme 4-3).[6] In the case of $H3BIM^+$ (or $H4BIM^{2+}$) - TCNQ system, the ΔpK_a criteria of the mixed PT state were derived as following ΔpK_a regions (ii and iii of Scheme 4-3).

i. $[HD^+][A^-] < \Delta pK_a = -0.7 < [D^{+\delta}][HA^{-\delta}]$

ii.
$$1 < \Delta pK_a < 2.5$$
$$H2BIM < [H2BIM]_x[H3BIM^+]_{1-x} < H3BIM^+$$

iii.
$$-3 < \Delta pK_a < -1$$
$$H3BIM^+ < [H3BIM^+]_x[H4BIM^{2+}]_{1-x} < H4BIM^{2+}$$

Scheme 4-3

Since the ΔpK_a criteria of mixed PT region changes in some extent according to the system, I can expect the PT state of H2BBIM system based on the results of H2BIM system. The ΔpK_a value between the $H3BBIM^+$ and $TCNQ^{-\bullet}$ is determined as ca. 0, which will deduce the complete PT reaction of $H3BBIM^+ \rightarrow H2BBIM + H^+$ assuming the ΔpK_a criteria of $H3BIM^+$. The ΔpK_a of $H4BBIM^{2+}$ - $TCNQ^{-\bullet}$ ($\Delta pK_a < -1$) will cause the mixed PT; $[H4BBIM^{2+}]_x[H3BBIM^+]_{1-x}$, or complete PT reaction; $H4BBIM^{2+} \rightarrow H3BBIM^+ + H^+$, if I apply the similar ΔpK_a criteria of $H4BIM^{2+}$ - $TCNQs^{-\bullet}$ system. Therefore the PT process is expected to dominate the complex formation between the $H3BBIM^+$ (or $H4BBIM^{2+}$) and $TCNQ^{-\bullet}$ rather than the CT one.

4-3-2. Electrocrystallization in Buffer Solution

The single crystals of $(H3BBIM^+)(TCNQ)(Cl^-)_{0.7}(H_2O)_{0.7}$ were obtained by the electrocrystallization method between the $[H3BBIM^+][I^-]$ and TCNQ in acetonitrile - buffer solution (KCl - HCl with pH = 1.20). During the electrocrystallization, both of the Cl^- and H_2O were incorporated into the crystal, which was supported by the result of elemental analysis. The electrocrystallization in dry acetonitrile solution gave no CT

complex due to the precipitation of neutral H2BBIM from solution. Since the $H3BBIM^+$ has highly acidity, the equilibrium of $H3BBIM^+ \rightleftarrows H2BBIM + H^+$ is largely shifted to the right side in dry acetonitrile solution. Thus, I adjusted the pH of electrocrystallization solvent, where the $H3BBIM^+$ can exist as a stable form. The Clark - Lubus's buffer solution (HCl-KCl aquaeous solution with pH of 1.20) was added to the acetonitrile solution, which shifted the above equilibrium to the left side. This method suppressed the deprotonation reaction of $H3BBIM^+$, and existed the cation species of $H3BBIM^+$ and $H4BBIM^{2+}$ in electrocrystallization solvent. It is noted that the stability of $TCNQ^{-\bullet}$, which is formed by the reduction of TCNQ in the Pt electrode, is closely related to the pH range of the electrocrystallization solvent. Highly acidic condition causes the following cyclic reaction.

$$TCNQ + e^- \rightarrow TCNQ^{-\bullet}$$
$$TCNQ^{-\bullet} + H^+ \rightleftarrows HTCNQ^{\bullet}$$
$$HTCNQ^{\bullet} \rightarrow 0.5H2TCNQ + 0.5TCNQ$$
$$0.5TCNQ + e^- \rightarrow 0.5TCNQ^{-\bullet}$$

However, the formation of the H2TCNQ was not observed during the electrocrystallization. It is thus considered that the reaction of $0.5TCNQ + e^- \rightarrow 0.5TCNQ^{-\bullet}$ was negligible in the electrocrystallization of TCNQ complex.

I tried the electrocrystallization of a complex using the another TCNQ derivative; F_4-TCNQ (2,3,5,6-tetrafluoro-TCNQ), Me_2-TCNQ (2,5-dimethyl-TCNQ), or BTDA-TCNQ(4,8-bis(dicyanomethylidene)-4,8-dihydrobenzo[1,2-c:4,5-c']bis[1,2,5]thiadiazole-TCNQ). However, the isolation of solid CT complex was failure. Since the electrocrystallization of Me_2-TCNQ complex in the similar condition to the case of TCNQ complex formation indicates no observable colour change of crystallization solvent, the HMe_2-$TCNQ^{\bullet}$ seems to be formed in the acidic electrocrystallization solvent. The low acidity of HMe_2-$TCNQ^{\bullet}$ (pK_a ~ ca. 5.0) may cause the following cyclic disproportion reaction easily.

Me_2-TCNQ + e^- → Me_2-TCNQ$^{-\bullet}$

Me_2-TCNQ$^{-\bullet}$ + H^+ → HMe_2-TCNQ$^{\bullet}$

HMe_2-TCNQ$^{\bullet}$ → 0.5Me_2-TCNQ + 0.5H2Me_2-TCNQ.

0.5Me_2-TCNQ + e^- → Me_2-TCNQ$^{-\bullet}$

On the other hand, the electrocrystallizations of F_4-TCNQ or BTDA-TCNQ complex changed the colour of crystallization solvent, thus the cyclic disproportion reaction are suppressed in contrast to the case of Me_2-TCNQ complex . High acidic characters of F_4-TCNQ$^{-\bullet}$ (pK_a ~ ca. 0) and BTDA-TCNQ$^{-\bullet}$ (pK_a ~ ca. 1) may suppress the formations of HF_4-TCNQ$^{\bullet}$ and HBTDA-TCNQ$^{\bullet}$, thus the adequate modification of crystallization condition will provide the single crystals of these complexes.

4-3-4 IR and UV-VIS Spectra of H2BBIM, H3BBIM$^+$, and H4BBIM^{2+}

The IR spectra are useful guide to distinguish the protonated species of H2BBIM system in the CT complexes. Fig. 4-2 indicates the IR spectra of H2BBIM, [H3BBIM$^+$][I^-], and [H4BBIM^{2+}][BF_4^-]$_2$ in the frequency range from 4000 to 600 cm^{-1}. The broad band in the frequency region from 3300 to 2200 cm^{-1} was accompanied by the multi band structures, 3028, 2498, 2968, and 2749 cm^{-1}, which were assigned to the N-H stretching mode (ν_{NH}).[7] The multi band structures of H3BBIM$^+$ were slightly shifted to the lower frequency region (3200 ~ 2000 cm^{-1}) compared with those of H2BBIM. In the case of [H4BBIM^{2+}][BF_4^-]$_2$, the broad ν_{NH} band has the absorption maxima at 3285 cm^{-1}, which is ascribable to the N-H•••F hydrogen bond ν_{NH} mode. These changes of ν_{NH} mode are related to the formation of intermolecular hydrogen bonds of N-H•••N (H2BBIM), N-H•••I^- (H3BBIM$^+$), and N-H•••F^- (H4BBIM^{2+}) types.

In the H2BBIM system, the N-H in-plane bending mode (ν^b_{NH}) appeared at frequency range from 1700 to 1500 cm^{-1}. The ν^b_{NH} band of H2BBIM was observed at 1584 cm^{-1}, and the ring stretching mode of benzoimidazole appeared at 1397 cm^{-1}.[7]

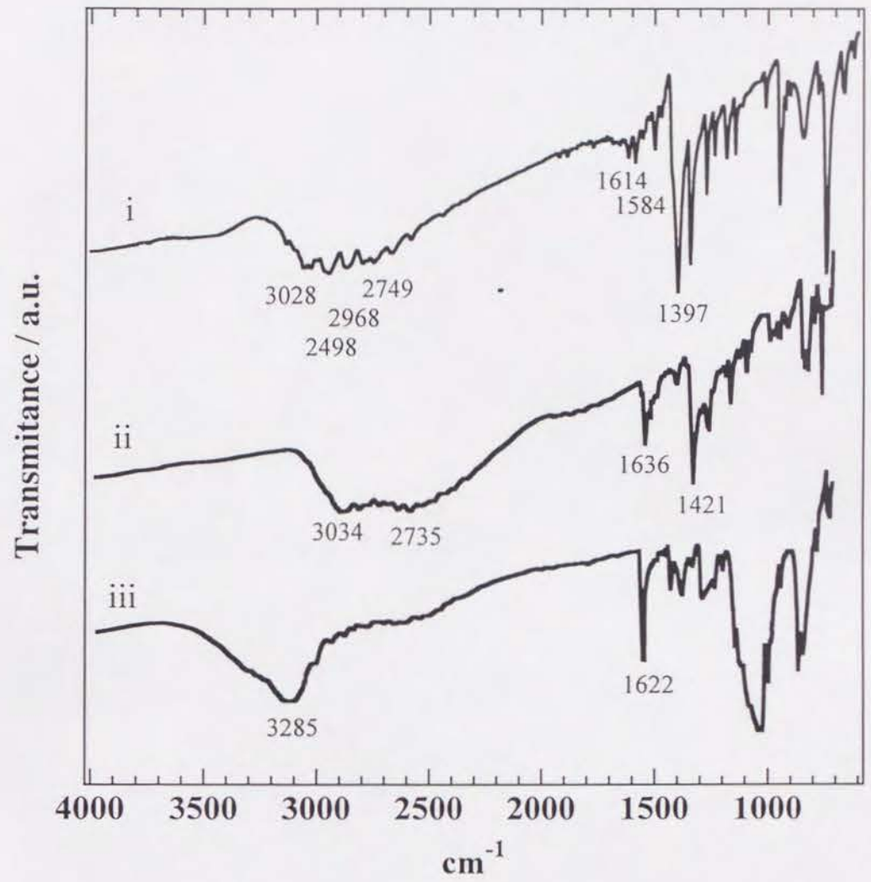

Fig. 4-2 Vibration spectra of each protonated species of i) H2BBIM, ii) [H3BBIM$^+$][I^-] , and iii) [H4BBIM^{2+}][BF_4^-]$_2$ at the frequency range of 4000 ~ 600 cm^{-1}.

The H3BBIM^{+} showed the absorptions at 1636, 1623, and 1605 cm^{-1}, which were assigned to the ν^{b}_{N+-H} and ν^{b}_{NH}, while the ν^{b}_{N+-H} of H4BBIM^{2+} was observed at 1618 cm^{-1} as a single band. These ν^{b}_{NH} mode can be used to examine the PT state of H2BBIM system in the CT complex.

4-3-5 Crystal Structure of H2BBIM (1)

Figure 4-3 illustrates the unit cell of H2BBIM viewed along the c-axis. One H2BBIM molecule is crystallographically independent. Since the dihedral angle between two benzoimidazole rings at the central C - C bond is 0.02°, the H2BBIM is nearly planar. Each H2BBIM molecule is inclined by about 45° to the c-axis, which are connected by the N-H•••N hydrogen bonds. There are no intermolecular contacts within the ab plane, which is shorter than the sum of the van der Waals radius,[8] and the highly cleavage character along the c-axis is reflected by one dimensional intermolecular interaction.

Figure 4-4 shows the hydrogen bond of H2BBIM viewed along the a-axis. Each H2BBIM molecule is connected by the four N-H•••N hydrogen bonds at the side-by-side direction of the molecular plane. The hydrogen bonds elongated along the c-axis, and the H2BBIM molecules form a non planar sheet structure due to the steric repulsions between the hydrogen atoms of benzene rings. In the case of H2BIM, the similar N-H•••N hydrogen bond formation with planar sheet structure was reported.[9]

The average N•••N distances (2.864 Å) of hydrogen bonds in the H2BBIM, N1•••N2 = 2.916(8) and N3••• N4 = 2.811(8)Å, are slightly shorter than that of H2BIM (2.872 Å).[9] The strength of hydrogen bond of H2BBIM is not changed by the expansion of π-electron system of the parent H2BIM. The positions of the hydrogen atoms based on the differential Fourier synthesis revealed no disorder, which indicated the localization of the proton within the asymmetrical double minimum potential of hydrogen bond. The N•••N distances of 4,5-dichloro-1*H*-imidazole (2.800 Å), 1*H*-imidazole (2.860 Å), and 4-nitro-1*H*-imidazole (2.871 Å) were reported by the structural analysis.[10] The average N•••N distance of H2BBIM is similar to that of 1*H*-imidazole,

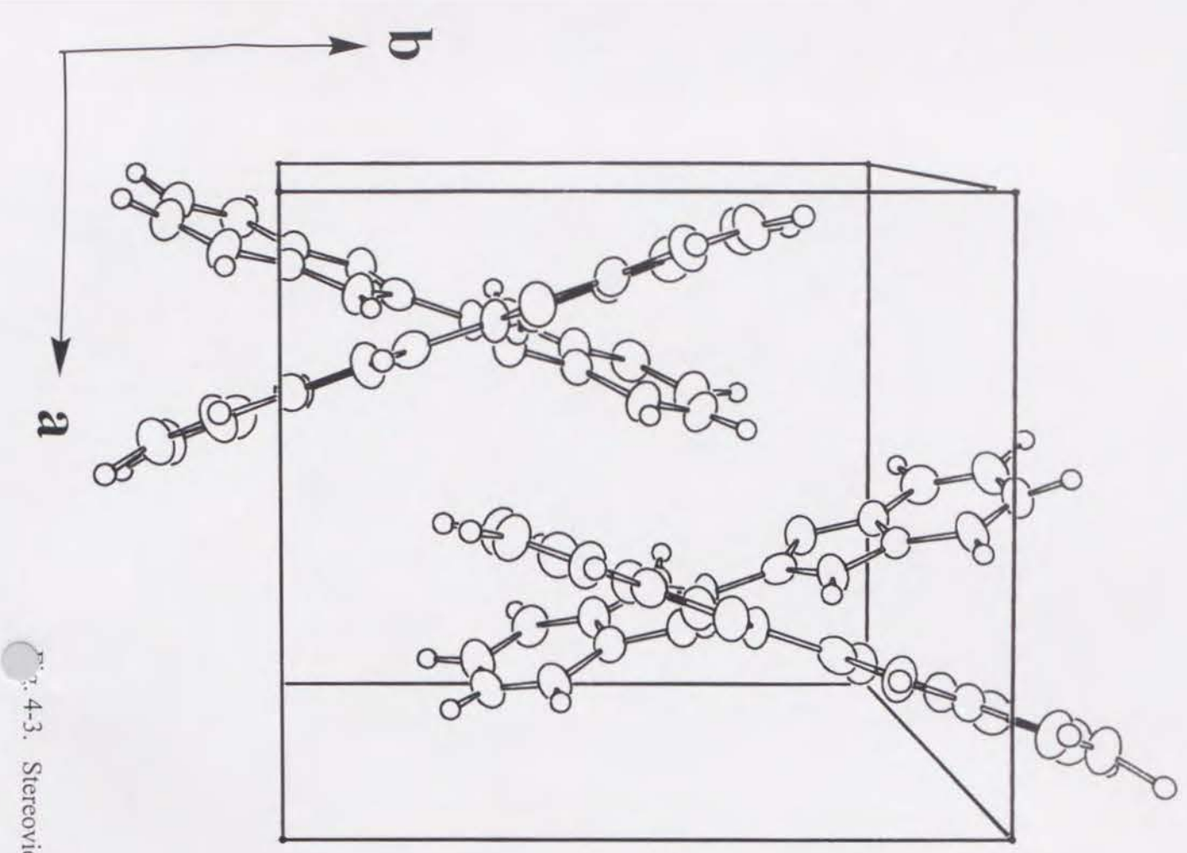

Fig. 4-3. Stereoview of unit cell of H2BBIM viewed along the c-axis.

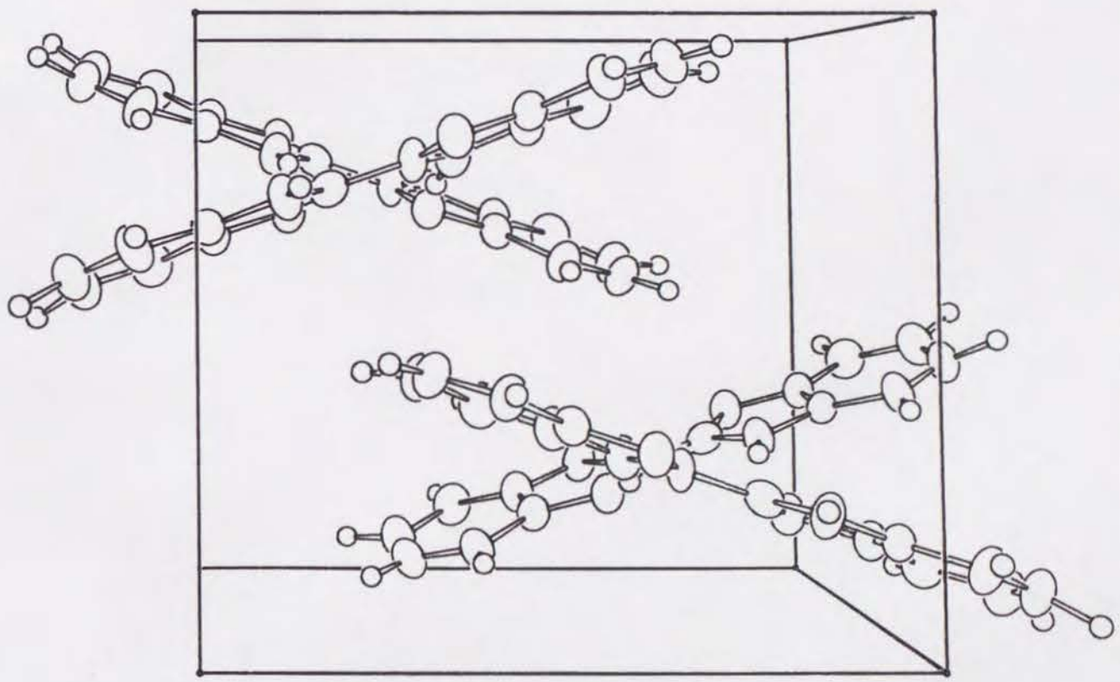

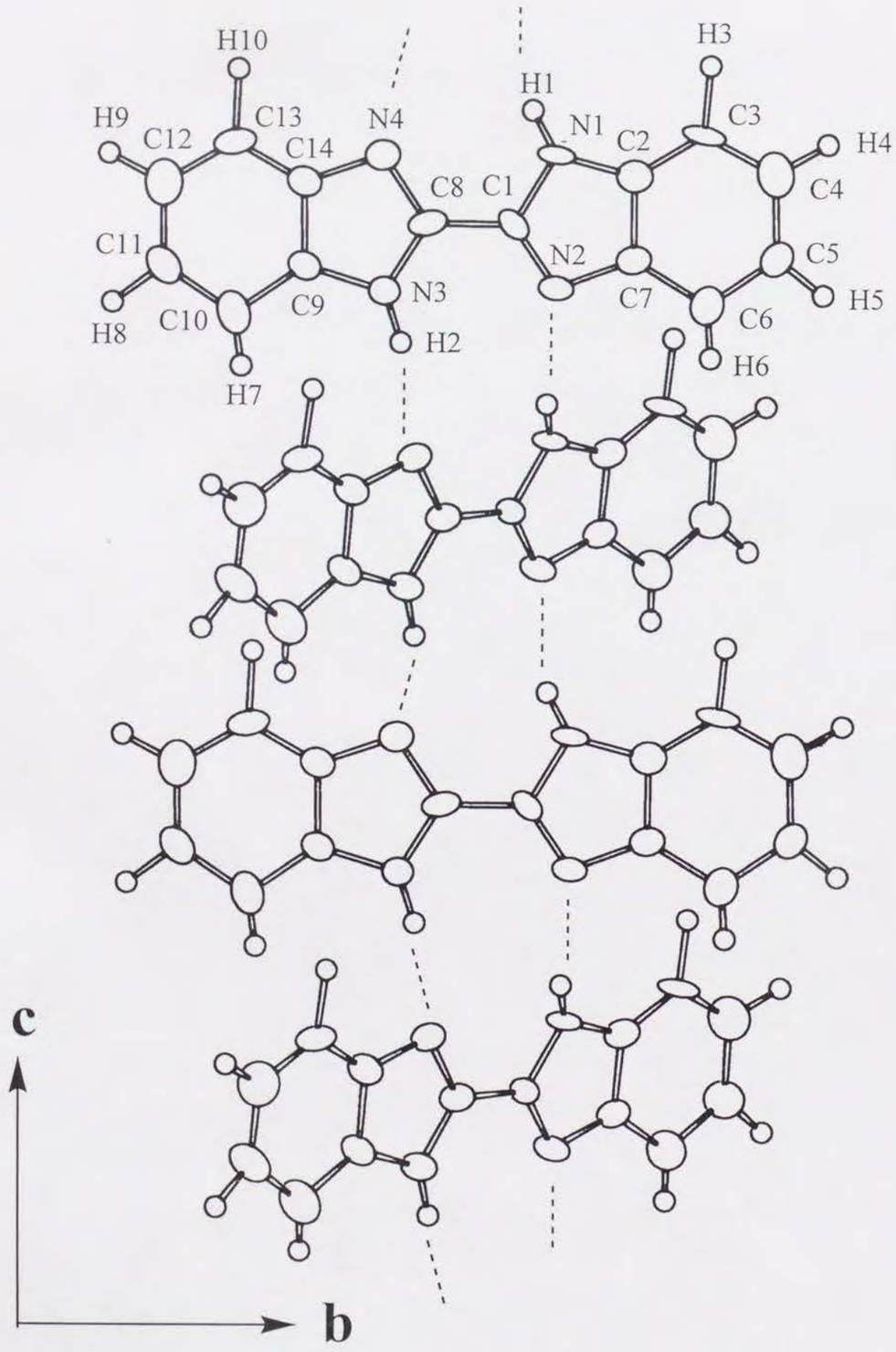

Fig. 4-4 Hydrogen bond of H2BBIM with atomic numbering scheme viewed along the a-axis. Dashed lines are N-H•••N hydrogen bond.

thus the strength of hydrogen bond is not influenced by the benzo substitution to the imidazole molecule.

4-3-6 Crystal Structure of [H4BBIM^{2+}][BF$_4^-$]$_2$ (4)

Half units of H4BBIM^{2+}(1) and H4BBIM^{2+}(2), one BF$_4^-$(1) and BF$_4^-$(2) molecules are crystallographically independent in the unit cell, and the mirror planes are located on the molecular short axis of H4BBIM^{2+} molecules (Fig. 4-5). Since the dihedral angles between two benzoimidazolium parts at the central C- C bond of H4BBIM^{2+}(1) and H4BBIM^{2+}(2) are 11.2 and 10.2°, respectively, the H4BBIM^{2+} molecules deviates from the planar structure.

Figure 4-6 showed a stereoview of the unit cell viewed along the b-axis. The H4BBIM^{2+} molecules are arranged in the ac-plane, and the BF$_4^-$ molecules are sandwiched by the H4BBIM^{2+} layers. In the ac-plane, the overlap of each H4BBIM^{2+} molecules occurred at benzoimidazole parts along the c-axis. The N-H•••F hydrogen bond between the H4BBIM^{2+} and BF$_4^-$ layers connects to each H4BBIM^{2+} layer along the b-axis.

The fundamental unit in the crystal is the N-H•••F hydrogen bond planar sheet structure, which is composed of the alternate arrangements of H4BBIM^{2+} and two BF$_4^-$ (Fig. 4-7a). The BF$_4^-$ anions between the H4BBIM^{2+} are located at above and below positions of the molecular plane of H4BBIM^{2+}. Table 4-5 summarizes the N•••F distances of the N-H•••F hydrogen bond. Among the N•••F distances of H4BBIM^{2+}(1); N11•••F41 (2.800 Å), N11•••F41'(2.909 Å), N12•••F42 (2.314 Å), and N12•••F42' (2.749 Å), the N12•••F42 distance is very short. Similar short distance is also observed at N21•••F31' among the H4BBIM^{2+}(2) ; N22•••F34 (2.745 Å), N22•••F34' (2.976 Å), N21•••F31 (2.840 Å), and N21•••F31' (2.307 Å), where the prime symbol corresponds to the atom generated by the symmetrcal operations.

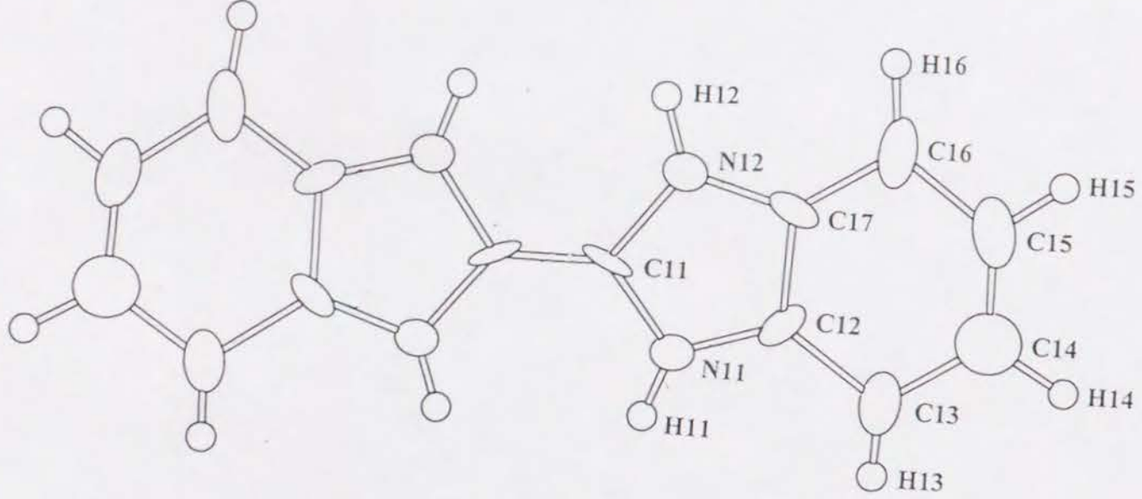

$H4BBIM^{2+}(1)$

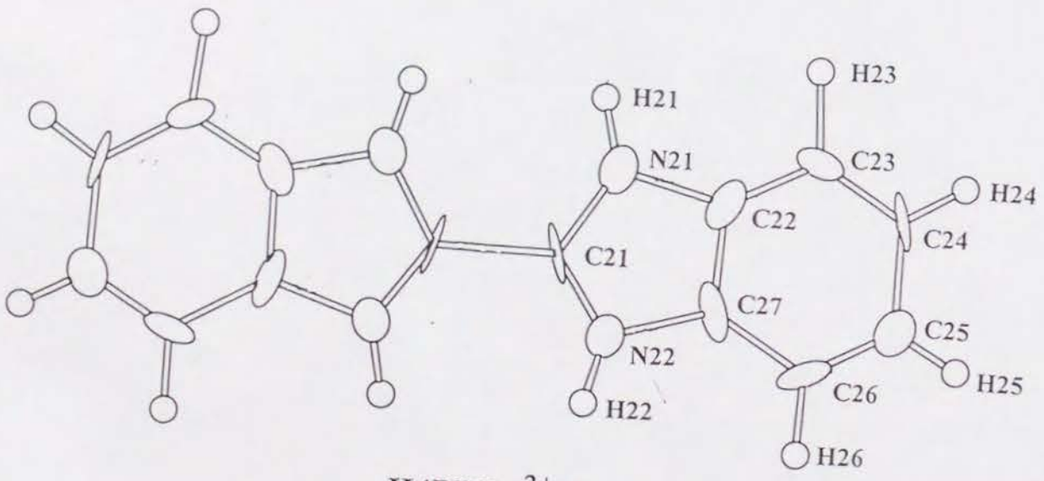

$H4BBIM^{2+}(2)$

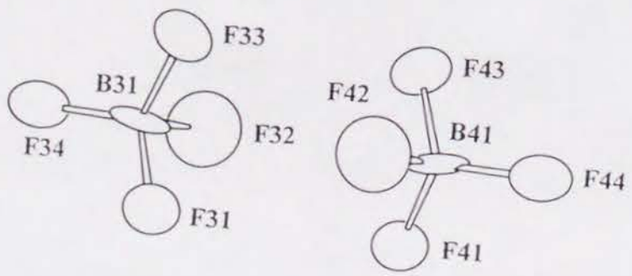

$BF_4^-(1)$

$BF_4^-(2)$

Fig. 4-5 Crystal structure of $[H4BBIM^{2+}][BF_4^-]2$. Crystallographically independent molecules, $H4BBIM^{2+}(1)$, $H4BBIM^{2+}(2)$, $BF_4^-(1)$, and $BF_4^-(2)$.

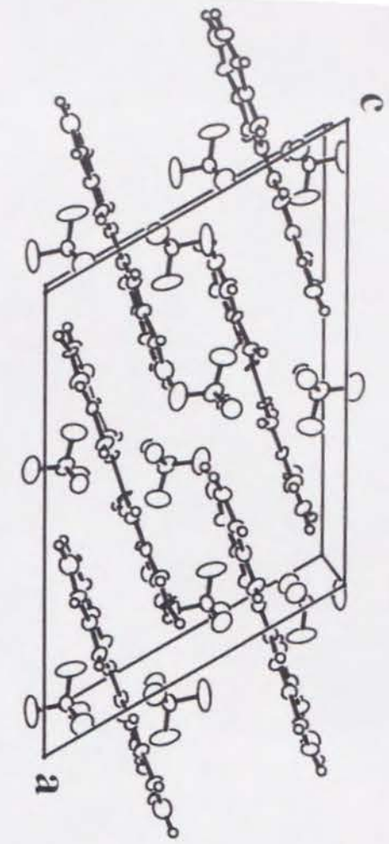

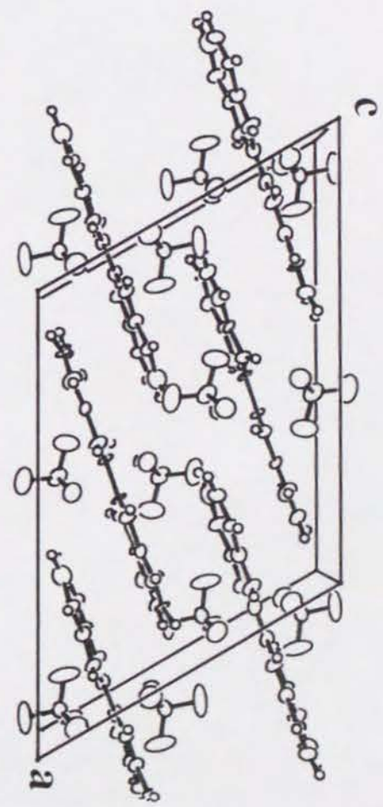

Fig. 4-6 Stereoview of unit cell of $[H4BBIM^{2+}][BF_4^-]2$ viewed along the b-axis.

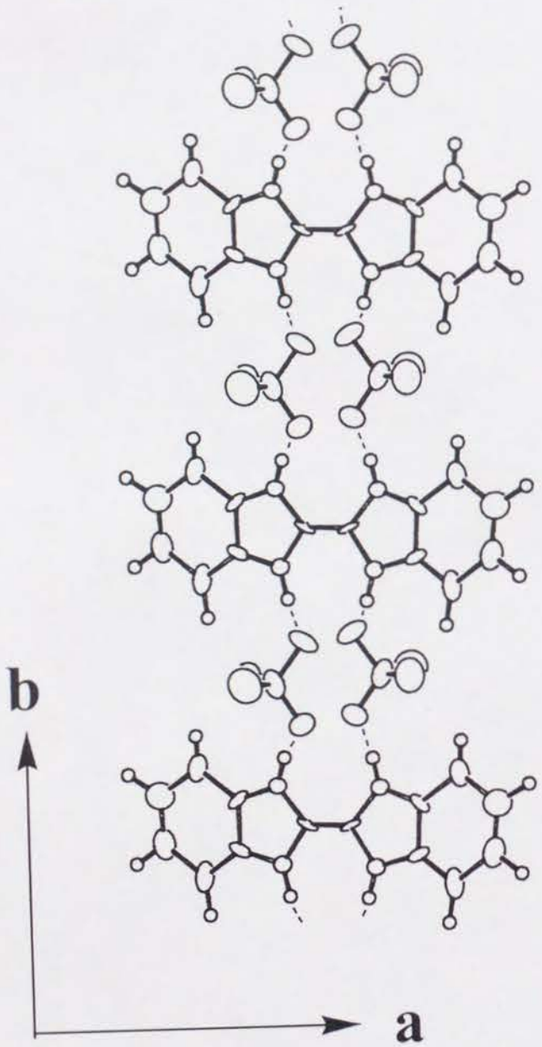

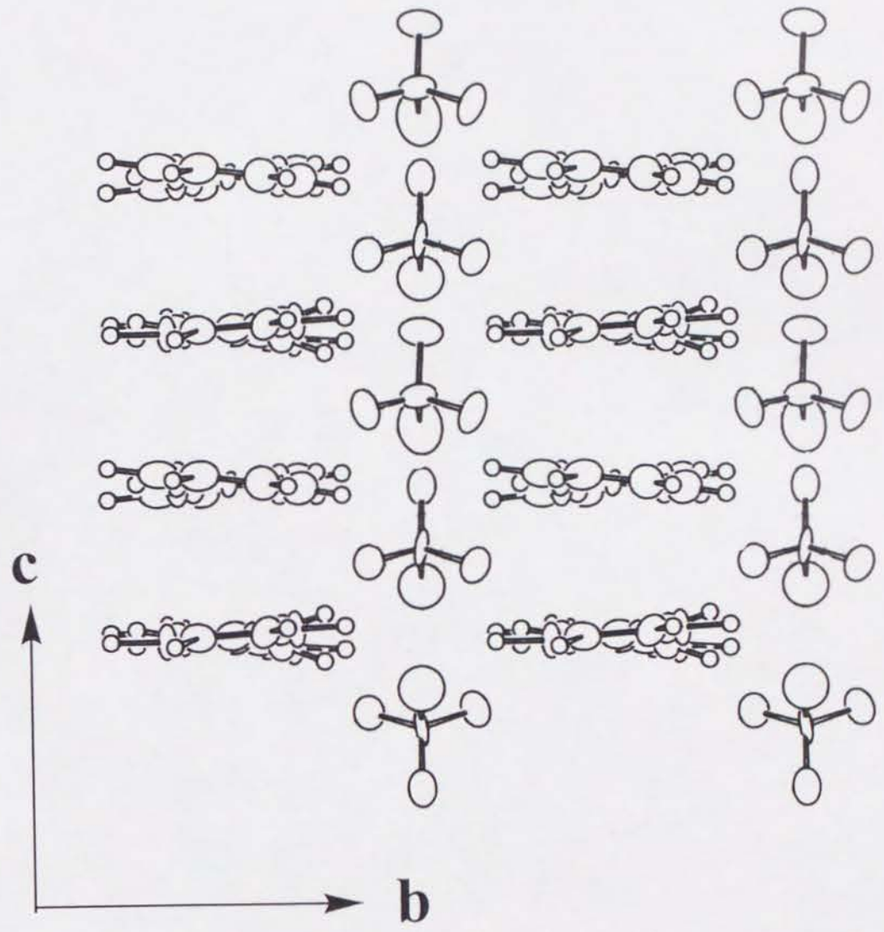

Fig. 4-7 Crystal structure of $[H4BBIM^{2+}][BF_4^-]_2$. a) hydrogen bond network viewed along the c-axis. b) Layer structures of $H4BBIM^{2+}$ and BF_4^- viewed along the a-axis.

Table 4-5. N-H•••F hydrogen bond distances (Å) of $[H4BBIM^{2+}][BF_4^-]_2$.

$H4BBIM^{2+}(1)$		$H4BBIM^{2+}(2)$	
N11•••F41	2.800(10)	N22•••F34	2.745(12)
N11•••F41'	2.909(11)	N22•••F34'	2.976(12)
N12•••F42	2.314(12)	N21•••F31	2.840(12)
N12•••F42'	2.749(12)	N21•••F31'	2.307(12)

The distances of N12•••F42 and N21•••F31' are contracted about 0.5 Å compared with the sum of the ion radius of NH_4^+ and F^- (2.84 Å).[8] The N•••F distances of [benzoimidazole][benzoimidazolium$^+$][BF_4^-] were reported as 2.870(4) and 2.896(3)Å,[11] while those of $[NH_4^+][F^-]$ and $[NH_3\text{-}NH_3^{2+}][F^-]_2$ were 2.69 and 2.62 Å , respectively.[12] It is thus the N12•••F42 and N21•••F31' hydrogen bonds are extremely strong among the N-H•••F hydrogen bonds.

Figure 4-7b indicates the $H4BBIM^{2+}$ and BF_4^- layers viewed along the molecular long axis of $H4BBIM^{2+}$. Since the mean interplanar distances between $H4BBIM^{2+}$ planes along the c-axis is determined as 3.61Å, a considerable intermolecular interaction by the $\pi - \pi$ overlap of benzoimidazole parts is expected along this direction. The intermolecular $\pi - \pi$ interaction within the $H4BBIM^{2+}$ layer is two dimensional (Fig. 4-6). Consequently, the two dimensional conductor will be formed from this crystal structure, if the carrier doping is possible. In the anion layer, the weak intermolecular contacts were found at F31•••F31' (3.056 Å) and F42•••F42' (3.016 Å), which are slightly longer than the sum of the van der Waals radius of fluorine (2.94 Å). The intermolecular interactions in the crystal $[H4BBIM^{2+}][BF_4^-]_2$ are observed as the hydrogen bond along the b-axis and the $\pi - \pi$ overlap of $H4BBIM^{2+}$ in the ac plane.

4-3-7 Crystal Structure of $(H3BBIM^+)(TCNQ)(Cl^-)_{0.7}(H_2O)_{0.7}$ (5)

One $H3BBIM^+$ and TCNQ molecule are crystallographically independent in the unit cell (Fig. 4-8). I used the non-centrosymmetric space group P1 instead of $P\bar{1}$ by the reason of non-symmetry of $H3BBIM^+$ molecule. The occupancy factors of Cl^- and O atoms were refined as 0.7, which had the positional disorder with two equivalent sites.

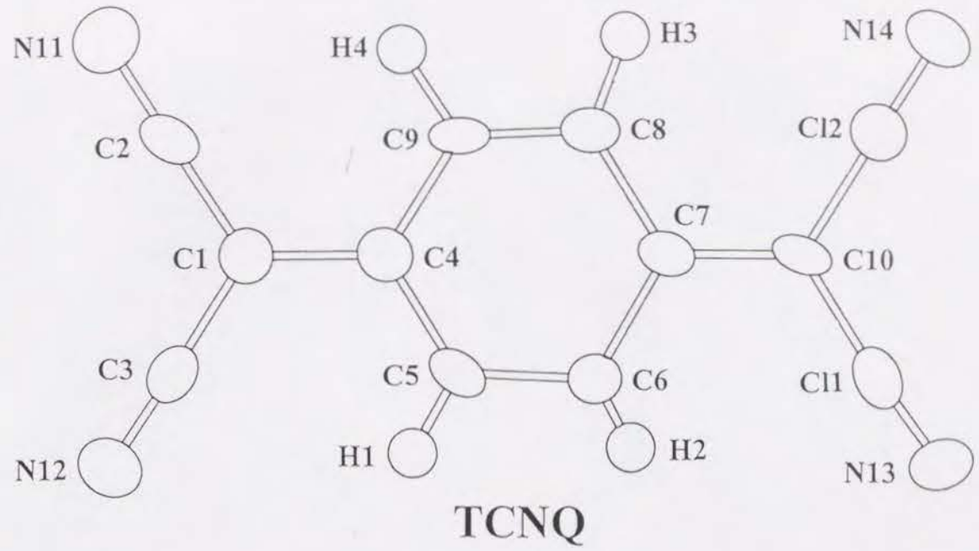

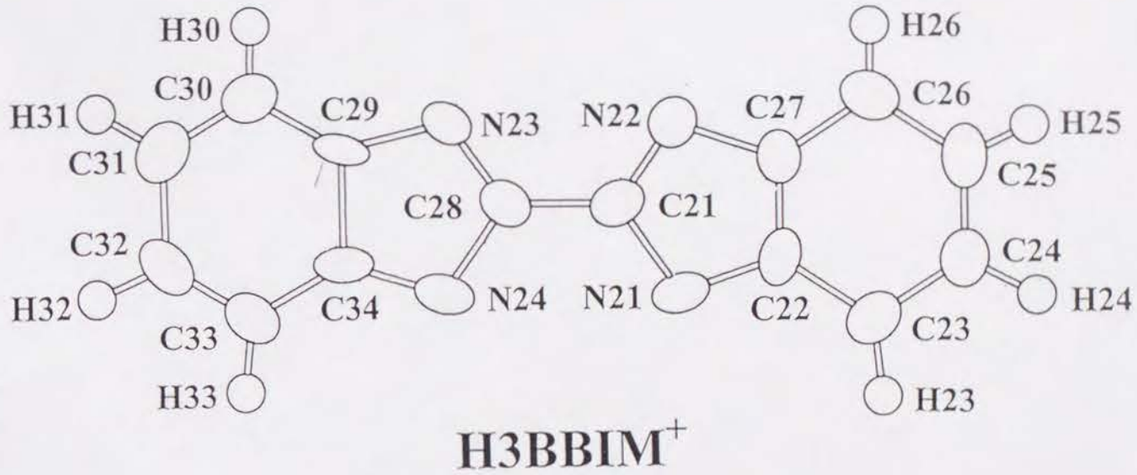

Fig. 4-8 Crystallographically independent molecules of $(H3BBIM^+)(TCNQ)(Cl^-)_{0.7}(H_2O)_{0.7}$ with atomic numbering scheme.

a

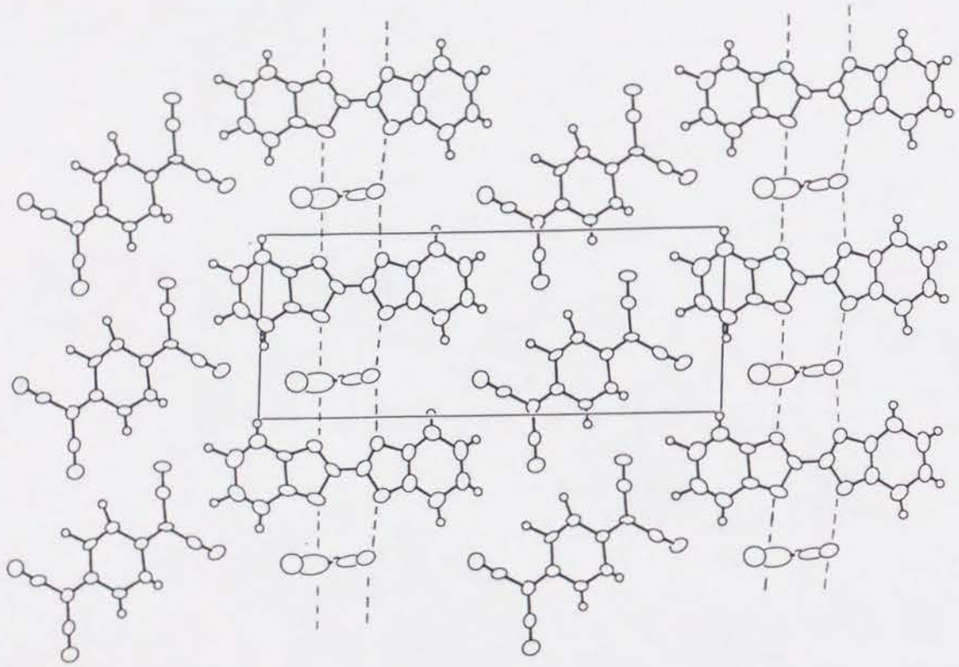

b

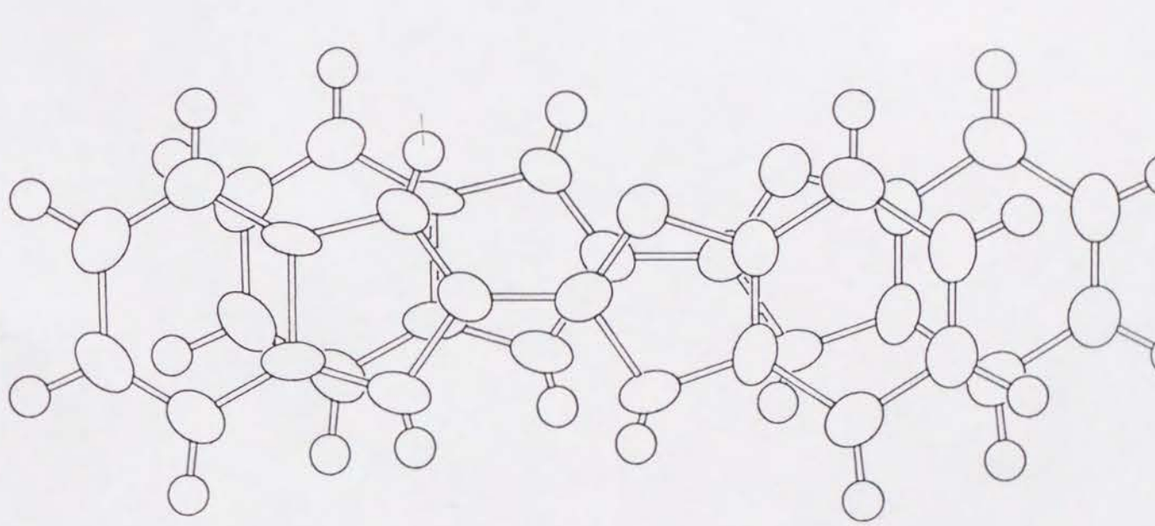

c

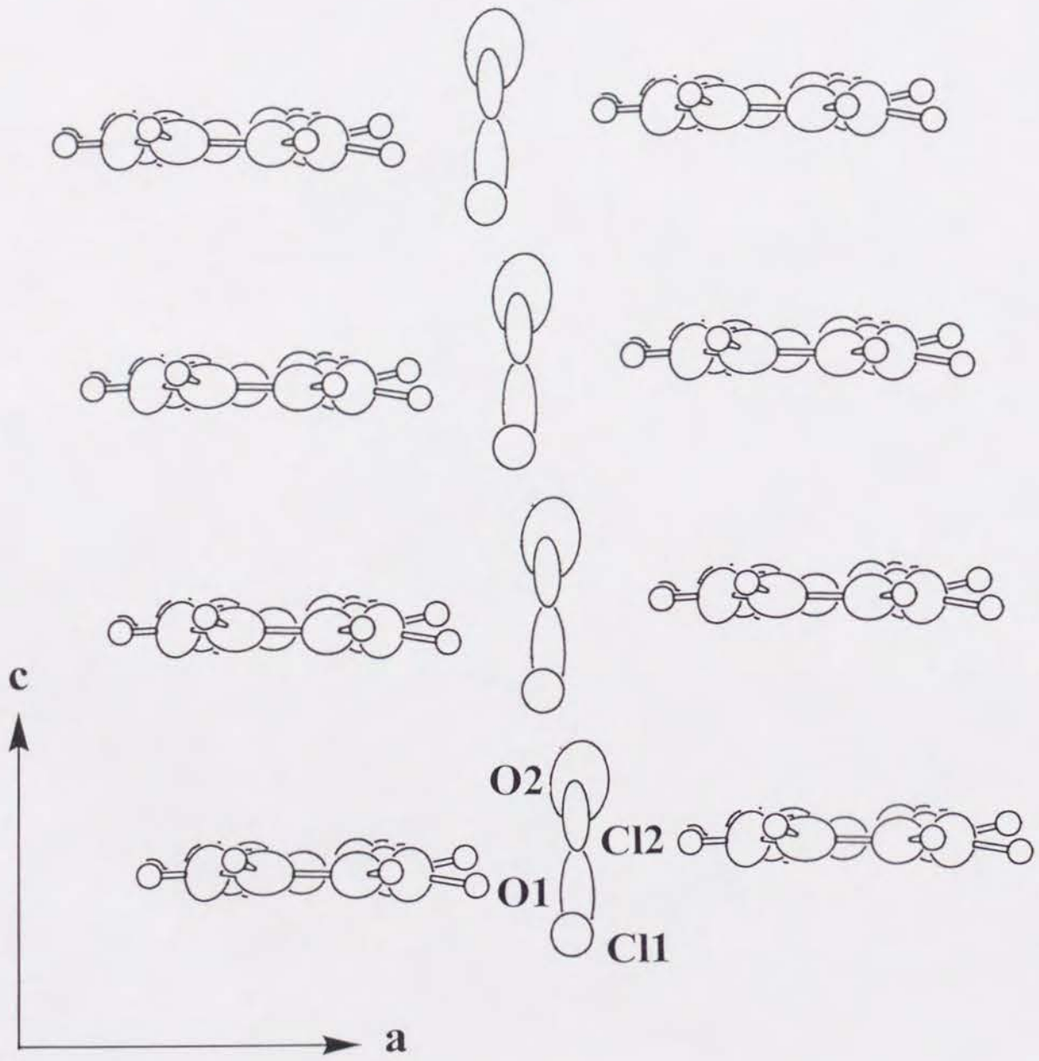

Fig. 4-9 Crystal structure of $(H3BBIM^+)(TCNQ)(Cl^-)_{0.7}(H_2O)_{0.7}$. a) Unit cell viewed along the c-axis, and the dashed lines along the a-axis are the hydrogen bonds. b) Overlap modes of TCNQ molecules and $H3BBIM^+$ molecules in columns. c) Stacking of $H3BBIM^+$ molecules and disordered Cl^- and H_2O having two equivalent sites viewed along the b-axis.

The hydrogen atoms of H_2O and amino protons were not detected, while those of benzene rings were found from the differential Fourier map. The protonated species of $H3BBIM^+$ have ambiguity from the result of structural analysis. The dihedral angle between two benzoimidazole parts at the central C - C bond (1.3°) indicates the nearly planar structure of $H3BBIM^+$.

Figure 4-9a shows a unit cell viewed along the c-axis. The crystal was composed of the segregated uniform stacks of $H3BBIM^+$ molecules and TCNQ molecules along the c-axis. The mean interplanar distances of TCNQ molecules and $H3BBIM^+$ molecules in each column are 3.25 and 3.47 Å, respectively. The overlap mode of TCNQ is the bond-over-ring type, which resembles to that of the highly conducting TCNQ salts, [13] while the effective overlap of $H3BBIM^+$ molecules is also observed (Fig. 4-7b). Along the a-axis, each $H3BBIM^+$ molecules are connected by the hydrogen bonds between amino proton of $H3BBIM^+$ and Cl^- or H_2O, which forms the hydrogen bond sheet structure as observed in the $[H4BBIM^{2+}][BF_4^-]_2$. The Cl^- and H_2O locate at the side-by-side space between two $H3BBIM^+$ molecules, and can participate to the hydrogen bonds (Fig. 4-9c). There are no interatomic contacts between the TCNQ and $H3BBIM^+$ molecules, which is shorter than the sum of the van der Waals radius.

The degree of CT (δ) of TCNQ molecule can be estimated from the bond lengths of TCNQ. I examined the correlation between the bond lengths and the δ from the results of structural analysis of some kinds of TCNQ complexes.[14] Table 4-6 summarizes the selected bond lengths a ~ d (see below Table 4-6) and δ of reference complexes. Eight kinds of TCNQ complexes having the various δ values ranging from 0 to 1.0 were used to deduce the correlation.

Table 4-6. Selected bond lengths of TCNQ complexes.[a)]

	a	b	c	d	δ[b)]
TCNQ	1.346	1.448	1.374	1.441	0
(TMTSF)(TCNQ)[c)]	1.354	1.438	1.375	1.429	0.21
(TMTSF)(TCNQ)[d)]	1.39	1.44	1.39	1.42	0.57
(TMPD)(TCNQ)$_2$	1.353	1.431	1.394	1.423	0.5
(TMTSF)(DMTCNQ)	1.360	1.441	1.398	1.423	0.5
(HMTTF)(TCNQ)	1.356	1.434	1.397	1.421	0.72
(TTF)(TCNQ)	1.356	1.433	1.402	1.423	0.59
(Rb^+)(TCNQ)	1.373	1.423	1.420	1.416	1.0

a) Cited from Ref. 14. The notations of TMTSF, TMPD, and HMTTF are tetramethyltetraselenafulvalene, *N,N,N',N'*-tetramethyl-*p*-phenylenediamine, hexa methylenetetrathiafulvalene. b) Degree of CT (δ) determined by experimental method. c) Red form. d) Black form.

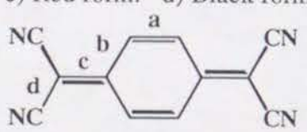

Fig. 4-10 indicates the nearly linear correlation between the bond lengths of a ~ d and the δ. Both of the a and c bonds increase linearly according to the increase of δ, while the b and d decrease. I tried to fit these data by the least-squares method. The linear correlation between the bond lengths a ~ d and δ are derived as the following equations.

$$\mathbf{a} = 0.0210\delta + 1.345 \qquad (4\text{-}1)$$

$$\mathbf{b} = -0.0178\delta + 1.442 \qquad (4\text{-}2)$$

$$\mathbf{c} = 0.0513\delta + 1.368 \qquad (4\text{-}3)$$

$$\mathbf{d} = -0.0198\delta + 1.437 \qquad (4\text{-}4)$$

The bond length c is the most sensitive to the change of the δ. Kistenmacher et al. used the parameter c / (b + d) to determine the δ, thus I also used this parameter. The following equation was derived from the equations 4-2, 4-3, and 4-4.

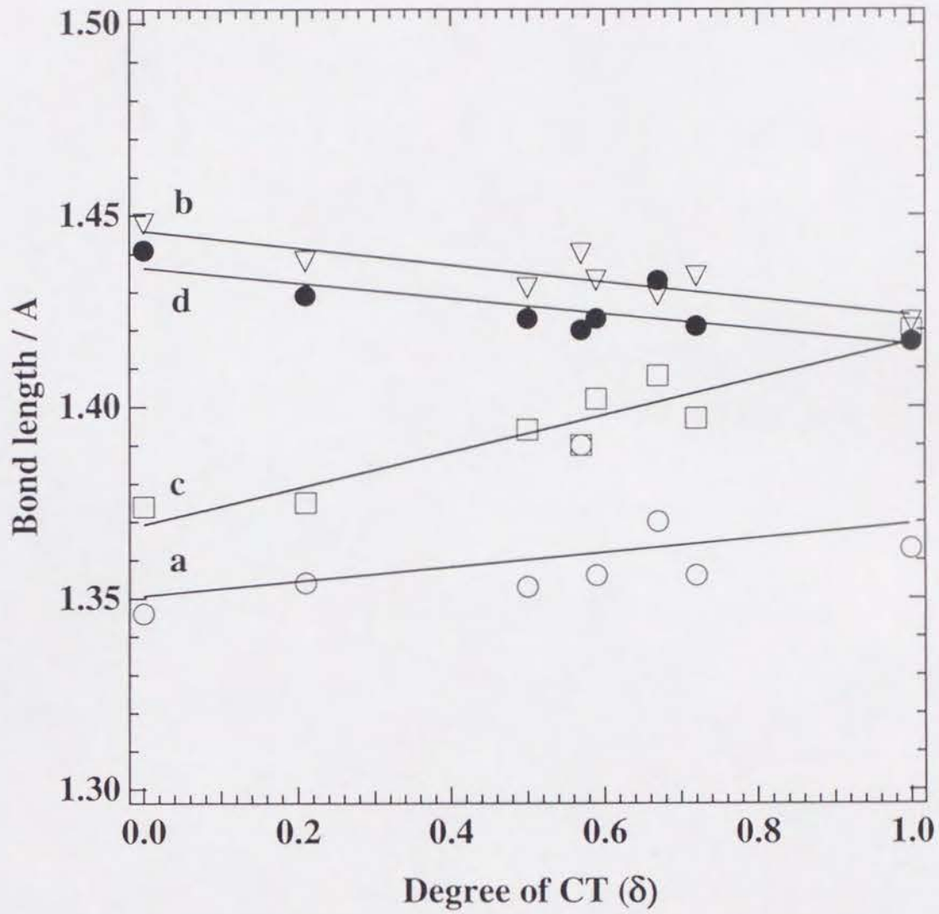

Fig. 4-10 The relation between the degree of CT (δ) and the selected bond lengths of TCNQ. The bond lengths a ~ d correspond to those of Table 4-6.

$$\frac{c}{b+d} = \frac{0.0513\delta + 1.3681}{2.8792 - 0.03756\delta} \qquad (4\text{-}5).$$

The δ value is expressed as equation 4-6.

$$\text{Degree of CT } (\delta) = 86.956\frac{c}{b+d} - 41.313 \qquad (4\text{-}6)$$

Using equation 4-6, the δ value in the complex (**5**) was deduced as 0.7.

The H2BBIM system exists as the stable cation within the solid complex as supported by the results of redox properties, magnetic and optical properties (see Sections 4-3-9 and 4-3-10). Since the chlorine and water existed as Cl^- and H_2O rather than the Cl^- and H_3O^+ (described later), the real chemical formula is expressed as $[H3BBIM^+]_{0.6}[H4BBIM^{2+}]_{0.4}[TCNQ^{-0.7}][Cl^-]_{0.7}[H_2O]_{0.7}$ based on the above δ value. The mixed PT state $[H3BBIM^+]_{0.6}[H4BBIM^{2+}]_{0.4}$ is needed to explain the total balance of charge in the solid CT complex. In the electrocrystallization solvent, the equilibrium $H3BBIM^+ \rightleftarrows H4BBIM^{2+} + H^+$ gives rise to the mixed PT state of $H3BBIM^+$ and $H4BBIM^{2+}$.

4-3-8 Electrical Conductivity of $(H3BBIM^+)(TCNQ)(Cl^-)_{0.7}(H_2O)_{0.7}$

In the ambient pressure, the conductivity at room temperature (σ_{RT}) was 2 ~ 20 Scm^{-1}, which was measured along the stacking axis of TCNQ. The temperature dependence of conductivity (σ) showed the semimetallic character in the temperature range from 300 to 280 K (Fig. 4-11a), and the semiconducting behaviour was observed from 280 to 100 K with the activation energy (E_a) of 0.04 eV. The abrupt decrease of σ was observed at 100 K, which changed the system to an insulator. The semimetallic conducting behaviour was reported for the narrow gap semiconductor; for examples, (*N*-methylphenazinium)(TCNQ) and (triethylammonium)$(I_3^-)_{0.3}$(TCNQ).[15] The semimetallic conductivity at high temperature region is arisen from the mobility term, but upon low temperature the decreasing of the activated carrier concentration changes the

a

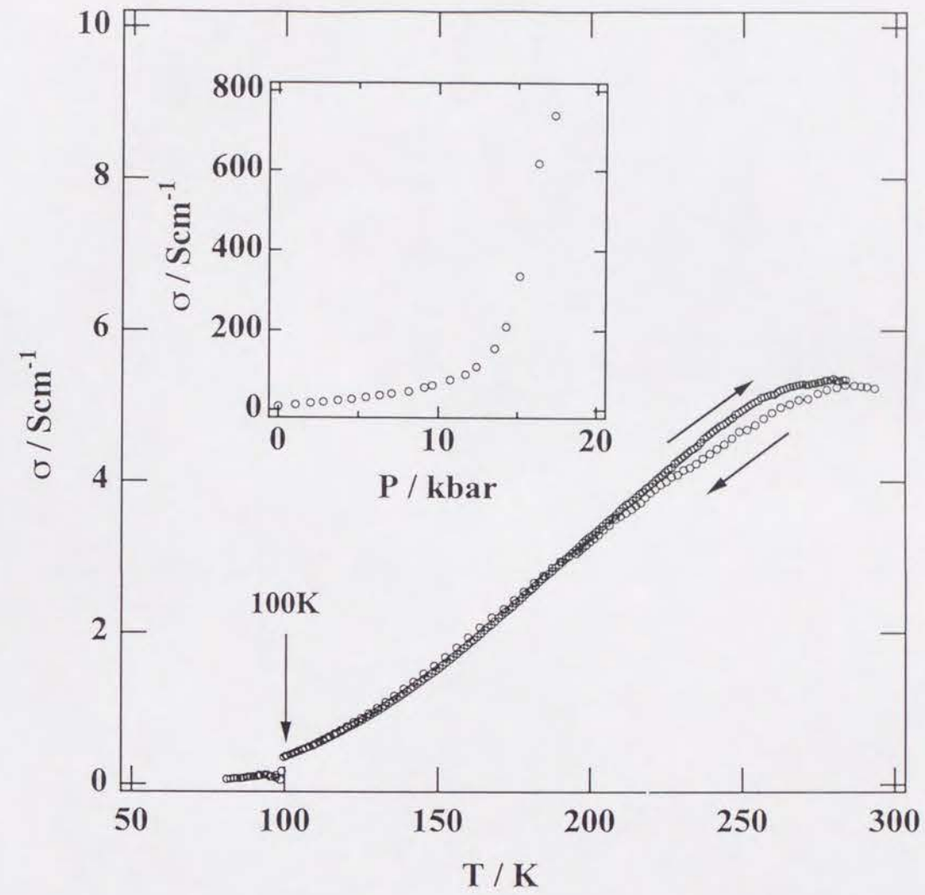

b

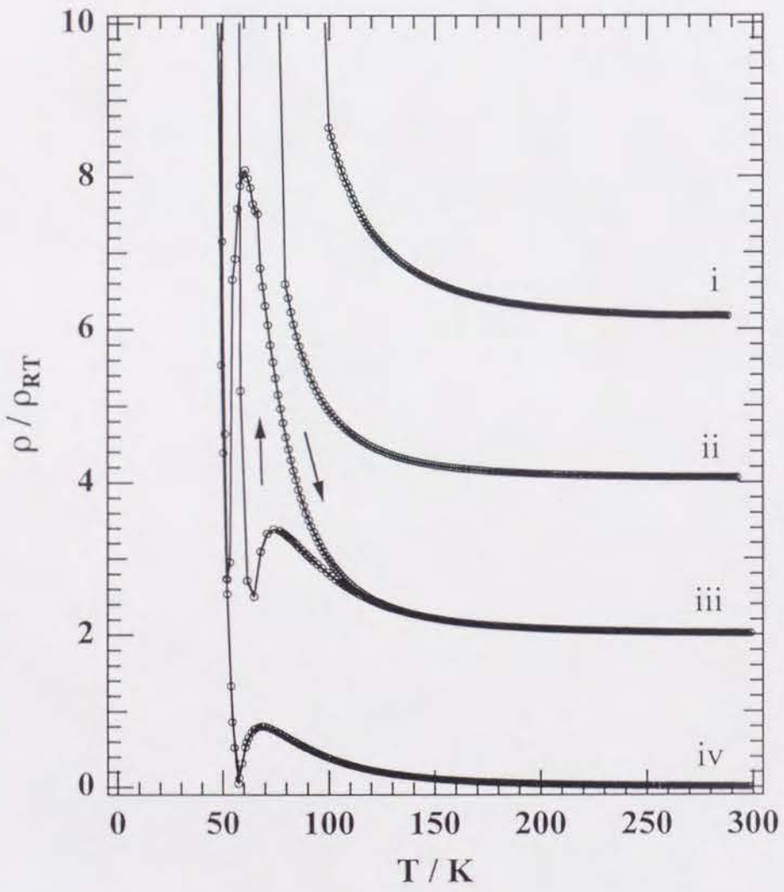

Fig. 4-11 The electrical conducting behaviour of $(H3BBIM^+)(TCNQ)(Cl^-)_{0.7}(H_2O)_{0.7}$. a) Temperature dependence of conductivity at ambient pressure, and inset shows the pressure dependence of room temperature conductivity. b) Temperature dependence of resistivity normarized at ρ_{RT} measured at 1 bar (i), 4.5 (ii), 13.4 (iii), and 18.0 (iv) kbar conditionsm, which are shifted to vertical axis to clarify the figure. The hysteresis was observed at 13.4 kbar (iii) measurement.

system to an insulator. The anisotropy of σ_{RT} (a : b : c = 10^{-6} : 10^{-6} : 1) in the complex (**5**) indicates highly one dimensional character of electronic structure.

I examined the pressure dependence of conductivity. The linear increase of σ_{RT} was observed from 1bar to 12 kbar, and abrupt increase of σ_{RT} occurred by the application of pressure above ca. 12 kbar. The σ_{RT} reached to ca. 800 Scm^{-1} under a pressure of 18 kbar (inset of Fig. 4-11a). The temperature dependencies of resistivities under the 4.5 (ii), 13.4 (iii), and 18.0 (iv) kbar were also shown in Fig. 4-11b. All of the temperature dependencies of resistivities under pressure indicated the semiconducting behaviour. The resistivity at 4.5 kbar showed similar conducting behaviour to that of the ambient pressure, but the transition temperature to the insulating state was decreased to 80 K compared with ambient pressure (100 K). In the 13.4 kbar condition, the resistivity hump appeared at 75 K in the cooling process, which accompanied by the hysteresis with the enhanced hump at 65 K in the heating process. The similar resistivity hump (65 K) was also observed at 18.0 kbar measurement with no hysteresis. Some kinds of phase transition may occur by the application of pressure about 12 kbar.

4-3-9 Magnetic Property of $(H3BBIM^+)(TCNQ)(Cl^-)_{0.7}(H_2O)_{0.7}$

The temperature dependence of molar magnetic susceptibility (χ_m) of complex $(H3BBIM^+)(TCNQ)(Cl^-)_{0.7}(H_2O)_{0.7}$, which was corrected of the core diamagnetism and no correlation of Curie impurity, indicates the broad maximum at around 80 K (Fig. 4-12). The paramagnetic χ_m was observed at all measured temperature region, and abrupt increase of χ_m at ca. 20 K was ascribable to the Curie impurity. The χ_m at room temperature was 4.3 x 10^{-4} emu mol^{-1}, and slightly increased up to 80 K with maximum value of 5.3 x 10^{-4} emu mol^{-1} at 80 K, and then the χ_m slightly decreased from 80 to 30 K. This temperature dependence of χ_m resembles to the one-dimensional antiferromagnetic system, but the experimental results can not best fitted to both of the Bonnier - Fisher and Hisenberg equations. From the electrical conductivity, the transition to the insulating state was observed at 90 ~ 100 K, which was slightly higher temperature than the broad maxim of χ_m. Therefore, the mobile carriers of

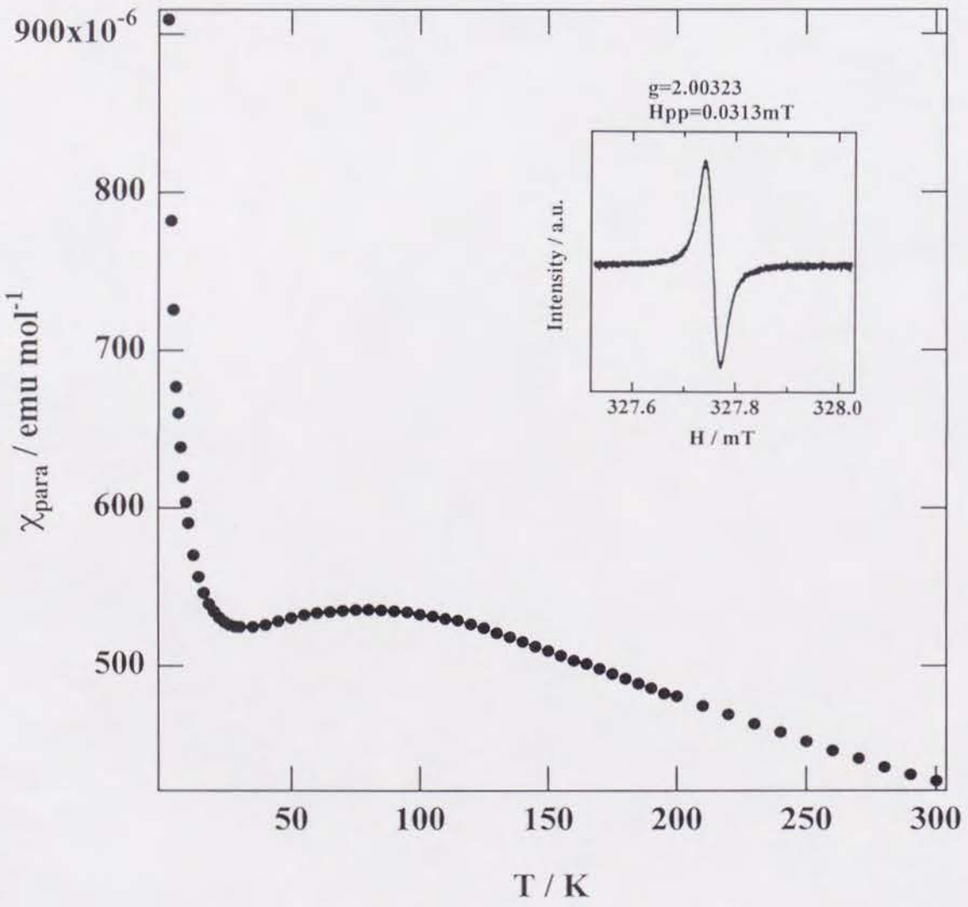

Fig. 4-12 Temperature dependence of molar magnetic susceptibility (χ_m) of $(H3BBIM^+)(TCNQ)(Cl^-)_{0.7}(H_2O)_{0.7}$. The inset is the electron spin resonance (ESR) spectrum at 297 K. The g-value and line width are 2.00323 and 0.0313 mT, respectively.

TCNQ chain disappeared at around 90 ~ 100 K, which will reflect the decreasing of χ_m at around 80 K. Similar magnetic behaviours, which accompanied the broad maxima of χ_m, were reported for the metallic [1,2-di(*N*-ethyl-pyridinium)ethylene][TCNQ]4 (σ_{RT} = 150 ~ 2200 Scm^{-1}) and the semimetallic [9,10-bis(4,5-dimethyl-1,3-dithiolo)-2-ylidene-9,10-dihydroanthracene][TCNQ]4 (σ_{RT} = 60 Scm^{-1}).[16] However, there is no explanations for the broad maxima of magnetic susceptibility.

The electron spin resonance at room temperature indicated the sharp absorption at the line width of 0.313 gauss with g-value of 2.0032 (inset of Fig. 4-12). Since this absorption is characteristic to the TCNQ anion radical,[15b] the opene shell species $H3BBIM^{\bullet}$ or $H4BBIM^{+\bullet}$ were not formed in the complex. The close shell $H3BBIM^+$ and $H4BBIM^{2+}$ exist in the complex in accordance with redox, structural, and optical properties.

4-3-10 Optical Property of $(H3BBIM^+)(TCNQ)(Cl^-)_{0.7}(H_2O)_{0.7}$

From the UV-VIS-NIR and IR spectra, I examined the electronic states of TCNQ and protonated states of H2BBIM system within the complex. The UV-VIS-NIR spectra of $(H3BBIM^+)(TCNQ)(Cl^-)_{0.7}(H_2O)_{0.7}$ was compared with the $[K^+][TCNQ^{-\bullet}]$ and $[H3BIM^+]_2[TCNQ^{-\bullet}][TCNQ^0]$ (Fig. 4-13). The completely ionic $[K^+][TCNQ^{-\bullet}]$, having the dimeric non uniform column, shows the CT absorption at 8.2 x 10^3 cm^{-1} (B-band), which is assigned to the transition of $2TCNQ^{-\bullet} \rightarrow TCNQ^{2-} + TCNQ^0$.[17] Both of the C- (11.5 x 10^3 cm^{-1}) and D- (16.4 x 10^3 cm^{-1}) bands are ascribable to the interdimer and monomer transitions of $TCNQ^{-\bullet}$, and the E band (27.6 x 10^3 cm^{-1}) is originated from intramolecular transition of $TCNQ^{-\bullet}$. The $[H3BIM^+]_2[TCNQ^{-\bullet}][TCNQ^0]$ has the charge separated non-uniform column of TCNQ. The TCNQ column was composed of the trimer unit of the $TCNQ^{-\bullet} \sim TCNQ^{-\bullet} \sim TCNQ^0$ (see Chapter 3). The CT transition from $TCNQ^{-\bullet}$ to $TCNQ^0$ revealed at 4.8 x 10^3 cm^{-1} (A-band), and the C-band (11.6 x 10^3 cm^{-1}) was enhanced compared with $[K^+][TCNQ^{-\bullet}]$. Both of D- (16.2 x 10^3 cm^{-1}) and E- (27.6 x 10^3 cm^{-1}) bands appeared at

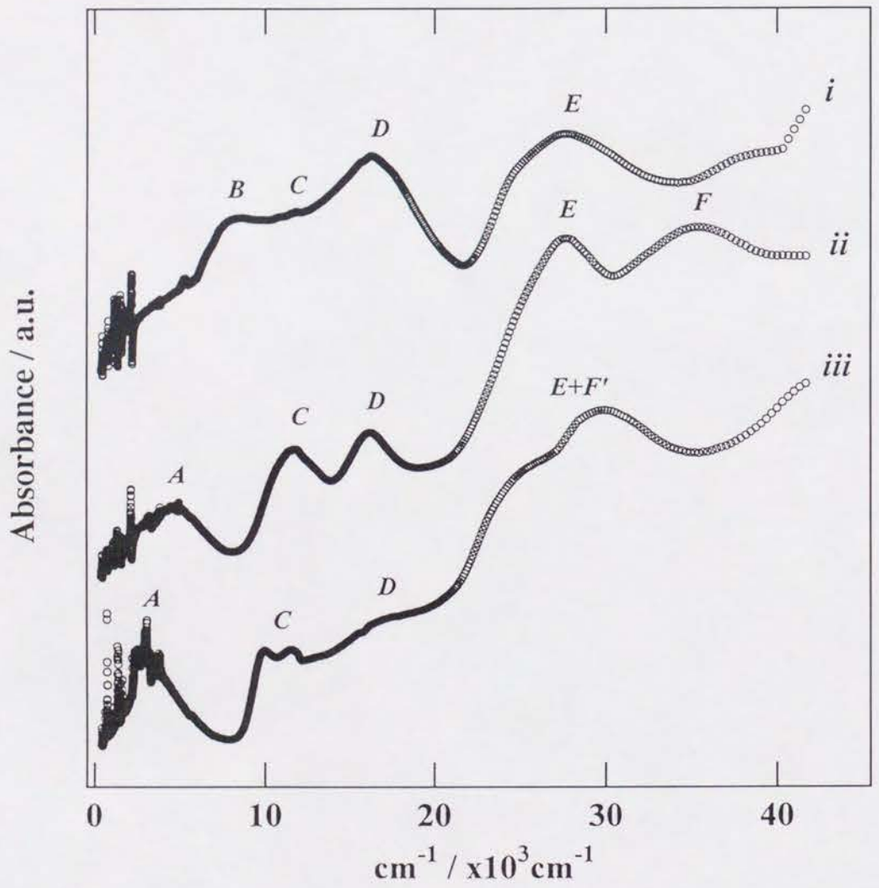

Fig. 4-13 UV-VIS-NIR spectra of i) $[K^+][TCNQ^{-\bullet}]$, ii) $[H3BIM^+]_2[TCNQ^{-\bullet}]_2[TCNQ^0]$, and iii) $(H3BBIM^+)(TCNQ)(Cl^-)_{0.7}(H_2O)_{0.7}$. See text to the assingment of A ~ F bands.

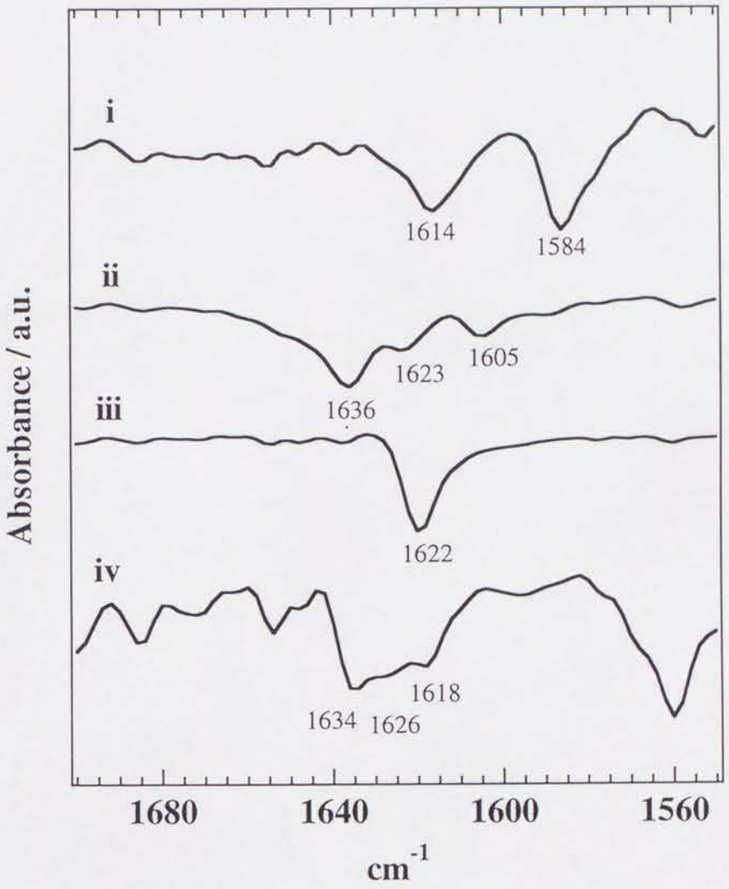

Fig. 4-14. Vibration spectra of i) H2BBIM, ii) $[H3BBIM^+][I^-]$, iii) $[H4BBIM^{2+}][BF_4^-]_2$, and iv) $(H3BBIM^+)(TCNQ)(Cl)_{0.7}(H_2O)_{0.7}$ at the frequency range from 1700 to 1550 cm^{-1}.

the similar energy region to those of the $[K^+][TCNQ^{-\bullet}]$, and the intramolecular transition of $H3BIM^+$ species (F-band) newly appeared at 35.5 x 10^3 cm^{-1}.

The CT transition (A-band) of $(H3BBIM^+)(TCNQ)(Cl^-)_{0.7}(H_2O)_{0.7}$ appeared at 3.2 x 10^3 cm^{-1}, which shifted to lower energy region compared with that of $[H3BIM^+]_2[TCNQ^{-\bullet}][TCNQ^0]$ in accordance with the high electrical conducting behaviour. The appearance of A-band indicates the mixed CT state of TCNQ column, which is consistent with electrical conductivity and crystal structure. The C-band splits to into two bands at 10.0 and 11.4 x 10^3 cm^{-1}, and resembles to the solution spectra of $TCNQ^{-\bullet}$ (11.2 and 12.0 x 10^3 cm^{-1} in acetonitrile). The D-band appeared at 16.8 x 10^3 cm^{-1}, and E-band was overlapped with the intramolecular transition of H2BBIM species (F'-band).

To examine the PT state of H2BBIM system in the complex, the ν^b_{N-H} mode of $(H3BBIM^+)(TCNQ)(Cl^-)_{0.7}(H_2O)_{0.7}$ was compared with those of H2BBIM, $H3BBIM^+$, and $H4BBIM^{2+}$ in the frequency range from 1700 to 1550 cm^{-1} (Fig. 4-14). The $(H3BBIM^+)(TCNQ)(Cl^-)_{0.7}(H_2O)_{0.7}$ has the absorptions at 1634, 1626, 1618 cm^{-1} (line iv in Fig. 4-14), which are consistent with $H3BBIM^+$ (1636, 1623, and 1605 cm^{-1}) and $H4BBIM^{2+}$ (1622 cm^{-1}). Since the absorption at 1584 cm^{-1} of H2BBIM is not observed at curve iv, the complex is composed of the $H3BBIM^+$ and $H4BBIM^{2+}$. The highly acidic electrocrystallization condition provides the equilibrium of $H3BBIM^+ \rightleftarrows H4BBIM^{2+} + H^+$, thus the mixed PT state of $[H3BBIM^+]_x[H4BBIM^{2+}]_{1-x}$ was realized during the complex formation.

There are two kinds of possibilities of the solvated form of chlorine and water in the complex; that is, i) $[Cl^-]_{0.7}[H_2O]_{0.7}$ and ii) $[Cl^-]_{0.7}[H_3O^+]_{0.7}$. The hydronium ion ($H_3O^+$) has some characteristic IR absorptions at 3150, 2555, 2100, 1685, and 1000 cm^{-1}.[18] Unfortunately, the absorptions at 2100, 1685 and 1000 cm^{-1} are overlapped with the intense bands of $TCNQ^{-\bullet}$ and $H3BBIM^+$. However, the absorption maxima of the O-H stretching band (ν^s_{OH}) appeared at around 3460 cm^{-1}, which was shifted by 310 cm^{-1} to the higher frequency region than the ν^s_{OH} of H_3O^+. In addition, there are no observable peak at around 2555 cm^{-1}. As a result, the solvent molecule in the

complex exists as $[Cl^-]_{0.7}[H_2O]_{0.7}$ form rather than the $[Cl^-]_{0.7}[H_3O^+]_{0.7}$ one. As a consequence, the real chemical formula is deduced as $[H3BBIM^+]_x[H4BBIM^{2+}]_{1-x}[TCNQ^{-(1.3-x)}][Cl^-]_{0.7}[H_2O]_{0.7}$, $0.3 < x < 1$.

From the nitrile stretching frequency (ν_{CN}) of TCNQ, I estimated the degree of CT (δ) in the complex.[19] The neutral TCNQ and complete ionizied $TCNQ^{-\bullet}$ have the b_{1u} modes at 2222 and 2196 cm^{-1}, respectively. The ν_{CN} of $(H3BBIM^+)(TCNQ)(Cl^-)_{0.7}(H_2O)_{0.7}$ appeared at 2192 cm^{-1}. Assuming the linear relation between the ν_{CN} and δ value, the δ is estimated as 0.85, which is larger than the estimated value of the structural analysis (δ = 0.7).

4-4 Conclusion

The 2,2'-bi-1*H*-benzoimidazole (H2BBIM) system has the multiplex CT and PT interaction as well as 2,2'-bi-1*H*-imidazole (H2BIM) one. From the examinations of the acid dissociation (pK_a) and redox properties (E_p) of $H3BBIM^+$ and $H4BBIM^{2+}$, it is concluded that the expansion of π-electron system increases both of the acidity and electron-accepting ability of the $H3BBIM^+$ and $H4BBIM^{2+}$. However, the close shell cation species; $H3BBIM^+$ and $H4BBIM^{2+}$, are expected to be stable rather than the open shell species; $H3BBIM^{\bullet}$ and $H4BBIM^{+\bullet}$. The crystal structures of close shell species; H2BBIM and $[H4BBIM^{2+}][BF_4^-]_2$, were composed of the hydrogen bond networks of N-H•••N and N-H•••BF_4^-, respectively. The hydrogen bond ability is not influenced by the dibenzo substitution.

The TCNQ complex with $H3BBIM^+$ was prepared by a novel electrocrystallization method. Since the $H3BBIM^+$ was unstable in the dry acetonitrile solution, the electrocrystallization was carried out in the mixed solvent system containing the buffer solution (pH = 1.20). The acidic crystallization condition stabilized cationic states, which succeeded the preparation of good quality of single crystals as the composition of $(H3BBIM^+)(TCNQ)(Cl^-)_{0.7}(H_2O)_{0.7}$. The crystal structure of this

was composed of the uniform segregated stacks of TCNQ and $H3BBIM^{+}$, and the degree of CT (δ) was estimated as 0.7 from the bond lengths of TCNQ, which deduced the real chemical formula of $[H3BBIM^{+}]_{0.6}[H4BBIM^{2+}]_{0.4}[TCNQ^{-0.7}][Cl^{-}]_{0.7}[H_2O]_{0.7}$ with mixed PT state of H2BBIM species.

The electrical conducting behaviour of $[H3BBIM^{+}]_{0.6}[H4BBIM^{2+}]_{0.4}[TCNQ^{-0.7}][Cl^{-}]_{0.7}[H_2O]_{0.7}$ was semiconducting, and changed to the insulator at around 100 K. Similar semiconducting character was observed by the application of pressure up to 18 kbar. The molar magnetic susceptibility indicated a broad maxima at around 80 K, which was slightly lower temperature than the transition temparature of the insulator in the electrical conductivity measurement.

The UV-VIS-NIR spectra of TCNQ complex showed the mixed CT state of TCNQ, while the IR measurement supported the mixed PT state of $H3BBIM^{+}$ and $H4BBIM^{2+}$ in the complex. The mixed PT state of $H3BBIM^{+}$ and $H4BBIM^{2+}$ is closely related to the mixed CT state of TCNQ. The control of x value in the $[H3BBIM^{+}]_{x}[H4BBIM^{2+}]_{1-x}[TCNQ^{-(1.3-x)}][Cl^{-}]_{0.7}[H_2O]_{0.7}$ will cause the filling change of the band structure of TCNQ chain. The crystal preparation in the pH controlled solvent is useful method to do the precise injection of carrier to the conduction band.

4-5 References

1) B.F.Fieselmann, D.N.Hendrickson, and G.D.Stucky., *Inorg. Chem.*, **17**, 2078 (1978).

2) D.D.Perrin and B.Dempsey, *Buffer for pH and Metal Ion Control*, Chapman and Hall, London (1974).

3) G.M.Sheldrick, "SHELXS-86", Program for Crystal Structure Determination," Univ. of Göttingen, Federal Republic Germany.

4) The lists of atomic coordinates, structure factors, and anisotropic thermal parameters for non-hydrogen atoms are summarized at Chapter 6.

5) a) R.C.Wheland, *J. Am. Chem. Soc.*, **98**, 3926 (1976); b) G.Saito and J.P.Ferraris, *Bull. Chem. Soc. Jpn.*, **53**, 2141 (1980).

6) G.Saito and T.Inukai, *J. Jpn. Association Cryst. Growth,* **16**, 2 (1989).

7) D.Boinnard, P.Cassoux, V.Petrouleas, J.M.Savariault, and J.P.Tuchagues, *Inorg. Chem.,* **29** (1979) 4114.

8) A.Bondi, *J. Phys. Chem.*, **68**, 441 (1964).

9) D.T.Cromer, R.R.Ryan, and C.B.Storm, *Acta Crystallogr., Sect. C*, **43**, 1435 (1987).

10) a) B.M.Craven, R.K.McMullan, J.D.Bell, and H.C.Freeman, *Acta. Cryst., Sect.* **B**, **33**, 2585 (1977); b) S.Nagatomo, S,Takeda, H.Tamura, and N.Nakamura, *Bull. Chem. Soc. Jpn.*, **68**, 2783 (1995).

11) A.Quick, D.J.Williams, B.Borah, and J.L.Wood., *J. Chem. Soc. Chem. Commun.*, 891 (1974).

12) a) R.C.Plumb and D.F.Hornig, *J. Chem. Phys.*, **23**, 947 (1955); b) M.Koronberg and D.Harker, *J. Chem. Phys.*, **10**, 309 (1942).

13) *Extended Linear Chain compunds*, edited by J.S.Miller, Prenum Press, New York (1982).

14) T.J.Kistenmacher, T.J.Emge, A.N.Bloch, and D.O.Cowan, *Acta. Cryst., Sect. B*, **38**, 1193 (1982).

15) a) J.S.Miller and A.J.Epstein, *Angew. Chem. Int. Ed. Engl.*, **26**, 287 (1987); b) M.A.Abkowitz, A.J.Epstein, C.H.Griffiths, J.S.Miller, and M.L.Slade, *J. Am. Chem. Soc.*, **99**, 5304 (1977).

16) a) G.J.Ashwell, D.D.Eley, M.R.Willis, and J.Woodward, *phys. state sol. (b)* **79**, 629 (1977); b) M.R.Bryce, A.J.Moore, M.Hasan, G.J.Ashwell, A.T.Fraser, W.Clegg, M.B.Hursthouse, and A.I.Karaulov, *Angew. Chem. Int. Ed. Engl.*, **29**, 1450 (1990).

17) a) J.B.Torrance, B.A.Scott, B.Welber, F.B.Kaufman, and P.E.Seiden., *Phys. Rev., B*, **19**, 730 (1979); b) E.M.Conwell, I.A.Howard, J.P.Pouget, C.S.Jacobsen, J.C.Scott, and L.Zuppiroli, "*Semiconductors and Semimetals*" Vol.27, edited by E.M.Conwell, Academic Press, Inc., New York (1988); c) J.Tanaka, M.Tanaka, T.Kawai, T.Takabe, and O.Maki, *Bull. Chem. Soc. Jpn.*, **49**, 2358 (1976).

18) a) C.C.Ferriso and D.F.Hornig, *J. Chem. Phys.*, **23**, 1464 (1955); b) A.S.Gilbert and N.Sheppard, *J. Chem. Soc. Farady Trans. II.*, **69**, 1628 (1973).

19) J.S.Cappell, A.N.Bloch, W.A.Bryden, M.Maxfield, T.O.Poehler, and D.O.Cowan, *J. Am. Chem. Soc.*, **103**, 2442 (1981).

Chapter 5. General Conclusion

I examined the multiplex proton-transfer (PT) and electron-transfer (CT) nature of the 2,2'-bi-1*H*-imidazole (H2BIM) molecular framework. This system has complicated PT and CT nature, having twenty-five independent species, and belongs to the Weitz type redox structure. Among twenty-five species, I focused on the cation species; 2-(2-1*H*-imidazolyl)-1*H*-imidazolium ($H3BIM^+$) and 2,2'-bi-1*H*-imidazolium ($H4BIM^{2+}$).

The acid dissociation and redox properties in solution are indispensable characters to evaluate the PT and CT nature, which are useful to explain the types of the obtained CT complex. In Chapter 2, both of the acid dissociation constants (pK_a) and redox potentials (E_{redox}) of various kinds of H2BIM systems were examined to compare the PT and CT nature of the representative electron and proton donor and acceptor molecules. I related the CT and PT nature of various kinds of molecules to the on-site Coulomb repulsion energy (U) of two step CT or PT processes. The U of CT process was classified into the electron donor and acceptor system, while U of PT one was closely related to the size of molecules.

The CT complex formations of $H3BIM^+$ and $H4BIM^{2+}$ with 7,7,8,8-tetracyanoquinodimethane (TCNQ) derivatives were examined to clarify the CT and PT interactions during the crystal preparation. The types of the obtained CT complexes were changed to completely ionic, mixed CT, and neutral CT types. From the redox character between $H3BIM^+$ (or $H4BIM^{2+}$) and TCNQ systems, the CT process is inert in this combination, while the PT process dominates the complex formation. The PT states of H2BIM system in the complex were changed from the initial $H3BIM^+$ (or $H4BIM^{2+}$) to $[H4BIM^{2+}]_x[H3BIM^+]_{1-x}$ (or $[H3BIM^+]_x[H2BIM]_{1-x}$) and H2BIM (or $H3BIM^+$) according to the differences of acidity between the $H3BIM^+$ (or $H4BIM^{2+}$) and anion radical of TCNQ. Since the TCNQ system has moderate proton accepting ability, the detailed analysis of CT and PT nature of TCNQs were needed to explain the mechanism of the CT complex formation.

The electrical conductivities of the CT complex of $H3BIM^+$ and $H4BIM^{2+}$ were not so high (10^{-5} ~ 10^{-10} Scm^{-1}). The structural analysis of $[H3BIM^+]_2[TCNQ^{-\bullet}][TCNQ]$ indicated that the extension of π – electron system is useful to construct the uniform stacking structure of $H3BIM^+$ and TCNQ chains. Thus, I tried to increase the electrical conductivity in the 2,2'-bi-1*H*-benzoimidazole (H2BBIM) system. The 2-(2-1*H*-benzoimidazolyl)-1*H*-benzoimidazolium ($H3BBIM^+$) and 2,2'-bi-1*H*-benzoimidazolium ($H4BBIM^{2+}$) were newly prepared and examined the redox and acid dissociation properties, which showed the stable existence of cation species. The single crystals of $(H3BBIM^+)(TCNQ)(Cl^-)_{0.7}(H_2O)_{0.7}$ was obtained by the novel electrocrystallizaton method in the mixed solvent system between the buffer solution and acetonitrile. This method was possible to isolate the TCNQ complex, which can not be obtain from dry acetonitrile due to the deprotonation reaction of $H3BBIM^+$. Since the crystal structure of TCNQ complex was composed of the segregated uniform stacks of $H3BBIM^+$ and TCNQ, the expansion of π-electron system was effective to increase the intermolecular overlap of H2BIM system. The electrical conductivity of $H3BBIM^+$ complex with TCNQ (2 ~ 20 Scm^{-1}) largely enhanced compared with $H3BIM^+$ and $H4BIM^{2+}$ ones. The real chemical formula of this was deduced as the $[H3BBIM^+]_{0.6}[H4BBIM^{2+}]_{0.4}[TCNQ^{-0.7}][Cl^-]_{0.7}[H_2O]_{0.7}$ from the structural analysis, and the IR measurements of ν_{NH} mode of the complex supported the mixed PT state of $[H3BBIM^+]_x[H4BBIM^{2+}]_{1-x}$ in the TCNQ complex.

The mixed PT state in the crystal is interesting character from a viewpoint of filling control of electron conducting band. The degree of CT in the TCNQ can be changed according to the mixing ratio of $H3BBIM^+$ and $H4BBIM^{2+}$, if the isostructural salt is obtained. The filling control of organic system is next subject to increase the T_c of organic superconductor as well as CuO_x system. However, the chemical method of free control of band filling is not established. Since the mixing ratio of PT state depends on the equilibrium between two kinds of protonated species, the changes of the pH of crystallization solvent vary the PT state in the complex. It is thus that the mixed PT state is possible to use as a method of band filling control in the electron conducting system.

However, there are some problems to apply this method. i) The stability of electron donor or acceptor molecules to the acidic or basic solvent. ii) The isostructural character in large ranges of filling control. iii) The precise determination of mixing ratio of PT. To clear these problems, the equilibrium between the macrocyclic ligand and ion can also be used to the filling control. This equilibrium is inert to the CT processes of electron donor and acceptor molecules, and the moderate size of ion is possible to determine the content of ion from structural and density measurements. However, the increasing of the ion size will cause to a large deformation of potential field in the crystal, which influences the conduction electron. The equilibrium of acid-base and ion-ligand systems will be useful chemical method to control the band filling.

Chapter 6 Supplemental Tables

Table 6-1. Atomic Parameters for $[H2BIM^0]_3[H3BIM^+]_2[I^-]_2$ (7).

Atom	x	y	z	B_{eq} / Å^2 a)
I(1)	0.46914	0.38807	0.05943	3.19
I(2)	0.03225	0.41600	0.94696	3.80
C_{11}	0.07141	0.85536	0.48602	2.80
C_{12}	0.07762	0.95811	0.51656	2.25
C_{13}	0.10711	1.12197	0.49374	4.23
C_{14}	0.07112	1.13623	0.69595	4.64
C_{15}	0.04299	0.68524	0.55312	3.77
C_{16}	0.07515	0.68167	0.33710	3.86
N_{11}	0.08443	0.78554	0.31053	2.63
N_{12}	0.10683	1.02844	0.39427	4.05
N_{13}	0.05623	1.02676	0.71626	2.94
N_{14}	0.04085	0.79073	0.61912	2.88
C_{21}	0.41890	0.83625	0.44947	2.57
C_{22}	0.43121	0.96145	0.49914	2.49
C_{23}	0.46164	1.12023	0.49977	3.88
C_{24}	0.43298	1.12319	0.65610	3.79
C_{25}	0.39665	0.67353	0.51982	4.84
C_{26}	0.42216	0.67892	0.32392	3.80
N_{21}	0.43727	0.77873	0.28734	4.21
N_{22}	0.46040	1.01644	0.36738	3.60
N_{23}	0.40618	1.01863	0.67298	2.62
N_{24}	0.39188	0.79192	0.60257	3.40
C_{31}	0.22760	0.40409	0.48597	2.58
C_{32}	0.27744	0.40264	0.52529	1.95
C_{33}	0.34276	0.40028	0.71228	3.14
C_{34}	0.34825	0.38980	0.42279	2.51
C_{35}	0.15587	0.41441	0.31650	2.74
C_{36}	0.15548	0.39823	0.56500	2.87
N_{31}	0.19516	0.40784	0.68177	2.28
N_{32}	0.30002	0.40100	0.74820	2.47
N_{33}	0.30009	0.40566	0.31660	2.38
N_{34}	0.20488	0.41163	0.23913	2.86
C_{41}	0.18620	0.84870	0.80421	3.13
C_{42}	0.19767	0.96159	0.85098	2.65
C_{43}	0.20188	1.12590	1.03732	3.88
C_{44}	0.22458	1.12183	0.84290	3.32
C_{45}	0.18376	0.68667	0.64049	3.66
C_{46}	0.15618	0.69287	0.82071	2.54
N_{41}	0.15621	0.79677	0.92834	2.77
N_{42}	0.18157	1.02498	1.07559	2.67
N_{43}	0.22498	1.01758	0.73514	3.69
N_{44}	0.19965	0.78791	0.62839	2.37
C_{51}	0.30403	0.84168	0.12805	3.03
C_{52}	0.31703	0.95612	0.16861	2.61
C_{53}	0.31377	1.12313	0.33357	3.98
C_{54}	0.34765	1.12351	0.11986	3.67
C_{55}	0.30708	0.67458	-0.00086	3.42
C_{56}	0.30708	0.67458	-0.00086	3.42
N_{51}	0.27070	0.79402	0.27797	3.03
N_{52}	0.29141	1.01877	0.35484	3.17
N_{53}	0.34779	1.01419	0.03008	3.25
N_{54}	0.32686	0.77608	-0.00539	2.05

a) $B_{eq} = (\frac{4}{3})(\frac{B_{11}}{(A^{\bullet})^2} + \frac{B_{22}}{(B^{\bullet})^2} + \frac{B_{33}}{(C^{\bullet})^2})$

Table 6-2. Interatomic distances (Å) and bond angles (deg) for $[H2BIM^0]_3[H3BIM^+]_2[I^-]_2$ (7) with estimated standard deviations in parenthesis.

H3BIM+(1)		H3BIM+(2)	
C11-C12	1.295(14)	C31-C32	1.587(14)
C11-N11	1.306(13)	C31-N31	1.248(14)
C11-N14	1.401(14)	C31-N34	1.271(13)
C12-N12	1.395814)	C32-N32	1.318(14)
C12-N13	1.484(14)	C32-N33	1.387(13)
N11-C16	1.327(13)	N31-C36	1.322(14)
N14-C15	1.333(13)	N34-C35	1.519(14)
C15-C16	1.530(14)	C35-C36	1.291(15)
N12-C13	1.263(15)	N32-C33	1.446(14)
N13-C14	1.423(14)	N33-C34	1.502(13)
C13-C14	1.528(15)	C33-C34	1.197(14)

H2BIM0(1)		H2BIM0(3)		H2BIM0(3)	
C21-C22	1.464(14)	C41-C42	1.449(14)	C51-C52	1.464(13)
C21-N21	1.411(14)	C41-N41	1.288(13)	C51-N51	1.416(12)
C21-N24	1.278(13)	C41-N44	1.251(13)	C51-N54	1.372(13)
C22-N22	1.463814)	C42-N42	1.480(14)	C52-N52	1.279(12)
C22-N23	1.385(14)	C42-N43	1.234(14)	C52-N53	1.299(12)
N21-C26	1.377(14)	N41-C46	1.389(14)	N51-C56	1.275(13)
N24-C25	1.378(13)	N44-C45	1.334(13)	N54-C55	1.519(13)
C25-C26	1.518(14)	C45-C46	1.269(14)	C55-C56	1.278(13)
N22-C22	1.463(13)	N42-C43	1.396(13)	N52-C53	1.284(13)
N23-C24	1.416(14)	N43-C44	1.401(14)	N53-C54	1.493(13)
C23-C24	1.520(15)	C43-C44	1.232(14)	C53-C54	1.492(13)

H3BIM+(1)		H3BIM+(2)	
N11-C11-N14	101.1(8)	N31-C31-N34	108.3(8)
N12-C12-N13	105.0(8)	N32-C32-N33	109.3(9)
C14-C13-N13	112.6(9)	C34-C33-N32	109.5(9)
C13-C14-N13	100.2(8)	C33-C34-N33	111.8(9)
C16-C15-N11	104.9(9)	C36-C35-N34	102.8(9)
C15-C16-N11	99.5(8)	C35-C36-N31	110.8(8)
C11-N11-C16	111.0(8)	C31-N31-C36	104.3(8)
C12-N12-C13	111.8(9)	C32-N32-C33	101.6(8)
C12-N13-C14	109.7(8)	C32-N33-C34	107.2(9)
C11-N14-C15	112.8(9)	C31-N34-C35	113.3(8)

H2BIM0(1)		H2BIM0(3)	
N21-C21-N24	115.4(9)	N51-C51-N54	109.2(8)
N22-C22-N23	116.0(8)	N52-C52-N53	117.0(9)
C24-C23-N22	112.0(9)	C54-C53-N52	125.4(9)
C23-C24-N23	104.3(8)	C53-C54-N53	100.5(8)
C26-C25-N24	103.7(9)	C56-C55-N54	109.0(8)
C25-C26-N21	108.1(9)	C55-C56-N51	111.6(9)
C21-N21-C26	102.8(8)	C51-N51-C56	108.2(8)
C22-N22-C23	99.5(8)	C52-N52-C53	109.3(9)
C22-N23-C24	107.9(8)	C52-N53-C54	103.5(8)
C21-N24-C25	109.2(9)	C51-N54-C55	100.1(7)

H2BIM0(2)	
N31-C31-N34	118.4(9)
N32-C32-N33	116.6(8)
C34-C33-N32	109.1(9)
C33-C34-N33	114.9(9)
C36-C35-N34	103.8(8)
C35-C36-N31	111.9(9)
C31-N31-C36	105.7(8)
C32-N32-C33	102.8(8)
C32-N33-C34	95.6(7)
C31-N34-C35	99.9(8)

Table 6-3. Atomic Parameters for [H4BIM^{2+}][PICRATE^{-}]$_2$ (7).

Atom	x	y	z	B_{eq} / Å^2 a)
C_{11}	0.35651	0.68554	0.27361	2.34
C_{12}	0.41656	0.70885	0.31432	2.57
C_{13}	0.44901	0.88397	0.23780	3.05
C_{14}	0.41786	1.03349	0.12350	3.49
C_{15}	0.35976	1.01673	0.08172	3.59
C_{16}	0.33065	0.85073	0.16209	2.83
N_{11}	0.44803	0.55362	0.42722	3.07
N_{12}	0.44822	1.22125	0.05521	4.19
N_{13}	0.26933	0.83838	0.11037	2.45
O_{11}	0.32568	0.51906	0.34230	3.76
O_{12}	0.42459	0.46358	0.52557	5.20
O_{13}	0.49934	0.52605	0.41020	4.88
O_{14}	0.49858	1.26299	0.10646	4.16
O_{15}	0.42899	1.31465	-0.06602	5.93
O_{16}	0.25329	0.85878	-0.02528	3.41
O_{17}	0.23677	0.81312	0.20809	3.95
C_{21}	0.14695	0.53202	0.71739	3.20
C_{22}	0.08424	0.48866	0.69536	2.96
C_{23}	0.05395	0.32320	0.76049	3.13
C_{24}	0.07915	0.17346	0.86556	2.69
C_{25}	0.13738	0.19259	0.91225	2.41
C_{26}	0.16852	0.36473	0.84354	2.58
N_{21}	0.05187	0.64905	0.58122	3.52
N_{22}	0.04609	-0.01348	0.94847	3.87
N_{23}	0.22985	0.37355	0.88775	3.40
O_{21}	0.17353	0.68510	0.66479	2.80
O_{22}	0.07671	0.72348	0.46890	3.86
O_{23}	0.00226	0.70084	0.58972	3.85
O_{24}	-0.00209	-0.05988	0.89314	5.71
O_{25}	0.07635	-0.12465	1.05428	6.87
O_{26}	0.24605	0.34944	1.02907	3.52
O_{27}	0.26360	0.40135	0.79207	3.27
C_{31}	0.22420	0.14297	0.46127	2.75
C_{32}	0.27621	0.04515	0.54466	2.80
C_{33}	0.33638	-0.17170	0.70312	2.89
C_{34}	0.36659	0.00553	0.63912	3.11
C_{35}	0.16504	0.37519	0.31440	3.56
C_{36}	0.13524	0.19565	0.37169	3.88
N_{37}	0.27871	-0.13403	0.63738	2.57
N_{38}	0.32864	0.14620	0.53893	2.70
N_{39}	0.22017	0.35137	0.36854	3.43
N_{40}	0.17154	0.05801	0.46179	3.27
H_{11}	0.49584	0.87195	0.26630	4.45
H_{12}	0.34709	0.15038	0.01178	4.79
H_{21}	0.51726	0.37801	0.73820	4.24
H_{22}	0.16573	0.06610	0.00174	4.41
H_{31}	0.09304	0.17049	0.35077	3.87
H_{32}	0.15258	0.50490	0.22772	4.45
H_{33}	0.40362	0.04505	0.65438	3.84
H_{34}	0.34541	0.68804	0.75639	4.56
H_{35}	0.24068	0.40400	0.33534	3.89
H_{36}	0.33809	0.30834	0.47610	4.87
H_{37}	0.23587	0.74161	0.66484	4.20
H_{38}	0.16563	0.89298	0.52733	4.60

a) $B_{eq} = (\frac{4}{3})(\frac{B_{11}}{(A^*)^2} + \frac{B_{22}}{(B^*)^2} + \frac{B_{33}}{(C^*)^2})$

Table 6-4. Interatomic distances (Å) and bond angles (deg) for [H4BIM^{2+}] [PICRATE$^-$]$_2$ (**5**) with estimated standard deviations in parenthesis.

PICRATE$^-$(1)		PICRATE$^-$(2)	
C11-C12	1.415(7)	C21-C22	1.494(8)
C12-C13	1.462(8)	C22-C23	1.293(7)
C13-C14	1.438(8)	C23-C24	1.323(7)
C14-C15	1.372(8)	C24-C25	1.383(7)
C15-C16	1.368(8)	C25-C26	1.382(7)
C16-C11	1.428(7)	C26-C21	1.465(7)
C11-O11	1.341(7)	C21-O21	1.176(7)
C12-N11	1.425(7)	C22-N21	1.494(8)
C14-N12	1.431(8)	C24-N22	1.508(8)
C16-N13	1.453(8)	C26-N23	1.461(7)
N11-O12	1.187(7)	N21-O22	1.217(7)
N11-O13	1.246(7)	N21-O23	1.206(7)
N12-O14	1.238(7)	N22-O24	1.210(7)
N12-O15	1.224(7)	N22-O25	1.250(7)
N13-O16	1.219(7)	N23-O26	1.257(7)
N13-O17	1.221(7)	N23-O27	1.230(7)
C13-H11	1.030(90	C23-H21	0.925(9)
C15-H12	0.965(9)	C25-H22	1.057(9)
H4BIM^{2+}			
C31-C32	1.451(8)		
C31-N39	1.395(8)	C32-N37	1.276(7)
N39-C35	1.347(7)	N37-C33	1.417(7)
C35-C36	1.323(8)	C33-C34	1.368(7)
C36-N40	1.336(7)	C34-N38	1.396(7)
N40-C31	1.31587)	N38-C32	1.356(7)

PICRATE$^-$(1)		PICRATE$^-$(2)	
C11-C12-C13	120.7(5)	C21-C22-C23	129.0(5)
C12-C13-C14	115.4(5)	C22-C23-C24	121.5(5)
C13-C14-C15	124.6(5)	C23-C24-C25	119.5(5)
C14-C15-C16	117.0(5)	C24-C25-C26	118.7(5)
C15-C16-C11	124.6(5)	C25-C26-C21	126.9(5)
C16-C11-C12	117.3(5)	C26-C21-C22	104.1(5)
011-C11-C12	121.0(5)	O21-C21-C22	129.5(5)
C11-C12-N11	123.4(5)	C21-C22-N21	114.1(5)
C12-N11-O12	119.2(5)	C22-N21-O22	118.7(5)
C12-N11-O13	115.6(5)	C22-N21-O23	120.7(5)
C13-C14-N12	116.3(5)	C23-C24-N22	123.8(5)
C14-N12-O14	119.1(5)	C24-N22-O24	117.2(5)
C14-N12-O15	120.1(5)	C24-N22-O25	114.4(5)
C15-C16-N13	114.5(5)	C25-C26-N23	117.3(5)
C16-N13-O16	118.2(5)	C26-N23-O26	116.7(5)
C16-N13-O17	118.5(5)	C26-N23-O27	120.4(5)
H4BIM^{2+}			
C31-N39-C35	105.3(5)	C32-N37-C33	111.3(5)
N39-C35-C36	110.1(5)	N37-C33-C34	103.2(5)
C35-C36-N40	107.3(5)	C33-C34-N38	109.4(5)
C36-N40-C31	110.1(5)	C34-N38-C32	106.1(5)
N39-C31-N40	107.2(5)	N37-C32-N38	110.0(5)
N39-C31-C32	125.2(5)	N37-C32-C31	125.9(5)

Table 6-5. Atomic Parameters for $(H3BIM^+)_2(TCNQ^-)_3$ (**13**).

Atom	x	y	z	B_{eq} / Å^2 a)
C_1	0.05294	0.41544	0.08950	2.02
C_2	0.02955	0.41361	-0.08146	1.84
C_3	0.02470	0.49798	0.16667	2.07
C_4	0.03680	0.32897	-0.33244	2.46
C_5	0.05776	0.33115	-0.15967	2.08
C_6	0.10819	0.24130	-0.07464	3.11
N_1	0.02083	0.32755	-0.46784	3.79
N_2	0.14538	0.17028	-0.00757	5.47
C_{31}	0.01857	-0.07850	0.31421	2.26
C_{32}	0.15426	-0.08846	0.18263	2.60
C_{33}	0.33308	-0.08215	-0.08027	3.80
C_{34}	0.37922	-0.11936	0.05782	3.99
C_{35}	-0.15621	-0.09174	0.57812	2.87
C_{36}	-0.20072	-0.04187	0.44053	3.21
N_{37}	0.19313	-0.06298	-0.00164	3.25
N_{38}	0.26955	-0.12328	0.22005	3.38
N_{39}	-0.01865	-0.11342	0.49746	2.50
N_{40}	-0.08870	-0.03385	0.27360	2.76
C_{41}	0.67185	0.54269	0.53487	2.10
C_{42}	0.69940	0.45936	0.45738	2.01
C_{43}	0.67851	0.45683	0.28840	1.71
C_{44}	0.62825	0.54509	0.20246	2.01
C_{45}	0.60028	0.62785	0.27951	2.07
C_{46}	0.62027	0.63035	0.45018	1.78
C_{47}	0.76272	0.28544	0.29575	2.24
C_{48}	0.70813	0.37085	0.20946	1.85
C_{49}	0.69421	0.36596	0.03527	2.18
C_{50}	0.61781	0.71785	0.69940	2.28
C_{51}	0.59042	0.71489	0.53324	2.11
C_{52}	0.53778	0.80438	0.45523	2.50
N_{50}	0.80618	0.21817	0.36844	3.23
N_{51}	0.68553	0.36191	-0.10420	3.73
N_{52}	0.64072	0.72127	0.83018	3.53
N_{53}	0.49357	0.87608	0.39786	3.61
H_1	0.08268	0.34999	0.14481	3.27
H_2	0.05208	0.50496	0.29085	3.99
H_{33}	0.37061	-0.07394	-0.21165	3.23
H_{34}	0.44046	-0.14339	0.05802	2.87
H_{35}	-0.20102	-0.10911	0.68329	2.58
H_{36}	-0.30333	-0.00966	0.44340	3.24
H_{37}	0.13803	-0.05470	-0.02494	4.62
H_{38}	0.28237	-0.12865	0.30500	3.35
H_{39}	0.02513	-0.13947	0.53830	2.64
H_{41}	0.68957	0.54312	0.65230	3.68
H_{42}	0.72803	0.39903	0.51743	3.42
H_{44}	0.61183	0.54352	0.09242	3.41
H_{45}	0.56680	0.68501	0.22615	3.01

a) $B_{eq} = (\frac{4}{3})(\frac{B_{11}}{(A^*)^2} + \frac{B_{22}}{(B^*)^2} + \frac{B_{33}}{(C^*)^2})$

Table 6-6. Interatomic distances (Å) and bond angles (deg) for $(H3BIM^+)_2(TCNQ^-)_3$ (**13**) with estimated standard deviations in parenthesis.

TCNQ(1)		TCNQ(2)	
C1-C2	1.449(7)	C41-C42	1.368(7)
C1-C3'	1.356(7)	C42-C43	1.423(7)
C2-C3	1.437(7)	C43-C44	1.432(7)
C2-C5	1.360(7)	C44-C45	1.359(7)
C4-C5	1.452(7)	C45-C46	1.431(7)
C5-C6	1.446(7)	C46-C41	1.427(7)
C4-N1	1.135(7)	C43-C48	1.407(7)
C6-N2	1.130(8)	C48-C49	1.437(7)
C1-H1	1.003(11)	C47-C48	1.425(7)
C3-H2	1.131(11)	C46-C51	1.406(7)
		C51-C52	1.429(7)
		C50-C51	1.437(7)
		C47-N50	1.142(7)
		C49-N51	1.139(7)
		C52-N53	1.139(7)
		C50-N52	1.142(7)
		C41-H41	1.002(11)
		C42-H41	0.958(11)
		C44-H44	0.941(11)
		C45-H45	0.924(11)
H3BIM+			
C31-C32	1.422(7)		
C31-N40	1.328(7)	C32-N37	1.336(7)
N40-C36	1.394(7)	N37-C33	1.375(8)
C36-C35	1.367(8)	C33-C34	1.334(8)
C35-N39	1.362(7)	C34-N38	1.360(8)
N39-C31	1.349(7)	N38-C32	1.354(7)
C33-H33	0.946(12)	N37-H37	0.655(11)
C34-H34	0.686(12)	N38-H38	0.713(11)
C35-H35	0.790(12)	N39-H39	0.684(11)
C36-H36	1.105(12)		

TCNQ(1)		TCNQ(2)	
C3'-C1-C2	120.6(4)	C41-C42-C43	121.3(5)
C1-C2-C3	119.6(4)	C42-C43-C44	117.3(4)
C2-C3-C1'	120.7(4)	C43-C44-C45	121.5(4)
C4-C5-C6	116.7(4)	C44-C45-C46	121.2(4)
N1-C4-C5	179.7(7)	C45-C46-C41	117.3(4)
C5-C6-N2	178.7(6)	C46-C41-C42	121.4(5)
		C49-C48-C47	116.9(4)
		C50-C51-C52	115.4(4)
		C48-C47-N50	178.3(5)
		C48-C49-N51	178.9(6)
		C51-C52-N53	178.1(6)
		C51-C50-N52	179.1(6)
H3BIM+			
C31-N40-C36	107.9(4)	C32-N37-C33	109.1(5)
N40-C36-C35	106.9(5)	N37-C33-C34	107.3(5)
C36-C35-N39	108.485)	C33-C34-N38	107.8(5)
C35-N39-C31	106.0(4)	C34-N38-C32	109.1(5)
N40-C31-N39	110.8(4)	N38-C32-N37	106.7(5)

Table 6-7 Atomic Parameters of H2BBIM.

Atom	x	y	z	B_{eq} / Å^2 a)
C1	0.22533	0.31116	0.74573	2.6
C2	0.16574	0.48415	0.66878	3.2
C3	0.13431	0.58406	0.60221	3.3
C4	0.08260	0.67658	0.66952	4.4
C5	0.06690	0.67042	0.81160	3.4
C6	0.09546	0.57015	0.88712	3.6
C7	0.14706	0.47345	0.80882	2.6
C8	0.27238	0.19108	0.74090	2.6
C9	0.33301	0.01620	0.80987	2.5
C10	0.36450	-0.08709	0.88701	4.0
C11	0.41291	-0.17869	0.80569	3.7
C12	0.43458	-0.16879	0.66725	4.4
C13	0.40253	-0.06697	0.60095	3.3
C14	0.35107	0.02453	0.66882	2.7
N1	0.21759	0.37801	0.63138	2.8
N2	0.18714	0.36309	0.85428	2.8
N3	0.28443	0.12472	0.85382	2.9
N4	0.31284	0.13589	0.62669	2.9
H1	0.26649	0.35865	0.56069	3.3
H2	0.26683	0.14245	0.94140	0.6
H3	0.13866	0.59884	0.48522	8.0
H4	0.07791	0.75761	0.62511	5.0
H5	0.04489	0.73358	0.87663	2.7
H6	0.08323	0.56921	0.97615	0.8
H7	0.34319	-0.08389	0.97581	2.0
H8	0.45531	-0.24713	0.86966	4.6
H9	0.48909	-0.23669	0.61998	7.5
H10	0.41993	-0.05347	0.47989	7.7

a) $B_{eq} = (\frac{4}{3})(\frac{B_{11}}{(A^*)^2} + \frac{B_{22}}{(B^*)^2} + \frac{B_{33}}{(C^*)^2})$

Table 6-8. Intramolecular bond distances (Å) and angles (deg) of H2BBIM.

Bond	Distance	Bond	Distance	Bond	Distance
C1-C8	1.449(6)	C1-N1	1.367(6)	C1-N2	1.287(6)
N1-C2	1.369(6)	N2-C7	1.395(6)	C2-C7	1.405(6)
C2-C3	1.353(6)	C3-C4	1.353(7)	C4-C5	1.418(7)
C5-C6	1.395(6)	C6-C7	1.45(6)	C3-H3	1.172(8)
C4-H4	1.023(9)	C5-H5	0.991(8)	C6-H6	0.891(8)
C8-N3	1.355(6)	C8-N4	1.358(6)	N3-C9	1.399(6)
N4-C14	1.390(6)	C9-C14	1.412(6)	C9-C10	1.438(6)
C10-C11	1.406(7)	C11-C12	1.394(7)	C12-C13	1.371(7)
C13-C14	1.345(6)	N3-H2	0.909(8)	C10-H7	0.897(8)
C11-H8	1.093(8)	C12-H9	1.060(9)	C13-H10	1.222(8)
N1-H1	0.887(8)	N3-H2	0.909(8)		
N1-C1-N2	114.8(4)	C1-N1-C2	106.8(4)	N1-C2-C7	104.0(4)
C2-C7-N2	110.9(4)	C1-N2-C7	103.4(4)	C2-C3-C4	120.4(4)
C3-C4-C5	119.6(4)	C4-C5-C6	123.3(4)	C5-C6-C7	114.2(4)
C6-C7-C2	120.9(4)	C7-C2-C3	121.5(4)	N3-C8-N4	113.7(4)
C8-N3-C9	105.5(4)	N3-C9-C14	107.1(4)	C9-C14-N4	108.8(4)
C8-N4-C14	104.9(4)	C9-C10-C11	112.3(4)	C10-C11-C12	123.4(4)
C11-C12-C13	120.1(5)	C12-C13-C14	120.5(4)	C23-C24-C9	119.5(4)
C14-C9-C10	123.5(4)				

H-bond		H-bond		H-bond	
N1•••N2	2.916(8)	N3•••N4	2.811(8)	N2•••H1	2.099(8)
N4•••H2	2.008(9)				
N1-H1•••N2	152.8(7)	N3-H2•••N4	160.8(7)	N2-H5•••N1	143(7)
N3-H6•••N4	165(5)				

Table 6-9. Atomic Parameters of $[H4BBIM^{2+}][BF_4^-]_2$.

Atom	x	y	z	B_{eq} / Å^2 a)
C11	0.95663	0.74900	0.22866	2.0
C12	0.81845	0.67063	0.15762	2.4
C13	0.73823	0.56616	0.11431	3.4
C14	0.65962	0.66386	0.08450	4.6
C15	0.66391	0.82821	0.09870	3.9
C16	0.74327	0.93473	0.14024	3.5
C17	0.81826	0.84113	0.17009	2.3
N11	0.90008	0.62924	0.19192	2.1
N12	0.90362	0.88617	0.21098	2.5
C21	0.55134	-0.73860	0.22794	2.5
C22	0.68795	-0.83635	0.15808	2.3
C23	0.76410	-0.91225	0.11396	2.7
C24	0.83607	-0.83024	0.08494	2.5
C25	0.83597	0.65340	0.09395	2.8
C26	0.76287	0.57584	0.13472	2.9
C27	0.68421	0.66515	0.16858	2.5
N21	0.59672	0.87854	0.20038	2.8
N22	0.59579	0.61323	0.21571	2.6
B31	0.43416	0.74829	0.06951	2.6
F31	0.48477	0.88918	0.12416	4.3
F32	0.36825	0.74871	0.10076	7.1
F33	0.39869	0.75001	0.04974	4.6
F34	0.48577	0.61256	0.11925	3.8
B41	0.93592	0.25730	0.07404	3.4
F41	0.98440	-0.39495	0.12000	4.0
F42	0.98710	-0.11622	0.12692	4.6
F43	0.86473	-0.25326	0.08910	7.2
F44	0.90888	-0.25052	0.04416	6.6
H11	0.91742	0.52369	0.18946	3.8
H12	0.92094	0.99207	0.21159	2.3
H13	0.73837	0.45738	0.10329	5.7
H14	0.59819	0.59663	0.04887	7.8
H15	0.61097	0.89715	0.06554	2.2
H16	0.75144	1.06523	0.15389	5.9
H21	0.58259	0.99069	0.19637	8.0
H22	0.57875	0.50137	0.25043	1.0

H23	0.75824	1.05626	0.11553	4.3
H24	0.88838	0.89039	0.04370	3.2
H25	0.88879	0.59705	0.07448	3.5
H26	0.76100	0.44751	0.14090	3.4

a) $B_{eq} = (\frac{4}{3})(\frac{B_{11}}{(A^*)^2} + \frac{B_{22}}{(B^*)^2} + \frac{B_{33}}{(C^*)^2})$

Table 6-10. Intramolecular bond distances (Å) and angles (deg) of $[H4BBIM^{2+}][BF_4^-]_2$.

Bond	Distance	Bond	Distance
C11-C11	1.327(4)	C21-C21	1.587(4)
C11-N11	1.353(3)	C21-N21	1.332(3)
N11-C12	1.329(3)	N21-C22	1.444(3)
C12-C13	1.488(4)	C22-C23	1.310(3)
C13-C14	1.463(4)	C23-C24	1.303(3)
C14-C15	1.349(4)	C24-C25	1.446(3)
C15-C16	1.489(3)	C25-C26	1.278(3)
C16-C17	1.393(3)	C26-C27	1.417(4)
C17-C12	1.400(3)	C27-C22	1.401(3)
C17-N12	1.359(3)	C27-N22	1.411(3)
N12-C11	1.396(4)	N22-C21	1.245(3)
N11-H11	0.850(4)	N21-H21	0.957(5)
C13-H13	0.899(5)	C23-H23	1.178(5)
C14-H14	1.081(5)	C24-H24	0.934(5)
C15-H15	0.978(5)	C25-H25	0.946(5)
C16-H16	1.076(5)	C26-H26	1.051(4)
N12-H12	0.914(4)	N22-H22	0.993(5)
B31-F31	1.405(3)	B41-F41	1.350(3)
B31-F32	1.408(3)	B41-F42	1.405(3)
B31-F33	1.354(3)	B41-F43	1.360(3)
B31-F34	1.367(3)	B41-F44	1.369(3)
Hydrogen-bond Distances			
N11•••F41	2.803(12)	N22•••F34	2.745(12)
N11•••F41'	2.909(11)	N22•••F34'	2.976(12)
N12•••F42	2.214(12)	N21•••F31	2.840(12)

N12•••F42'	2.749(12)	N21•••F31'	2.307(12)

N11-C11-N12	104.85(8)	N21-C21-N22	114.79(8)
C11-N11-C12	110.44(8)	C21-N21-C22	107.04(9)
N11-C12-C17	109.48(8)	N21-C22-C27	102.25(8)
C12-C17-N12	104.28(9)	C22-C27-N22	109.14(8)
C17-N12-C11	110.86(9)	C27-N22-C21	106.67(8)
C12-C13-C14	111.72(9)	C22-C23-C24	120.38(7)
C13-C14-C15	121.65(9)	C23-C24-C25	121.79(8)
C14-C15-C16	127.29(9)	C24-C25-C26	119.12(8)
C15-C16-C17	110.87(9)	C25-C26-C27	119.14(8)
C16-C17-C12	124.67(9)	C26-C27-C22	119.45(7)
C17-C12-C13	123.7(9)	C27-C22-C23	120.02(8)

Hydeogen-Bond		Hydrogen-Bond	
N11•••F41	2.803(12)	N22•••F34	2.745(12)
N11•••F41'	2.909(11)	N22•••F34'	2.976(12)
N12•••F42	2.314(12)	N21•••F31	2.840(12)
N12•••F42'	2.749(12)	N21•••F31'	2.307(12)

Table 6-11 Atomic Parameters of $(H3BBIM^{+})(TCNQ)(Cl^{-})_{0.7}(H_2O)_{0.7}$.

Atom	x	y	z	B_{eq} / Å^{2} a)
C1	0.02657	0.58954	0.47015	4.3
C2	0.11211	0.52750	0.34780	3.3
C3	-0.15094	0.59636	0.40083	2.5
C4	0.11099	0.64123	0.64429	5.0
C5	0.02023	0.70221	0.75866	3.1
C6	0.09671	0.75544	0.92515	2.9
C7	0.28035	0.74539	0.99357	2.5
C8	0.37421	0.68099	0.87724	3.5
C9	0.29061	0.63494	0.70850	3.6
C10	0.35988	0.79605	1.16176	3.7
C11	0.26563	0.85974	1.28098	2.6
C12	0.54459	0.78894	1.23716	4.2
N11	0.83607	0.47431	0.25233	3.2
N12	-0.29304	0.59948	0.33721	2.8
N13	0.20568	0.90705	1.38557	2.9
N14	0.68649	0.78337	1.30077	3.1
H1	-0.09382	0.70971	0.70472	5.2
H2	0.03973	0.78651	0.99716	5.6
H3	0.49723	0.66309	0.93580	6.0
H4	0.35419	0.58766	0.62443	4.9
C21	0.70092	0.22608	0.39270	3.4
C22	0.60713	0.32645	0.61462	3.6
C23	0.50461	0.38685	0.72850	3.2
C24	0.60219	0.43918	0.86589	3.3
C25	0.77282	-0.43347	0.88618	4.5
C26	0.87516	-0.37335	0.76226	4.1
C27	0.77571	-0.32103	0.62633	4.0
C28	0.70189	-0.15883	0.23597	4.6
C29	0.79465	0.05663	0.01518	3.9
C30	0.88162	-0.00127	-0.10869	5.0
C31	0.79402	-0.05240	-0.22971	2.8
C32	0.60104	-0.04520	-0.22939	2.8
C33	0.51476	0.01035	-0.12497	3.2
C34	0.60172	0.06401	0.00213	2.8
N21	0.54960	0.26841	0.46771	3.8

N22	0.83440	0.25505	0.48332	2.9
N23	0.83677	0.11976	0.16070	3.0
N24	0.55110	0.12609	0.13911	4.0
H23	0.37935	0.39904	0.69981	5.6
H24	0.54009	0.48501	0.95556	5.5
H25	0.82341	0.47091	0.98368	3.8
H26	0.99327	0.37071	0.76229	6.1
H30	1.00200	-0.00373	-0.10609	5.0
H31	0.85780	-0.09673	-0.30947	5.3
H32	0.54609	-0.08858	-0.30665	5.4
H33	0.39061	0.00783	-0.12176	6.0
O1	0.18505	0.17183	0.49173	5.8
O2	0.19907	0.20079	0.23405	5.4
Cl1	0.21942	0.24413	0.12750	2.9
Cl2	0.17909	0.08848	0.39020	3.1

a) $B_{eq} = (\frac{4}{3})(\frac{B_{11}}{(A^{*})^2} + \frac{B_{22}}{(B^{*})^2} + \frac{B_{33}}{(C^{*})^2})$

Table 6-12. Intramolecular bond distances (Å) and angles (deg) of $(H3BBIM^{+})(TCNQ)(Cl^{-})_{0.7}(H_2O)_{0.7}$.

TCNQ				H3BBIM^{+}	
C1-C2	1.409(4)	C21-C28	1.433(5)	C33-C34	1.363(4)
C1-C3	1.411(4)	C21-N22	1.257(4)	N21-H5	0.641(6)
C1-C4	1.412(4)	N22-C27	1.433(4)	C23-H23	0.996(7)
C2-N11	1.199(4)	C27-C22	1.298(4)	C24-H24	1.036(6)
C3-N12	1.137(4)	C22-N21	1.360(4)	C25-H25	0.927(8)
C4-C5	1.399(4)	N21-C21	1.407(4)	C26-H26	0.905(6)
C5-C6	1.387(4)	C22-C23	1.432(4)	N23-H7	0.765(6)
C6-C7	1.461(4)	C23-C24	1.407(4)	C30-H30	0.923(7)
C7-C8	1.466(4)	C24-C25	1.318(4)	C31-H31	0.991(8)
C8-C9	1.321(4)	C25-C26	1.439(4)	C32-H32	1.003(8)
C9-C4	1.421(4)	C26-C27	1.413(4)	C33-H33	0.953(9)
C7-C10	1.366(4)	C28-N23	1.274(4)	N24-H8	0.689(8)
C10-C11	1.472(4)	N23-C29	1.400(4)		
C10-C12	1.460(4)	C29-C34	1.486(4)		
C11-N13	1.073(4)	C34-N24	1.343(4)		
C12-N14	1.137(4)	N24-C28	1.413(4)		

C5-H1	0.923(6)	C29-C20	1.350(5)		
C6-H2	0.765(6)	C30-C31	1.318(4)		
C8-H3	1.035(6)	C31-C32	1.481(4)		
C9-H4	1.058(6)	C32-C33	1.288(4)		
C4-C1-C2	123.11(8)	C21-N21-C22	104.98(8)	C28-N23-C29	112.26(8)
C4-C1-C3	122.46(8)	N21-C22-C27	109.43(8)	N23-C29-C34	102.78(8)
C1-C2-N11	178.27(8)	C22-C27-N22	108.60(8)	C29-C34-N24	107.32(8)
C1-C3-N12	177.23(8)	C27-N22-C21	106.61(8)	C34-N24-C28	107.92(8)
C5-C4-C9	116.7(8)	N21-C21-N22	110.89(8)	N24-C28-N23	109.68(8)
C4-C5-C6	123.54(8)	C22-C23-C24	113.97(8)	C29-C30-C31	119.75(8)
C5-C6-C7	117.5(8)	C23-C24-C25	123.12(8)	C30-C31-C32	119.33(8)
C6-C7-C8	118.71(8)	C24-C25-C26	122.39(8)	C31-C32-C33	122.49(8)
C7-C8-C9	118.77(8)	C25-C26-C27	113.97(8)	C32-C33-C34	119.46(8)
C8-C9-C4	124.68(8)	C26-C27-C22	123.16(8)	C33-C34-C29	118.73(8)
C7-C10-C12	121.91(8)	C27-C22-C23	123.33(8)	C34-C29-C30	120.14(8)
C7-C10-C11	121.82(8)	C28-C21-N22	124.75(8)	C21-C28-N23	125.82(8)
C10-C12-N14	178.94(8)	C28-C21-N21	124.35(8)	C21-C28-N24	124.50(8)
C10-C11-N13	174.55(8)				

Acknowledgements

This work has been carried out under the supervision of Prof. Gunzi Saito at Kyoto University. The author would like to thank Professor Gunzi Saito (Kyoto University) for his continuos encouragement and stimulating discussions.

The author is grateful to Professor Hideki Yamochi (Kyoto University) for many experimental supports and discussions, and Professor Takayoshi Nakamura (Hokkaido University) for helpful advises and encouragement.

The X-ray crystal structural analysis have be carried out at University of Osaka. The author wishes to acknowledge Dr. Masami Kusunoki and Mr. Ken-ich Sakaguchi for experimental supports.

The author wishes to thank to Professor Norimich Kojima (Tokyo University) for useful discussion of magnetic experiment, and also thanks Dr. Ken-ich Sugiura (Univ. of Osaka) for valuable discussion.

The author thanks Research Associate Toshiro Ban (Kyoto Univ.), Dr. Akihiro Otuka (Kyoto Univ.), Dr. Tokutaro Komatsu (Tokyo Univ.), Dr. Sachio Horiuch (Kyoto Univ.), and all the members of Saito laboratory for various useful discussion and encouragement.

The author is grateful to Honorary Prof. Yoshio Matsunaga (Hokkaido Univ.) for his continuos encouragement and stimulating discussions during his study at Hokkaido University.

The author is very grateful to his parents for their continuous encouragement and invaluable support during his study at the graduate school.